“SS CYRIL AND METHODIUS” UNIVERSITY IN SKOPJE

SCHOOL FOR DOCTORAL STUDIES

FACULTY OF CIVIL ENGINEERING

Study program:

STRUCTURAL ENGINEERING

EXPERIMENTAL AND ANALYTICAL INVESTIGATION ON RC FRAMES INFILLED WITH AUTOCLAVED AERATED CONCRETE BLOCKS

Candidate:

MSc. Valon VESELI, grad. civil. eng.

- DRAFT-Doctoral Dissertation -

Mentor:

Prof. Dr. Sc. Sergey CHURILOV

November 2025

РЕЗИМЕ

Во оваа докторска дисертација презентирани се интегралните резултати добиени од спроведените оригинални експериментални и аналитички истражувања извршени на армирано бетонски рамовски систем со исполна од блокови од автоклавиран аериран бетон (гасбетон) (AAC). Разгледуваниот систем за градење се применува во региони кои се карактеризираат со изразена до висока сеизмичност, но се уште постојат нејастотии околу неговото однесување, но и практично проектирање.

Експерименталните истражувања вклучуваат тестирање на однесувањето на прототип модели во голем рамер на АБ рамки без и со AAC исполна, при услови на реално симулирани вертикални и земјотресни хоризонтални оптоварувања. Спроведената специфична и детална студија за аналитичко моделирање опфаќа развој на напреден експериментално верификуван нелинеарен микро-модел и реализација на многу важни и релевантни параметарски студии на тестираните прототипски модели на АБ рамки без и со AAC исполна, при симулирани услови на товарење. Во моментов, развојот на сеизмички безбедни АБ системи за градење со исполна од AAC всушност се од голема важност бидејќи овие типови на конструкцции интензивно се применуваат во сите региони, вклучително и во многу области со висока сеизмичност.

По воведното поглавје 1 кое дава кратка презентација на предметот и целите на реализираните конкретни експериментални и аналитички истражувања, следува Поглавје 2, кое содржи краток преглед на карактеристиките на земјотресните оштетувања на АБ рамовски системи на згради со исполна, вклучително и специфични типови на оштетување на истражуваните АБ рамовски згради со исполна од автоклавен гасобетон (AAC). Накратко е резимирана потребата од надградба на сеизмичка безбедност на АБ рамоввски згради со AAC исполна.

Согласно целните на аналитичките истражувања, во Глава 3 накратко се претставени основните претпоставки за формулирање на имплементираниот напреден концепт на нелинеарно микро-моделирање на тестираните прототипски модели на АБ рамки без и со исполна од автоклавиран аериран бетон (AAC).

Во Глава 4 се претставени добиените резултати од спроведените експериментални тестови на конструирани прототипски модели на АБ рамки со и без AAC исполна. Со оглед на остварената почетна апликација на пропишаните вертикални товари при тестовите, специфичните интерактивни нелинеарни одговори на моделите беа успешно регистрирани при симулирано циклично и постепено еднонасочно оптоварување. Експерименталната програма беше усогласена со поставените специфични истражувачки цели. Извршените обемни и скапи експериментални истражувања беа реализирани согласно на целите на предметното истражување.

Добиените експериментални резултати за тестираните прототип модели на АБ рамки без и со AAC исполна беа од големо значење за експериментална валидација на

формулираните микро-аналитички модели. Експериментално докажаните нелинеарни микро-модели беа успешно имплементирани за реализација на планираните параметарски анализи за проучување на ефектите од различни нивоа на постојаните аксијални оптоварувања во различни катови на реалниот нелинеарен одговор на применетите АБ рамки. Во Глава 5 презентирани се резултатите добиени од реализираната параметарска анализа на ефектот од симулирани различни нивоа на аксијални оптоварувања (N1, N2 и N3) за нелинеарен одговор на тестираната АБ рамка без ААС исполна. Аналогно, во Глава 6 се изложени добиените резултати од параметарско аналитичко истражување на ефектот на симулирани различни нивоа на аксијални оптоварувања (N1, N2 и N3) за нелинеарен одговор на тестираната АБ рамка со ААС исполна. Во Глава 7 се претставени резултатите добиени од аналитичкото проучување на ефектите во зависност од насоката на оптоварување врз нелинеарниот одговор на АБ рамката со ААС компоненти на исполна долж полураспон. Добиените резултати претставуваат важен придонес за практично моделирање и разбирање на нелинеарниот одговор на рамовските АБ згради со ААС исполна. Во Глава 8 е дадено резиме на најважните сознанија кои се однесуваат на формулирање на микро-аналитички модели.

Во поглавјето 9, презентирани се резултатите добиени од завршената параметарска анализа со користење на експериментално верифицирани микро-модели, кои претставуваат "аналитички експерименти". Во поглвјето 10, предложен е нов AACF нелинеарен макро-модел применлив за практично моделирање и сеизмичка анализа на интегрални повеќекатни АБ рамовски згради со исполна од ААС. Главата 11 ги содржи заклучоците извлечени од реализираните интегрални истражувачки активности како и општи насоки за идните истражувања. Во последното 12то поглавје прикажана е листа на литературата што е користена за овие специфични истражувачки цели.

SUMMARY

This doctoral dissertation presents the results obtained from experimental and analytical study conducted on a reinforced concrete (RC) frame system with infill walls made of autoclaved aerated concrete (AAC) elements. The investigated building system is widely used in regions characterized by moderate to high seismicity; however, there still exist ambiguities regarding its behavior and practical design.

The experimental study involved large-scale testing of RC bare frame model and RC frame with AAC infill, under vertical and monotonic loads. The specific and detailed analytical study conducted includes the development of advanced, developed nonlinear micro-model and the execution of extensive and relevant parametric studies on the tested prototype models of RC bare frames and RC frames with AAC infill, under loading conditions. At present, the development of seismically safe RC building systems incorporating AAC infill is of great importance, since these structural types are increasingly applied worldwide, including in many high-seismicity areas.

Following the introductory Chapter 1, which provides a brief overview of the subject, objectives, and scope of the conducted experimental and analytical research, Chapter 2 presents a concise review of the characteristics of earthquake-induced damage in RC frame building systems with infill walls, including specific types of damage observed in RC frame buildings with AAC element infill. The chapter also summarizes the need to enhance the seismic safety of RC frame buildings with AAC infill.

In accordance with the objectives of the analytical research, Chapter 3 outlines the fundamental assumptions adopted in formulating the implemented advanced concept of nonlinear micro-modelling of the tested prototype RC bare frame and RC frame with AAC infill.

Chapter 4 presents the results obtained from the conducted experimental tests on the constructed prototype RC bare frame and RC frame with AAC infill. Considering the applied initial vertical loading during testing, the specific interactive nonlinear responses of the models were successfully recorded under simulated cyclic and monotonically increasing horizontal loading. The experimental program was carefully aligned with the defined research objectives. These extensive and costly experimental studies were carried out in accordance with the aims of the study.

The experimental results obtained for the tested prototype RC frames, both RC bare frame and RC frame with AAC infill, were of great significance for the experimental validation of the formulated micro-analytical models. The experimentally verified nonlinear micro-models were then successfully implemented for performing the planned parametric analyses aimed at studying the effects of different levels of sustained axial loads at various story levels on the nonlinear response of the analyzed RC frames.

Chapter 5 presents the results obtained from the parametric analysis examining the effect of different simulated levels of axial load (N_1, N_2, and N_3) on the nonlinear response of the tested bare RC bare frame. Analogously, Chapter 6 presents the results of the parametric analytical study on the influence of simulated varying axial load levels (N_1, N_2, and N_3) on the nonlinear response of the tested RC frame with AAC infill. Chapter 7 discusses the analytical study of the effects of the loading direction on the nonlinear response of the RC frame with AAC infill components along the half-span. The obtained results represent a significant contribution toward practical modelling and understanding of the nonlinear response of RC frame buildings with AAC infill walls.

Chapter 8 summarizes the key findings related to the formulation of micro-analytical models.

In Chapter 9, the results from the final parametric analyses performed using the experimentally verified micro-models are presented, representing a series of "analytical experiments." Chapter 10 proposes a new nonlinear macro-model (AACF model) applicable for practical modelling and seismic analysis of multi-story RC frame buildings with AAC infill. Chapter 11 contains the conclusions derived from comprehensive experimental and analytical research, as well as general recommendations for future investigations. The final Chapter 12 provides the list of references used for the specific research objectives of this dissertation.

ACKNOWLEDGEMENT

Firstly, I would like to express my gratitude to the professors of the doctoral study program at the Faculty of Civil Engineering, Ss. Cyril and Methodius University and to the entire staff for the support that they have given to me during my doctoral studies.

Special thanks are extended to the Faculty's management, Dean - Prof. Dr. Sc. Goran Markovski and to Prof. Dr. Sc. Elena Dumova-Jovanoska, responsible for PhD studies, for their respected support and success in organizing the PhD studies.

I am expressing sincere gratitude to my mentor Prof. Dr. Sc. Sergey CHURILOV for the continuous and highly valuable support that he has given to me during my studies at Faculty of Civil Engineering and during the period of preparation of this dissertation.

I am particularly indebted to Prof. Dr. Danilo Ristic for the opportunity that he has given me to explore results obtained from the conducted innovative experimental tests in the newly established ReSIN Laboratory of Industrial Science and Technology, Skopje.

It was great privilege for me to be enrolled in continuation of the research project initiated in ReSIN Laboratory, devoted to development of advanced technology for seismic protection of RC frame buildings with AAC infill. For the extended support, I am expressing deep gratitude to the Faculty of civil engineering, my mentor and to the entire staff of the ReSIN Laboratory, Skopje.

I am also extending my gratitude to the Faculty of Civil Engineering, University of Prishtina, for the extended support to my studies in Skopje.

Finally, deep gratitude is also accorded to my family members for their continuous support and understanding that enabled me successful performance of all my research activities.

MSc. Valon Veseli, Grad. Civil. Eng.

TABLE OF CONTENT

LIST OF FIGURES

LIST OF TABLES

1 CHAPTER 1 - INTRODUCTION

1.1 Subject of the Conducted Research

This doctoral dissertation entitled “Development of seismically safe RC frame building systems with autoclaved aerated concrete infill based on nonlinear tests and analytical investigation”, explore obtained experimental and numerical research results and critically examines the seismic performance of reinforced concrete (RC) frames with autoclaved aerated concrete (AAC) infills. The research is mainly focused on formulation of experimentally verified analytical micro-models capable to closely simulate the existing complex interaction effects between these materials under very strong earthquake loads. The research addresses a vital gap in current seismic design practices, where the nonlinear behaviour of AAC-infilled structures is not fully understood or accounted for. Through a combination of experimental testing and numerical modelling, this work contributes to create ideas and to develop novel practical, data-driven guidelines that enhance both the structural resilience and sustainability of buildings in earthquake-prone areas.

The ultimate goal of the present study is to refine analytical nonlinear modelling concept based on conducted experimental tests of large-scale prototype models, to fill the existing research gap with upgraded scientific knowledge, to improve design standards, to propose a method for practical implementation of the AAC infill in structural analysis and to provide clear recommendations for safely integrating AAC into modern multi-story building construction systems with assured seismic safety in the regions with pronounced seismicity.

1.2 Background and Related Work

Some of the most significant recent studies are briefly summarized to demonstrate high interest in this specific research field. For example, comprehensive overview of the long development history of the autoclaved aerated concrete (AAC) material was given in literature by many authors, since its invention in Sweden in the 1920s [1]. Boggelen outlines the material’s inception as a solution to address both housing shortages and the demand for energy-efficient materials. AAC gained popularity for its favorable lightweight features, isolation capability and fire-resistant properties, is becoming today widely adopted across Europe and other regions for its sustainable building benefits. The unique properties of AAC elements, such as their thermal insulation, fire resistance, and lightweight structure, making them ideal for modern construction was highlighted in respective study [2]. The authors emphasize the importance of AAC in energy-efficient building systems and explore recent technological advancements that have improved its production and performance. This research underscores AAC's role in sustainable construction, especially for regions focused on reducing energy consumption in buildings. The technical document presented by Xella Group [3] presents the Ytong Modular Building System as an advanced approach to housing construction using AAC elements. The system offers solutions for fast, energy-efficient, and cost-effective housing, particularly in

areas where sustainable construction is a priority. The guide elaborates on how Ytong blocks contribute to energy savings and quick installation, making them suitable for a wide range of building applications. This construction guide [4] discusses the YTONG building materials and their application in construction systems. It covers the advantages of Ytong materials, such as thermal and acoustic insulation, fire resistance, and lightweight properties, which are key to modern, sustainable architecture. The guide provides detailed instructions on how to use Ytong blocks efficiently in various types of construction projects. Gökmen's thesis [5] focuses on the seismic performance of buildings constructed with reinforced AAC vertical panels. The study explores how AAC panels, reinforced with steel, behave under cyclic loading and earthquake conditions, evaluating their ability to withstand lateral forces. The findings highlight the nonlinear behavior of AAC panels, noting that while they improve a building's stiffness, they are prone to cracking under high-magnitude seismic loads. Gökmen's work provides critical insights into the use of AAC in seismic design and suggests improvements in reinforcement techniques to enhance the ductility and energy dissipation capacity of AAC-infilled buildings. Brightman's thesis [6] presents an early study into the shear capacity of AAC as a structural material, specifically focusing on shear wall specimens. The study details the development of a test setup to evaluate the performance of AAC shear walls under lateral forces typical of seismic events. The research provides preliminary results on the failure modes of AAC, showing that AAC shear walls demonstrate initial stiffness but suffer from brittle failure once cracking initiates. Brightman's work laid the groundwork for further investigations into the seismic behavior of AAC, particularly its use in shear wall systems. A recent study by Löfman and Molander [7], KTH Royal Institute of Technology examines the structural performance of reinforced AAC under seismic conditions. Löfman and Molander investigate how reinforcement improves the load-bearing capacity and ductility of AAC structures, focusing on cyclic tests to simulate seismic forces. Their research shows that proper reinforcement can significantly enhance the seismic resilience of AAC, reducing cracking and improving energy dissipation. The study contributes to the development of design guidelines for the use of AAC in seismically active regions, providing valuable data for future code improvements. Soulis' research [8] investigates the seismic performance of both single and three-story reinforced concrete (RC) frames with masonry infill using nonlinear numerical models. The study focuses on the infill-frame interaction during seismic events and how this affects the overall lateral stiffness and strength of the structure. The findings reveal that masonry infills contribute significantly to the initial stiffness of the RC frame but undergo rapid degradation after cracking begins. Soulis highlights the importance of incorporating nonlinear behavior into design models to accurately predict the seismic response of masonry-infilled structures. The work of Yu at al. [9] provides a numerical analysis of RC frames with infill panels subjected to progressive collapse triggered by seismic events. The authors simulate the dynamic behavior of infilled RC frames and study how local failures in the structure (e.g., column loss) can lead to a cascade of failures under seismic loading. The study shows that infill walls can significantly alter the failure of mechanisms, acting as secondary support but also increasing stiffness and potential brittleness, which requires careful consideration in seismic design. Specifically targeted study by Gaudio et al. [10] proposes a simplified analytical method for predicting seismic losses in masonry-infilled RC buildings. Del Gaudio et al. developed the

model to estimate structural damage and economic losses after seismic events, considering the effects of infill materials on overall building performance. Their findings demonstrate that while masonry infills can improve lateral load resistance, they also increase vulnerability to certain types of damage, leading to higher repair costs after earthquakes. The study emphasizes the need for cost-effective design strategies to reduce post-seismic recovery expenses. Hashemi et al. [11] conducted detailed investigation of the collapse mechanisms of RC columns in infilled frame structures under multi-axis hybrid simulation. Their research examines how combined vertical and horizontal loading affects RC columns and the surrounding infill materials. The study reveals that nonlinear interactions between the columns and infill panels can accelerate column failure under seismic conditions, highlighting the need for advanced simulation methods to predict collapse in infilled RC buildings. This comprehensive report by NZSEE [12] provides guidelines for the design and construction of moment-resisting RC frames with infill panels in regions with high seismic hazard. It emphasizes the importance of accounting for the nonlinear response of infill materials during earthquakes and provides recommendations for enhancing the ductility and seismic performance of infilled frames. The guidelines serve as a framework for engineers to improve the safety and resilience of infilled structures in earthquake-prone areas. Detailed experimental investigation of mechanical properties of autoclaved aerated concrete (AAC) masonry as conducted by Bhosale et al. [13]. The authors explore the compressive strength, shear capacity, and failure modes of AAC under various loading conditions. The study highlights AAC's lightweight nature and thermal properties, making it suitable for sustainable construction. However, the results show that while AAC masonry offers initial stiffness, it exhibits brittle failure after reaching its maximum load, emphasizing the need for reinforcement when used in seismic zones. Tomaževič and Gams' research [14] focuses on the seismic performance of confined AAC masonry buildings using shaking table tests. Their findings reveal that confined AAC masonry improves the seismic resilience of structures by reducing cracking and increasing energy dissipation. The study includes numerical modelling to simulate the behavior of these buildings under various seismic intensities. Results suggest that confined AAC masonry performs better than unreinforced AAC in absorbing seismic energy, making it a viable option for buildings in high-seismicity areas. The recent paper by Filippou et al. [15] presents the finite element model (FEM) for simulating the seismic behavior of masonry-infilled RC frames, including AAC infills. They develop a detailed numerical simulation to capture the nonlinear behavior of infill panels and their interaction with the RC frame during seismic events. The model accurately predicts cracking patterns, stiffness degradation, and shear failure, making it a valuable tool for understanding the behavior of AAC infills under earthquake loads. The study demonstrates that AAC infills contribute significantly to the lateral load resistance of RC frames but are prone to early cracking under high cyclic loading.

Ding et al. [16] investigates the hysteretic behavior of a new autoclaved lightweight concrete (ALC) external panel connector system designed for steel frames. Their study focuses on the energy dissipation capacity and ductility of the new ALC connectors, aiming to enhance the seismic performance of steel-framed buildings. The findings show that the proposed connector design improves seismic resilience, particularly in reducing panel displacement and preventing

connector failure under cyclic loading, offering a potential solution for improving AAC panels' connection to steel structures in seismic zones.

Markulak et al. [17] conducted cyclic tests on single bay steel frames with different types of masonry infill, including AAC, to evaluate their seismic performance. The study demonstrates that AAC infills increase the initial stiffness of the frame, but suffer from early stiffness degradation after cracking. The findings highlight the importance of considering infill-frame interaction and the need for reinforcing AAC to improve its seismic resilience. The results provide insights for improving seismic design codes that address AAC-infilled steel frames. The possible use of AAC as a strengthening solution for existing RC buildings in seismic regions was experimentally studied by Okasha et al. [18]. The authors propose adding AAC infill walls to enhance lateral stiffness and improve the seismic resistance of aging RC structures. Experimental results show that AAC infills increase the building's load-bearing capacity while reducing drift during seismic events. The paper provides practical retrofitting solutions for engineers to improve the seismic safety of older RC buildings using modern AAC infill techniques. Mollaei et al. [19] have studied behavior of AAC elements under blast loading, representing an extreme form of lateral force that shares characteristics with seismic loading. The findings reveal that AAC elements, while effective at absorbing low-magnitude shocks, undergo significant deformation under high blast pressures. The study emphasizes the importance of reinforcing AAC structures in high-risk environments, suggesting potential improvements in design methodologies for using AAC in both seismic and blast-resistant buildings. A recent study by Cardinale et al. [20] resulted in development of bio-aerated autoclaved concrete (Bio-AAC) as a more sustainable version of traditional AAC. The research focuses on integrating biodegradable materials into AAC production to reduce the carbon footprint of building materials. The study shows that Bio-AAC retains the lightweight and insulating properties of AAC while offering improved environmental sustainability, making it an ideal candidate for green building projects. A specific study by Huang et al. [21] resulted in proposing the new infill material model for predicting the seismic behavior of masonry-infilled self-centering beam moment frames. Huang et al. use numerical simulations to analyze how the new material model improves the energy dissipation and ductility of self-centering frames under seismic loading. The findings suggest that the new model outperforms traditional materials in minimizing residual deformations after an earthquake, offering a promising solution for seismic-prone regions. The recent research by Xiong [22] proposes a simplified model for studying the behavior of AAC masonry infilled frames with basalt fiber grating strips. The study describes how these fiber-reinforced connections improve the flexibility and seismic resilience of AAC-infilled RC frames. Results show that the use of basalt fiber strips significantly reduces crack propagation and improves energy dissipation under seismic loading. Comprehensive seismic performance assessment of AAC masonry buildings is presented in Costa et al. [23]. They evaluate the lateral load resistance and failure modes of AAC buildings using shake table tests and numerical models. The findings show that AAC masonry buildings can perform well under moderate seismic forces, but require additional reinforcement to prevent catastrophic failures during high-magnitude earthquakes. This most recent study by Li [24] was devoted to study of seismic performance of full-scale AAC panel-

assembled walls using both experimental testing and numerical modelling. The research demonstrates that AAC panels provide good initial stiffness but require reinforcement to prevent early cracking under seismic loading. The findings contribute to the development of design codes for using AAC panels in seismically active regions. Specific and novel research was focused on investigation of seismic performance of self-insulating AAC block walls as presented in Liu [25]. The study introduces use of finite element analysis to simulate the behavior of these walls under seismic forces. The results show that AAC self-insulating elements improve the thermal efficiency of buildings while providing moderate seismic resistance. To improve material modeling specific test methods have been developed and applied by ASTM [26] along with respective material failure criterion by Menetrey [27]. In respective recent studies, various numerical macro and micro models for static and dynamic analysis of masonry-infilled frames have been developed and implemented [28-34]. During the last decade intensive and important innovative research has been conducted mainly focused on development of advanced construction technology [35-38]. "Generally, the current sophisticated analytical studies have been realized implementing the most advanced computer software [41], [43], while for practical purposes respective guides for design and construction have been developed and used [38], [46].

1.3 Motivation for the Study

Although many studies have been conducted in the past devoted to studying the behavior of brick-infilled reinforced concrete (RC) frames under seismic loads, fewer papers made clear reference to satisfactory improvement of the performance with reliable damage reduction and qualitative upgrading of seismic safety of modern multi-story AAC-infilled RC frames. Japanese, Italian, Turkish and American literature further underscores the demand for the novel and specific future research. In many countries, there is a very developed knowledge about the seismic behavior of several types of RC framed construction systems. However, the AAC-infilled RC frame structures are not sufficiently studied and properly advanced to achieve global safety with damage limitation providing their successful practical application in regions characterized with high seismicity.

1.4 Objectives of the Study

The behaviour of AAC-infilled reinforced concrete frames exposed to seismic events with high intensity represents at present very important challenges since solutions of such complex issues are not adequately addressed in the current construction practice including proper technological advancements and qualitative upgrading of the related seismic design codes. By combining the results obtained from the conducted experimental tests with introduced and advanced computational micro-modelling concept, this research offers a deeper understanding of the nonlinear interactions that occur under the induced seismic forces. The findings are filling the critical gap in design practices and provide advanced practical guidelines applicable to enhance structural safety. Moreover, this research aims to influence updates to seismic design standards

by presenting new insights into AAC's performance. As a sustainable material, AAC has significant potential, but its safety in earthquake zones must be rigorously validated, ensuring that environmental benefits do not come at the cost of structural integrity. Scientific contributions achieved along such important goals represented the main stated objectives of the presently realised extensive experimental and analytical investigations.

2 CHAPTER 2 - SEISMIC DAMAGE OF RC FRAMED BUILDINGS WITH AAC INFILL

2.1 Current Trends in Construction

The intensified use of AAC products during the last decade resulted due to the newest successful developments in the field, tracing the scope of the current modern trends in construction. Generally, such trends mainly resulted due to long-term research efforts and innovative developments of novel AAC products with qualitatively improved characteristics.

Today, autoclaved aerated concrete (AAC) material is quite popular in engineering practice. However, its first development steps are dating back to the beginning of the twentieth century [1]. During the existence of this material, its wide and widespread use worldwide has been noticeable. At the same time, considering the permanent upgrading of its physical and mechanical characteristics, the AAC material enjoys the reputation of being also the building material of the future.

- ***Origin of the aerated autoclaved concrete:*** At the very beginning, this material was presented through several patents. For example, in 1880, the German researcher Michaelis patented his innovative steam-curing process. In 1889, the Check researcher Hoffman successfully patented a "method of aerating" concrete by use of carbon dioxide. Then, in 1914, the American researchers Aylsworth and Dyer patented a method in which they used aluminum powder and calcium hydroxide to provide porosity of a cement mass. The development of modern AAC material is the result of the 1920 patent of the Swedish researcher Axel Eriksson. His method is based on the use of a mixture of limestone and ground slate to create an aerated mix. Chemically, the combination of cement, lime, gypsum, finely ground sand and aluminum powder creates a mixture that can expand considerably, leading to the necessary porosity of a material.
  The real breakthrough of the material in the construction industry took place in 1923. The same researcher, architect Axel Eriksson came to the conclusion that a moist foamed mass may undergo a pressurized steam curing process, which is presently known as "autoclaving". In his application for a patent, he stated two most important conclusions, namely: (1) The material is hardened fast thanks to the autoclaving process and (2) there is almost no shrinkage following the steam-curing unlike the ordinary air-curing. Later, it was discovered that it was also possible to use alternative materials such as, for example, pulverized ash instead of lime/cement. In that way, a possibility is given to achieve lower costs by avoiding expensive constituent materials for the binder.
- ***Original commercial production:*** The great success of Eriksson immediately aroused a great interest in commercial production. In 1929, the first big commercial factory to produce artificially made crystallized stone blocks was built. These were suitable for application in construction of different types of structures. At first, the blocks were referred to as "Yxhult", but in 1940, they were renamed "YTONG" because the new

name was easier to pronounce. In 1934, there started to operate a competing factory that produced AAC elements under the commercial name "Siporex" following 1937. In addition, in 1935, Siporex was the first producer of reinforced AAC elements suitable for use as roof and floor structure panels. The extraordinary characteristics of the new material led to the construction of many factories to produce AAC material throughout Europe, out of which 6 were in Sweden.

- ***Present products of AAC material:*** Over the past decades, the technology of production has improved significantly. For example, the production of unreinforced ordinary AAC elements has become increasingly possible worldwide. For these reasons, this construction material has increasingly been applied in the construction industry in many markets. Today, AAC can be considered suitable construction material, an extraordinary temperature isolator, a good sound absorber and attractive decorative material. Presently, it is possible to produce materials with a density of 300 - 800 kg/m^3, with lambda values of 0.08 (thermal conductivity) at a density of 300 kg/m^3. Also, the products are adaptable to the EU standards (EN 771-4 and EN 772-16) which provides a great preciseness of the products. For example, the difference in geometry is less than 1 mm for AAC elements and less than 3 mm for AAC panels. In the course of the entire past period, there have been many great achievements and advancements in the domain of the improvement of technology of production and in the domain of the improving the quality of final products.
- ***Future application of AAC material:*** Since 1990 till now, the development of the AAC materials market has experienced great revolutionary advancements. With the international introduction of the so-called "green policies" and strict regulations in construction, pressure has been exerted upon producers. Increasingly required are more energy-efficient materials, low-density blocks and panels, high product accuracy, high surface quality, etc. The application of the material has increasingly been extended to the construction of residential buildings, commercial buildings, integrated units and industrial structures. In fact, AAC is becoming increasingly the construction material of the future.

2.2 Modern RC Framed Buildings with AAC Infill

For the last two decades, modern RC framed buildings with AAC infill have increasingly been constructed in the region of Southeast Europe. This region is characterized by a quite pronounced seismicity, where in some regions, the buildings are located in zones of the highest intensity (IX), as for example, the Skopje region in the Republic of North Macedonia. Such a tendency has led to the intuitive creation of corresponding structural systems, which has opened up numerous questions to which no adequate answer has been given based on relevant scientific research.

a) Typical framed buildings with AAC infill: Following the analogy of building multi-storey buildings of the type of reinforced concrete frame systems with infill of hollow bricks or

corresponding fired clay blocks, AAC elements of different dimensions and different strength, or generally different physical-mechanical characteristics are being more intensively used as an infill. These AAC elements are more frequently produced in installed new factories for their production. The physical-mechanical characteristics of the applied elements vary a lot and generally depend on the components used of constituent materials and the technology of production itself.

Following the traditional principles of design of RC frame buildings, numerous multi-storey structures have already been constructed. The number of storeys of the structures has continuously increased and buildings with a height of nine or ten storeys have already been constructed in Skopje, Figs. 2.2.1 - 2.2.3. During construction, these structures are visibly different due to the different infill materials used in both external facade and internal partition walls.

However, with the completion of the facade finishing and internal finalization of the walls, the appearance of the buildings is almost identical with the applied brick or clay block infill. Now, comparisons of applied types of infill from the aspect of strong and weak points including also the aspects of the speed of construction and finalization are very much of a current interest.

Figure 2.2.1. Typical building system applied in SE Europe (Skopje): RC frame with AAC infill (RCF-AAC).

Figure 2.2.2. Typical multi-storey RCF-AAC building system with garage at two ground floors.

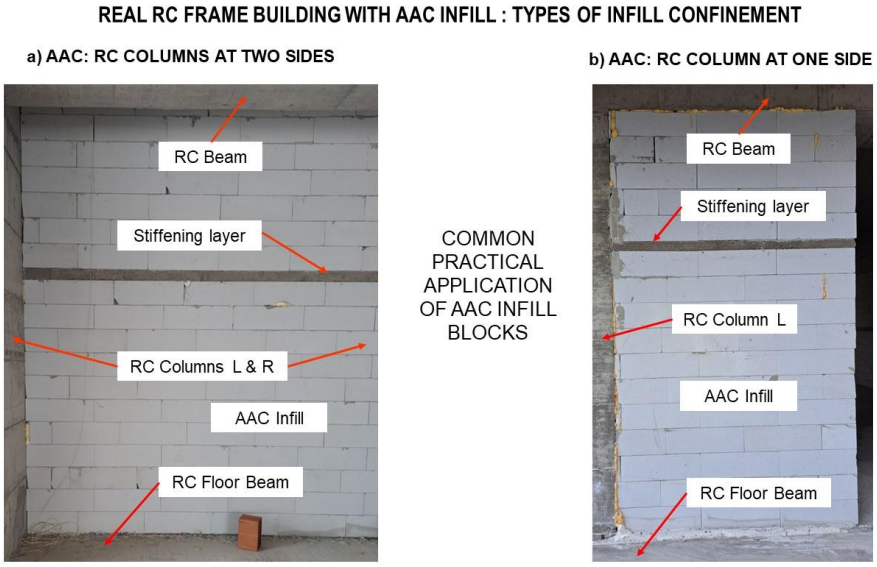

Figure 2.2.3. Indication of different geometry and construction options of AAC infill in RC frame buildings.

To improve the stability of the AAC element infill, reinforced concrete (RC) stiffening layers are sometimes introduced, as illustrated in Fig. 2.2.3. However, their actual contribution to the overall stiffness, strength, and stability of the infilled frame system remains highly debatable. This uncertainty primarily arises from the weak mechanical connection between the stiffening layers and the adjacent RC columns or walls. Several experimental and analytical studies have highlighted this issue, reporting that such stiffening measures often provide only limited

enhancement of the global stiffness and energy dissipation capacity of the system [35-37]. While constructing AAC block infills, the mortar joints are typically of small thickness, and their effectiveness largely depends on the quality and properties of the applied bonding materials.

b) Limited targeted seismic vulnerability assessments: Although numerous experimental and numerical studies have been conducted on RC framed buildings with AAC infill, most of them primarily focus on the mechanical characterization, stiffness degradation, and interaction behavior between the infill and the surrounding RC frame. However, relatively few studies have addressed seismic vulnerability and performance assessment of such systems in a systematic manner. There is still a lack of targeted studies that explore a wider range of parameters including connection detailing, boundary conditions, and infill-frame interaction mechanisms within the context of vulnerability assessment. Further analytical and experimental research is therefore required to better capture the response of these structures under higher-intensity earthquake scenarios.

c) Consideration of ACC infill in design as added mass: Due to the inability to practically include the interactive phenomena between RC frames and AAC infill, in the current design practice, the present AAC infill is simply considered only as an added mass distributed along storeys and their corresponding supporting RC elements in the form of floor slabs or supporting beams.

Accurate modeling of RC frames with AAC infills is not feasible due to limited understanding of their combined nonlinear behavior and specific failure mechanisms. Numerous such research gaps are evident. To provide reliable knowledge, results from performed specifically targeted experimental and analytical research are necessary.

d) Problems with seismically exposed AAC infilled frame buildings: The designed AAC infilled frame buildings in seismic areas are essentially characterized by: (1) an integrated ductile RC frame representing the major supporting system of the building; (2) an integrated non-ductile AAC infill; (3) consequently, this creates a highly complex system of mutual interaction that remains insufficiently explored.

Depending on the mechanical characteristics of the supporting frame system and the specific mechanical characteristics of the AAC infill that vary in a very wide range, the potential conditions for many different types of critical failure modes are proposed. The most common variations of the critical failure modes of AAC infill can be classified into several distinctive groups: (1) Diagonal cracks ranging from fine to major (failure) cracks; (2) Local failure cracks in the activated frame corner regions; (3) Failure cracks in the AAC contact regions; (4) Failure cracks expressing horizontal multi-layer sliding; (5) Random distribution of fine and major cracks; and (6) Fracture due to complex interactive degrading combinations.

(e) Objectives of the present research: Considering the complex nature of possible damage to AAC infilled frame buildings located in seismic regions, there have arisen the principal and dominant objectives of the considered investigations:

- Realization of experimental investigation of the nonlinear behavior of prototype models of RC frames without and with AAC infill. The results from these specific experimental investigations are expected to provide valuable insights into the behavior, failure mechanisms, stiffness and strength degradation, and interaction processes of the tested RC frames with AAC infill. These findings will serve as a basis for understanding the key factors influencing the seismic performance of such systems and, at the same time, will create the necessary conditions for the successful formulation of efficient nonlinear micro-models applicable for simulation of their overall nonlinear response. Experimental investigation of the nonlinear behavior of prototype models of RC frames without and with AAC infill should provide valuable insights into the structural behavior, failure mechanisms, stiffness and strength degradation, and overall seismic performance of such systems. The results of this study will also serve as a basis for the formulation of efficient nonlinear micro-models applicable to the simulation of their nonlinear response.
- Development and experimental validation of nonlinear simplified-micro models suitable for general application.
- Development of practical approaches for incorporating AAC infill calculations in structural analysis projects
- This work introduces a practical method for including AAC infills in structural calculations, enabling a more evaluation of stiffness, strength, and seismic performance of RC frame buildings. The proposed approach directly improves the safety assessment and design reliability of such structures, establishing a clear connection between analytical modeling and real structural behavior. In this way, the thesis provides a practical contribution toward developing more consistent design recommendations for AAC infilled RC frames.

2.3 Typical failure mechanisms

To appropriately understand the complex nature of the induced nonlinear seismic response of various building structures and structural components, the typical failure mechanisms of seismic damage are classified into five specific damage categories: (1) Damage to RC frames; (2) Damage to RC framed buildings with brick masonry infill; (3) Damage to RC framed buildings with AAC infill; (4) Damage of brick masonry buildings, and (5) Damage of AAC buildings.

2.3.1 Damage to RC Frames

The bearing reinforced concrete frame structures should be adequately designed to avoid failure under expected seismic effects. For the strongest seismic effects, the valid design

regulations anticipate that these structures could exhibit nonlinear behavior. However, with the provided satisfying ductility of the columns and the beams, the damage incurred should remain in the frames of repairable damage categories, while the structure should not experience total failure.

Nevertheless, in real practice we have witnessed heavy damage to bearing frame structures, occurrence of irreparable damage, or even total failure of these systems during strong earthquakes.
Such failures have been consistently observed in both experimental investigations and post-earthquake assessments, where reinforced concrete columns and beam-column joints exhibited severe cracking, crushing, and shear failure due to insufficient strength and ductility (Fig. 2.3.1).

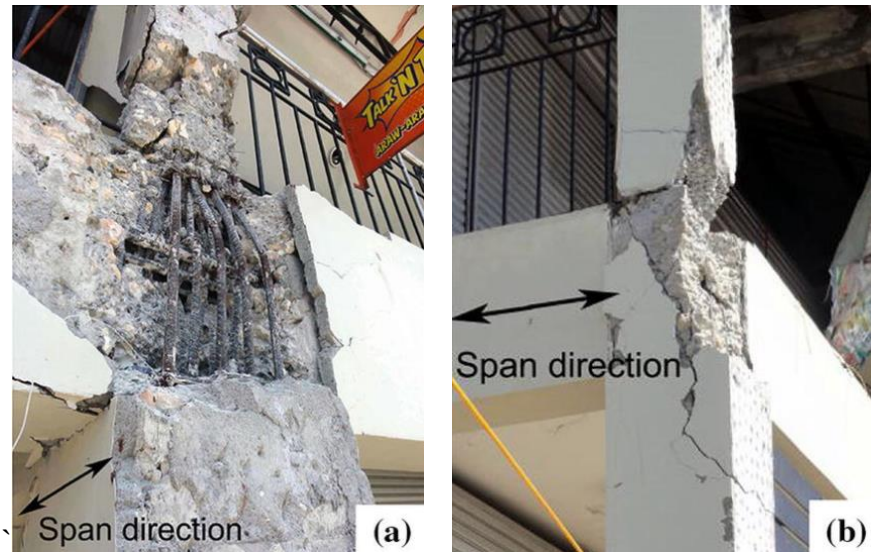

Figure 2.3.1. Beam-column joint damage in RC frame; crushing and spalling due to insufficient shear capacity. Source: Brzev et al., 2017 [61].

Collapse-type damage in RC frames has been reported in several studies, confirming the vulnerability of these structures under multi-directional seismic actions (Fig. 2.3.2) [11, 53, 54, 59]. These results are in full agreement with the seismic assessment provisions prescribed by Eurocode 8, Part 3 [59], which underline the need for detailed modelling of inelastic behavior and proper evaluation of local and global damage mechanisms in RC frame structures.

Figure 2.3.2. Partial collapse of RC framed building after strong earthquake; typical soft-storey failure. Source: Dogan et al., 2024, [67].

According to Hashemi et al. (2017), the collapse of RC columns can occur through combined axial and lateral deformation mechanisms when ductility capacity is exceeded (Fig. 2.3.3), while similar findings have been emphasized by Dolšek & Fajfar (2002) and Stavridis & Shing (2010) through nonlinear analytical and pseudo-dynamic tests on masonry-infilled frames.

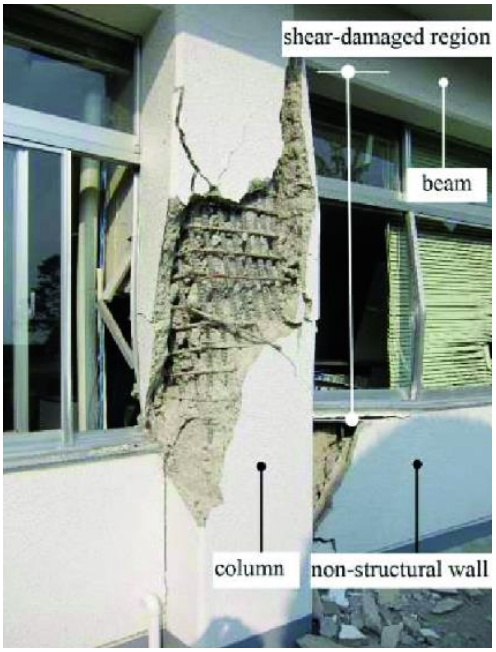

Figure 2.3.3. Shear-damaged RC column with crushed concrete core and exposed reinforcement after seismic loading. Source: Kumamoto Earthquake, Japan, [66].

The heaviest damage occurs in columns of high ground floors or other critical locations due to insufficient strength and ductility of these structures. During the construction of buildings located in seismic regions, it is essential to ensure that the seismic safety of RC frame systems is adequately addressed through proper design and detailing in accordance with current seismic codes. In addition to providing high quality design procedures, it is very important to make an adequate reliable assessment of the expected intensity of seismic effects on the considered location.

2.3.2 Damage to RC Framed Buildings with Brick Masonry Infill

Different seismic regions worldwide are characterized by mass construction of RC framed buildings with brick masonry infill, Fig. 2.3.4 and Fig. 2.3.5. The quality of design and construction of structures depends on numerous factors that are partially of pure technical nature or, quite often, of combined technical and economic nature.

Figure 2.3.4. Example of frame building with brick masonry infill in India (photo credit: S. Brzev, EERI 2012) [61].

Figure 2.3.5. Typical example of an RC frame building with clay hollow block masonry infill, representative of common construction practice in South-East European countries.

If the problems related to insufficient seismic protection of the buildings are of technical nature, it is necessary to anticipate corresponding conditions and measures that will lead to improvement of the quality of design. This includes improvement of seismic regulations, providing of corresponding technical training for the engaged design staff, improvement of the norms for obligatory verification of the construction materials as well as improvement of the methods and procedures of high-quality construction.

Figure 2.3.6. Observed seismic damage of traditional RC frame building with masonry infill.

However, if the problems of insufficient seismic protection of structures are dominantly of economic nature, it is necessary to take corresponding effective measures. The most important would be to enable construction of structures at much lower costs, but the construction systems should be adequately adapted to provide satisfying seismic protection. In both cases, the solution to the complex problems of seismic protection should be based on corresponding scientific knowledge and developed corresponding methodologies of design and construction.

For example, on Fig. 2.3.6, earthquake excitation induces different types of complex damage in the traditional reinforced concrete frame building with masonry infill. Several failure modes can be clearly identified. The most evident is the out-of-plane failure of the masonry infill walls, where the blocks have detached and fallen outward due to insufficient anchorage to the surrounding RC frame [67]. In addition, in-plane diagonal cracking and shear failure of the infill panels are observed, indicating excessive horizontal deformation demand [53], [54]. The partial collapse of infill walls between floors suggests poor bond and lack of proper confinement at the wall-frame interfaces [59]. Moreover, the beam-column joints and column ends show signs of crushing and spalling, typical of insufficient ductility and poor detailing in seismic zones [61]. These failure mechanisms confirm that both structural (RC frame) and non-structural (infill masonry) components play a significant role in the global seismic response. Therefore, the design methods and applied construction technologies must ensure adequate connections between infill and frame, sufficient ductility of RC members, and appropriate stiffness balance to avoid concentration of damage in specific stories or elements. For different infill types constructed with various geometrical and mechanical properties, the design should provide optimal technical conditions for their effective seismic protection.

2.3.3 Damage to RC Framed Buildings with AAC Infill

Like frame structures with clay brick or hollow block infill, reinforced concrete (RC) framed buildings with autoclaved aerated concrete (AAC) infill exhibit a combined interaction between ductile and flexible RC frame elements and brittle, non-ductile AAC infill walls. This interaction results in a complex system response during strong ground motion, where stiffness and strength incompatibilities often lead to severe local and global damage mechanisms.

Under moderate to strong seismic excitations, several characteristic failure modes are typically observed in such systems. The main in-plane failure mechanisms of infilled RC frames under lateral loading are schematically illustrated in Fig. 2.3.7 [69]. These include sliding shear along horizontal joints, corner crushing in compression zones, diagonal cracking through the infill panel, formation of plastic hinges in columns, and column shear failure. Such mechanisms represent the progressive sequence of damage, starting from minor diagonal tension cracks to more severe crushing, sliding, and eventual loss of load-bearing capacity.

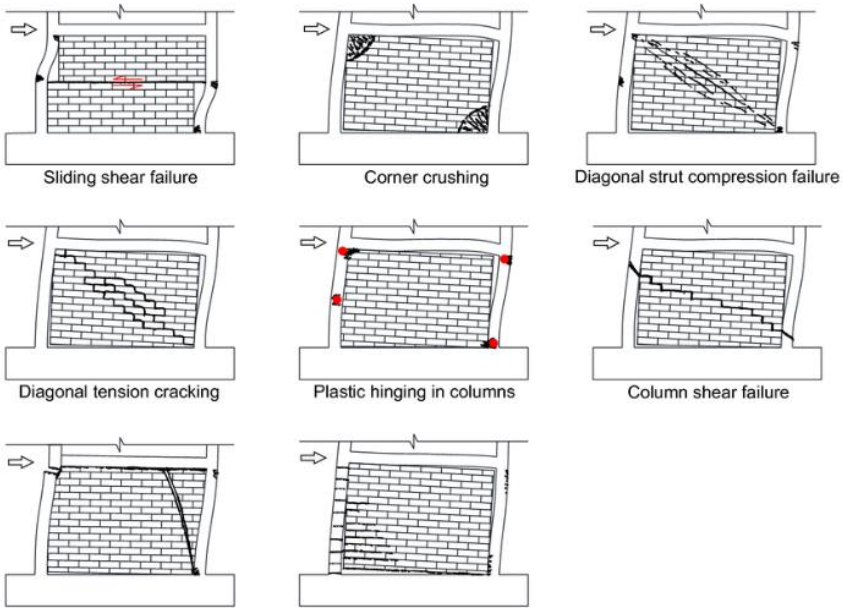

Figure 2.3.7. Typical in-plane damage mechanisms in infilled RC frames [69].

Another frequent mode is the out of plane failure, where the infill walls detach and collapse outward due to insufficient anchorage to the RC frame. This occurs because AAC infills, lightweight and of low cohesion, have weak connection with surrounding beams and columns. In some cases, sliding shear failure along the horizontal mortar joints develops when poor adhesion or thin adhesive layers are used, leading to progressive separation of AAC courses [24], [26].

Infilled walls with openings tend to exhibit local crushing around lintel regions and corner separation near the beam-column joints, where stress concentrations are the highest. When the stiffness contrast between the infill and the surrounding frame is significant, soft-storey

mechanisms may appear, characterized by concentrated inter-storey drifts and partial collapse of infills at the lower levels [10], [53], [54].

Experimental and numerical studies confirm these behaviors. Costa et al. (2008) [24] and Liu et al. (2020) [26] reported that AAC walls, despite their low density and energy-absorbing properties, suffer rapid degradation once diagonal cracking initiates. Dolšek & Fajfar (2002) [53] and Stavridis & Shing (2010) [54] demonstrated through pseudo-dynamic and nonlinear FE analyses that interaction between infill and RC frame significantly modifies the global stiffness and energy dissipation capacity of the structure. Furthermore, Del Gaudio et al. (2021) [10] highlighted that damage patterns in infilled RC buildings often transition from local cracking to partial collapse, depending on the type of bonding and detailing at frame-infill interfaces.

Due to these complex interaction effects between RC frames and AAC infills, detailed experimental investigations and nonlinear micro-modelling approaches are required to capture the combined behavior. Verification of the analytical models through experimental calibration enables reliable prediction of both local failure mechanisms and global seismic performance, as emphasized by Hashemi et al. (2017) [11] and consistent with the principles of Eurocode 8, Part 3 [59].

2.3.4 Damage of Brick Masonry Buildings

Brick masonry buildings represent one of the most widely spread construction systems worldwide. Their load-bearing capacity relies solely on the strength and integrity of masonry walls, without the contribution of an additional reinforced concrete or steel frame. This makes them particularly vulnerable to seismic actions, since masonry is a brittle material with limited tensile and shear resistance.

During earthquakes, two principal categories of failure mechanisms are typically observed: in-plane and out-of-plane failure modes. The in-plane failure of masonry walls occurs when the seismic action acts parallel to the wall's plane, inducing shear and bending stresses. Depending on the level of horizontal force and the material properties, several sub-mechanisms can develop: (1) diagonal shear cracking, forming an "X-shaped" crack pattern due to tensile stress exceeding the low tensile capacity of mortar joints; (2) sliding shear failure, when poor bonding or weak mortar causes horizontal displacement along bed joints; (3) toe crushing or rocking failure, where the wall rotates around its base corners due to overturning moments and insufficient vertical confinement; and (4) flexural cracking, which develops in tension zones at the wall edges. The most typical in-plane failure mechanisms of brick masonry walls are schematically illustrated in Fig. 2.3.8 [14], [15], [29], [70].

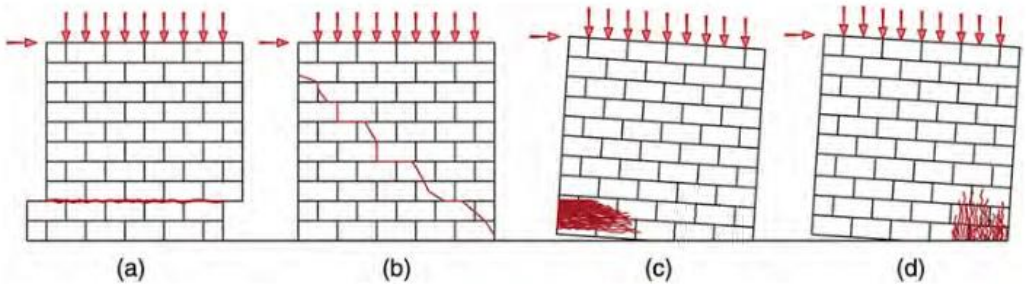

Figure2.3.8. Typical in-plane failure mechanisms of brick masonry walls, [70].

These mechanisms usually lead to degradation of lateral load-bearing capacity and, in advanced stages, to partial collapse of wall piers and spandrels.

The out-of-plane failure mechanism develops when inertial forces perpendicular to the wall plane causes the wall to bulge or overturn. This occurs particularly in walls insufficiently tied to orthogonal walls, floors, or roof diaphragms.

Once the flexural strength or anchorage capacity is exceeded, the wall separates and collapses outward, which can lead to severe life-safety hazards. This type of failure is especially common in upper stories, parapets, or façade walls not adequately connected to the diaphragms.

Experimental studies such as those by Tomaževič and Gams (2012) [14], Lourenço (1996) [15], and D'Altri et al. (2020) [29] confirm that the failure mode of masonry structures depends strongly on the material composition (brick or stone), quality of mortar, wall slenderness, and boundary conditions. Analytical and numerical models of masonry walls developed by Furtado et al. (2016) [33] and Dolšek & Fajfar (2002) [53] further demonstrate that out-of-plane instability can interact with in-plane deformation, resulting in combined failure mechanisms.

The seismic provisions of Eurocode 8, Part 3 [59] emphasize that for unreinforced masonry structures, both in-plane shear and out-of-plane flexural failure modes should be explicitly considered in vulnerability assessment, and proper connection detailing between intersecting walls and diaphragms is crucial to mitigate out-of-plane collapse. A positive example of a built monumental masonry structure is Louis Kahn Plaza in India, which represents a completely stable brick masonry structure, Fig. 2.3.9.

Figure 2.3.9. Example of brick masonry building: Louis Kahn Plaza in Ahmedabad, India.

Figure 2.3.10. Example of traditional adobe masonry building: Governor's photo archives (photograph courtesy 1912), New Mexico History Museum, Santa Fe, New Mexico.

Brick masonry structures may also be built of local cheap traditional materials that provide conditions for their long-term use. An example is the New Mexico History Museum built in the city of Santa Fe in 1912, Fig. 2.3.10. The structure is built as a traditional adobe building and has been in use for more than 100 years since it has been appropriately protected by adequate maintenance measures.

Figure 2.3.11. Illustrated seismic damage of traditional masonry building.

As illustrated in Fig. 2.3.11, total collapse represents the most severe form of seismic damage in traditional masonry buildings, typically resulting from the loss of wall integrity and lack of proper connections between orthogonal walls, floors, and roofs. However, masonry structures can also experience a variety of other failure modes depending on material quality, construction technique, and ground motion intensity.

Common in-plane failure modes include diagonal shear cracking, forming characteristic “X”-shaped cracks due to tensile stresses exceeding the mortar bond strength, and sliding shear failure, which occurs along horizontal mortar joints in walls with weak bonding. In some cases, toe crushing and rocking mechanisms develop when walls rotate about their base corners under lateral forces.

In contrast, out-of-plane failures occur when seismic inertia forces act perpendicular to the wall plane, causing the wall to bulge, separate, or overturn outward. These failures are often observed in facades, gable walls, and parapets that are insufficiently tied to the transverse walls or roof diaphragms.

The collapse observed in this case (Fig. 2.3.11) likely results from a combination of out-of-plane wall instability and in-plane shear cracking, leading to a complete loss of load-bearing capacity. Similar behavior has been reported in past earthquakes affecting unreinforced masonry buildings, where weak mortar, irregular openings, and absence of horizontal ties significantly contributed to the progressive collapse mechanism,[14], [15], [29], [59].

2.3.5 Damage of AAC Masonry Buildings

Using the evident engineering advantages of modern AAC materials such as low density, good thermal insulation, and ease of construction numerous technological advances have led to the realization of AAC masonry buildings. Despite these benefits, the seismic behavior of AAC

masonry remains critical due to its intrinsic brittleness, low tensile strength, and limited ductility compared to traditional brick masonry.

Under seismic excitation, two main categories of damage mechanisms can be observed in AAC masonry walls: in-plane and out-of-plane failure modes.

The in-plane failure modes typically develop when horizontal seismic forces act parallel to the wall plane. The most characteristic response is diagonal cracking, forming through the thin adhesive joints due to the low tensile strength of AAC and brittle nature of its cellular structure. Unlike clay brick masonry, where cracks often follow mortar joints, in AAC walls the cracks frequently propagate through the elements themselves, indicating a homogeneous but fragile failure pattern. In some cases, shear sliding along adhesive joints occurs when the thin-bed mortar loses cohesion, producing a stepped crack pattern. Compressive crushing in the compressed diagonal or at the corners of wall piers is also common when vertical load combines with lateral drift.

The out-of-plane failure modes are mainly governed by the lightweight nature and low flexural capacity of AAC panels. Due to insufficient anchorage to floor and roof diaphragms, infill or load bearing AAC walls may experience out-of-plane bending and detachment, especially in areas with large slenderness ratios (height-to-thickness > 15). Partial collapse can occur when flexural tensile stresses exceed the tensile strength of AAC or when connections between walls and slabs fail. Experimental campaigns by Costa et al. (2008) [24] and Liu et al. (2020) [26] confirmed that poor diaphragm connections and weak horizontal bonding are critical triggers for such failures.

Compared to traditional brick masonry, AAC structures exhibit faster stiffness degradation once cracking initiates, as the porous microstructure limits the redistribution of stresses. Studies by Taha Ali Okasha et al. (2020) [19], Mollaei et al. (2022) [20], and Li et al. (2024) [25] indicate that AAC walls demonstrate a brittle shear response under cyclic loading, with limited residual strength beyond first cracking. Numerical simulations, such as those by Dolšek & Fajfar (2002) [53], further emphasize the need for detailed nonlinear modeling to account for cracking localization and strength softening specific to AAC materials.

Hence, the failure behavior of AAC masonry buildings is governed by the combined effects of material brittleness, adhesive joint performance, wall slenderness, and boundary restraint conditions. Understanding these mechanisms through targeted experiments and refined micro-models is essential to ensure reliable seismic design and safe implementation of modern AAC structural systems.

Examples of AAC masonry structures constructed by application of AAC elements are shown in Fig. 2.3.12 and Fig. 2.3.13.

Figure 2.3.12. Building system based on application of AAC elements (Myanmar, 2017).

Figure 2.3.13. Modular building system based on application of common AAC elements.

Figure 2.3.14. Building system based on application of common AAC panels.

Figure 2.3.15. Confined AAC masonry house constructed in Bovec, Slovenia.

Figure 2.3.16. Example of construction of strengthened AAC elements building.

Figure 2.3.17. Example of construction of strengthened AAC panel building.

Figure 2.3.18. Example of constructed typical multi-storey AAC building.

Figure 2.3.19. Illustrated seismic damage of commonly constructed AAC building.

Figure 2.3.20. Illustrated observed seismic damage of typical AAC building.

To provide successful composing of all constituent segments of a structure, the AAC material products are adequately geometrically adapted for such specific purposes.

In recent years, AAC structures have been increasingly built using a building system based on the application of common AAC panels (Fig. 2.3.12). The main purpose of using such a system is to increase the speed of construction of the structures.

Fig. 2.3.15, Fig. 2.3.16 and Fig. 2.3.17 show characteristic examples of constructed AAC structures with a height of up to 3 storeys. However, such structures are mainly located in regions in which seismic effects are not so pronounced.

To get an insight into the behavior of these structures under seismic effects, it is necessary to perform corresponding investigations with seismic testing of models. The seismic design of the model of the building shown in Fig. 2.3.18 can be stated as a characteristic example. The investigations have shown that such structures possess almost satisfying seismic stability in the case of lower-intensity earthquakes. However, under higher intensities, the systems are susceptible to irreparable and critical damage, as shown in Fig. 2.3.19 and Fig 2.3.20. In AAC masonry buildings, several failure mechanisms may develop depending on the geometry, joint properties, and boundary conditions of the walls.

The most typical damage pattern is in-plane diagonal shear cracking, which forms through the AAC elements themselves because of the material's low tensile strength and brittle cellular structure. Once these cracks initiate, they propagate rapidly across the wall, often intersecting at mid-height and leading to triangular shear wedges. Another frequent failure is sliding along thin adhesive joints, especially in walls built with poor bonding or uneven mortar layers, where relative displacement occurs between element courses. Compressive crushing can also appear at the compressed corners or near openings due to the combined effect of axial load and lateral drift.

In addition to in-plane mechanisms, out of plane failures are commonly observed when the walls are not adequately connected to the floor or roof diaphragms. These include wall detachment, bending-induced cracking, and in some cases partial or complete overturning of slender panels. The lack of confinement and the low flexural capacity of AAC panels contribute to this behavior. Furthermore, corner separation between orthogonal walls and cracking around window and door openings are frequent, indicating stress concentration and inadequate tie behavior.

These mechanisms collectively highlight the brittle seismic response and low energy dissipation capacity of AAC masonry, emphasizing the importance of improved connection detailing and experimental calibration of analytical models. Similar observations were reported by Costa et al. (2008) [24], Okasha et al. (2020) [19], Liu et al. (2020) [26], and Li et al. (2024) [25], who confirmed that AAC buildings, while lightweight and thermally efficient, are particularly vulnerable to both in-plane shear and out-of-plane flexural failures when subjected to strong seismic excitation.

2.4 Need for Seismic Safety Upgrading of RC Framed Buildings with AAC Infill

To use the advantages of the modern AAC material and enable its successful application also in areas with pronounced seismic intensity, it is necessary to perform corresponding experimental and analytical investigations.

Realizing the evident need for scientific knowledge in this domain that will provide considerable improvement of the seismic protection of the structures, the programme of the investigations considered has been conceptualized to reach the following research goals:

1. To enable construction of multi-storey buildings with corresponding seismic protection, application of RC frames in the role of a main load bearing system of the building has been anticipated.
2. To enable intensive application of AAC elements and use all of their realized advantages, application of AAC elements for construction of all facade and interior walls has been anticipated.
3. To get new scientific knowledge on the interactive nonlinear behavior of RC frames with AAC infill, experimental laboratory testing of large-scale models without and with AAC infill has been realized.
4. Using the experimental results, corresponding simplified micro-models have been formulated and verified.
5. The verified simplified micro-models have successfully been applied to provide additional scientific knowledge on the effect of the level of axial loads on the nonlinear behavior of frame structures with AAC infill (parametric analysis).
6. Based on the formulated simplified micro-models, practical calculation models for RC frames with AAC infills have been developed. These models enable engineers to adequately account for infill behavior in the design and construction of buildings requiring seismic protection.

3 CHAPTER 3 - LABORATORY TESTING OF LARGE-SCALE RC FRAME MODELS WITHOUT AND WITH AAC INFILL UNDER CYCLIC AND MONOTONIC LOADING

3.1 Testing of Material Parameters

To develop an accurate understanding of the behavior of structures composed of reinforced concrete (RC) frames and infill walls with AAC (Autoclaved Aerated Concrete) elements, it is essential to determine the basic mechanical parameters of the constituent materials. Parameters such as compressive strength, flexural strength, yield point, and ultimate strength, in addition to serving as a verification of material quality in practice, are also input data for numerical modeling and for the calibration of experimental and parametric analyses.

The laboratory tests were carried out in accordance with the relevant European standards [55], [56], [57], [58], under controlled temperature and humidity conditions, to ensure reliable and comparable results. For each material, specific testing methods were applied, adapted to its nature, to determine characteristic values that are later used in performance-based structural assessment.

3.1.1 Compressive Strength of AAC elements

The compressive strength tests of the autoclaved aerated concrete (AAC) elements were performed in accordance with the requirements of EN 772-1:2011 methods of test for masonry units - Part 1: Determination of compressive strength, which specifies the procedure for preparing, conditioning, loading, and evaluating masonry specimens under compression. The tested specimens were regular-type AAC elements, typically used for non-load-bearing masonry infill in RC frame structures. The mother elements, having nominal dimensions of 600 × 250 × 200 mm, were produced by Ytong and characterized by an average dry density of about 500 kg/m³ and declared thermal conductivity between 0.12 and 0.13 W/mK.

To enable uniform stress distribution and facilitate comparison with reference literature, the elements were cut into cube specimens of 100 × 100 × 100 mm, as prescribed in Annex A of EN 772-1 for the testing of small masonry samples.

The cutting was carried out using a precision diamond-blade saw, ensuring clean surfaces and minimal damage to the porous AAC matrix. The top and bottom faces of each cube were ground and leveled to achieve planarity and smooth contact with the compression plates, in accordance with Clause 7.2.2 of EN 772-1. Before testing, the specimens were conditioned in a controlled laboratory environment at 20 ± 2 °C and relative humidity of 60 ± 5% for at least 48 hours, ensuring moisture equilibrium as required by Clause 7.3 of the standard. The compression tests were performed using a servo-hydraulic universal testing machine with a maximum load capacity of 200 kN.

The specimens were placed centrally between two parallel steel plates, and load was applied continuously and without shock at a constant rate of 0.05 MPa/s, corresponding to the standard's requirement that the time to failure should be between 1 and 2 minutes. The compressive strength ($f_a$cc) of each specimen was calculated as the ratio of the maximum applied load (F_{max}) to the loaded cross-sectional area (A), as per Equation (1) of EN 772-1:

$$f_{acc} = \frac{F_{max}}{A}$$

After testing, the failure patterns and crack propagation were observed. The AAC samples exhibited typical brittle failure modes, characterized by vertical splitting and crushing along the loaded faces, consistent with the cellular microstructure of the material.

The purpose of this test program was to establish the fundamental compressive load-bearing capacity of AAC, which represents a key mechanical parameter influencing the in-plane and out-of-plane behavior of AAC masonry infill within RC frame systems.

Figure 3.1.1 Compressive strength test of AAC elements

The detailed results of the tests are presented in Table 3.1.1, which summarizes the applied loads, calculated compressive strengths, and normalized values for each specimen. Here, "solid strength" denotes Force/Area, while "normalized strength" is the solid strength adjusted by the unit and shape factors.

Table 3.1.1 Compressive strength test of AAC elements

No.	Specimen	Dimensions (mm)	Area (mm^2)	Force (kN)	Solid Strength (MPa)	Unit Factor	Shape Factor	Normalized Strength (MPa)
1	M1	100 × 100 × 100	10 000	25.1	2.5	0.8	1.0	2.0
2	M2	100 × 100 × 100	10 000	26.0	2.6	0.8	1.0	2.1
3	M3	100 × 100 × 100	10 000	26.2	2.6	0.8	1.0	2.1
4	M4	100 × 100 × 100	10 000	26.5	2.7	0.8	1.0	2.1
5	M5	100 × 100 × 100	10 000	28.3	2.8	0.8	1.0	2.3
Mean (μ)					2.64			2.12
Standard deviation (SD)					0.11			0.11
Coefficient of variation (COV %)					4.32 %			5.17 %

3.1.2 Flexural Strength of AAC elements

Since AAC is a brittle material, flexural tests were conducted to determine its indirect tensile capacity. The specimens had dimensions of 500 × 100 × 100 mm and were tested in accordance with EN 772-1, Figure 3.1.2. Each test was performed using a three-point bending setup, where each specimen was placed on two simple supports with a span of 400 mm and loaded monotonically at mid-span under displacement control until failure. The load and mid-span deflection were recorded continuously, and the modulus of rupture (flexural tensile strength) was calculated based on the maximum load at failure using the relation provided in EN 772-1. All specimens were tested under dry conditions at room temperature to minimize moisture influence.

Figure 3.1.2. Flexural strength test of AAC elements

The detailed results of the flexural tests, including the applied loads, specimen dimensions, and the corresponding calculated flexural strengths, are presented in Table 3.1.2. These results provide the necessary parameters for further analytical and numerical modeling of AAC infilled frames.

Table 3.1.2 Flexural strength test of AAC elements

Specimen No.	**Test Date**	**Dimensions (a × b × h) [mm]**	**Span (L) [mm]**	**Area [mm²]**	**Load (F) [kN]**	**Flexural Strength [MPa]**
M1	04/10/2024	500 × 100 × 100	400	50,000	0.8	0.50
M2	04/10/2024	500 × 100 × 100	400	50,000	0.8	0.50
M3	04/10/2024	500 × 100 × 100	400	50,000	0.8	0.40
M4	04/10/2024	500 × 100 × 100	400	50,000	0.7	0.40
Mean (μ)					0.775	0.45
Standard deviation (SD)					0.05	0.05
Coefficient of variation (COV %)					6.45 %	11.1 %

The flexural tensile strength (modulus of rupture) of AAC specimens was calculated according to EN 772-1 using the three-point bending formula:

$$f_{tb} = \frac{3FL}{2bh^2}$$

where:

- f_{tb}= flexural strength (MPa)
- F= maximum load at failure (N)
- L= span between supports (mm)
- b= width of specimen (mm)
- h= height of specimen (mm)

3.1.3 Flexural Testing - Mortar Prism

The mortar used for the AAC infill was a factory-produced thin-bed adhesive mortar of the YTONG TM type, specifically formulated for bonding autoclaved aerated concrete elements. As an industrial dry mix, the internal proportions of the constituents Portland cement as the primary binder, finely graded silica sand as the mineral filler, lime components for improved workability, and polymer additives for enhanced adhesion and reduced shrinkage are predefined and strictly controlled by the manufacturer, ensuring constant quality and

reproducible mechanical performance in every batch. The dry mortar was prepared by gradually adding the prescribed quantity of clean potable water under mechanical stirring until a uniform, cohesive, and lump-free mixture was obtained. After the initial blending, the mixture was allowed to rest briefly and then remixed to achieve the final consistency suitable for thin-layer application (Figure 3.1.3).

The prepared mortar was applied uniformly on all horizontal and vertical contact surfaces between the AAC elements, following the standard YTONG thin-bed construction technique, which ensures minimal joint thickness, high bonding capacity and a homogeneous structural behavior of the infill. During construction and specimen preparation, care was taken to avoid excessive water absorption by the blocks, thus maintaining the intended adhesion performance. After placement, all specimens were stored under controlled laboratory temperature and relative humidity as prescribed in EN 1015-11, ensuring proper hydration of the cementitious binder and stable strength development throughout the 28-day curing period before mechanical testing.

The flexural strength of mortar prisms was examined to determine the bonding capacity and tensile resistance of the mortar used with AAC elements. The specimens were prepared as 40 × 40 mm cross-section beams with a 100 mm span and were tested according to EN 1015-11. The shorter span was adopted to ensure failure within the central third of the specimen and to avoid premature cracking near the supports, as recommended for thin mortar joints. The age of the specimens at testing was 28 days, representing the standard tensile performance of the hardened mortar in accordance with EN 1015-11

Figure 3.1.3 Flexural strength test of Mortar

The examination of the specimens and the corresponding laboratory results, including the fracture load and calculated flexural strength, are presented in Table 3.1.3. These results provide key input for understanding the role of mortar in the overall performance of AAC infill walls.

Table 3.1.3 Flexural strength test of Mortar

Parameter	Unit	M1	M2	M3	Mean (μ)	SD	COV (%)
Cross-Section (b×h)	mm	40×40	40×40	40×40	–	–	–
Span Length (L)	mm	100	100	100	–	–	–
Age of Specimen	days	28	28	28	–	–	–
Unit Weight (ρ)	kg/m³	1780	1780	1780	1780	–	–
Fracture Load (F)	kN	1.18	1.21	1.20	1.20	0.01	1.0
Flexural Strength	MPa	2.76	2.83	2.84	2.81	0.04	1.3
Standard	–				EN 1015-11		

3.1.4 Mortar Strength

The mortar used for bonding the AAC elements was tested according to EN 1015-11. Prisms measuring 40 × 40 × 160 mm were prepared and cured under standard laboratory conditions (20 ± 2 °C and 65 ± 5% RH) until the 28-day test. Each set of six prisms was first tested in three-point bending, and the resulting halves were then tested in compression as 40 × 40 × 40 mm cubes. The loading rates followed EN 1015-11 (≈ 50 ± 10 N/s for bending and 2400 ± 200 N/s for compression). Maximum loads were recorded and converted into flexural and compressive strengths using standard formulas (Figure 3.1.4).

Figure 3.1.4 Compressive strength test of Mortar

This indicates that mortar itself has a limited load-bearing role but is essential as a bonding agent ensuring the integrity of the infill system. The detailed numerical values obtained from the laboratory testing are summarized in Table 3.1.4.

Table 3.1.4 Compressive strength test of Mortar

Parameter	Unit	C1	C2	C3	C4	C5	C6	Mean (μ)	SD	COV (%)
Sample Type	–	CUBE	CUBE	CUBE	CUBE	CUBE	CUBE	–	–	–
Cross-sectional Area (A)	mm²	1600	1600	1600	1600	1600	1600	1600	–	–
Age of Specimen	days	28	28	28	28	28	28	–	–	–
Max Load (Fm)	kN	15.4	16.2	15.9	16.7	16.1	15.8	16.02	0.45	2.8
Compressive Strength (fc)	MPa	9.62	10.12	9.94	10.44	10.06	9.87	10.01	0.28	2.8
Standard	–							EN 1015-11		

3.1.5 Compressive Strength of Concrete

The concrete used for casting the RC frame elements was a normal-weight Portland cement concrete produced in accordance with the specifications provided for structural concrete in EN 206. The mixture consisted of CEM II/A-L 42.5R cement, natural river aggregates with a maximum nominal size of 16 mm, potable mixing water, and standard chemical admixtures for workability retention. The aggregates were combined in appropriate proportions to achieve a well-graded composition suitable for structural elements, while the water-cement ratio was selected to satisfy both strength and workability requirements. All materials were mixed in a rotary drum mixer following the manufacturer's recommended mixing sequence to ensure uniformity and homogeneity of the fresh concrete. After mixing, the concrete was placed into molds in two layers and compacted using a vibrating table to eliminate entrapped air and ensure adequate density. Specimens were demolded after 24 hours and transferred to a controlled curing environment. Curing was performed in water tanks at a constant temperature of 20 ± 2 °C for 28 days, following the requirements of EN 12390-2. Throughout the curing period, the specimens were fully submerged to prevent moisture loss and to allow the concrete to achieve its design hydration and strength development. Concrete specimens were tested in the form of 150 × 150 × 150 mm cubes in accordance with EN 12390-3 (Figure 3.1.5). A total of five cubes were prepared and tested to verify the concrete class used in the RC frame system. Before testing, the unit weight of all specimens was measured, yielding an average density of 2380 kg/m³, consistent with normal-weight structural concrete. Compression testing was performed under load control at a rate of 0.6 ± 0.2 MPa/s until failure, as prescribed by the standard. The compressive strength was calculated by dividing the maximum load by the loaded area. Statistical parameters including mean, standard deviation (SD), and coefficient of variation (COV) were computed to evaluate the consistency and reliability of the concrete strength results.

Figure 3.1.5 Compressive strength of concrete

The detailed numerical values obtained from the laboratory testing:

Table 3.1.5 Compressive strength test of concrete

No.	Specimen	Age (days)	Dimensions (mm)	Mass (g)	Density (kg/m³)	Area (cm²)	Force (kN)	Compressive Strength (MPa)
1	M1	28	150×150×150	7540	2234	225.0	690.1	30.7
2	M2	28	150×150×150	7703	2282	225.0	649.3	28.9
3	M3	28	150×150×150	7862	2329	225.0	804.3	35.7
4	M4	28	150×150×150	7585	2247	225.0	701.5	31.2
5	M5	28	150×150×150	7648	2266	225.0	684.8	30.4
Mean (μ)	–	–	–	7668	2272	–	705.98	31.38
SD	–	–	–	119	36.9	–	54.4	2.48
COV (%)	–	–	–	1.55	1.63	–	7.7	7.9

3.1.6 Mechanical properties of steel reinforcement

Steel reinforcement bars were tested in accordance with EN ISO 6892-1:2019, under room temperature conditions (20 ± 5 °C) using a servo-hydraulic universal testing machine equipped with an electronic extensometer for precise strain measurement (Figure 3.1.6). The tests were carried out on five different diameters Ø6 mm, Ø10 mm, Ø12 mm, Ø16 mm, and Ø18 mm to determine the yield strength ($Rp_{0.2}$), ultimate tensile strength (Rm), strength ratio (Rm/Rp), and elongation at fracture (A%). Each bar was tested under displacement-controlled loading, with a strain rate $\leq 0.002\ s^{-1}$ up to yielding and increased thereafter until rupture, in full compliance with the standard procedure. The force-elongation curves were continuously recorded to capture both the elastic and plastic phases of behaviour. For every diameter, three specimens were tested to ensure representative results. The measured data were processed to obtain mean values, standard deviation (SD), and coefficient of variation (COV) for each mechanical parameter. These results provide a statistically reliable assessment of the steel quality and verify compliance with Eurocode 2 requirements for ductile reinforcing steel used in seismic-resistant RC

Figure 3.1.6 Test of steel reinforcement bars

The detailed results obtained from the tensile tests are presented in the following tables. Table 3.6 summarizes the results for the Ø6 mm reinforcement bars, representing small-diameter steel typically used in secondary structural members and distribution reinforcement. Table 3.1.7 provides the results for the Ø10 mm bars, showing the measured values of yield strength, ultimate strength, strength ratio (Rm/Rp), and elongation. Table 3.1.8 presents the corresponding results for the Ø12 mm bars, which are commonly used as longitudinal reinforcement in beams and columns. Table 3.1.9 contains the results for the Ø16 mm bars, typically serving as primary reinforcement in elements subjected to higher bending and axial loads. Finally, Table 3.1.10 summarizes the results for the Ø18 mm bars, representing the largest diameter tested in the program. Together, these tables provide a comprehensive overview of the mechanical performance of the reinforcing steel used in the experimental investigation. The obtained results confirm that all tested bar diameters satisfy the required strength and ductility criteria, demonstrating their suitability for seismic-resistant reinforced concrete (RC) structures in accordance with EN ISO 6892-1:2019 and Eurocode 2 specifications.

Table 3.1.6 Results for Ø6 mm bars

Specimen	**Gauge L_0 (mm)**	**Total Lt (mm)**	**Yield Strength (N/mm^2)**	**Ultimate Strength (N/mm^2)**	**Rm/Rp**	**Elongation (%)**
M1	30	300	545.0	640.0	1.17	17.0
M2	30	300	552.0	648.5	1.17	16.4
M3	30	300	560.5	653.2	1.17	16.8
Mean (μ)			552.5	647.2	1.17	16.73
SD			7.8	6.7	0.00	0.31
COV (%)			1.4	1.0	0.0	1.8

Table 3.1.7 Results for Ø10 mm bars

Specimen	Gauge L_o (mm)	Total Lt (mm)	Yield Strength (N/mm^2)	Ultimate Strength (N/mm^2)	Rm/Rp	Elongation (%)
M1	50	500	631.5	755.1	1.20	11.20
M2	50	500	609.7	756.6	1.24	10.00
M3	50	500	644.7	747.7	1.16	11.60
Mean (μ)			628.6	753.1	1.20	10.93
SD			17.7	4.8	0.04	0.83
COV (%)			2.8	0.6	3.3	7.6

Table 3.1.8 Results for Ø12 mm bars

Specimen	Gauge L_o (mm)	Total Lt (mm)	Yield Strength (N/mm^2)	Ultimate Strength (N/mm^2)	Rm/Rp	Elongation (%)
M1	60	520	566.0	672.3	1.19	16.00
M2	60	520	587.5	677.6	1.15	14.40
M3	60	520	574.7	662.6	1.15	16.00
Mean (μ)			576.1	670.8	1.16	15.47
SD			10.8	7.6	0.02	0.92
COV (%)			1.9	1.1	2.0	6.0

Table 3.1.9 Results for Ø16 mm bars

Specimen	Gauge L_o (mm)	Total Lt (mm)	Yield Strength (N/mm^2)	Ultimate Strength (N/mm^2)	Rm/Rp	Elongation (%)
M1	80	550	586.2	756.9	1.29	13.60
M2	80	550	635.3	760.3	1.20	14.00
M3	80	550	583.4	757.2	1.30	16.00
Mean (μ)			601.6	758.1	1.26	14.53
SD			29.2	1.9	0.06	1.29
COV (%)			4.9	0.2	4.4	8.8

Table 3.1.10 Results for Ø18 mm bars

Specimen	Gauge L_o (mm)	Total Lt (mm)	Yield Strength (N/mm^2)	Ultimate Strength (N/mm^2)	Rm/Rp	Elongation (%)
M1	90	600	560.0	690.5	1.23	15.0
M2	90	600	573.5	705.3	1.23	15.2
M3	90	600	568.0	698.1	1.23	15.4
Mean (μ)			567.2	698.0	1.23	15.20
SD			6.8	7.4	0.00	0.20
COV (%)			1.2	1.1	0.0	1.3

3.2 Prototype walls testing program

A program for experimental testing of large-scale RC frame models under cyclic and monotonic loading has been realized to derive experimental results needed for this study. This chapter presents the basic concept of the specifically designed large-scale prototype models that were selected and tested. The testing concept harmonized with the objectives of the experimental investigation by aligning the boundary conditions, load configurations, and instrumentation with the predefined research goals, ensuring simulation of the nonlinear behavior of the RC bare frame and RC frame with AAC infill.

The program of experimental studies has been also harmonized with the available experimental conditions in the RESIN Laboratory (part 3.3), applied for realization of the complex experimental tests of the constructed models. In the RESIN laboratory, several necessary conditions were ensured for accurate control of the prescribed quasi-static loading, including stable temperature and humidity, precise displacement control of the loading actuator, synchronized data acquisition, and fixed boundary supports of the tested models. The tests were realized considering a step-by step loading with the predefined respective magnitudes of displacements and forces to enable study of the characteristics of behavior of the tested physical models.

The experimental study involved realization of specific experimental tests of constructed four large-scale physical models of representative RC frame without and with AAC infill. The first two RC bare frame, M1-A and M1-B, were tested respectively under cyclic and monotonic loading. To derive the related comparative results, the second two RC frame models with AAC infill, M2-A and M2-B, were also tested under cyclic and monotonic loading (Table 3.2.1).

Table 3.2.1 Geometrical and loading characteristics of the tested RC frame models

Wall	Length (mm)	Height (mm)	Thickness (mm)	Axial Load (kN)	Load Application
M1-A	2650	1980	–	62.5	Cyclic
M1-B	2650	1980	–	62.5	Monotonic
M2-A	2650	1980	125	62.5	Cyclic
M2-B	2650	1980	125	62.5	Monotonic

The test results provided identification of the main parameters of the real nonlinear behavior of the tested individual models. In addition, the obtained experimental results were of great importance for the realization of the planned extensive analytical study of the seismic performances of the tested specific structural segments and for detailed validation of the developed advanced nonlinear micro-models.

3.3 RESIN Laboratory details

The Regional Seismic Innovation Network Laboratory (ReSIN Laboratory of Industrial science and Technology) located in Skopje, was planned to support PhD research of young scientists from the region. With such objectives, the creation of the ReSIN Lab was initiated. Then, it was established and is currently led by Prof. Danilo Ristic. The created ReSIN Lab represents a well promoted open laboratory, following the successful completion of the international long-term innovative NATO Science for Peace project (2010-2013), Brussels, Belgium, with participation of five different countries.

The planned testing program for experimental laboratory testing of large-scale RC frame models without and with AAC infill under cyclic and monotonic loading has been realized in the recently developed and established RESIN Laboratory testing facility in Skopje integrating a total of 15 principal components, including:

I) A laboratory testing frame (LTF): The laboratory testing frame represents a stiff reinforced concrete structure designed with a specific geometry and other conditions to enable successful installation of test models and testing equipment (Figure 3.3.1). The structure is primarily composed of two identical parallel reinforced concrete frames with external dimensions of length at plan L = 340.0 cm and height h = 330.0 cm. Each frame is composed of a left and a right column with cross-section proportions a/b = 60.0 x 30.0 cm that are mutually connected in the upper zone by a reinforced concrete horizontal beam of the same dimensions. In the lower zone, the reinforced concrete columns are connected by a reinforced concrete base beam with cross-section proportions a/h = 120.0 cm x 40.0 cm, representing the base support for the fixation of the tested experimental models to the laboratory floor. To provide conditions for application of fixation nuts on the lower side, the reinforced concrete base beam was elevated from the floor by 10.0 cm. To enable successful fixation of experimental models and hydraulic actuators, a system of regularly distributed openings formed by metal tubes with external diameter of ∅ 42.0 mm was made in the base RC beam as well as the vertical and horizontal segments of both RC frames. The laboratory testing frame is specifically conceptualized in this way to represent an adaptable independent testing unit that can be transported, mounted and used on any laboratory location according to the needs.

II) Model installation system (MIS): The model installation system consists of a series of important metal elements with appropriate dimensions and different lengths that have corresponding threads and nuts at their ends for fixed fastening (without a gap) of the experimental models in compliance with the expected large forces via the corresponding openings made at suitable locations.

III) Hydraulic Actuators (Vertical and Horizontal): Both the vertical (VHA) and horizontal (HHA) hydraulic actuators are specifically designed for the performance of cyclic experimental tests in the field of earthquake engineering and other advanced structural studies. Each actuator can apply a maximum force of ±300 kN and allows for a piston stroke (maximum displacement) of ±300 mm. These actuators enable the application of controlled cyclic and

monotonic loads in both vertical and horizontal directions, ensuring simulation of seismic loading conditions on structural specimens.

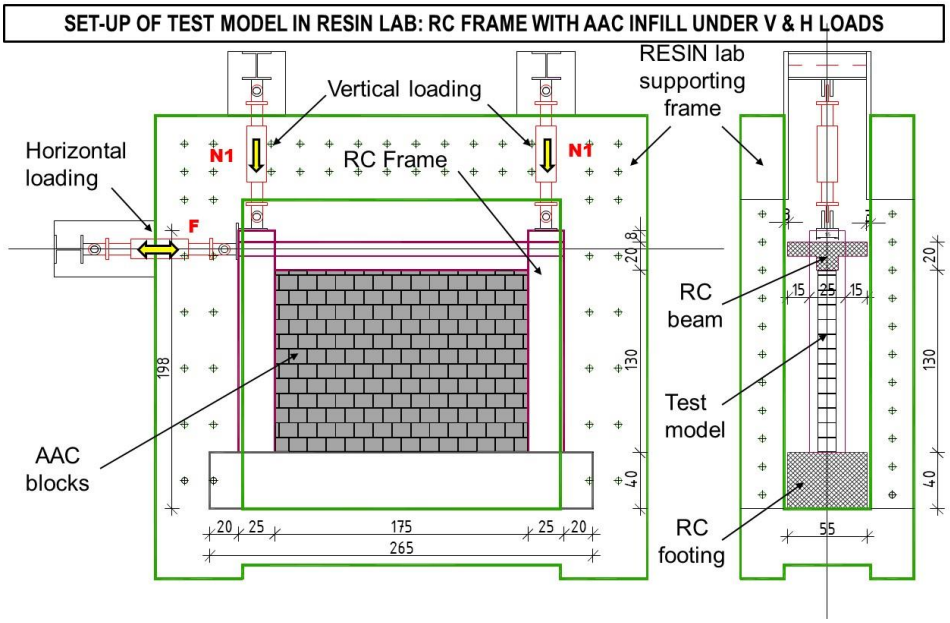

Figure 3.3.1 Set-up of test model in RESIN lab: RC frame with AAC infill under V and H loads.

IV) Connecting support of the vertical hydraulic actuator (CVHA): The connecting support of the vertical hydraulic actuators represents a specific steel structure which is fixed to both rigid RC beams on two sides. At its risen top, the CVHA structure has a specially designed strong supporting hinges at the formed piston rod. The hinge sustains the reaction forces from the vertical actuator. This hinge enables rotation of the vertical piston with eliminated friction, enabling thus the necessary horizontal displacement of the upper part (the top) of the model, which is simultaneously applied during the test, by the horizontal piston.

V) Connecting support of the horizontal hydraulic actuator (CHHA): The used connecting support of the horizontal hydraulic actuator represents a specific two-part steel structure fixed to both left frame columns, while between the two parts, a specially designed strong supporting hinge is formed to continuously sustain the two-sign reaction forces from the horizontal actuator. Also, this hinge enables adequate rotation of the top of the piston in the case of possible small displacements of its front part during the performance of complex simultaneous cyclic tests.

VI) Hydraulic Actuator Oil Source Reservoirs (VASR and HASR): The oil source reservoirs for both the vertical and horizontal actuators are designed as independent hydraulic units, each with sufficient capacity to ensure stable operating conditions of the respective actuator during testing. Their configuration provides continuous oil supply, pressure stability, and efficient cooling, allowing precise control of the hydraulic actuators throughout the cyclic or monotonic experimental procedures.

VII) Actuator Controlling Systems (VACS and HACS): Both the vertical and horizontal actuator systems are managed through dedicated electronic control units integrated with specialized software. These control systems enable real-time monitoring and regulation of key mechanical parameters such as force, displacement, and velocity at each discrete stage of an experimental test. Independent yet synchronized software interfaces are used for both actuators to allow coordinated multi-directional loading, ensuring accuracy, repeatability, and reliability of the applied loading protocols during complex nonlinear testing.

VIII) Instrumentation system (IS): The instrumentation system represents installed electronic measuring devices capable of measuring forces, deformations, strains, etc.

IX) Experiment execution system (EES): The Experiment Execution System (EES) represents a specialized control and data acquisition software developed for managing and automating experimental tests in the RESIN Laboratory. The system enables full control of hydraulic actuators, synchronization of applied loads, and continuous recording of force, displacement, and time histories.

In the RESIN setup, the EES is configured to execute both monotonic and cyclic loading protocols by defining control parameters such as loading amplitude, frequency, number of cycles, and displacement increments. The software interfaces directly with the servo-hydraulic control units and the data acquisition system, allowing real-time feedback between measured and commanded quantities. During testing, all parameters' forces, actuator strokes, displacements, and reaction loads are monitored through high-precision sensors, and the data are logged automatically at a high sampling rate for post-processing and comparison with numerical simulations.

This integrated setup ensures accurate, repeatable, and fully automated execution of experimental tests, eliminating operator influence and improving the reliability of the obtained results.

X) Data acquisition system (DAS): The data acquisition system consisted of a multi-channel electronic unit connected to all displacement transducers and load cells installed on the test model. The system enabled continuous automatic recording of the measured quantities horizontal and vertical loads, displacements, and strains throughout the test. It operated with a sampling frequency of 10 Hz and 16-bit resolution, providing real-time digital conversion and storage of mechanical response data for subsequent processing and analysis.

XI) Test data input port (TDIP): The Test Data Input Port represents the dedicated software module used for defining and importing the complete loading protocol of the experimental test. Through this interface, the sequence of control parameters such as load increments, displacement amplitudes, loading rate, and hold durations was entered and synchronized with the data acquisition and actuator control systems. This ensured precise execution of the prescribed quasi-static cyclic or monotonic loading history according to the predefined testing program.

XII) Laboratory computer (LC): The laboratory computer served as the central unit for actuator control and data acquisition. It operated with dedicated software used for managing cyclic and monotonic loading protocols, recording measured parameters, and storing experimental data. The LC was connected to the servo-hydraulic control system through a digital communication interface, enabling real-time transmission of commands and feedback signals. During testing, all sensor data including load, displacement, and actuator stroke were continuously logged at a fixed sampling frequency to ensure synchronization and precision. The acquired data were stored in structured project files for subsequent processing, visualization, and comparison with numerical simulations.

3.4 Bare frame models specific details

The experimental program was realized to study the behavior and influence of the AAC infill to RC frames effects of the AAC infill in the implemented RC frames.

The experimental program was divided into two phases.

The experimental program within Phase - 1 included an experimental study of the behavior of RC bare frame under vertical and monotonic loads. To provide a comparative insight into the effects of applied horizontal load upon the behavior, testing of two identical models M1-A and M1-B was performed considering different loading patterns.

In the case of the tested model M1-A, in addition to the vertical load, cyclic horizontal loading with a gradually increased amplitude of positive and negative deformations was applied. This experimental test provided an insight into the real hysteretic response of the model and the failure mechanisms upon cyclic load reversals.

In the case of the tested model M1-B, in addition to the vertical load, monotonic loading with gradually increased displacements was applied.

The main design characteristics of the experimental models M1-A and M1-B are presented in part 3.4.1. The experimental testing results for the tested prototype models M1-A and M1-B are presented in parts 3.4.2 and 3.4.3., respectively.

Finally, part 3.4.4 contains a summary of major observations derived from the conducted experimental study within phase-1, based on comparative analysis of the experimental results obtained.

3.4.1 Bare RC frame models M1-A and M1-B

For bare frame models M1-A and M1-B, a large scale (M = 1: 2) was initially adopted. This provided conditions to: (1) achieve the obtaining of highly reliable experimental results and (2) enable the use of identical materials that are also constructed during the construction of real frame systems. The adopted large scale for the construction of experimental models

considerably increases financial expenses. Nevertheless, in this way, increased reliability and representativeness of the experimental results obtained is provided.

- ***Geometry of Models M1-A and M1-B:*** The main geometrical characteristics of the experimental models M1-A and M1-B that represent RC bare frame models are shown in Fig. 3.4.1. The rigid base of the model representing the footing segment was constructed as a reinforced concrete beam with cross-section a/h = 55/40 cm and total length of 265 cm. Fig. 3.9. shows the reinforcement of the footing beam consisting of bars ϕ 16 mm, namely four bars in the lower zone and four bars in the upper zone. The stirrups were constructed of reinforcement ϕ 6 mm and were placed at a distance of e = 15 cm. Both RC columns of the frame structure were constructed with a cross-section 25 x 25 cm and a height of 130 cm, Fig. 3.4.2. The RC columns were reinforced with longitudinal reinforcement consisting of symmetrically placed eight bars with a diameter of 10 mm (8ϕ10). The stirrups were adopted as ϕ6/15 in the middle segments and ϕ6/7.5 cm in the vicinity of the fixation zones. The horizontal RC floor beam was designed in the form of a typical square "T" section 20 x 20 cm having RC floor slab with a thickness of 10 cm.
- ***Construction of Models M1-A and M1-B:*** The construction of models M1-A and M1-B was carried out in a vertical position analogously to the usual construction practice. In doing so, corresponding openings were made for fixation of the model to the experimental laboratory frame and devices were incorporated for the fixation of the corresponding hydraulic actuators.

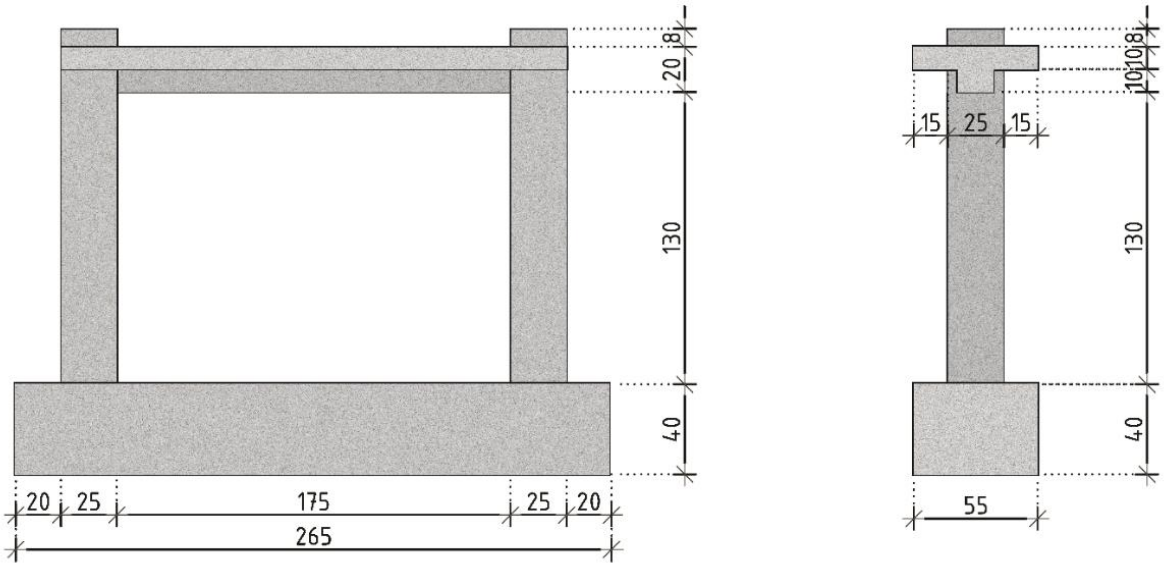

Figure 3.4.1 Geometry of designed and constructed large scale RC frame prototype models (M1-A, M1-B, M2-A, M2-B) tested without and with AAC infill.

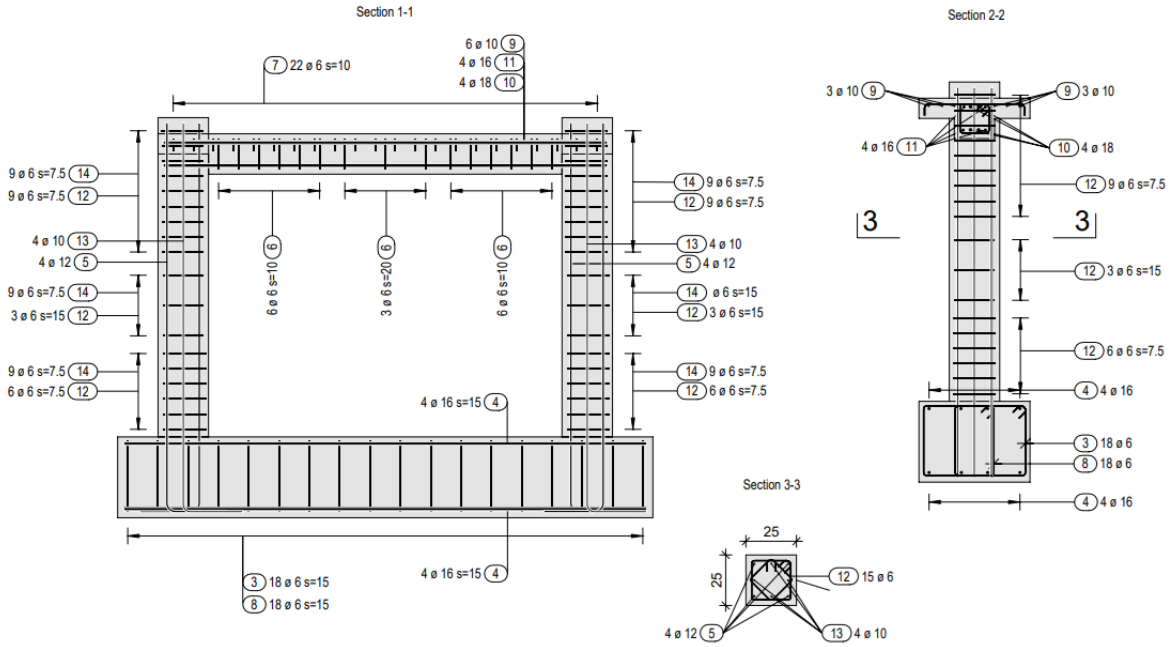

Figure 3.4.2 Reinforcement of designed and constructed bare RC frame prototype models (M1-A, M1-B, M2-A, M2-B) tested without and with AAC infill.

3.4.2 Testing protocol and results for bare frame model M1-A (cyclic loading)

For experimental testing of the bare frame model M1-A, the laboratory testing frame is shown in Fig. 3.4.4. The experimental test was carried out under the effect of vertical and cyclic horizontal loads marked as loading type L11. As shown in Fig. 3.10, the vertical compressive load on both the RC columns was applied with identical intensities N1 = 62.5 kN using two hydraulic actuators. The horizontal cyclic load was applied using a horizontal hydraulic actuator (with push-pull) action located at the level of the RC top beam.

The loading process upon experimental model M1-A is schematically shown on Fig. 3.10. and was realized in two planned phases. In the first phase, vertical load was slowly-incrementally applied with a small incremental gradual increase of the load identically on both RC columns at each successive discrete step.

Following the application of the constant vertical load $N_1 = 62.5$kN on both columns, the testing proceeded with the second phase, consisting of cyclic horizontal loading of the prototype model M1-A. The cyclic loading was performed under displacement control, where the actuator movement was governed by the prescribed sequence of displacement commands rather than by force control. To capture the initiation and propagation of fine cracks in the concrete, very small and precisely adjusted displacement increments were applied. The loading process was executed through successive positive and negative displacement cycles, gradually increasing in amplitude up to the target limits of +19.9 mm and −19.8 mm, thereby reproducing the full quasi-static cyclic loading protocol.

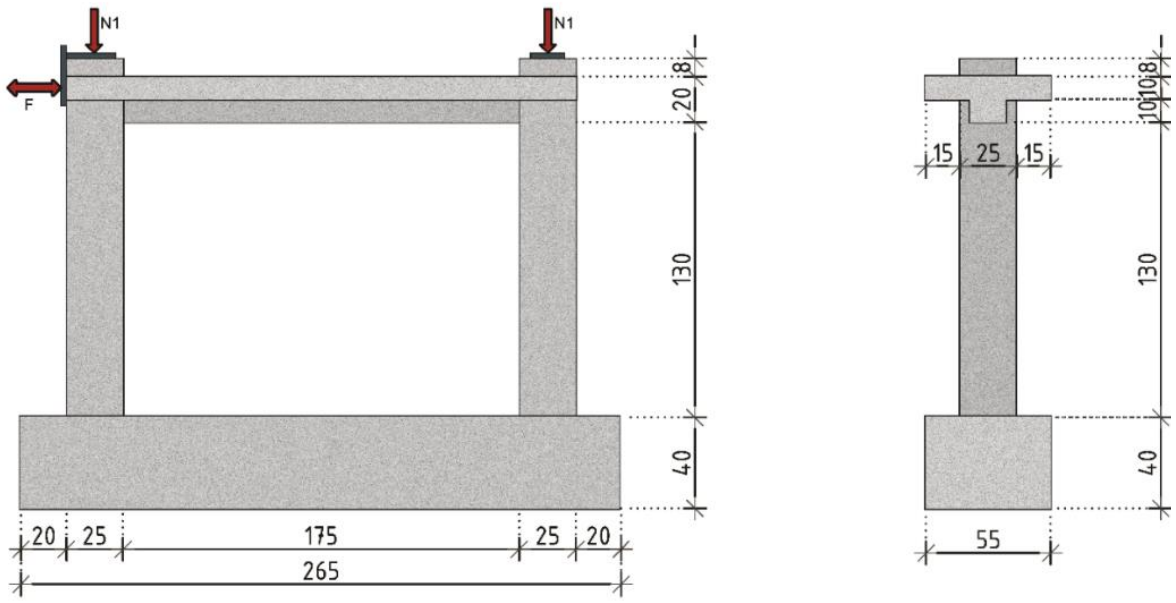

Figure 3.4.4 Bare Frame model M1-A under cyclic loading pattern L11(NL+CL)

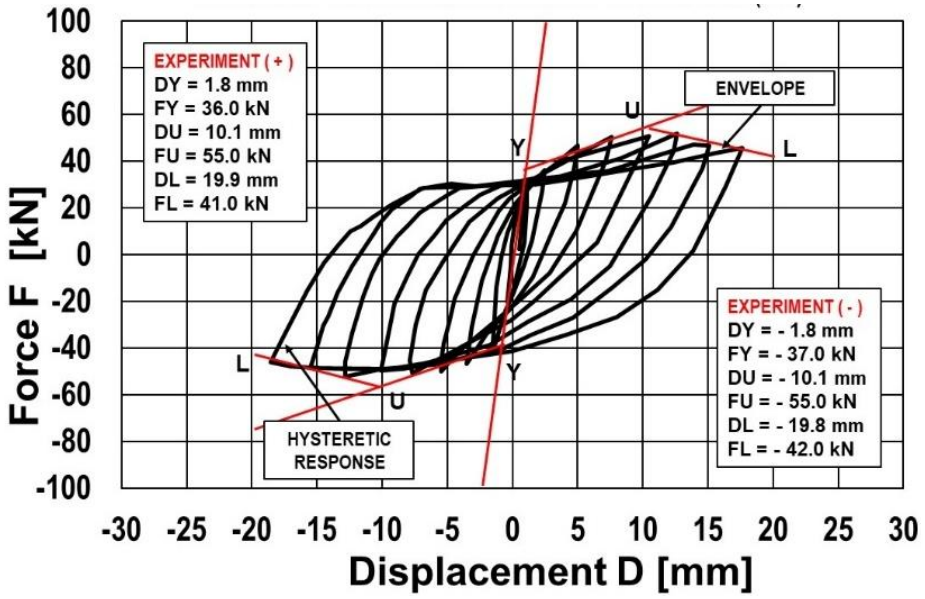

Figure 3.4.5 Bare Frame model M1-A: Response of tested of RC frame under vertical and cyclic load (L11: NL+CL).

Through the applied data acquisition system of the displacements at each step Di (mm) as well as the measured value of the corresponding restoring force Fi (mm), a large set of numerical values was obtained during the entire process of the experimental test.

Using the recorded numerical values of force and deformation, graphic presentation of the hysteretic behavior of the bare frame model M1-A was enabled for quite large range of cyclic deformations, Fig. 3.4.5. The obtained hysteretic relationship very successfully and correctly

represents the cyclic response of the model considering that almost symmetrical hysteretic relationship was obtained in the domain of positive and negative deformations. The resulting hysteretic relationship was used to define the envelope curve on both the positive and negative sides, representing the overall nonlinear response of the tested specimen. To derive the envelope, the peak points of force displacement cycles were identified for each loading direction. These maximum points were connected to form the ascending and descending branches of the envelope, defining the yielding point (Y), the ultimate force point (U), and the point corresponding to the maximum deformation (L). This procedure allowed for a clear visualization of stiffness degradation and strength evolution during cyclic loading. The obtained hysteretic response showed almost symmetrical behavior and confirmed a stable nonlinear performance and satisfactory ductility of the tested prototype model M1-A.

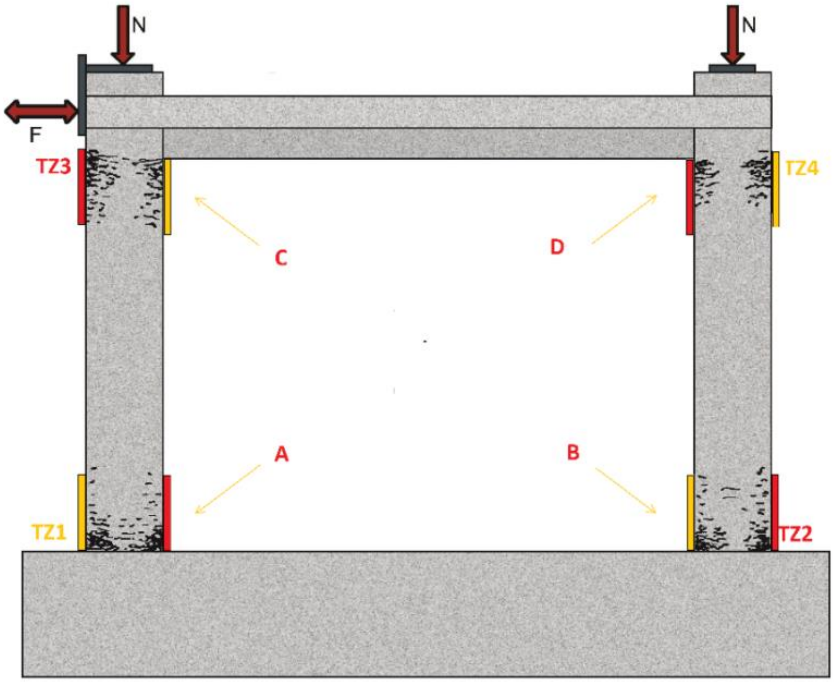

Figure 3.4.6 Bare Frame model M1-A: Recorded crack zones of tested of RC frame under vertical and cyclic load (L11).

During the experimental testing, propagation of cracks in the concrete was continuously monitored at predefined load intervals, Figure 3.4.6. The development of cracks and their progression along critical regions were marked on the specimen surface and correlated with the applied load and displacement values recorded by the data acquisition system. This procedure enabled continuous observation of the cracking pattern and its evolution throughout the loading process. The zones of propagation of cracks, ranging from initial to considerable, are graphically illustrated in Fig. 3.4.6. The recorded localized tension zones (TZ1 through TZ4) for the positive deformations are shown in yellow color, while for the negative deformations they are shown in red near the corners of the RC frame indicated by A, B, C, and D. During the test, several types of cracks were observed, including flexural cracks that initiated near the column bases (zones TZ1 and TZ2) due to bending moments under cyclic horizontal loading, shear cracks that appeared diagonally in the lower parts of the columns and in the joint regions

(zones TZ3 and TZ4) caused by the combined action of vertical and horizontal forces, and interface cracks that formed along the beam-column connections and propagated toward the mid-span, reflecting local separation between the concrete layers. The progression of these cracks became more pronounced in the tension zones on the loaded side, with gradual widening during successive displacement cycles. During testing, three main types of cracks were identified. Flexural cracks were formed at the beam-column joints because of bending moments, while shear cracks developed diagonally near the column ends where shear demand was higher. In addition, localized concrete crushing zones were observed at the base of the columns (TZ1 and TZ2) under compressive loading. The overall crack distribution and the nearly symmetrical formation of tension zones confirm the accuracy and stability of the experimental setup and the symmetric hysteretic behavior of the tested RC frame.

3.4.3 Testing protocol and results for bare frame model M1-B (monotonic loading)

For the experimental testing of the prototype model M1-B, the same laboratory testing frame was used. The experimental test set-up was identical, Fig. 3.3.1. However, in this case, the test was realized under loading type L12, represented with identical vertical load and monotonically increasing horizontal load. The process of loading the bare frame model M1-B was equivalent, and it is schematically presented in Fig 3.4.7. Analogously, in this case, the loading process was also realized in two phases. Provided in the first phase was step-by-step loading with a vertical load in an equivalent way up to the same level of compressive forces in each of both RC columns to the amount of N1 = 62.5 kN each.

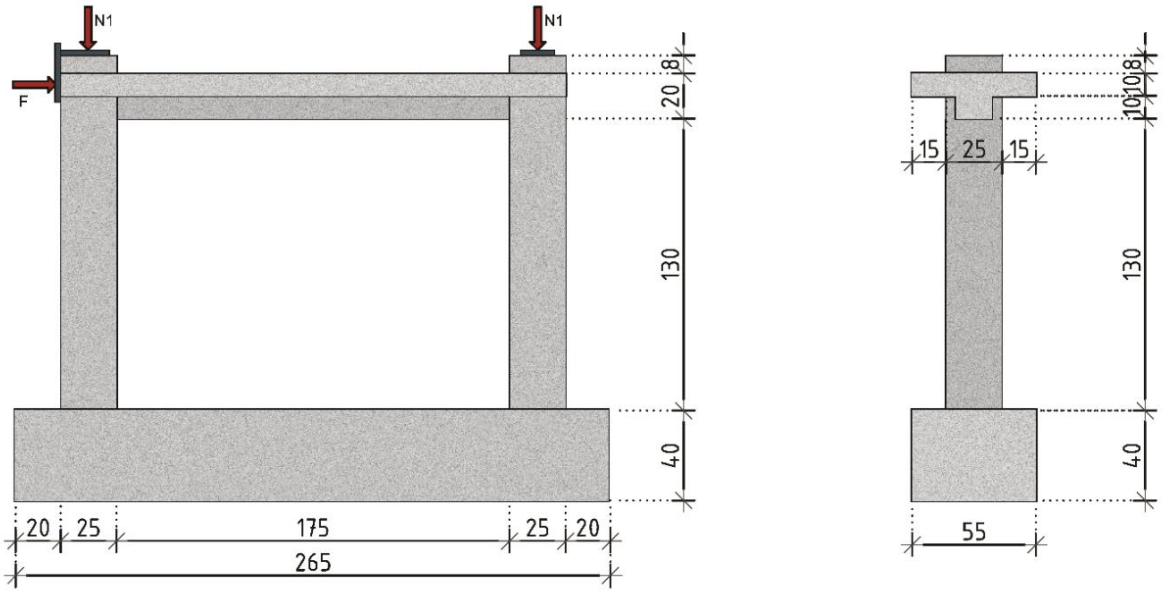

Figure 3.4.7 Bare frame model M1-B tested under monotonic loading pattern L12 (NL+ML).

In the second phase, the test was continued with representative monotonic loading. The main test objective was to investigate if it is possible to use monotonic loading concept (L12) to closely define envelope curve or nonlinear relationship like that recorded under cyclic loading (L11) to model M1-A.

Using the values recorded during this experimental test, the corresponding envelope nonlinear relationship for the positive horizontal deformations and obtained horizontal forces is presented graphically in red color in Fig. 3.4.8. Presented with a broken red line (left) is the symmetric envelope relationship for the negative deformations. Theng the identified resulting points Y, U and L, with respective numerical values for displacements and forces, the straight segments of the envelope curve were also defined. For each loading direction, the envelope was obtained by first extracting, from every load displacement cycle, the peak measured values of force and the corresponding displacements. These peak points (one for each cycle) were then ordered according to the increase of displacement and connected to form the ascending branch of the curve. The first point of this branch corresponds to the yielding point Y (DY, FY), the next characteristic point corresponds to the maximum recorded restoring force U (DU, FU), while the last point represents the maximum attained deformation L (DL, FL). In this way, three characteristic segments were defined: the initial elastic quasi elastic part from the origin to Y, the strength development part from Y to U, and the post-peak/softening part from U to L. The same procedure was applied symmetrically for the negative displacements, using the peak values recorded in the opposite loading direction, which resulted in an almost symmetrical envelope for the tested RC frame.

The strains in the reinforcement bars were not monitored during the experimental program for several practical and methodological reasons. First, the primary objective of the test was to characterize the global nonlinear response of the RC frame and to establish the envelope curve for numerical modelling, which is governed mainly by the horizontal restoring forces and the global lateral displacements of the system rather than by local strain measurements in individual reinforcing bars. Second, installing strain gauges on internal reinforcement would have required direct intervention during the placement of the bars and the concrete casting process, which could have altered the real construction characteristics, complicated the fabrication of the specimens, and increased the risk of sensor damage during vibration and compaction of the fresh concrete. In large-scale tests, strain gauges embedded inside concrete elements are also prone to failure due to harsh loading conditions, which may lead to unreliable readings.

Furthermore, the behavior of the reinforcement in the critical regions was evaluated indirectly through observable indicators such as crack formation patterns, changes in stiffness, yielding of the global response, and attainment of maximum load capacity. These parameters provide sufficiently reliable information for defining the nonlinear structural characteristics required for the purposes of this study. Therefore, although the absence of direct reinforcement strain measurements represents a limitation, it did not compromise the validity of the experimental program, because the test was primarily focused on capturing the global response of the RC frame and deriving the necessary macroscopic parameters for nonlinear modelling.

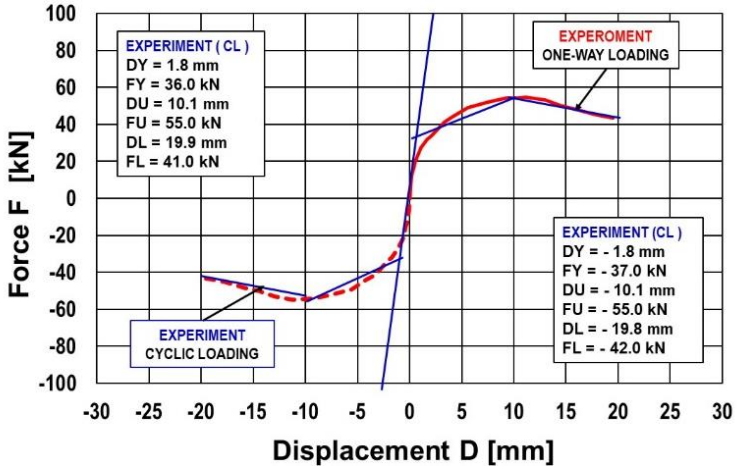

Figure 3.4.8. Bare frame model M1-B: Response of tested of RC frame under vertical and monotonic load (L12: NL+ML).

If the envelope curves defined under cyclic loading (L11) and under monotonic loading (L12) are compared, it is evident that there is a very good correlation between the recorded experimental results in the two testing cases (Fig 3.11).

During the experimental testing, also in this case, there was continuous monitoring of the process of occurrence of fine cracks in concrete and their propagation through the same four tensile zones (TZ1 through TZ4) located in the four corners A, B, C and D of the experimental frame. The recorded cracks zones are shown in yellow color on Fig. 3.4.9. The locations of the zones of cracks recorded for the positive deformations are almost identical for both different types of loading (L11 and L12) showing almost identical structure of destruction and length of occurrence at the corner segments of both RC columns of the experimental model M1-B.

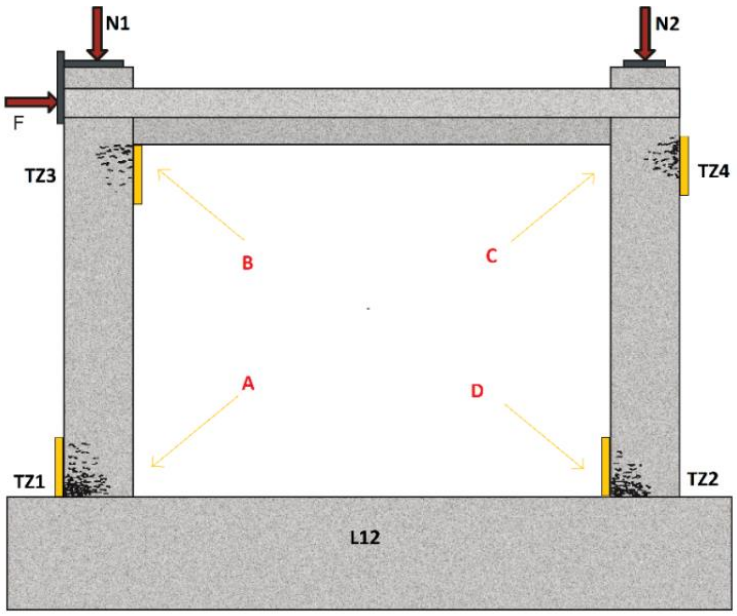

Figure 3.4.9 Bare frame model M1-B: Schematic view of crack pattern of tested of RC frame under vertical and monotonic load (L12)

3.4.4 Discussion of test results for bare frame models M1-B and M1-B

Following the experimental tests of models M1-B and M1-A, which represent RC bare frames, the main conclusions are summarized in Table 3.4.1 and Table 3.4.2. In addition, the corresponding crack patterns for both models are illustrated in Figure 3.4.10 and 3.4.11.

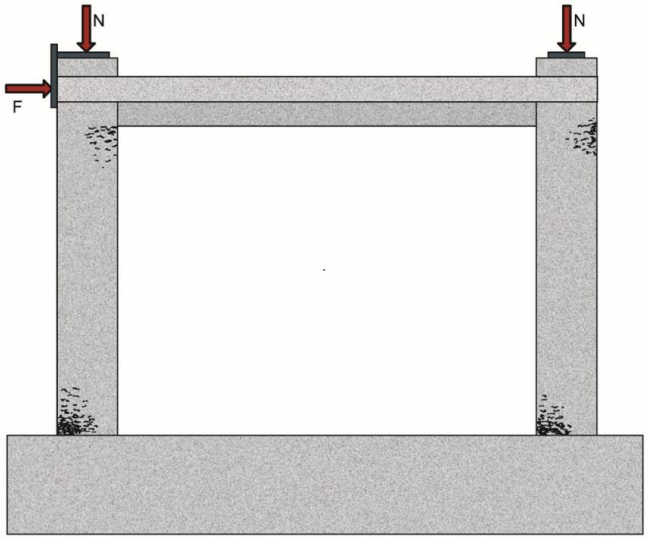

Figure 3.4.10 Model M1-B: Schematic view of crack pattern of tested RC bare frame under vertical and monotonic loading

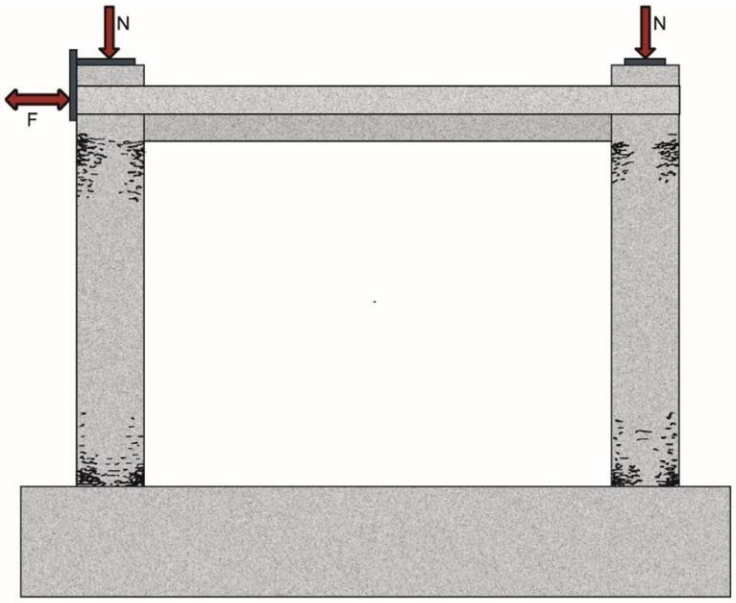

Figure 3.4.11 Model M1-A: Schematic view of crack pattern of tested RC bare frame model under vertical and cyclic loading

Table 3.4.1. Model M1-B: Observations from experimentally tested of RC bare frame model under vertical and monotonic loading

Model M1-B: Tested RC frame model without AAC infill under vertical and monotonic loading		
1	**Initial response**	
	a	Initial stiffness was defined considering yielding point: K0=FY/DY = 20.0 kN/mm
	b	Testing results indicate that the effect of cracking point was insignificant. Elastic nearly linear force-displacement relation was observed up to related yield point.
2	**Crack development**	
	a	The first cracks appeared in the tension zones, down and up, of the two columns for the applied force level F=18.2 kN, (See recorded force displacement relation).
	b	Similar, progressive crack development patterns were recorded for the larger force levels, spreading along the column's heights. Orientation of the cracks was dominantly horizontal.
	c	Critical cracks appeared when maximum restoring force was recorded F = 55.0 kN. The length of the critical cracks was nearly equal to l = 2.5 a, where a represent the size of the square cross section of RC frame column.
3	**Load-displacement response**	
	a	The recorded nonlinear force-deformation or pushover curve shows good regularity. It is in good correlation with the envelope curve defined from the recorded hysteretic response of the RC frame model tested under the effect of cyclic horizontal loads.
	b	Post yielding response was characterized with limited increase of restoring force.
	c	After the maximum force point, the behavior is characterized with slow softening. Only limited reduction of restoring force was recorded. With achieved this property confirmed was that prominent ductility of the tested model was recorded.
4	**Failure mechanism**	
	a	With the propagation of the cracks in the tensile zones and with the simultaneous occurrence of compressive failure of concrete, there occurs a state of heavy damage and then total failure of the tested frame system.
	b	The experimental tests show that under simulated larger deformations, there is severe deterioration of the initiated plastic hinges.
	c	The induced displacement near to ultimate displacement capacity was leading to collapse
5	**Comparison with cyclic behavior**	
	a	The stiffness of the RC frame was continuously reduced with the increase of deformations and becomes gradually smaller during larger deformations. The recorded push-over curve appears similar with envelope curve recorded under cyclic loading.
	b	During the experimental test of frame model M1-B under monotonic recorded were identical locations of occurrence of cracks and crush in concrete. Damage progression was limited to zones close to fixations of the columns.
	c	Envelope curve for cyclic loading evidently shows the regularity of stiffness deterioration also under segments of unloading. Differences in strength, stiffness, and ductility cyclic exist mainly due to different history of loading.
6	**Key observations**	
	a	Under induced large relative deformations follows a phase in which the restoring force is gradually reduced, leading to a critical state of failure.
	b	The initiation and propagation of cracks occur in the critical tension zones (TZ1 through TZ4) located in the segments close to the fixations of the columns.
	c	Overall structural response is nonlinear mainly due to induced nonlinearity in RC columns.

Table 3.4.2. Model M1-A: Observations from experimentally tested of RC bare frame model under cyclic loading

Model M1-A: Tested RC frame model without AAC infill under simulated cyclic loading		
1	**Initial behavior and elastic response:**	
	a	Initial stiffness was defined considering yielding point: K0=FY/DY = 20.5 kN/mm
	b	Testing results showed that the effect of first alternative cracking's was insignificant. Nearly linear force-displacement relation was observed up to alternative yield points.
2	**Progressive damage and crack patterns**	
	a	Development and propagation of cracks with increasing cycles occur in the critical alternative tension and compression zones located close to the fixations of the columns into the foundation RC beam and into the RC floor beam with slab.
	b	During the experimental tests of the prototype models M1-A and M1-B, recorded were completely identical locations of occurrence of cracks in concrete and their propagation in limited zones close to the cross-sections of fixation of the columns.
	c	Transition from flexural to shear cracks was not observed. The full nonlinear behavior of the tested model was dominated only by flexural failure only.
3	**Hysteretic behavior**	
	a	The recorded hysteretic response of the tested RC frame without AAC infill under simulated cyclic loading showed very good symmetry, harmonized hysteretic cyclic curves and very good ductility of about 5.
	b	The resulting hysteretic curves are regular in shape, well pronounced and exhibit satisfying symmetry. Regular stiffness degradation was observed with increasing displacement cycles.
	c	Expected gradual strength degradation and satisfying ductility was recorded.
4	**Failure mechanism:**	
	a	The experimental tests show that, under simulated larger deformations, there is deterioration of the initiated plastic hinges. With the propagation of the cracks in the tensile zones and with the simultaneous occurrence of compressive failure of concrete, there occurs a state of heavy damage and then total failure of the frame system.)
	b	After large relative deformations are induced, there follows a phase in which the restoring force is abruptly reduced, leading to a critical sequence of damage leading to failure.
	c	Maximum recorded lateral load amounts to F = 55.0 kN and displacement D = 17.5 mm.
5	**Energy dissipation**	
	a	The recorded hysteretic curves are regular, well pronounced and with satisfying symmetry. Large energy dissipation capacity was resulting since any pinching effect is not present.
	b	Hysteretic damping is significant since hysteretic response curves are forming large areas.
6	**Ductility**	
	a	The resulting envelope curves are well pronounced and exhibit satisfying symmetry. The recorded displacement ductility is satisfactory as was recorded for monotonic loading.
	b	The conducted test indicated gradual plastic hinge formation followed with stable rotation response capacity.

3.5 Infilled frame model specific details

The second part of the experimental program consisted of laboratory testing of the prototype models M2-A and M2-B. These models represent the RC frame configuration upgraded with an AAC infill panel placed along the entire span length and over the full height of the frame.

The prototype model M2-A was tested under the combined action of a constant vertical load and reversed cyclic horizontal loading. The horizontal load was applied in displacement control by following a predefined loading history with gradually increasing amplitudes in successive cycles. The results from this test are presented in part 3.5.2.

The prototype model M2-B was tested under the simultaneous action of vertical loads and a horizontal load of the monotonic type. The results of this test are presented in part 3.5.3.

To enable a direct comparison of the influence of the AAC infill on the nonlinear behavior of the RC frame, both tests were carried out on frames with identical geometry, reinforcement and support conditions. Furthermore, the installation of the specimens in the experimental frame and the loading procedure were kept the same as in the tests on prototype models M1-A and M1-B, so that the results could be compared on the same basis.

The final structural characteristics of the infilled models M2-A and M2-B are given in part 3.5.1, while the key observations and conclusions obtained from these tests are presented in part 3.5.4.

3.5.1 RC frame models with infill M2-A and M2-B

These experimental investigations were highly important since they provided the most favorable conditions for research into the quality effects of the AAC infill into buildings constructed by the application of modern RC bearing frame systems. In the case of all four prototype models, the RC frame structures were constructed as identical, which enabled favorable conditions for comparison of the obtained experimental results. The models with the AAC infill segments are briefly described.

• ***Construction of Models M2-A and M2-B with AAC Infill***: The construction process of prototype models M2-A and M2-B started with the construction of the two RC frame structures. Both frames were built in the same way and at the same scale (1:2) as the frames used for the prototype models M1-A and M1-B, and they were cast in a vertical position. The geometrical and structural characteristics of the frame structures are presented in detail in part 4.3.1. In the second phase, the prototype models M2-A and M2-B were completed by constructing the AAC infill. The AAC infill walls were constructed at the same 1:2 scale, using AAC elements with reduced dimensions consistent with the model scale, and with the same arrangement foreseen for the test frame, so that the behavior of the infilled frame could be directly compared with the bare-frame tests. The proportions of the prototype elements were Lp = 200 mm (length), Hp = 200 mm (height) and Dp = 250 mm (thickness). In accordance with the adopted scale for

construction (M = 1: 2), the AAC elements in the form of infill were constructed to have the following dimensions: Lm = 100 mm (length), Hm = 100 mm (height) and Dm = 125 mm (thickness). The construction of the infill made of AAC elements was carried out using the same procedure as in the construction of the frame models. The elements were laid course by course inside the RC frame, with level and vertical alignment controlled at each layer, following the geometry of the 1:2 test model. As bonding material, YTONG TM thin-bed adhesive mortar, specifically developed for AAC masonry units, was used. This ensured a uniform bonding layer and a construction technique fully compatible with the AAC system applied in the prototype frames.

3.5.2 Testing protocol and results for infilled frame model M2-A (cycling loading)

Experimental testing of prototype model M2-A, subjected to vertical and cyclic horizontal loading, was conducted following the same procedure used for model M1-A. Because both specimens were constructed with an identical RC frame including the same geometry, reinforcement detailing, boundary conditions, and loading protocol, the experimental setup ensured a consistent and controlled basis for comparison. This creates technically efficient conditions for distinguishing the structural effects caused specifically by the AAC infill. In practice, this means that any differences in stiffness, strength, cracking progression, deformation pattern, or energy dissipation observed between M1-A (bare frame) and M2-A (infilled frame) can be attributed directly to the AAC infill itself, rather than to variations in the RC frame or the testing process. Figure 3.5.1 provides a schematic presentation of the tested specimen with symbols of the applied loads on the experimental model marked as loading pattern L21. In the first phase, identical loads as for model M1-A with N1 = 62.5 kN were applied on both columns. In the second phase, applying the stepwise displacement time history, the prototype model M2-A was subjected to reversed cyclic load by controlling the displacement adopted with gradual increase of its amplitudes.

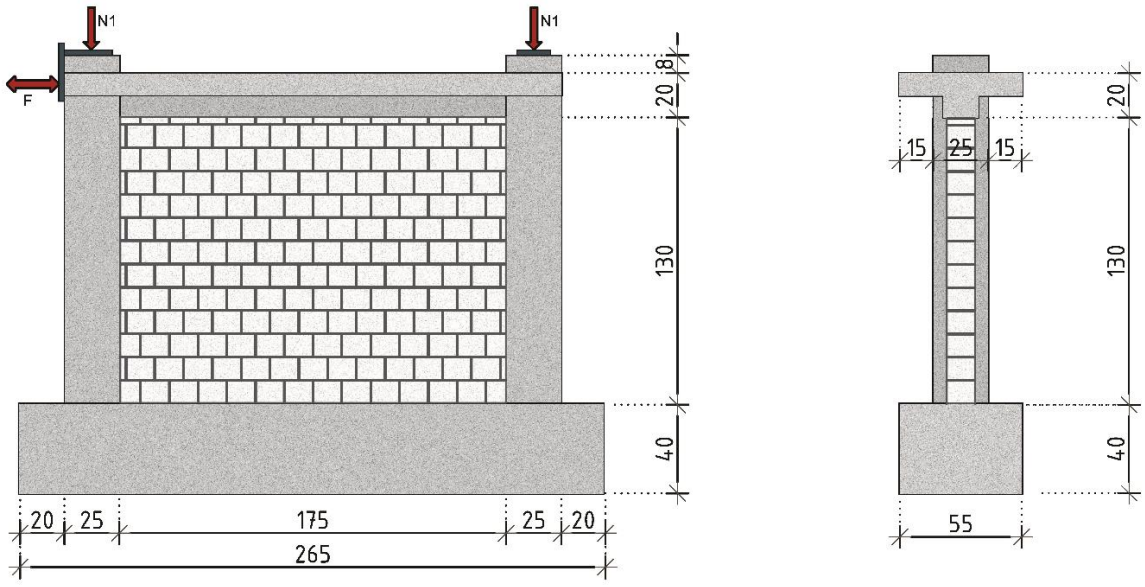

Figure 3.5.1 Prototype model M2-A tested with AAC infill under loading pattern L21 (NL+CL).

During the experimental test, the numerical values of the measured forces and displacements at each step were successfully recorded. Fig. 3.5.2 graphically shows the recorded hysteretic response of the tested prototype model M2-A under the effect of vertical and reversed cyclic horizontal loads. Based on recorded hysteretic response, defined were the representative envelope relationships by means of the defined characteristic points Y, U and L for the case of positive and negative deformations.

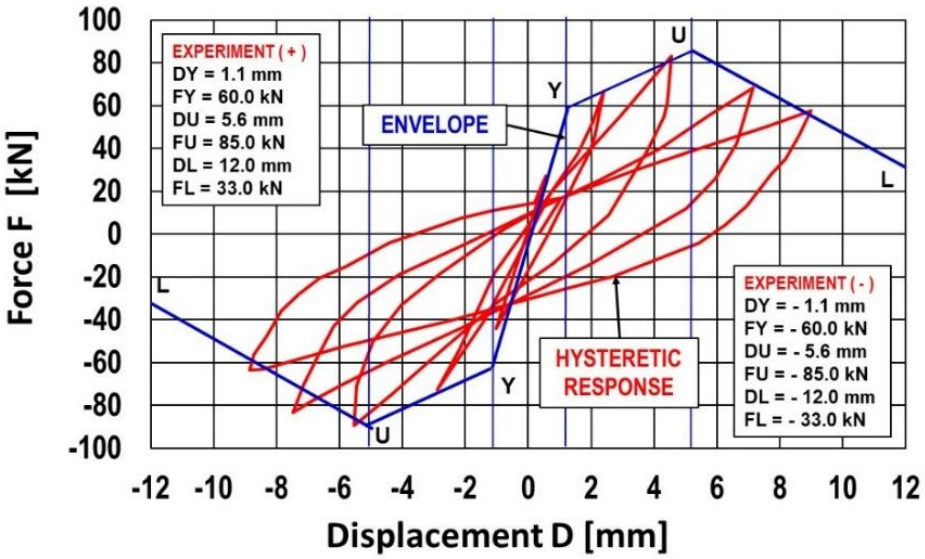

Figure 3.5.2 Prototype model M2-A: Response of tested of RC frame with AAC infill under vertical and reversed cyclic load (L21: NL+CL).

In Figure 3.5.3 graphically are presented the zones of recorded cracks during the experimental test of the model M2-1, both in the bearing RC frame segment and in the AAC infill segment. Due to the nature of the cyclic horizontal load, the occurred tension zones with cracks generally show symmetric locations and distributions.

For example, the tension zones in the reinforced concrete frame (TZ1 through TZ4) where cracks were recorded generally agreed with those recorded during the experimental test M1-A on the RC frame without an AAC infill, Fig. 4.16. In addition, the experimental test verified that the presence of the AAC infill did not cause almost any remarkable effects regarding the induced damage to the RC frame.

The recorded zones of occurrence of cracks under induced positive relative deformations are shown in yellow color on Fig. 3.5.3. Similarly, the occurred zones of cracks under negative deformations are marked with red color. However, the occurrence of fine cracks in the AAC infill is quite different, with a tendency to involve much larger surfaces, Fig. 4.12. For example, in the case of induced positive deformations, fine cracks occurred in a widened diagonal zone distributed along the diagonal between the corner points C and B of the frame. The activated zone is schematically marked on the left side by points c1 - C - c2 located in the upper zone of the left column, whereas on the right side, it is marked by points b1 - B - b2 located on the lower side of the right RC column. Due to the significant stiffness and lower ductility of the

AAC elements and due to the corresponding nonlinear deformations in the formed interface zones on the respective surfaces of the materials, recorded initially were very fine cracks with the tendency to increase in the diagonal zone. A considerable increase in the width of the cracks was observed during the induced larger relative deformations.

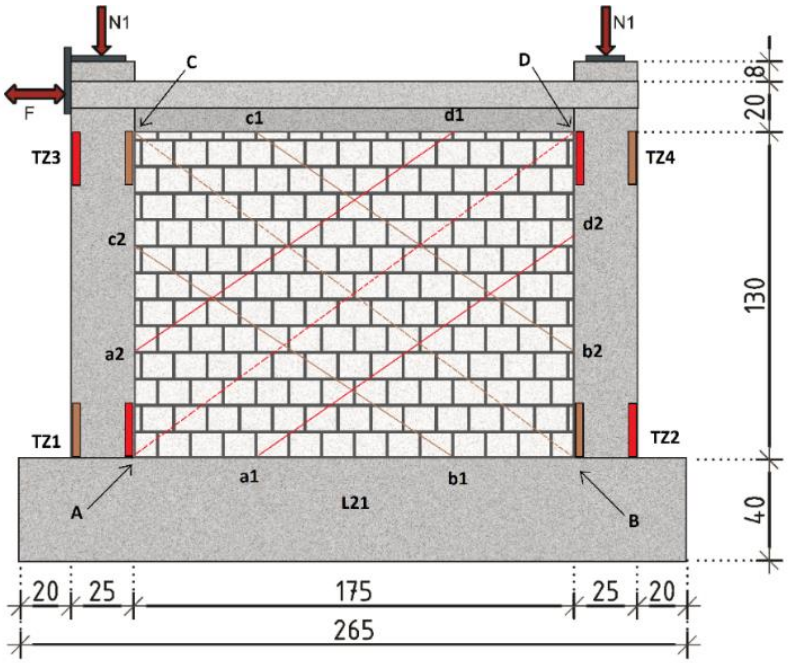

Figure 3.5.3 Prototype model M2-A: Recorded crack zones of tested of RC frame with AAC infill under vertical and reversed cyclic load (L21).

During the experimental test, the forces and displacements were continuously recorded at each loading step. The obtained hysteretic response of the prototype model M2-A under combined vertical and reversed cyclic horizontal loads is presented in Figure 3.5.3. The curve exhibits a stable and nearly symmetric shape in both positive and negative directions, confirming consistent behavior of the system. The initial linear part of the envelope indicates a pronounced stiffness typical of the elastic phase, followed by a gradual transition to nonlinear response as cracking initiated in the tension zones of the RC frame.

At the beginning of loading, the frame and the AAC infill acted monolithically. The first visible cracks appeared at beam-column joints and column bases at relatively low load levels, marking the end of the elastic stage. With the continuation of cyclic loading, additional flexural cracks formed along the beams and columns, while the AAC infill developed a diagonal cracking pattern extending from the upper corner of one column to the lower corner of the opposite column. This diagonal crack indicates the activation of compression-tension fields within the infill and the development of shear interaction along the interface with the RC frame. Fine cracks initially covered wide surfaces of the AAC panel and gradually widened with increasing relative deformations. The recorded cracking zones for positive and negative displacements are shown in yellow and red on Fig. 3.5.3, respectively.

As loading cycles progressed, the hysteretic loops revealed a moderate stiffness degradation, accompanied by slight pinching of the curves. This behavior reflects the progressive cracking of concrete, frictional sliding along the AAC-RC interfaces, and localized crushing of the AAC in compression zones. Despite these effects, the strength degradation remained limited, and the structure preserved stable hysteretic behavior up to the ultimate stage. At higher drift levels, significant diagonal cracking of the AAC infill dominated the overall response, while flexural cracks at beam ends and column bases became more pronounced. The ultimate failure mode was characterized by diagonal cracking and partial crushing of the AAC infill, followed by local separation at beam-column joints. The maximum lateral load and displacement capacity were reached shortly before the complete loss of load-carrying ability, which was mainly governed by the degradation of the infill's diagonal strut mechanism.

The area enclosed by the hysteresis loops demonstrates effective energy dissipation throughout the cyclic loading process, confirming favorable damping characteristics of the RC-AAC composite system. Although the AAC infill itself exhibits brittle behavior, the overall structural assembly showed moderate ductility due to the deformability of the RC frame, which allowed redistribution of internal forces after cracking. This combination of energy absorption and ductile response reflects a balanced seismic performance of the tested specimen.

During induced negative deformations, activation was an almost symmetrical zone with cracks occurring. This zone occurred as a diagonal between the corner points of the RC frame indicated by A (down) and B (up), on the left and the right RC column. In this case, the symmetric zone with the occurring cracks was defined by points a1 - A - a2 on the left column and points d1 - D - d2 on the right column.

With the induced cyclic loading with horizontal load, recorded was a complex alternating transformation of the diagonal zones with occurred cracks with a tendency for successive propagation. In addition, there were also observed critical localized zones that suffered visible damage due to concentrated local compressed zones, generally along segments a1 - A - a2, b1 - B - b2, c1 - C - c2 and d1 - D - d2. Summarizing all the experimentally recorded phenomena leading to initial fine cracks and then failure of the AAC infill, it was generally observed that the nonlinear behavior of the RC frames with AAC infill was extremely complex. The experimental evidence obtained clearly confirmed that only qualitatively advanced methods can assure possibility to closely analytically simulate the complex nonlinear phenomena arising from the specific behavior of different materials and their contact effects. The new approach created should be based on application of the advanced concept of detailed nonlinear micro-modelling of all complex nonlinear behavior origins and sources. The main objective of the second part of this research was focused on such original and specific modelling directions.

3.5.3 Testing protocol and results for infilled frame model M2-B (monotonic loading)

The schematic presentation of the loading of the experimental prototype model M2-B representing an RC frame with an AAC infill is given in Fig. 3.5.4. This specific type of model loading is marked as L22.

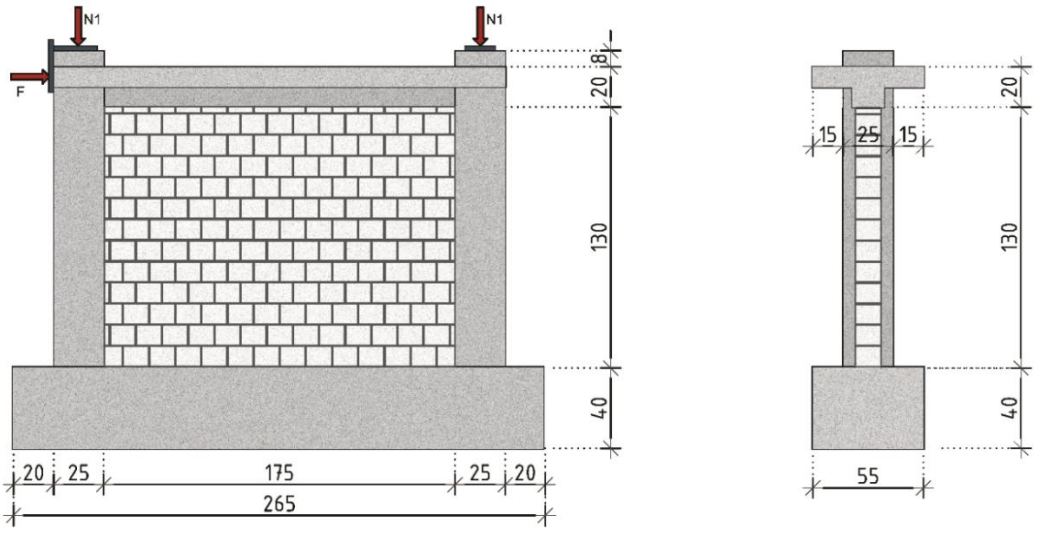

Figure 3.5.4 Prototype model M2-B tested with AAC infill under loading pattern L22 (NL+ML).

In the first phase, loading of both columns by identical vertical loads of N1 = 62.5 kN was performed. In the second phase, the prototype model M2-B was slowly loaded with a monotonously increasing load induced by means of slow and continuous increase of positive relative deformation.

The experimentally obtained nonlinear response of the prototype model M2-B is presented in Fig. 3.5.5. At the initial stage of loading, the specimen showed a clear linear behavior with relatively high initial stiffness, which reflects the joint action of the RC frame and the AAC infill. The departure from linearity occurred at the load level corresponding to the first visible cracking in the frame members, which can be taken as the yield point of the system.

With the increase of the lateral displacement, cracking started to develop progressively. First cracks appeared in the tension zones of the RC frame (beam-column joints and column ends), while at higher displacement levels diagonal cracking initiated in the AAC infill. This sequence shows that the frame governed the response at low drifts, whereas the infill started contributing and, at the same time, degrading at larger drifts.

The load-displacement curve obtained from the test has the typical shape of a pushover response: after the elastic part, the curve enters a gradual yielding range, followed by a slight strength reduction toward the ultimate point. This behavior indicates that the specimen was able to maintain its load-carrying capacity over a certain displacement range before softening.

The observed failure mechanism was governed by the damage in the infill (diagonal cracking and crushing in the compression zone) combined with the widening of the flexural cracks in the RC frame. Damage developed in a stable sequence - first in the frame, then in the infill - and finally led to a reduction of the lateral resistance.

When the envelope points (Y, U and L) from the monotonic test M2-B are compared with those obtained from the cyclic test M2-A, the monotonic loading program is able to reproduce the same envelope curve with satisfactory accuracy. This confirms that, for this type of RC frame with AAC infill, the monotonic test can be used as a reliable basis for calibrating the analytical model.

This is important because the full cyclic numerical simulations with detailed micro-modeling require very long computation times (in our case more than 100 hours for one analysis). By using the experimentally verified monotonic loading as the reference loading case, the computation time was reduced to about 10 hours, i.e. roughly 10-15 times shorter, while still preserving the essential features of the structural response.

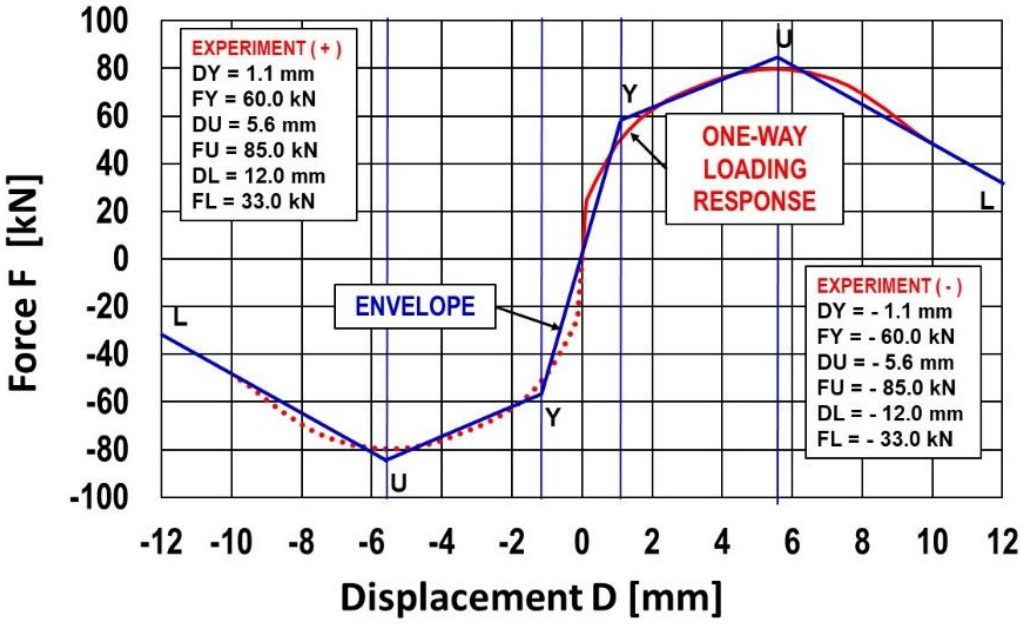

Figure 3.5.5. Force-Displacement pushover curve and envelope of frame model M2-B with AAC infill (L22: NL+ML).

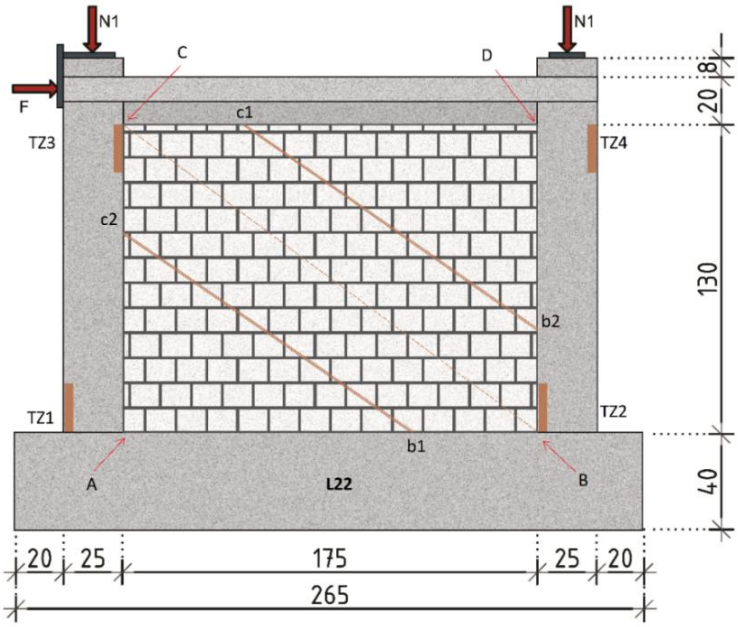

Figure 3.5.6. Prototype model M2-B: Recorded crack zones of tested of RC frame with AAC infill under vertical and monotonic load (L22).

It is acknowledged that, in most experimental studies, the cracking behavior of masonry infills is typically illustrated through individual crack orientations and locations. However, due to the specific characteristics of AAC material and its brittle nature, the cracks observed in the present experimental model did not appear as distinct, well-defined lines but rather as diffuse zones of microcracking extending diagonally across wider areas. For this reason, the cracking behavior was represented by shaded zones indicating the approximate regions of concentrated cracking and damage. This approach was considered more appropriate for accurately reflecting the actual failure mechanism observed during testing, as the fine cracks in the AAC infill could not be distinctly traced or measured individually. Figure 3.5.6 shows the zones with cracks in the RC frame as well as in the AAC infill during the effect of vertical and monotonic loading (L22). Since in this case, positive relative deformations were gradually induced, an analogous state of occurred cracks and damages was obtained. For example, in the RC frame of model M2-B, recorded analogous zones of cracks in the same zones (TZ1 through TZ4) as those in the tested model M1-B, but in the case of induced positive deformations only. Analogously, in the existing AAC infill, activated was a corresponding zone exposed to compression along diagonal C-B. In the wider diagonal zone defined by the contact zones c1 - C - c2 and b1 - B - b2, during the experimental test, there were observed the first fine cracks in the vicinity of the diagonal, being quite extended to a formed wider diagonal zone. Local damage to the AAC infill was also recorded due to compressive stress at the contact zones c1 - C - c2 and b1 - B - b2. Following the recorded phenomena of damage to the RC frame and AAC infill of the tested prototype model M2-A as well as the recorded phenomena of damage to the tested model M2-B, it was evident that there was a great similarity in both cases, where in the second case, the effects were recorded as reduced to a corresponding half due to the nature of the monotonic loading.

3.5.4 Influence of AAC Infill on Frame Behavior for model M1-B and M2-B

To present the effect of the AAC infill on the nonlinear behavior of RC frames with AAC infill, the results obtained from the performed experimental investigations were integrated and they are graphically presented in Fig. 3.5.7.

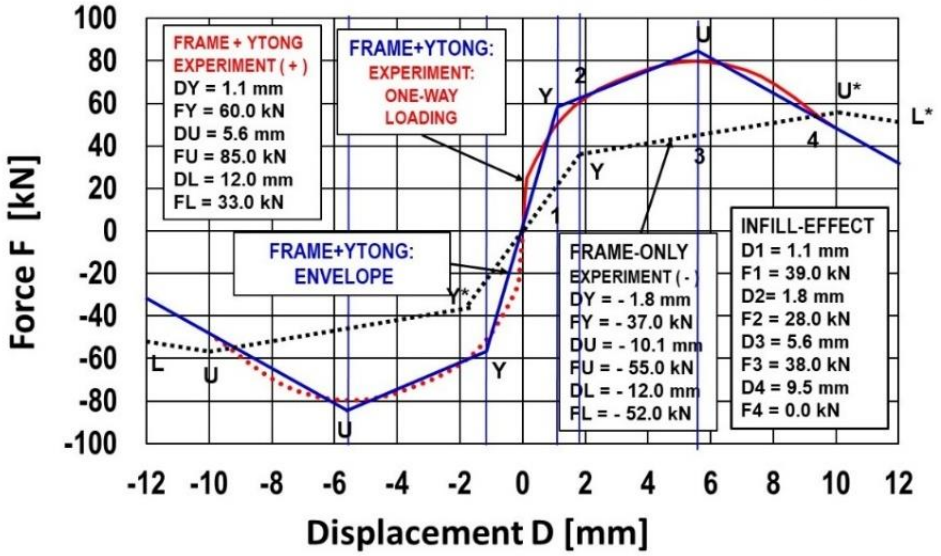

Figure 3.5.7 Comparison of the Force-Displacement pushover and envelope curves of bare frame model M1-B and frame model with AAC infill M2-B (L22: NL+ML)

The cumulative envelope curve defined with the experimental test of the model M2-B is shown in red color. The blue color indicates the corresponding envelope defined by rectilinear segments. Marked with a broken line is the experimentally defined envelope for the tested RC frame without an infill, model M1-B. From the presented experimental results, it is evident that to achieve the resisting force, the presence of the AAC infill cannot be neglected. In addition, due to the greater ductility of the RC frame and the significant stiffness of the AAC infill, extensive fine cracks and/or complete failure of the AAC infill takes place in the case of much smaller deformations. The part marked with the red arrow labeled “infill-effect” represents the phase where the AAC infill starts to actively contribute to the lateral load-resisting mechanism of the RC frame. At this stage, as the horizontal displacement increases beyond the initial yielding of the bare frame, the infill comes into compression along its diagonal, forming a strut-like action between the opposite corners of the frame. This interaction increases the overall lateral stiffness and strength of the system, as reflected by the steep rise of the load-displacement curve. The listed force values (F1-F4) correspond to successive load increments recorded as the infill becomes more engaged and transfers part of the shear forces through the contact interfaces. The behavior in this region indicates the development of a composite response between the frame and the infill, where the AAC elements temporarily enhance the stiffness and load capacity until diagonal cracking and local crushing start to occur, leading to a gradual reduction of strength beyond the peak point

3.5.5 Participation of AAC Infill Restoring Force in Total Restoring Force

Figure 3.5.8 shows the experimental results in a similar way, but in this case, in addition to the cumulative envelope relationship, the recorded envelope relationship resulting from the AAC infill is presented below with dashed line.

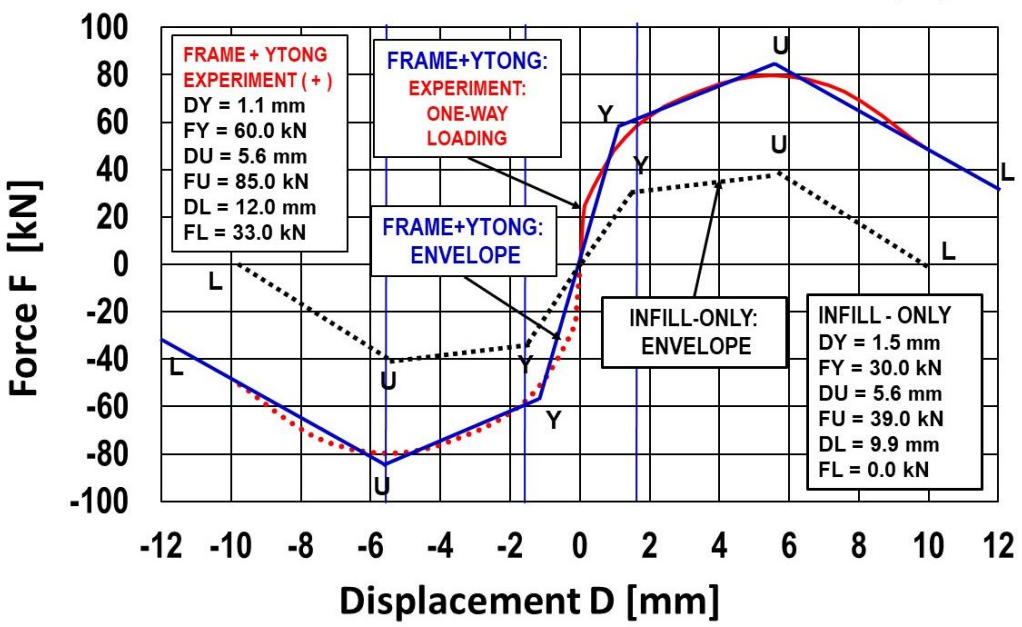

Figure 3.5.8. Prototype model M2-B: Envelope of AAC infill-only in tested RC frame with AAC infill under vertical and monotonic loading (L22: NL+ML)

From the stated figure, it is evident that the infill of AAC elements has great and non-negligible effects on the actual nonlinear behavior of the RC frames treated separately.

In addition to the evident great effect on the increase of the initial stiffness and resisting force, the AAC infill also exhibits abrupt damage in the case of relatively small deformations. For example, from Fig. 3.5.8, it is evident that total failure of the AAC infill takes place at induced relative deformations of only 8 to 10 mm. This phenomenon complicates very much the conditions for the definition of qualitatively improved technical measures for the reduction of damage to the AAC infill in the case when structures are exposed to earthquakes of higher intensities. At present, the creation of new and qualitatively improved innovative technical solutions for seismic protection of RC frame buildings with AAC infill, is of top priority and urgent need.

3.5.6 Discussion of test results for bare frame models M2-A and M2-B

Following the experimental tests of models M2-A and M2-B, which represent RC frames with AAC infill walls, the main conclusions are summarized in Table 3.5.1 and Table 3.5.2. In addition, the corresponding crack patterns for both models are illustrated in Figures 3.5.9 and 3.5.10.

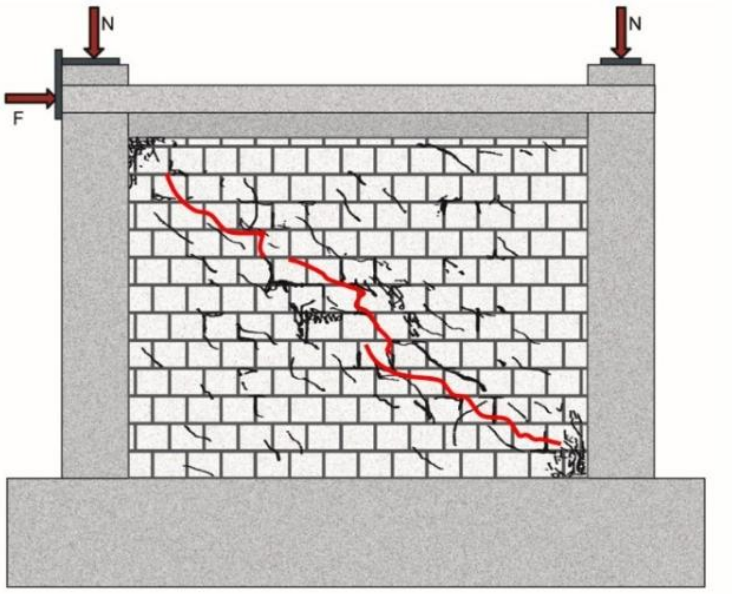

Figure 3.5.9. Model M2-B, schematic view of crack pattern of tested RC frame model with AAC infill under vertical and monotonic loading

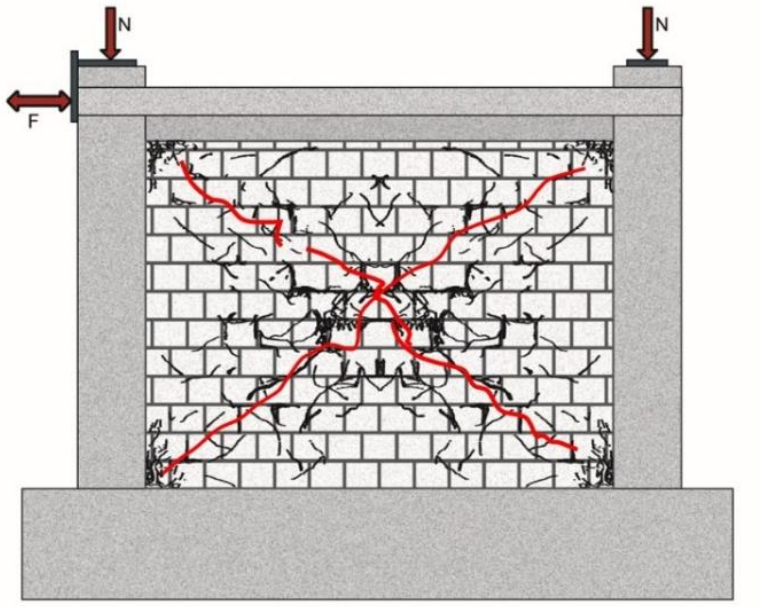

Figure 3.5.10. Model M2-A, schematic view of crack pattern of tested RC frame model with AAC infill under cyclic loading

Table 3.5.1. Model M2-B: Discussion of results from experimentally tested of RC frame model with AAC infill under vertical and monotonic loading

Model M2-B: Tested RC frame model with AAC infill under vertical and monotonic loading		
1	**Initial response**	
	a	Initial stiffness was defined considering yielding point: K0=FY/DY = 54.54 kN/mm
	b	Similar as under cyclic load, elastic behavior can be approximated up to the and yield point defined with displacement of DY = 1.1 mm. However, formation of the first cracks was observed in the region of corners of compressed diagonal under load level F = 30.0 kN.
2	**Crack development**	
	a	The first cracks appeared in infill for small displacements (1-2 mm) along diagonal. For larger displacements failure of infill was observed, while frame restoring force was not reduced due to large frame ductility capacity.
	b	The results from experimental investigations prove that the initial and propagated cracks occur, first, in the infill segment. The cracks in the RC frame structure are of a local character and are more pronounced in the case of considerably larger deformations.
	c	Initial and critical crack formation in RC columns had similar patterns as cracks in the tested frame without AAC infill.
3	**Load-displacement response**	
	a	With the performed experimental investigation of the nonlinear behavior of RC frame with AAC infill, but with alternate horizontal loading of the type of monotonic loading, very similar envelope curves and almost the same conclusions are obtained and drawn. Therefore, instead of the complex cyclic loading, during realization of the following extensive refined analytical studies, monotonic loading was defined and implemented.
	b	The recorded pushover curve indicates that maximum restoring force FU= 60.0 kN was reached for induced smaller displacement DU = 1.1 mm.
	c	After reaching the maximum restoring force, the recorded pushover curve was exposed to rapid softening. After failure of AAC infill, restoring force of only RC frame remain.
4	**Failure mechanism**	
	a	The presence of the AAC infill leads to a pronounced increase in initial stiffness. However, in the case of relatively small deformations, its stiffness significantly deteriorates due to the occurrence of cracks and/or failure of the AAC infill.
	b	Following the extensive damage to the AAC infill, the stiffness is reduced and generally becomes close to the stiffness of the RC frame without the considerable effect of the infill.
	c	The recorded peak load amounts to F = 85.0 kN while the recorded ultimate displacement amounted to d = 10.0 mm. For larger displacements than peak force displacement observed was rapid strength reduction directly leading to collapse.
5	**Comparison with cyclic behavior**	
	a	The ductility of the RC frame is quite large and does not change due to the presence of the AAC infill. The differences in strength, stiffness, and ductility manifested with pushover curve and envelope curve recorded during cyclic loading test are not significant.
	b	The ductility of the AAC infill is very low due to considerable fine cracks and heavier damage occur even at relatively small deformations.
	c	Different damage progression in AAC infill was observed during monotonic loading test and during cyclic loading test. Damage progression during monotonic loading test was manifested along one diagonal while it was recorded along two diagonals during cyclic loading test.
6	**Key observations**	
	a	The existing AAC infill suffer large irreparable damage under induced larger relative displacements. However, the RC frame structure is not exposed to failure due to its large ductility. Large nonstructural damage result in costly repair or large economic loss.
	b	Failure of AAC infill is observed for small deformations. The RC frame structure remain safe for larger deformations due to provided its satisfactory ductility.
	c	Recorded overall pushover response curve was very similar to the envelope curve obtained from test under cyclic loading. Therefore, instead of the complex cyclic loading, monotonic loading was simulated during realization of extensive analytical micro-modelling studies.

Table 3.5.2. Model M2-A: Discussion of results from experimentally tested of RC frame model with AAC infill under simulated cyclic loading

Model M2-A: Tested RC frame model with AAC infill under simulated monotonic loading		
1	**Initial behavior and elastic response**	
	a	Initial stiffness was defined considering yielding point: K0=FY/DY = 54.5 kN/mm
	b	Elastic behavior can be approximated up to the and yield point defined with displacement of DY = 1.1 mm. However, formation of the first cracks was observed in the region of corners of the two compressed diagonals under load level F = 30.0 kN.
2	**Progressive damage and crack patterns**	
	a	The results from experimental investigations prove that the initial and propagated cracks occur, first, in the infill segment. The cracks in the RC frame structure are of a local character and are more pronounced in the case of considerably larger deformations. Development and propagation of cracks in AAC infill with increasing cycles was recorded along diagonals and in the corners exposed to concentrated compression stresses.
	b	Under cyclic load, alternative crack patterns were recorded near fixation ends of columns and were similar to that recorded in the case of tested model without AAC infill.
	c	Transition from flexural to shear cracks was not observed. However, plastic hinges were formed due to cracks in tension zines and due to crush of concrete in compression zones.
3	**Hysteretic behavior**	
	a	The nonlinear hysteretic response of RC frame model with AAC infill under the effect of cyclic loads was very complex due to the interactive effects of ductile RC frame and the non-ductile infill of AAC elements. The recorded hysteretic loops were nearly symmetrical in shape, but with manifested presence of some pinching effect.
	b	AAC infill increases initial stiffness and contributes to the increase of the resistance force, but it also experiences extensive damage or failure in the case of induced relatively small relative deformations. Stiffness degradation appeared with increasing displacement cycles
	c	The presence of the AAC infill leads to a pronounced increase in initial stiffness. However, in the case of relatively small deformations, its stiffness significantly deteriorates due to the occurrence of cracks in the AAC infill under induced cyclic load. Following the extensive damage to the AAC infill, the stiffness is reduced and generally becomes close to the stiffness of the RC frame without the considerable effect of the infill.
4	**Failure mechanism**	
	a	Under applied cyclic loads, the existing AAC infill suffer large irreparable damage or failure depending on the level of induced relative displacements.
	b	Although the structure did not suffer failure, the large nonstructural damages result in costly and economically unjustified post-earthquake repair expenses. Sequence of damage leading to failure of RC frame mainly followed common ductile frame response.
	c	The recorded maximum lateral load amounted to F = 85.0 kN for recorded displacement amounting to D = 5.6 mm. After this stage, rapid reduction in restoring force was observed due to experienced failure in AAC infill.
5	**Energy dissipation**	
	a	With assured regularity of the formed repeated hysteretic cycles demonstrated was respectable energy dissipation capacity for larger displacements.
	b	The repeated open hysteretic cycles will result in good damping characteristics during structural seismic response induced with strong earthquakes.
6	**Ductility**	
	a	The ductility of the RC frame is quite large and does not change due to the presence of the AAC infill. The ductility of the AAC infill is very low due to considerable fine and large cracks and heavier damage occur even at relatively small deformations. Ductility improvement of AAC infill is not possible. To improve the protection of the AAC infill against seismic loads, it is necessary to create some t innovative technical solutions.
	b	Under applied cyclic loads (through considered predefined displacement history), the observed plastic hinges in RC columns shoved very good ductility and rotation capacity.

4 CHAPTER 4 - ADVANCED MODELLING OF RC FRAMED BUILDINGS WITH AUTOCLAVED AERATED CONCRETE (AAC) INFILL

The new knowledge obtained from the performed experimental investigations of the nonlinear behavior of RC frames without and with infill of AAC elements confirmed the inevitable need for qualitative improvement of the concepts of analytical investigations by introducing the use of a new advanced approach based on micro-modeling.

The need for the development and application of nonlinear analytical models based on the micro-modelling concept arises from the necessity for detailed simulation of the interactive nonlinear effects arising from several different and complex nonlinear phenomena.

1. Complex fluctuation of stiffness: Due to the nature of the cyclic loads from seismic excitations and due to the different nonlinear characteristics of the ductility of RC frames and the non-ductile AAC infill, there is a complex time variation of the stiffness of the system. The complexity of the stiffness variation arises from the induced spread distribution of specific stress-strain nonlinearities of all materials.

2. Complex variation of restoring force: The occurrence of multiple loading and unloading cycles in the entire time-domain of positive and negative deformations results in a complex variation of restoring force. Such complex variations can be closely analytically only by the application of advanced nonlinear micro-models.

3. Complexity of the envelope relationship: The conditional complex variations of the stiffness and the effective restoring force give rise to a very specific resulting envelope relationship. Such relationships can be realistically only by application of experimentally verified nonlinear micro-models.

4. Complexity of crack propagation: Through the evidence gained from the experimental investigations realized the nonlinear behavior of RC frames with AAC infill, a very specific and complex mode of occurrence and propagation of recorded cracks was identified.

Due to their propagation through larger surfaces of the infill with a variable intensity as well as due to the occurrence of localized cracks in the RC frames, an advanced concept of micro-modeling is necessary to be applied for their realistic and detailed simulation.

5. Complexity of damage patterns: Development of damage occurs first in the AAC infill. The occurrence of larger deformations of the infill, widening of the cracks and/or local failure in the critical zones of the AAC infill take place. Additionally, in the RC frame, firstly initially and then intensive localized damage. Such complexity of damage patterns can be analytically using detailed nonlinear analytical models.

6. Top priority for the upgrading of seismic codes: To enable closely simulation of the presented and experimentally verified complexity of the nonlinear phenomena, it is necessary to apply formulated advanced nonlinear micro-models.

Moreover, the use of the developed advanced micro-models opens the possibility to direct further research activities toward the development of new advanced technologies for quality reduction of heavy seismic damages to buildings with RC frames and infill of AAC elements.

The created advanced technical solutions for the protection of the AAC infill against large cumulative damage open the possibility for qualitative improvement of the seismic codes which is presently of top priority for these types of modern building structures.

The research topic addressed through the present experimental and analytical studies is highly complex. In conventional design practice, infill walls in RC frame structures are most often considered merely as additional mass [53].

In seismic regions, building design follows advanced procedures that account for the stochastic nature of earthquake excitations. These procedures require: (1) reliable estimation of the maximum expected seismic intensity, (2) consideration of the frequency content of ground motion, (3) realistic representation of the mechanical properties of materials, (4) accurate mathematical modeling, and (5) identification of critical loading patterns [52]. Each of these steps involves uncertainties that influence the overall design reliability.

During strong earthquakes, buildings may survive without collapse but still experience extensive damage to infill components, whose repair is often costly or unfeasible [54]. Predicting cumulative building damage under seismic loading therefore remains a significant and challenging issue.

The inherent incompatibility between ductile RC frames and rigid non-structural infill walls further complicates both design and service performance [54]. It is now widely recognized that infill effects cannot be ignored, as numerous studies have demonstrated their considerable impact on the global stiffness, strength, and energy dissipation capacity of RC frames [52-54].

Accordingly, specific experimental and analytical research is required to develop effective and practical measures to limit cumulative damage and enhance the overall seismic performance of buildings. In this context, the present study investigates the behavior of RC frame buildings with autoclaved aerated concrete (AAC) infills, aiming to optimize the use of AAC elements as efficient and lightweight infill materials in modern multi-story construction.

4.1 Basic Modelling Concepts

The development of analytical models for analysis of structures or their components in engineering practice has long been limited to and associated with simple procedures due to the complexity of the nonlinear behavior of construction materials. Generally, the development process in this domain can be presented through the realized achievements in different time periods.

1. ***Time period up to1945:*** Earthquake engineering as a specific scientific field did not exist in significant form. Considering the evident great need for improving the seismic safety of buildings in reasonable way, in Japan and the USA, the term "seismic load" was introduced. Then its level in horizontal direction was simply defined and considered in the design.
   The defined horizontal seismic load represented, in fact, a certain percentage of the vertical load, i.e., of the building weight. The analytical modelling of the buildings was quite simplified, treating the weight of a structure only as a "discrete" mass connected with the soil by a linear element with defined "equivalent stiffness".
   Modelling buildings with several included discrete masses corresponding to the number of building stories was difficult since there were no computers, no developed numerical models and no experimental knowledge on the nonlinear behavior of buildings or materials under earthquake loads [42]. The urgent need to avoid critical stability conditions or avoid intensive failure of structures was the main motivation and objective of the involved structural engineers and corresponding construction companies.
2. ***Time period from 1945 to 1980:*** In this period, the most intensive development of earthquake engineering took place [42]. The availability of "main frame" computer systems led to fast development of numerical methods as well as the first software programs for successful and rapid analysis of large engineering structural systems [52]. Specific research laboratories for earthquake engineering studies were established at Berkeley University in the USA and Tokyo University in Japan. Parallel to the realization of the important experimental investigations, the methods for seismic analysis of structures and computer software solutions were increasingly improved.
   This development trend was abruptly expanded to numerous scientific centers worldwide that became bearers of national programs for efficient seismic protection of engineering structures in all civil engineering fields.
3. ***Time period from 1980 until now:*** In this period, a very important development of earthquake engineering took place since the scientific achievements went in the following two parallel and extraordinarily important directions:
   - Development and improvement of national regulations and standards for more successful design of seismically resistant structures in seismic regions, and,
   - Development and improvement of computer software packages based on improved nonlinear analytical models through specific experimental studies.

Considering the numerous complex problems incurred in the modern earthquake engineering profession, innovative experimental studies presently represent the topmost priority [29], [42], [53].

Due to the evident complexity of nonlinear analytical modelling as well as due to the different needs and purposes of the performed analyses, the concepts of analytical modelling can be considered and classified into three general categories, Fig. 4.1.1 [29], [30], [31].

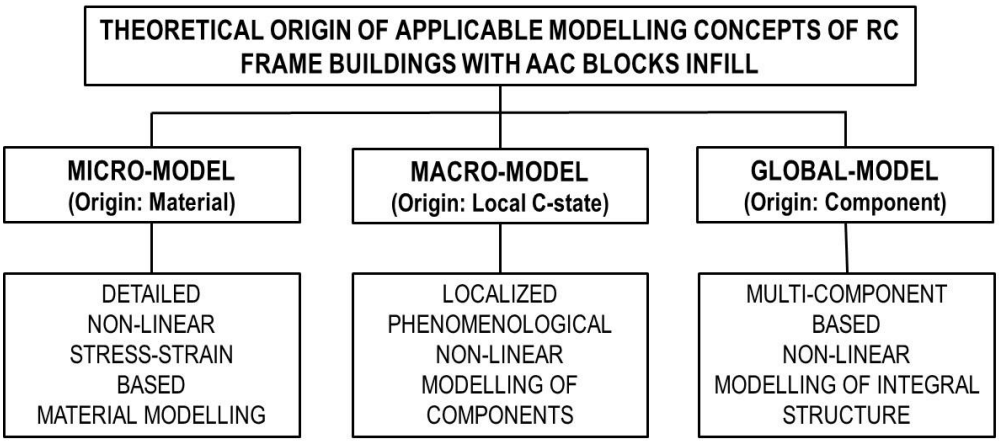

Figure 4.1.1. Theoretical origin of modelling concepts of RC frame buildings with masonry infill, elaboration based on [29], [30], [31].

a) Use of nonlinear global model: The nonlinear global analytical model is basically quite simplified for the purpose of modelling a structure. The structure is modelled by the application of nonlinear models of different constituent components. Although these models are the simplest, their application is very useful due to more successful monitoring of the correctness of the results obtained from the performed static or dynamic analyses.

b) Use of nonlinear macro model: The nonlinear macro-model of a building is somewhat more complex and represents a certain model improvement since it additionally includes some more important local nonlinear effects.

c) Use of nonlinear micro-model: The nonlinear micro-model represents the best modelling option and great achievement in the modern numerical modelling process since it is based on analytical simulation of the nonlinear stress-strain relations of the constituent structural materials. To formulate a nonlinear micro-model, specific experimental investigations are necessary. With generated experimental data, it is possible to perform needed verification of the formulated complex analytical nonlinear micro-models.

4.2 Micro-Modelling of RC Frame

Numerous analytical models have been developed to model RC frame bearing structures. Applying the general modeling concept based on the application of matrix analysis of structures, analytical macro-models and analytical global models have been formulated for

closely analysis in the domain of the linear behavior of structures. Using the results from experimental investigations of the nonlinear behavior of constituent components, advanced computer software for analysis of nonlinear static or dynamic behavior of systems has been developed. During this development process, the initial approach involving matrix analysis of structures has adequately been transformed into the application of a more general concept based on the use of the finite element method. However, to model the existing nonlinear interactive and local effects in the analysis, there has arisen a need for the development of the most advanced and detailed modelling approach. Such detailed modelling approach is referred to as micro-modelling concept. The micro-modelling approach represents a detailed nonlinear finite element strategy in which the behavior of individual materials and their interfaces is simulated explicitly, allowing the study of local phenomena such as cracking, crushing, bond-slip and stress redistribution between different components [29], [30], [31]. In contrast, macro-modelling and simplified micro-modelling approaches represent the structure or masonry wall as a homogenized continuum using equivalent mechanical properties to approximate the global behavior with less computational effort [29], [31]. Therefore, micro-modelling is particularly suitable for research studies or calibration of simplified analytical models, whereas macro-modelling remains more practical for large-scale design problems where computational efficiency is essential. To use the advanced micro-modelling concept, it is essential to define nonlinear stress-strain relations of constituent materials and to introduce analytical nonlinear simulation models [42], [52].

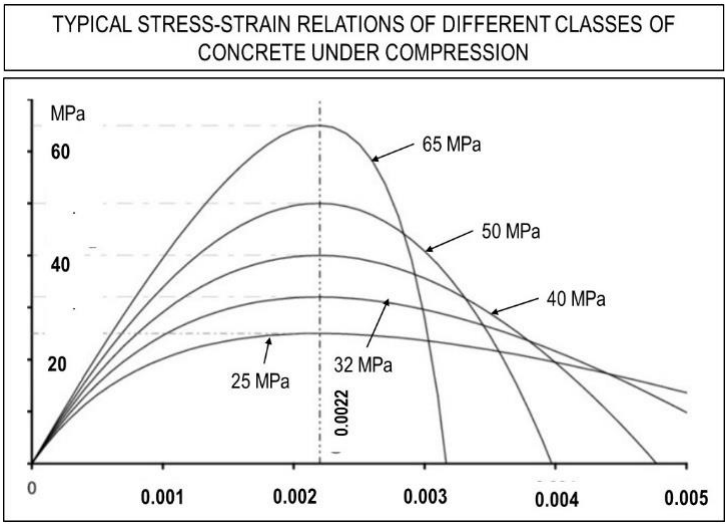

Figure 4.2.1. Typical stress-strain relations of different classes of concrete under compression, elaboration based on [42], [52].

The typical stress-strain relations of different concrete classes under uniaxial compression are presented in Fig. 4.2.1. It is evident that the experimentally defined stress-strain relations for different concrete classes are quite different. Therefore, the formulated analytical models should be based on defined realistic strength and deformability representing parameters. To derive generally applicable procedures for modelling concrete material, corresponding types of nonlinear finite elements have been developed. The specific development in this area is very

complex from the theoretical, numerical and software development aspects [42], [52]. Typical stress-strain relations of reinforcing steel are very much different from the nonlinear behavior of concrete. For example, during tension-compression cyclic loading, the nonlinear behavior of steel is almost symmetrical.

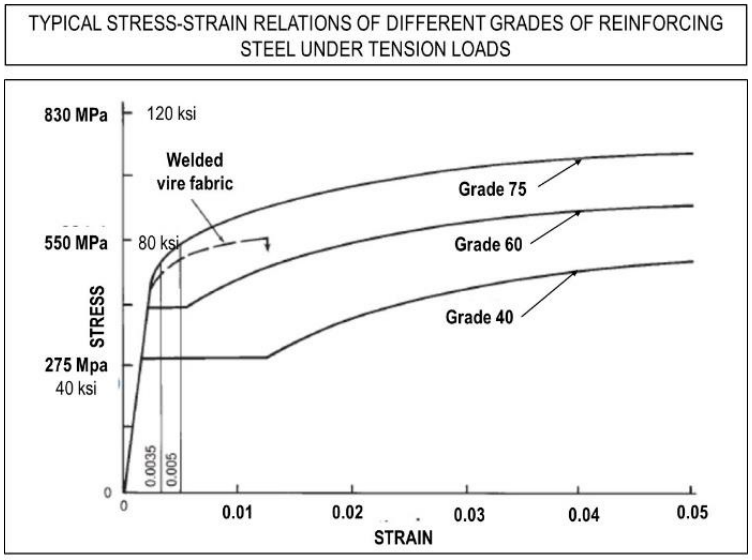

Figure 4.2.2. Typical stress-strain relations of reinforcing steel with different grades.

Modern program packages include different types of nonlinear analytical micro-models, but in all of them, adopted is identical nonlinear steel behavior under compression and tension stresses. Regarding concrete, nonlinear behavior in tension and compression is drastically different. Under the effect of compression loads, concrete exhibits high strength and stable nonlinear behavior. On the contrary, under the effect of tensile stresses, concrete exhibits far less bearing capacity, suffering cracks that have a great effect on analytical modelling Fig. 4.2.2. The finite elements for the behavior of concrete in the nonlinear domain are far more complex, and it is much more difficult to achieve convergence during advanced computer analyses [29], [31], [42].

4.3 Micro-Modelling of Masonry Infill

Analytical modelling of the complex nonlinear behavior of masonry infill (components) represents a subject of study by many experts worldwide [8], [16], [18], [53], [54]. To incorporate the effects of brick-masonry infill with its resistance degrading characteristics into the nonlinear resistance characteristics of reinforced concrete frames, there have been proposed numerous simplified nonlinear models calibrated with the results from the experimental tests [8], [53], [54], as follows: (1) nonlinear analytical models based on the concept of representing the infill panels through equivalent nonlinear diagonal struts have been widely adopted to simulate the interaction between the infill and the surrounding RC frame.; 2) a family of nonlinear models based on the application of equivalent nonlinear components of a more complex type; (3) a family of simplified nonlinear models based on the finite element concept.

In this FEM case, simplification is done with the introduced assumption of “smeared field models”, i.e., models in which the entire field is defined by averaged “smeared” characteristics; and (4) simplified models representing some related combined types.

Figure 4.3.1. Damage types of infill in building with RC frames (China 2008, Wenchuan earthquake).

However, the general nonlinear behavior of the masonry infill is characterized by much greater complexity, Fig. 4.3.1. From the presented figure, it is evident that the masonry may potentially suffer several different forms of damage like (1) Diagonal failure mode; (2) Semi-diagonal failure mode; (3) Localized failure mode, and (4) Distributed localized failure modes. Regarding the cases of existence of numerous openings for windows and doors, the behavior of the brick-masonry infills becomes even more complicated.

To achieve as realistic as possible simulation of the nonlinear behavior of a brick masonry infill, various nonlinear micro-models have been developed [29], [30], [31], [54]. To enable application of analytical micro-models, there have been formulated respective stress-strain-based analytical relations of the individual materials. Using the respective nonlinear finite elements, modelling of the specific nonlinear behavior characteristics as possible.

4.4 Micro-Modelling of AAC Infill

Modelling of the nonlinear behavior of AAC infill using the micro-modelling concept is particularly demanding because AAC is more brittle than conventional clay brick masonry and has lower tensile strength and fracture energy, while its key nonlinear mechanical parameters (such as strength, fracture energy, stiffness, and tension/compression softening) vary widely with density class, moisture content, and manufacturing technology [13], [26], [46], [48]. For example, when the infill consists of AAC masonry elements, the adopted micro-model must be capable of reproducing the representative nonlinear effects observed in practice (Fig. 4.4.1). The AAC units are discretized with sufficiently small nonlinear finite elements to capture cracking, crushing, and stiffness degradation within the AAC elements. The mortar joints are

modeled with small nonlinear elements that reflect their distinct mechanical response. To represent the interactions both between AAC elements and mortar and between the infill and the surrounding RC frame, nonlinear interface elements are assigned at the relevant contacts, enabling the simulation of bond-slip, opening/closing, shear transfer, and strength/energy degradation.

Figure 4.4.2 illustrates the uniaxial compression stress-strain responses of AAC prisms of different grades, highlighting the wide scatter in strength and deformability obtained experimentally. A similarly broad dispersion is observed for the elastic modulus (Fig. 4.4.3). Accordingly, to ensure a correct micro-model definition, the nonlinear properties of the constituent materials as well as the interface parameters are obtained experimentally and used for model calibration/validation, relying on modern and precise testing setups (Fig. 4.4.4).

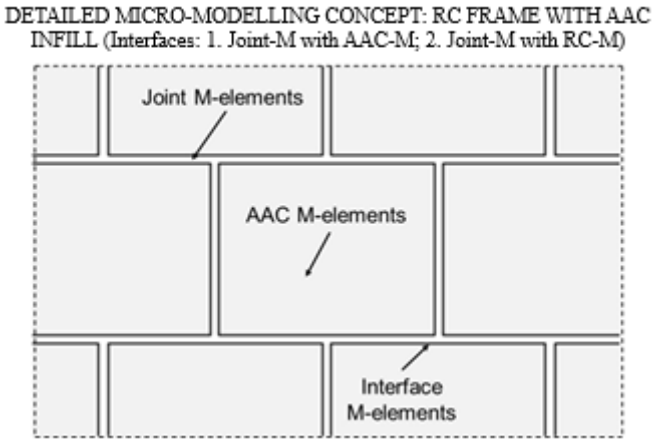

Figure 4.4.1. Detailed micro-modelling concept of RC frame with AAC infill (elaboration based on [29], [30], [31]).

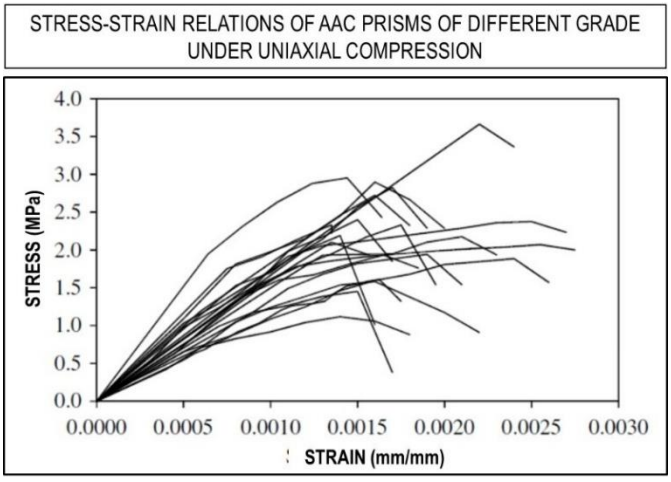

Figure 4.4.2. Stress-strain relations of AAC prisms of different grades under uniaxial compression (elaboration based on [13], [14], [48]).

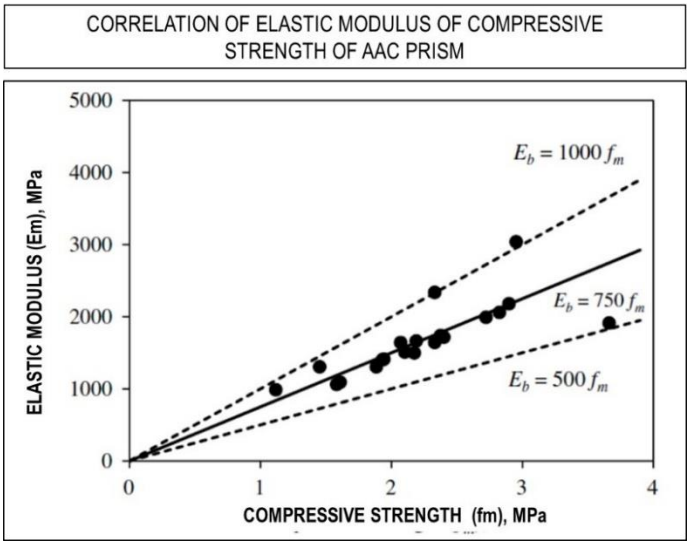

Figure 4.4.3. Correlation of elastic modulus and compressive strength of AAC prism (elaboration based on [13], [46], [48]).

Figure 4.4.4. Laboratory equipment for testing of stress-strain relations of structural materials (concrete, steel, AAC elements, AAC panels, illustration based on [13], [46], [48]).

4.5 Micro-Modelling of AAC Joints

The material used for forming AAC joints, typically thin-layer mortar or adhesive, often exhibits nonlinear mechanical characteristics that differ significantly from those of the AAC elements themselves. Its mechanical response depends on the joint thickness, mortar type, surface preparation, and curing conditions. These joints act as localized zones of weakness that strongly influence global stiffness, cracking pattern, and load transfer between AAC elements [13], [14], [19].

In micro-modelling, the mechanical properties of the joint material compressive strength, tensile strength, elastic modulus, and fracture energy are obtained through specific experimental tests on small specimens or prism assemblies, in accordance with EN 1052-1 and EN 12602 [46]. The stress-strain law for the joint material is typically defined by a nonlinear curve that accounts for the progressive degradation under tensile and compressive loads.

For reliable simulation, finite elements representing the mortar joints must reproduce both cohesive behavior and the potential for localized failure. In practice, these are modeled as separate continuum elements or as interface elements with traction-separation laws calibrated to experimental data [29], [30], [31]. This allows the model to capture the initiation and propagation of cracks, bond-slip effects, and strength degradation under cyclic or monotonic loading conditions.

To improve the understanding of the modelling strategy, schematic representations of AAC joints and interface elements are provided in Figures 4.5.1 and 4.6.1. Figure 4.5.1 shows the detailed representation of a typical AAC joint, where thin mortar layers are modeled as either continuum or nonlinear interface elements between the AAC elements. The nonlinear properties of these layers, including stiffness degradation, tensile cracking, and shear slip, are calibrated using the results of experimental tests [13], [14], [19], [46].

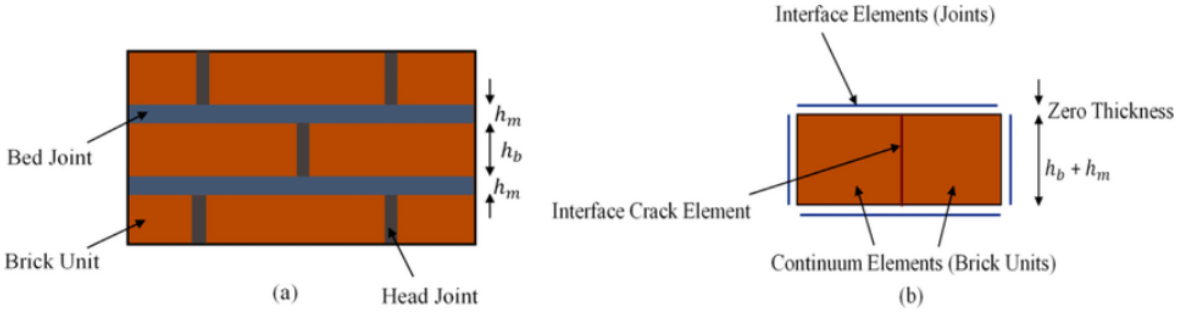

Figure 4.5.1. Schematic representation of AAC element joint micro-modelling; a) Actual AAC masonry specimen used for calibration of joint parameters; b) Idealized micro-modeling approach representing thin mortar layers as nonlinear interface elements.

In DIANA FEA, these joints can be represented using interface elements such as 8-node Interface or 6-node Line Interface (for 2D analyses), which allow separate definition of normal and shear behavior through traction-separation laws. The constitutive relationships can be defined as softening in tension and plasticity or frictional behavior in shear, following Mohr-Coulomb or Total Strain Crack (TSC) models [41]. Figure 4.6.1 illustrates the layout of the adopted interface configuration for AAC infill micro-modelling, including both AAC-mortar and mortar-RC contacts [29], [31], [54].

4.6 Micro-Modelling of AAC Interfaces

During the nonlinear response of AAC infilled RC frames subjected to significant lateral or cyclic loads, partial debonding and sliding can occur at the contact surfaces between different materials. These interactions, particularly between AAC elements, mortar joints, and surrounding RC frame members are critical to the overall structural behavior. To realistically simulate these effects, nonlinear interface micro-elements are introduced into the model [29], [31], [54].

Two main types of interface elements are typically defined: (1) AAC-mortar interfaces, representing the contact between AAC elements and joint material, which govern internal cohesion and cracking inside the infill panel; and (2) mortar-concrete interfaces, representing the contact between the infill panel and the RC frame, where separation or sliding under cyclic loading can lead to stiffness degradation and pinching in the global load-displacement response (Fig. 4.6.1).

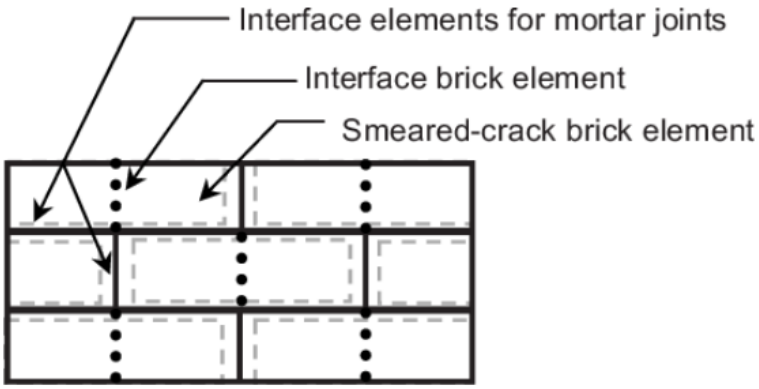

Figure 4.6.1. Finite element discretization of masonry infill with interface elements *(adapted for AAC from [54]; see also [29], [31]).*

These interface elements are formulated using traction-separation laws or Coulomb friction-based models that include both normal and tangential behaviors. Under increasing load, they allow for progressive softening in tension (opening) and reduction of shear resistance (sliding), reproducing realistic detachment and energy dissipation mechanisms.

The advantage of such detailed nonlinear interface modelling lies in its ability to reproduce experimentally observed local damage mechanisms, such as separation along frame-infill boundaries, diagonal cracking, and partial crushing near corners [14], [54]. This leads to a highly realistic simulation of the composite behavior of RC frames with AAC infill. However, the modelling process becomes significantly more complex when openings for doors and windows are included, since these create irregular stress distributions and concentration zones that require refined meshing and additional interface calibration [8], [19], [26].

5 CHAPTER 5 - NUMERICAL SIMULATION OF THE EXPERIMENTAL RESULTS FOR RC BARE FRAME

Presented in the previous chapter (Chapter 4) were the results obtained from the performed laboratory testing of the constructed large-scale models representing RC frames without and with AAC infill. The realized experimental investigations enabled the obtaining of fundamental knowledge on the real nonlinear (hysteretic) behavior of the tested models up to deep nonlinearity. Chapter 5 contains the results from the realized complementary analytical study carried out based on experimental results recorded during the testing of the experimental models M1-A and M1-B, representing an RC bare frame. To enable the numerical representation of the structural response under increasing lateral displacement, the monotonic loading type was selected as a representative simulation scenario, intended to replicate the gradual nonlinear behavior of the frame under one-directional loading. Specifically, the experimental test of the prototype model M1-B tested under the effect of vertical loads and monotonic loading was used for the analytical studies presented in this chapter. The results from the realized analytical studies carried out are presented in five successive sub-chapters. The first main chapter 5.1 contains the main considerations regarding the existing research gap that directly implicates the evident importance of these studies and then continues with the corresponding details for the explanation of the formulated advanced modeling concept. Part 5.1 shows the analytical studies directed to experimental validation of the formulated simplified micro-analytical model since an identical vertical load of N1 = 62.5 kN was during both experimental and analytical studies. Parts 5.2 and 5.3 show the obtained analytical results obtained under simulated increased vertical loads to N2 = 125.0 kN and to N3 = 280.0 kN, based on implementation of experimentally verified analytical model (part 5.1). The two additional analytical studies represent the two specific and very successful “analytical experiments” since the applied detailed analytical model was fully verified with the results from the performed experimental tests. The formulated experimentally verified analytical models are of high importance because numerous innovative projects and other specific studies can be successfully realized with their application. Finally, in part 5.4 briefly are summarized the major findings are from the conducted micro-modeling study of the tested model M1-B representing RC bare frame.

5.1 Parametric study - RC bare frame Model (M1-B)

5.1.1 Importance of the Conducted Analytical Study

In the past, many studies were dedicated to studies of the effect of infill on behavior of framed building structures. The most frequently considered in the studies was a brick infill or a similar infill type such as, for example, hollow ceramic elements of different dimensions. During the last years, the AAC infill has been most frequently applied in frame structures in the form of constructed masonry with AAC elements of different sizes. Due to evidently different mechanical characteristics of the masonry constructed of AAC elements, there is an evident

that needs to address interactive effects. The present extensive experimental and analytical studies were aimed at providing a contribution to the following two important research domains: (1) To obtain reliable experimental results with the experimental tests on large-scale prototype models of RC frames without and with AAC infill, and (2) To use the obtained experimental results for experimental verification of the formulated advanced nonlinear micro-analytical models.

The studies presented in this chapter were dedicated to formulation, verification and advanced research application of the developed simplified micro-model of the tested RC bare frame (M1-B).

5.1.2 Introduction to Parametric Study

The numerical parametric study was conducted to examine the influence of different axial load levels on the nonlinear lateral behavior of the RC bare frame. The main objective of this study was to understand how varying axial compression in the columns affects the overall stiffness, strength, and ductility of the frame. Such evaluation is of great importance because in real multistory structures, the axial load ratio in columns varies significantly between the upper and lower stories, directly influencing the seismic performance and the ability of the frame to dissipate energy.

All other parameters, including geometry, material properties, and boundary conditions, were kept constant to ensure that the axial load remained the only variable affecting the response. The nonlinear static analyses were performed using DIANA FEA with the same numerical modeling approach presented in previous sections, ensuring consistency between the experimental and analytical evaluations.

5.1.3 Simulation of RC bare frame model M1-B under Three Axial Load Levels

During conducted research activities in the past, sufficient study attention was not paid to study of the effect of dynamically induced different levels of axial forces in RC columns directly producing important modifications of their nonlinear behavior. For example, during intensive seismic response, variations of axial forces are possible in many cases. Such variations may reach quite big differences of 80% to 100% or more. The variation of the axial forces induces important fluctuation (change) of the moment bearing capacity of the affected RC cross-sections.

To investigate the effect of the changed axial forces on the nonlinear behavior of RC bare frames, a corresponding experimental-analytical research program was realized as follows:

Firstly, conducted was targeted experimental testing of the constructed large-scale RC bare frame model under simulated interactive effects of vertical loads of N1 = 62.5 kN in both columns and gradually increased monotonic loading (M1-B).

To study the effect of different axial load levels on nonlinear behavior of the RC frame, the analytical study was performed for two additional levels of axial loads defined as N2 = 125.0 kN and N3 = 280.0 kN. These studies were only possible by assured application of the previously formulated analytical micro-model. The completed study of nonlinear behavior of the RC bare frame under three levels of axial loads, N1, N2 and N3, were of great importance for study of the effects of the AAC infill in the case of the same loading conditions. Specifically, in the next Chapter 6, presented results obtained from the conducted experimental-analytical study of nonlinear behavior of RC bare frame, carried out with simulated three levels of axial loads N1, N2 and N3.

Based on the research results obtained from studied identical RC frames without and with an AAC infill and consequently for simulated three identical levels of axial loads, the effects of the AAC infill on the nonlinear behavior of RC frames were very successfully identified, evaluated and presented.

The selected axial load levels of 62.5 kN, 125 kN, and 280 kN correspond approximately to 5%, 10%, and 25% of the total axial load-bearing capacity of the column section, which was calculated as 1.22 MN for a 25×25 cm column reinforced with 4Ø12 + 4Ø10 longitudinal bars and concrete of class C25/30. The axial load-bearing capacity of the column was determined through a standard analytical approach based on the material properties and cross-sectional characteristics. The calculation considered the combined contribution of concrete and longitudinal reinforcement to axial resistance, following the fundamental design expressions prescribed in Eurocode 2. This provided a realistic estimation of the total column capacity, which served as a reference for defining the three representative axial load levels used in parametric analysis. These load levels were intentionally chosen to represent typical ranges of axial load ratios in RC frames and are summarized in Table 5.1.1, which presents the corresponding values expressed as a percentage of the total column capacity.

Table 5.1.1. Axial load levels used in parametric study

Axial Load Level	**Axial Load (kN)**	**Percentage of Column Axial Capacity (1.22 MN)**
N_1	62.5	5.1 %
N_2	125	10.2 %
N_3	280	22.95 %

These load levels were intentionally chosen to represent typical ranges of axial load ratios in RC frames:

- *Low load (62.5 kN)* - corresponding to lightly compressed columns or upper stories,
- *Medium load (125 kN)* - representing average working conditions,

- *High load (280 kN)* - representing a heavily compressed column zone near lower stories.

This range allows the assessment of both beneficial and adverse effects of axial compression on the frame response. All other mechanical parameters, modeling assumptions, and loading conditions were kept unchanged to ensure that the obtained differences in structural performance are solely attributed to the variation in axial load.

5.1.4 Geometry of the Bare RC Frame (M1-B)

A detailed description of the geometrical characteristics of the models M1-A and M1-B is given in the previous Chapter 3, specifically in part 3.3.1. Using the detailed data on the real geometrical characteristics, the applied concept of the experimental test, the procedure of application of the interactive vertical and horizontal load of the type of monotonic loading as well as the data on the defined characteristics of the materials, there were created the main pre-conditions for the formulation of an advanced nonlinear micro-model (Part 5.1.4), which was applied in the realization of the extensive analytical studies presented in this chapter.

5.1.5 Simplified Micro-Model of Bare RC Frame (M1-B)

To create optimal conditions for formulation of representative simplified micro-model for the tested RC bare frame, several optimal modeling assumptions were identified and introduced. The corresponding conceptual details used as the basis for the formulation of the applied simplified micro-analytical model are briefly explained to enable an adequate interpretation of the results obtained from analytical studies.

i. ***Concept of simplified micro-model:*** To provide the necessary accuracy of the formulated simplified micro-model, the concept of rational simplification was adopted but with assured conditions for close simulation of the experimentally verified reality. To provide the necessary accuracy, the advanced analytical approach based on the application of the modern concept of the finite element method (FEM method) was selected. In that way, the general conditions were created for improved accuracy through the increase of the number of finite elements, i.e., reduction of their dimensions. To provide conditions for simulation of the nonlinear behavior of the tested model, introduced were finite elements adapted for successful simulation of the nonlinear behavior of the corresponding materials and other existing nonlinear phenomena. To provide conditions for detailed nonlinear behavior simulation of different materials, selected were nonlinear finite elements formulated based on the fundamental nonlinear stress-strain relationships. To provide conditions for the application of the intended simplified micro-modeling concept, the well-known advanced software DIANA [40] was used. This software is developed for solving various complex problems of similar types and represents one of the most powerful software worldwide today. The numerical simulations were carried out with applied

interaction loads completely spaced in two-dimensional (2D) planes. For these reasons and particularly to reduce the complexity of the model and necessary computation time, for the needs of the present analytical studies, the representative 2D simplified micro-model was formulated. The formulated 2D simplified micro-model was provided with advanced capability to realistically simulate complex nonlinear interactive effects with considered in modeling representative effects of all the existing materials, elements and components.

ii. ***Modelling of concrete elements in the 2D micro-model:*** Contribution of the various concrete elements included in tested RC model, Fig. 5.1.1, considered are in the formulated 2D micro-model all constituent structural components with their respective thicknesses as follows: (1) RC Foundation segment with a thickness of 550 mm; (2) RC columns with a thickness of 250 mm; (3) RC beam with a thickness of 150 mm; (4) RC plate with a thickness of 550 mm; (5) Steel plate with RC bottom layer with a thickness of 150 mm;

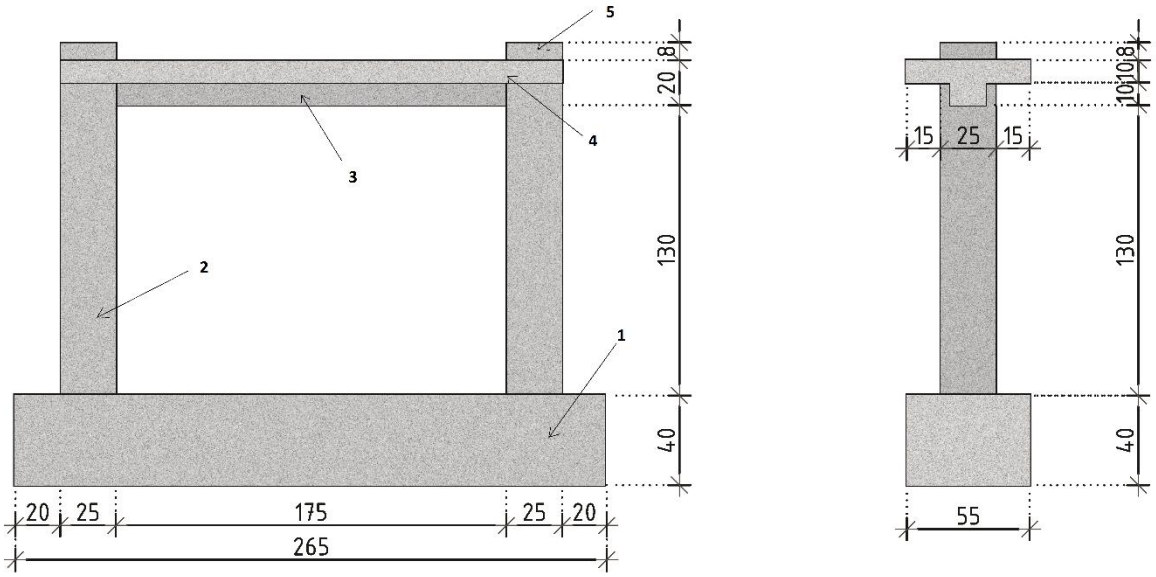

Figure 5.1.1. Concept of formulated nonlinear analytical model of the tested large-scale prototype model (M1-B) representing RC bare frame.

iii. ***Modeling of reinforcing bars in 2D micro model:*** (1) The reinforcing bars in the RC footing were modeled with upper and lower single bar-lines including also the existing steel hoops. The cross-section area of the modeled, representative "single" reinforcing bar was calculated as the sum of the cross-section areas of all the projected reinforcing bars along the respective single line; (2) The reinforcing bars in both RC columns were modeled with three parallel representative reinforcement lines. In the cross-section, the columns were reinforced by a regularly distributed total of 8ϕ10 mm longitudinal bars. Accordingly, the alternative reinforcement on the left and the right side included an equivalent total area corresponding to 3ϕ10 mm, whereas the modeled reinforcement in the middle of the cross-section included an area of 2ϕ10 mm. The existing stirrups were modeled in compliance with their number and position. (3) The reinforcing bars

in the RC floor beam were modeled by respective reinforcement in the upper and the lower zone, with a cross-section defined in accordance with the reinforcement. In addition, the stirrups were modeled at the actual locations and with the actual cross-sections.

iv. ***Modeling of vertical and horizontal loading segments:*** To provide conditions for correct simulation of the applied vertical loads, corresponding RC segments with end steel plates were included over the columns of the simplified micro-model. In that way, the applied loads were realistically distributed analogously to the system applied in the experimental test. Analogously, to provide conditions for simulation of the distributed horizontal load, an RC segment with end steel plate was included in the analytical model.

v. ***The concept of the created FEM mesh:*** While creating the final appearance of the applied FEM mesh, special attention was paid to enabling a needed accuracy and on achieving execution economy by shortening the computer time to acceptable frames. As is evident from the formulated analytical model, the size of the finite elements by which the concrete material is modeled is quite small and is of the order of 4 x 4 cm. With the adopted quite small finite elements, satisfying accuracy of the developed model was provided.

vi. ***Modeling boundary conditions:*** In the formulation of the FE model, the boundary conditions were specified in compliance with the real fixed support of the RC footing of the model on the rigid laboratory experimental frame. Therefore, fixed boundary conditions were simulated for all nodal points in the base of the formulated model.

vii. ***Concept of simulated loading patterns:*** Analogously to the experimental test of model M1-B, in the first phase, vertical load to the specified amount of N1 = 62.5 kN was gradually applied on each of both RC columns. This process was realized by an incremental increase of the loads. In the second phase, loading with horizontal load was carried out. The loading process was realized by application of small incremental deformations to provide conditions for required convergence of the final solutions.

viii. ***Possibility for model upgrading to simulate an AAC infill:*** During the formulation of the analytical model for simulation of the behavior for the tested model M1-B representing an RC bare frame, the necessary conditions were created for its upgrading and simulation of the nonlinear behavior of the tested model M2-B representing the RC bare frame.

ix. ***Material FEM elements and modeling parameters:*** Selection of the appropriate FEM models of different materials and/or other, present, specific nonlinear behavior sources was adapted to the available modeling options in the DIANA computer software [40], selected as an appropriate and advanced option for solving complex problems of this type. Extended modelling experience was also of great help [4-47].

During analytical modeling of the RC bare frame, model M1-B, representative options of finite elements defined with a corresponding set of representative input parameters were selected. The following parameters for the concrete and steel were applied:

(1) FE type for concrete: For modeling of concrete, the Q8MEM finite element was selected, which is generally typical for the formulation of the 2D analytical models. It represents a four-node quadrilateral isoparametric element having 8 degrees-of-freedom representing translational displacements Ux and Uy of each node. It includes linear interpolation functions and 2 x 2 Gauss integration points. In the FE simulation study, concrete material was characterized with the following representative input parameters: Young's modulus 21000 N/mm^2; Poisson's ratio 0.2; Tensile strength 2.0 N/mm2; Mode-I tensile fracture energy 0.169 N/mm; Compressive strength 25 N/mm^2. The quality of the concrete was verified by testing sample cubes proportioned 20x20x20 cm.

(2) FE type for steel: For modeling of steel, an option simulating embedded longitudinal bars connected to mother concrete elements was provided in the DIANA computer software. Based on test results, for the steel material, the following representative input parameters were considered: Young's modulus 200000 N/mm^2; plastic hardening total strain-yield stress; and total strain-yield stress defined with four (strain, stress N/mm^2) points: P_0: 0., 0.; P_1: 0.00119, 240; P_2: 0.01, 280; P_3: 0.1, 280.

5.2 Low Axial Load N1: Validation of Nonlinear Micro-Model Based on Test Results of RC Bare Frame (M1-B)

Fig. 5.2.1 shows the developed nonlinear model of the tested RC Bare Frame used for analysis of its response under simulated level of axial load N1 = 62.5 kN and monotonic loading. Following the performed nonlinear analysis by application of the DIANA computer software, in accordance with the corresponding specified input data, a complete solution was obtained in the form of large files.

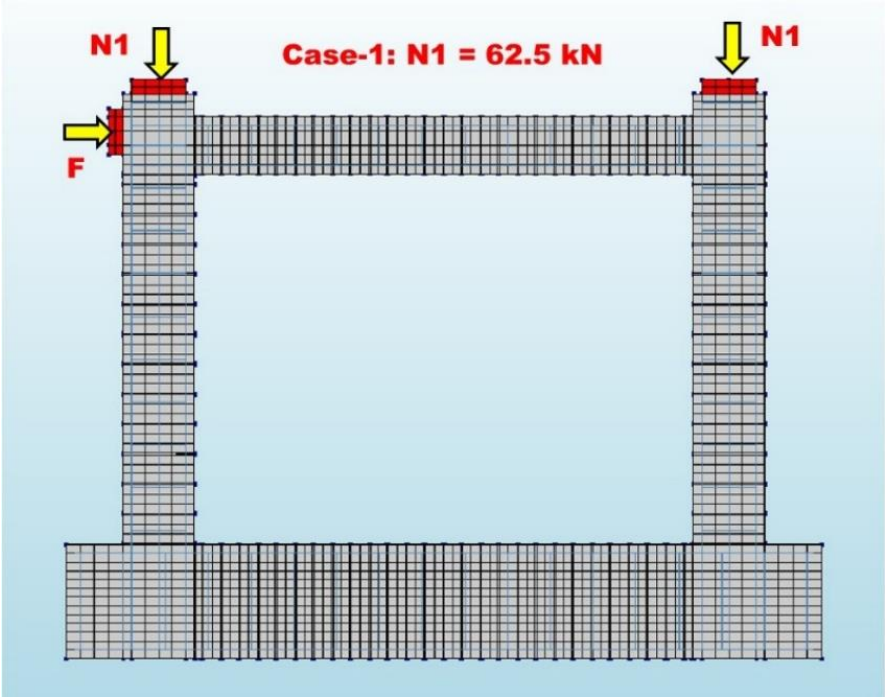

Figure 5.2.1 Developed nonlinear model of RC Bare Frame model M1-B under axial load N1=62.5 kN and monotonic loading.

One part of the files contains the results from the solution in the form of numerical values. The second part of the files contains a graphic presentation of the corresponding results in the form of individual video presentations of the corresponding parameters, whose values are marked with a corresponding colour.

The video presentations were made to enable monitoring of the change of the computed physical quantities of the simulated nonlinear response.

In the case of this specific analysis, a selection of the characteristic time from the video presentations was made and the representative states (images) were presented in a total of 32 electronic files, Table 5.2.1.

The stated table that presents the analytical phase A1-1 shows the computed nonlinear response of the tested RC bare frame (M1-B) under simulated vertical load N1 = 62.5 kN and monotonic loading (Chapter 5.1).

Table 5.2.1. list of included relevant data like for example: (1) mesh of the micro-model (file - 0); (2) six characteristic distributions of displacements (files 1 - 6); (3) six characteristic distributions of Cauchy total stresses (files 7 - 12); (4) six characteristic distributions of total strains (file 13 - 18); (5) two characteristic distributions of propagation of cracks in concrete (files 19 - 20); (6) six characteristic distributions of stresses in reinforcement (files 21 -26) and (7) six characteristic distributions of total strains in reinforcement (files 27 - 32).

To get an insight into the most characteristic results, presented in this text that refers to part 5.2, are a total of 10 selected characteristic figures indicated as Fig. 5.2.1, Fig. 5.2.1 through Fig. 5.2.9. in the stated basic Table 5.2.1 showing the analytical phase A1-1. In all the included figures, the obtained characteristic results are very clearly presented.

For example, Fig. 5.2.1, Fig. 5.2.2 and Fig. 5.2.3 show the distributions of displacements DX(mm), DY(mm) and DXY(mm) for the respective computation time steps. From the stated figures, displacement DX is the most pronounced (Fig. 5.2.1), displacement DY is smaller (Fig. 5.2.2), while displacement DXY is quite expressed, Fig. 5.2.3.

Fig. 5.2.4 and Fig. 5.2.5 show the computed Cauchy total stresses SXX and SYY, respectively. The values of both total stresses are characterized by the occurrence of two different zones (compression and tension), however, in both cases, compressive stresses dominate.

Fig. 5.2.6 and Fig. 5.2.7 show the predicted distributions of cracks in concrete for the solution steps 30 and 130, respectively. In Fig. 5.2.8, the zones of occurred cracks are enlarged since they correspond to higher values of induced displacements. However, in both cases, the occurred distributions of cracks in concrete are generally of a local character as it was recorded in the conducted experimental test.

Fig. 5.2.9 and Fig. 5.2.10 showcase the computed distributions of reinforcement stresses SXX and SYY, respectively for the same solution step 130.

From the stated figures, it is evident that pronounced compressive and tensile stresses occur in the reinforcement. At segments where cracks occur in concrete, the tensile stresses are transferred to the reinforcement bars.

Fig. 5.2.11 comparatively shows the nonlinear force - deformation relationships obtained by experimental test and FE simulation by application of the formulated nonlinear micro-model. Considering the great complexity of the analytical simulation, it can be concluded that the analytical and the experimental curves show a very good agreement although, in certain zones, there is a certain mutual deviation. However, the occurred difference between the values of the maximum restoring force obtained experimentally and analytically is minimal and amounts to only 1.8%.

The value of the maximum resisting force, i.e., the bearing capacity of the RC bare frame under horizontal loads represents one of the most important parameters. Besides this, the nonlinear force-deformation relationship obtained by applying the developed model is generally in good correlation with the experimentally defined envelope curve by means of the experimental test on the model M1-B.

Finally, the results obtained from the realized analytical study enabled direct verification of the developed model of a reinforced concrete under vertical and horizontal loads.

Considering the realized general benefits offered by the formulated detailed and verified micro-model, an opportunity is opened for realization of new analytical research activity that is of very high scientific importance.

Consequently, presented further in this chapter are the results obtained from the performed two specific additional analytical studies with simulation of higher levels (N2 and N3) of vertical loads. The results obtained from the analytical study, presented in parts 5.2 and 5.3, are generally of the highest importance for modern structural and seismic engineering.

Table 5.2.1. Analytical phase A1-1: Computed nonlinear response of the tested RC bare frame model (M1-B) under vertical load N1=62.5 kN and monotonic-loading (Ch. 5.1)

ANALYTICAL PHASE A1-1: **Study of capability of formulated model based on results obtained from tested RC Bare Frame (M1-B) simulating vertical load N1=62.5 kN and monotonic loading (Ch. 5.1)**					
File	Presented FEM parameter	Notation	Load step	E-Plotted	Shown/Fig.
0	Mesh of micro-model	Geometry	-	yes	+ / 5.1.0.
1	Displacement-x (mm)	TDtX	30	yes	
2	Displacement-x (mm)	TDtX	130	yes	+ / 5.1.1.
3	Displacement-y (mm)	TDtY	30	yes	
4	Displacement-y (mm)	TDtY	130	yes	+ / 5.1.2.
5	Displacement-xy (mm)	TDtXY	30	yes	
6	Displacement-xy (mm)	TDtXY	130	yes	+ / 5.1.3.
7	Cauchy total stresses-x (N/mm^2)	SXX	30	yes	
8	Cauchy total stresses-x (N/mm^2)	SXX	130	yes	+ / 5.1.4.
9	Cauchy total stresses-y (N/mm^2)	SYY	30	yes	
10	Cauchy total stresses-y (N/mm^2)	SYY	130	yes	+ / 5.1.5.
11	Cauchy total stresses-xy (N/mm^2)	SXY	30	yes	
12	Cauchy total stresses-xy (N/mm^2)	SXY	130	yes	
13	Total strains-x (mm/mm)	EXX	30	yes	
14	Total strains-x (mm/mm)	EXX	130	yes	
15	Total strains-y (mm/mm)	EYY	30	yes	
16	Total strains-y (mm/mm)	EYY	130	yes	
17	Total strains-xy (mm/mm)	EXY	30	yes	
18	Total strains-xy (mm/mm)	EXY	130	yes	
19	Crack widths: plane princ./comp. (mm)	Ecw	30	yes	+ / 5.1.6.
20	Crack widths: plane princ./comp. (mm)	Ecw	130	yes	+ / 5.1.7.
21	Reinforcement CT stresses-x (N/mm^2)	SXX	30	yes	
22	Reinforcement CT stresses-x (N/mm^2)	SXX	130	yes	+ / 5.1.8.
23	Reinforcement CT stresses-y (N/mm^2)	SYY	30	yes	
24	Reinforcement CT stresses-y (N/mm^2)	SYY	130	yes	+ / 5.1.9.
25	Reinforcement CT stresses-xy (N/mm^2)	SXY	30	yes	
26	Reinforcement CT stresses-xy (N/mm^2)	SXY	130	yes	
27	Reinforcement of total strain-x (mm/mm)	EXX	30	yes	
28	Reinforcement of total strain-x (mm/mm)	EXX	130	yes	
29	Reinforcement total strain-y (mm/mm)	EYY	30	yes	
30	Reinforcement total strain-y (mm/mm)	EYY	130	yes	
31	Reinforcement total strain-xy (mm/mm)	EXY	30	yes	
32	Reinforcement total strain-xy (mm/mm)	EXY	130	yes	
Number of plotted figures from analytical study using formulated micro-model					32
Number of figures presented showing representative results					10

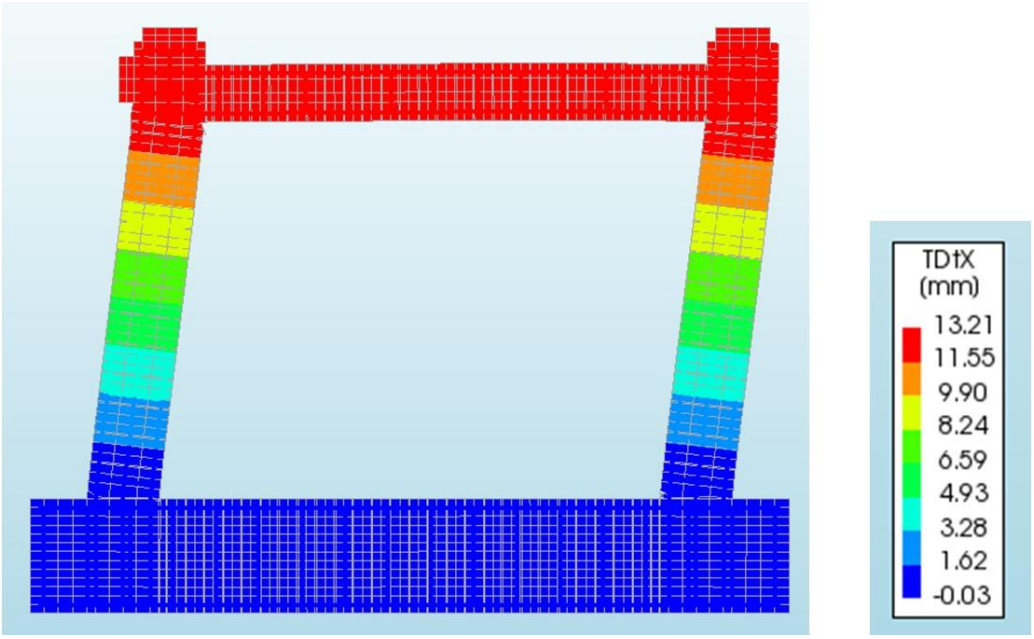

Figure 5.2.2. Response of RC Bare Frame M1-B under axial load N1=62.5 kN and monotonic loading: Computed displacements DX for loading step 130.

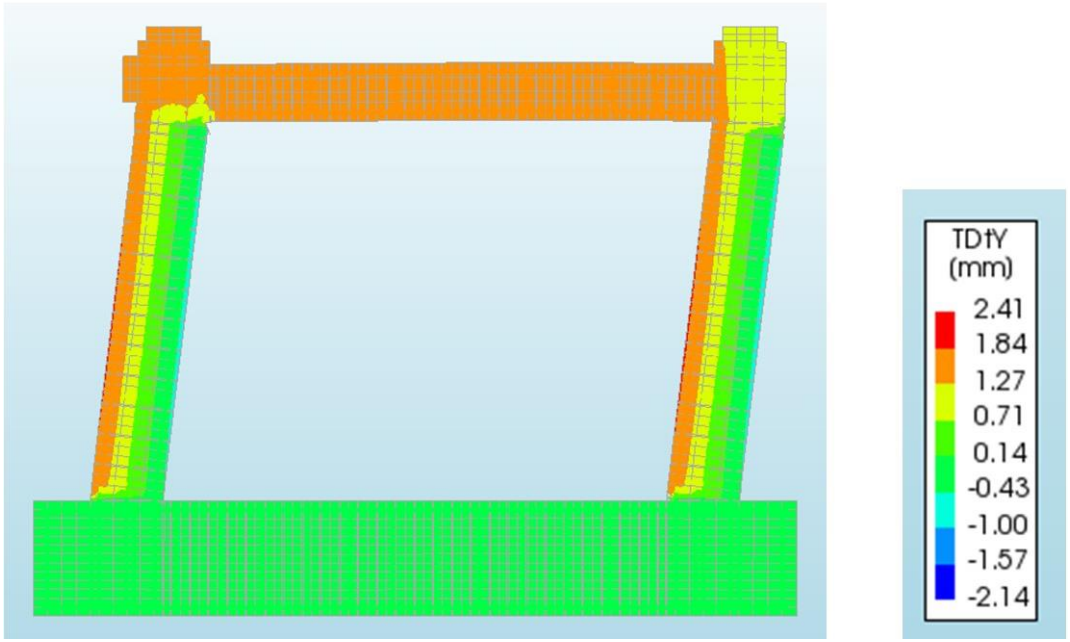

Figure 5.2.3. Response of RC Bare Frame model M1-B under axial load N1=62.5 kN and monotonic loading: Computed displacements DY for loading step 130.

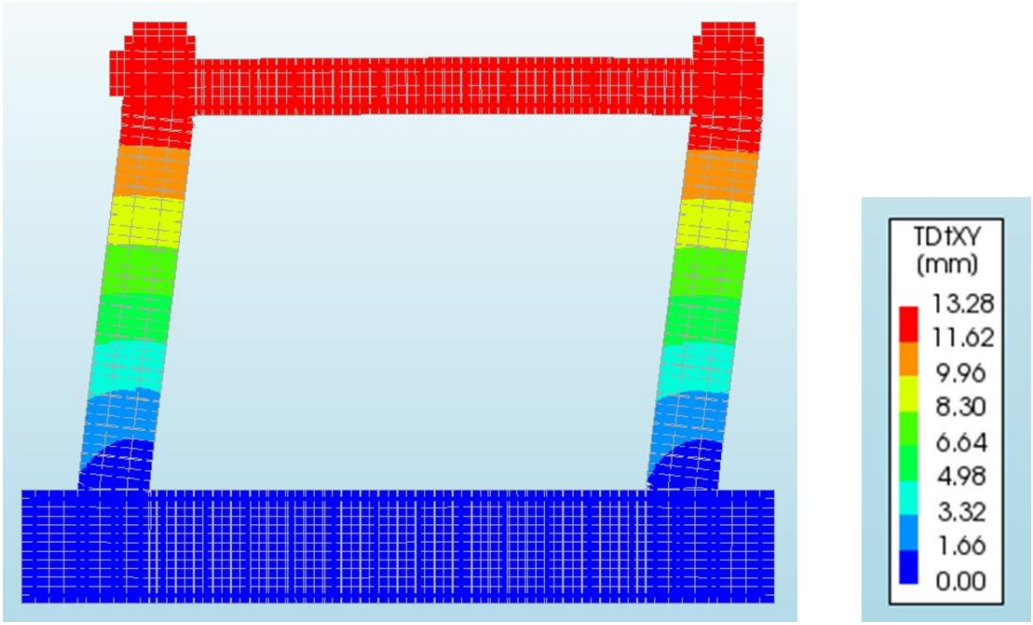

Figure 5.2.4. Response of RC Bare Frame model M1-B under axial load N1=62.5 kN and monotonic loading: Computed displacements DXY for loading step 130.

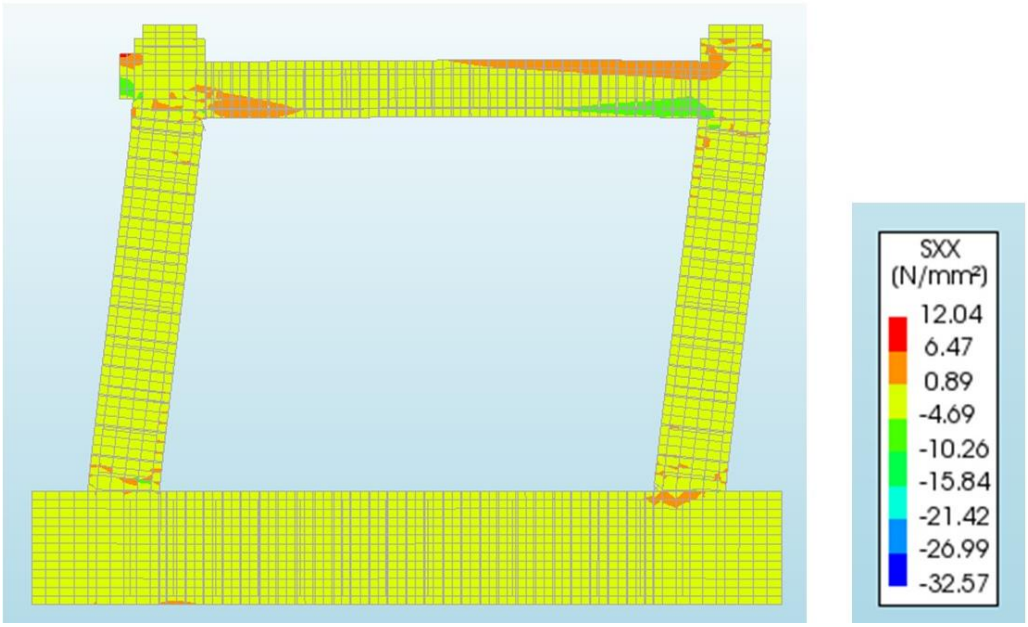

Figure 5.2.5. Response of RC Bare Frame model M1-B under axial load N1=62.5 kN and monotonic loading: Computed Cauchy total stresses SXX for loading step 130.

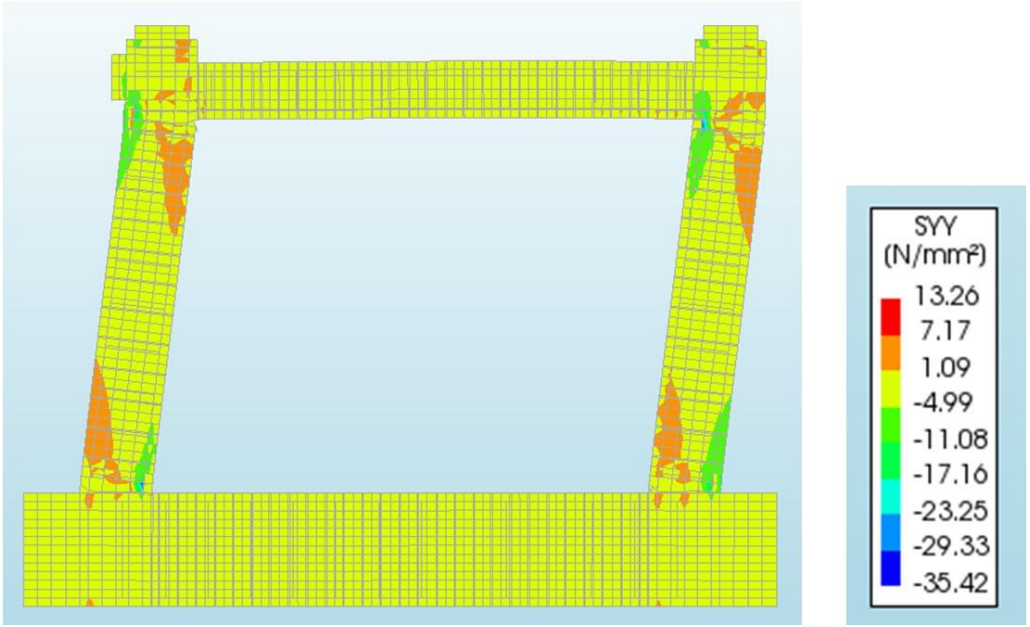

Figure 5.2.6. Response of RC Bare Frame model M1-B under axial load N1=62.5 kN and monotonic loading: Computed Cauchy total stresses SYY for loading step 130.

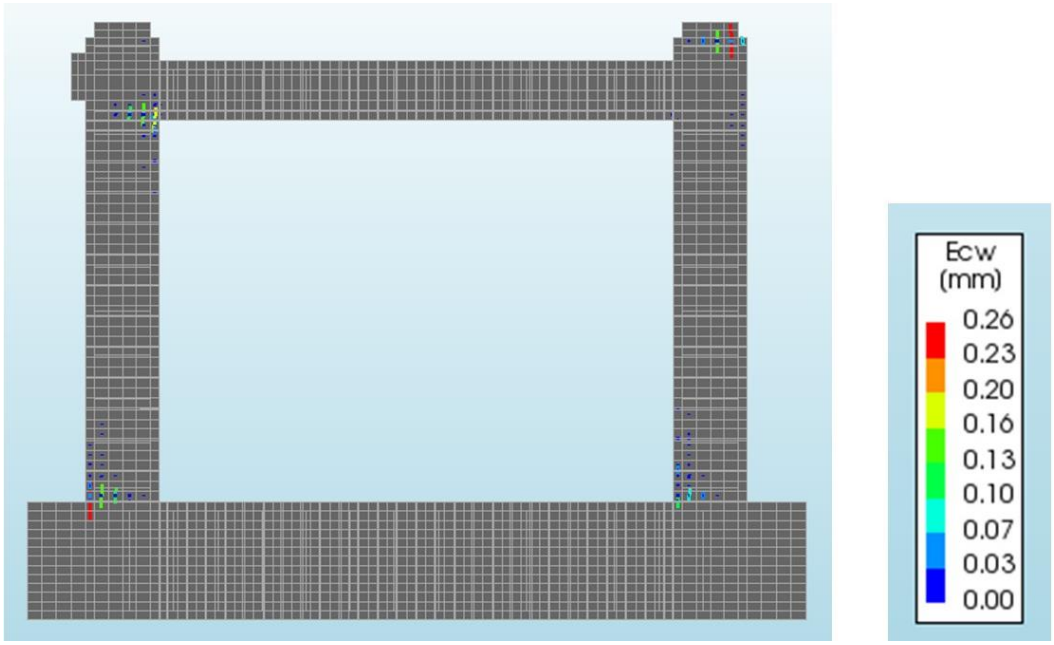

Figure 5.2.7. Response of RC Bare Frame model M1-B under axial load N1=62.5 kN and monotonic loading: Computed crack distribution for loading step 30.

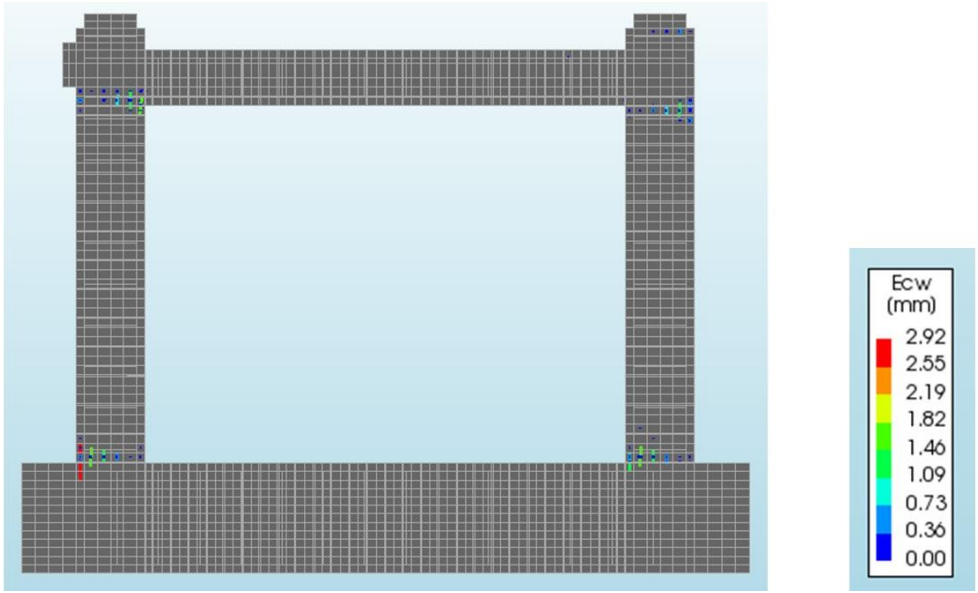

Figure 5.2.8. Response of RC Bare Frame model M1-B under axial load N1=62.5 kN and monotonic loading: Computed crack distribution for loading step 130.

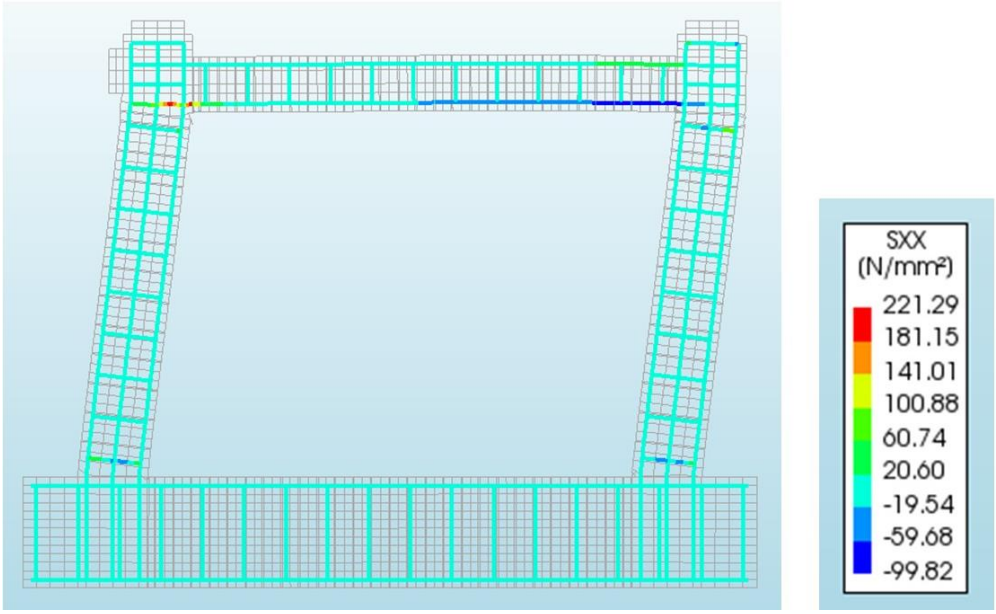

Figure 5.2.9. Response of RC Bare Frame model M1-B under axial load N1=62.5 kN and monotonic loading: Computed reinforcement stresses SXX for loading step 130.

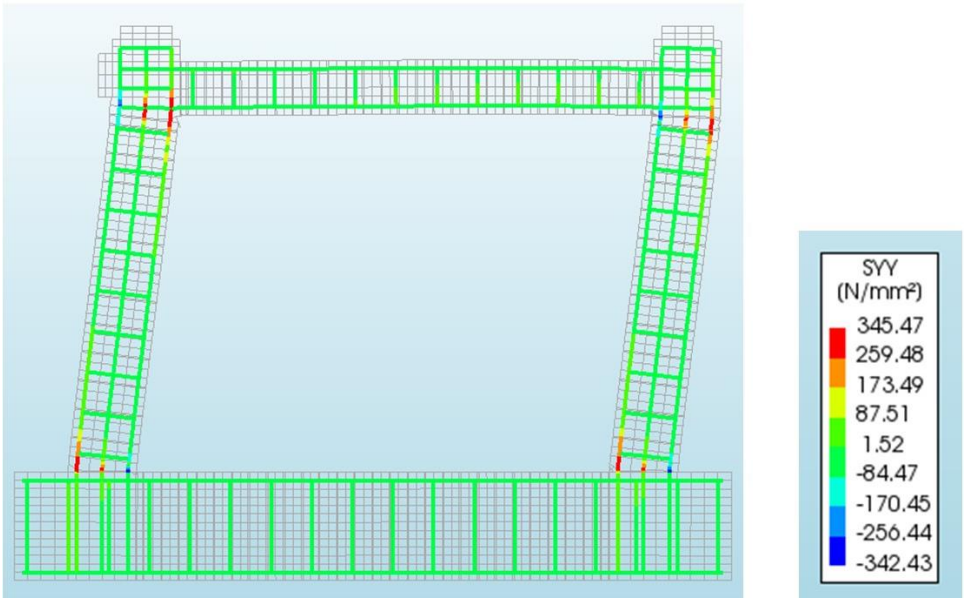

Figure 5.2.10. Response of RC Bare Frame model M1-B under axial load N1=62.5 kN and monotonic loading: Computed reinforcement stresses SYY for loading step 130.

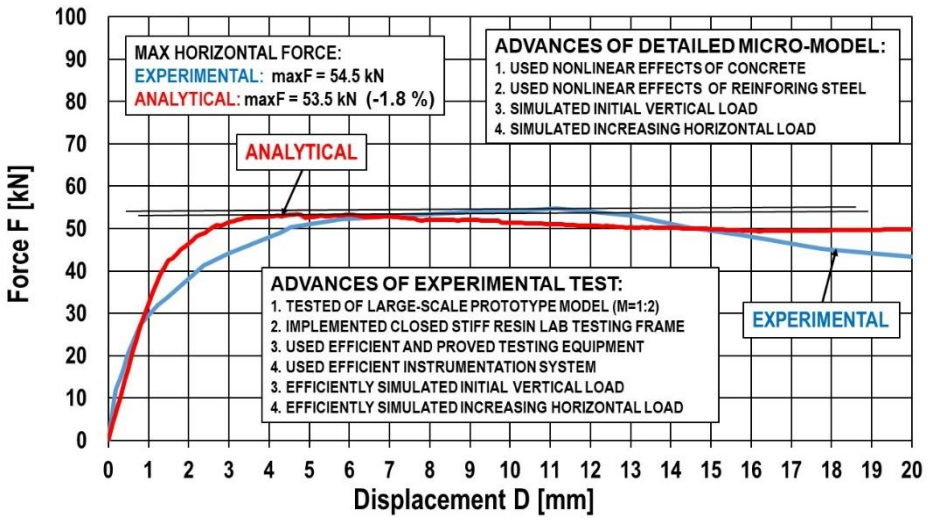

Figure 5.2.11. Comparison of experimental and numerical force-displacement curves under axial load N1=62.5 kN and monotonic loading.

5.3 Medium axial load N2: Micro-Modelling and nonlinear response of RC bare frame (M1-B1)

This specific analytical study was conducted considering the formulated and experimentally verified model and modified intensity of vertical load while preserving the same monotonic horizontal loading pattern. In this case, on both RC columns the vertical load was increased to N2 = 125 kN as shown in Fig. 5.3.1.

The results obtained from the performed study are analogously presented and analyzed in an identical way due to their extensiveness.

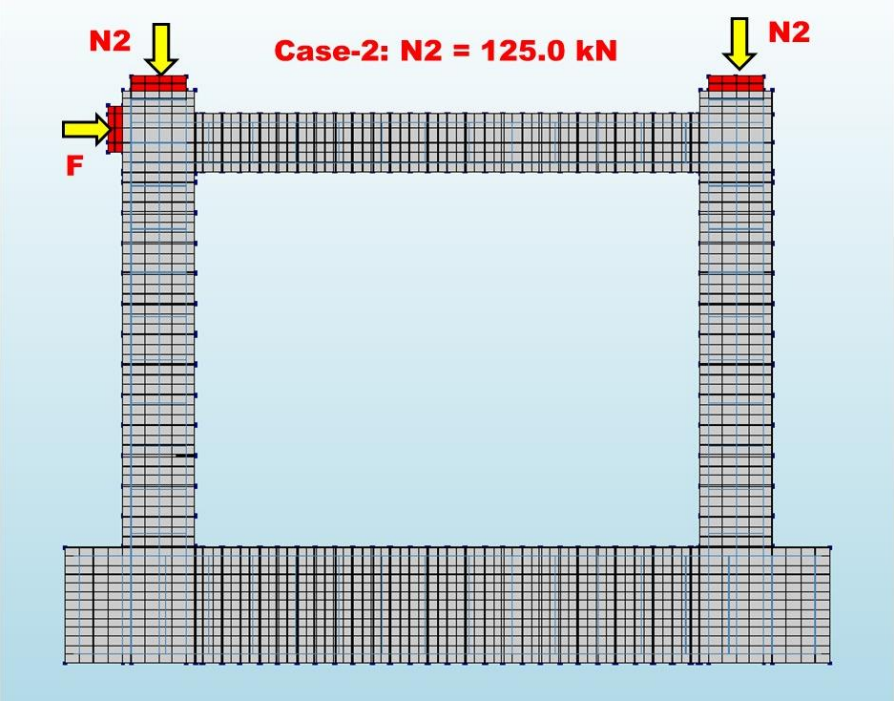

Figure 5.3.1. FE model of RC Bare Frame with axial load N1=125.0 kN and monotonic loading.

Summarized in Table 5.3.1 are the results obtained from the analytical phase A1-2 representing the computed nonlinear response of the tested RC bare frame model (M1-B) under simulated vertical load N2 = 125.0 kN and monotonic loading (Chapter 5.2). For the selected characteristic solution step 130, Fig. 5.3.2, Fig. 5.3.3 and Fig. 5.3.4 show the distributions of displacements DX, DY and DXY, respectively. Although these distributions generally show similarities with the previous solution, there are certain differences due to the increased level of vertical loads. Fig. 5.3.5 and Fig. 5.3.6 show the distributions of the computed total Cauchy stresses in concrete SXX and SYY, respectively, for the same solution step 130.

Due to the presence of reinforcement, the distribution of stresses in concrete is considerably changed. In the tensile zones, the tensile stresses are transferred to the reinforcement to a dominant amount.

Fig. 5.3.7 and Fig. 5.3.8 comparatively show the distributions of cracks in concrete for two solution steps, 30 and 130, respectively. Although the zones of occurred cracks are approximately the same, the propagation of the zones and cracks is considerable for the solution step 130 which indicates a state with considerably increased displacements DXY. In the last two figures, Fig. 5.3.9 and Fig. 5.3.10, respectively, the reinforcement stresses SXX and SYY are presented. It is evident that stresses SYY are dominant in the critical zones since reinforcement dominantly sustains the tensile stresses. To demonstrate the occurred difference in the model responses, comparatively are presented the computed envelope curves for axial load amounting to N1 = 62.5 kN and for an increased amount of axial load to the value of N2 = 125.0 kN, Fig. 5.2.10. From the results obtained, it is evident that the difference in the values of the computed maximum forces is considerable and amounts to 28.9%. With the conducted study it was verified that the variation of axial force during seismic response can greatly affect nonlinear response and could not be neglected in the process of modern seismic resistant design.

Table 5.3.1. Analytical phase A1-2: Computed nonlinear response of the tested RC bare frame model (M1-B) under vertical load N2=125.0 kN and monotonic loading (Ch. 5.2)

ANALYTICAL PHASE A1-2: Details of the RC bare frame mode (M1-B1) under vertical load N2=125.0 kN and monotonic-loading (Ch. 5.2)					
File	Presented FEM parameter	Notation	Load step	E-Plotted	Shown
0	Mesh of micro-model	Geometry	-	yes	+ / 5.2.0.
1	Displacement-x (mm)	TDtX	30	yes	
2	Displacement-x (mm)	TDtX	130	yes	+ / 5.2.1.
3	Displacement-y (mm)	TDtY	30	yes	
4	Displacement-y (mm)	TDtY	130	yes	+ / 5.2.2.
5	Displacement-xy (mm)	TDtXY	30	yes	
6	Displacement-xy (mm)	TDtXY	130	yes	+ / 5.2.3.
7	Cauchy total stresses-x (N/mm2)	SXX	30	yes	
8	Cauchy total stresses-x (N/mm2)	SXX	130	yes	+ / 5.2.4.
9	Cauchy total stresses-y (N/mm2)	SYY	30	yes	
10	Cauchy total stresses-y (N/mm2)	SYY	130	yes	+ / 5.2.5.
11	Cauchy total stresses-xy (N/mm2)	SXY	30	yes	
12	Cauchy total stresses-xy (N/mm2)	SXY	130	yes	
13	Total strains-x (mm/mm)	EXX	30	yes	
14	Total strains-x (mm/mm)	EXX	130	yes	
15	Total strains-y (mm/mm)	EYY	30	yes	
16	Total strains-y (mm/mm)	EYY	130	yes	
17	Total strains-xy (mm/mm)	EXY	30	yes	
18	Total strains-xy (mm/mm)	EXY	130	yes	
19	Crack widths: plane princ./comp. (mm)	Ecw	30	yes	+ / 5.2.6.
20	Crack widths: plane princ./comp. (mm)	Ecw	130	yes	+ / 5.2.7.
21	Reinforcement CT stresses-x (N/mm2)	SXX	30	yes	
22	Reinforcement CT stresses-x (N/mm2)	SXX	130	yes	+ / 5.2.8.
23	Reinforcement CT stresses-y (N/mm2)	SYY	30	yes	
24	Reinforcement CT stresses-y (N/mm2)	SYY	130	yes	+ / 5.2.9.
25	Reinforcement CT stresses-xy (N/mm2)	SXY	30	yes	
26	Reinforcement CT stresses-xy (N/mm2)	SXY	130	yes	
27	Reinforcement of total strain-x (mm/mm)	EXX	30	yes	
28	Reinforcement of total strain-x (mm/mm)	EXX	130	yes	
29	Reinforcement total strain-y (mm/mm)	EYY	30	yes	
30	Reinforcement total strain-y (mm/mm)	EYY	130	yes	
31	Reinforcement total strain-xy (mm/mm)	EXY	30	yes	
32	Reinforcement total strain-xy (mm/mm)	EXY	130	yes	
Number of plotted figures from analytical study using formulated micro-model					32
Number of figures presented showing representative results					10

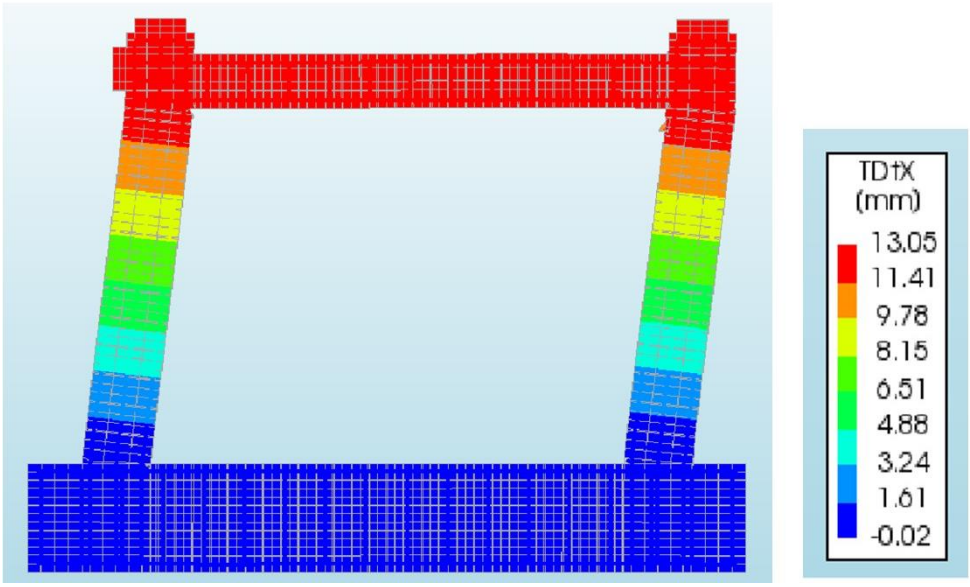

Figure 5.3.2. Response of RC Bare Frame model M1-B1 under axial load N1=125.0 kN and monotonic loading: Computed displacements DX for loading step 130.

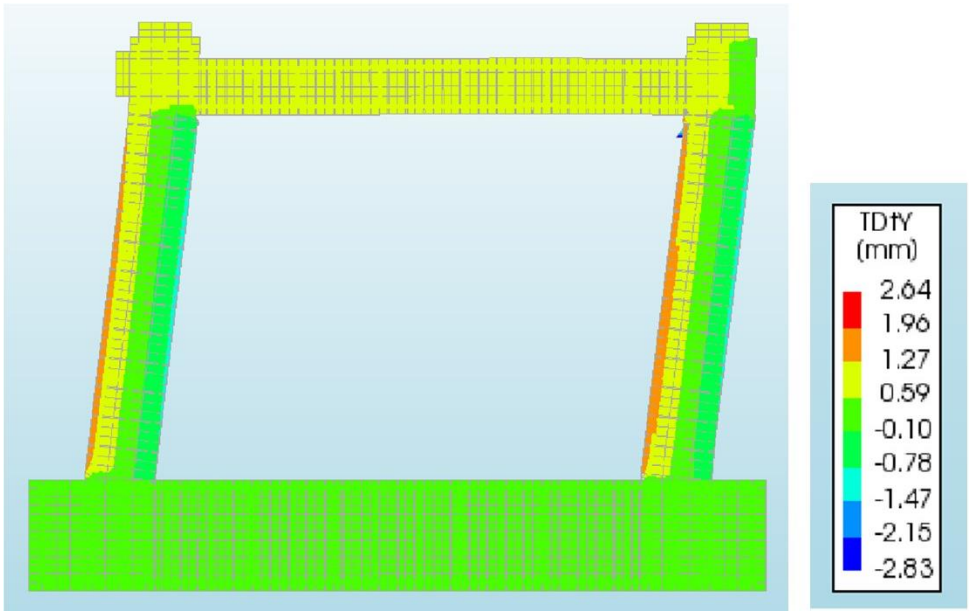

Figure 5.3.3. Response of RC Bare Frame model M1-B1 under axial load N1=125.0 kN and monotonic loading: Computed displacements DY for loading step 130.

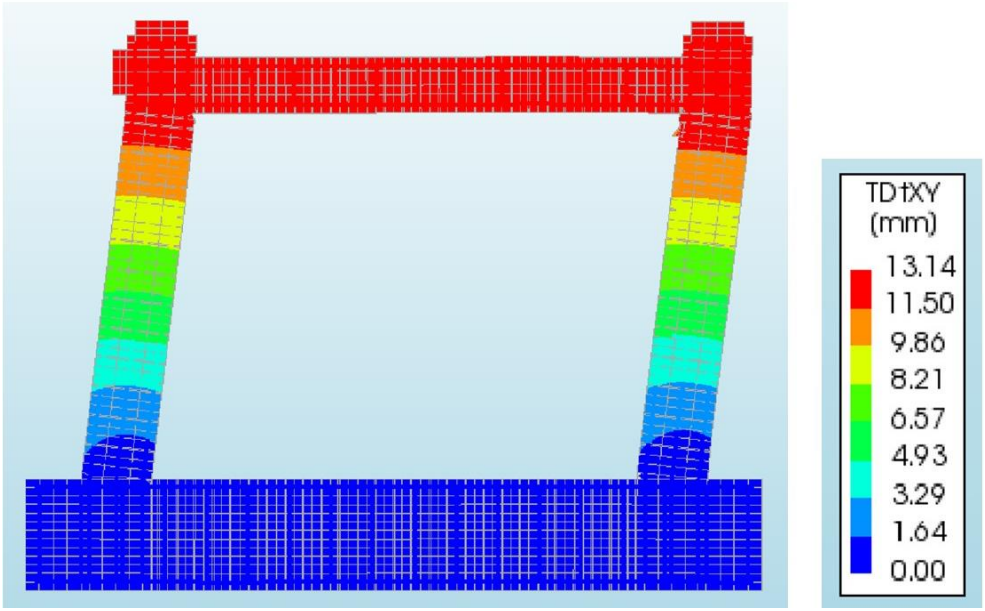

Figure 5.3.4. Response of RC Bare Frame model M1-B1 under axial load N1=125.0 kN and monotonic loading: Computed displacements DXY for loading step 130.

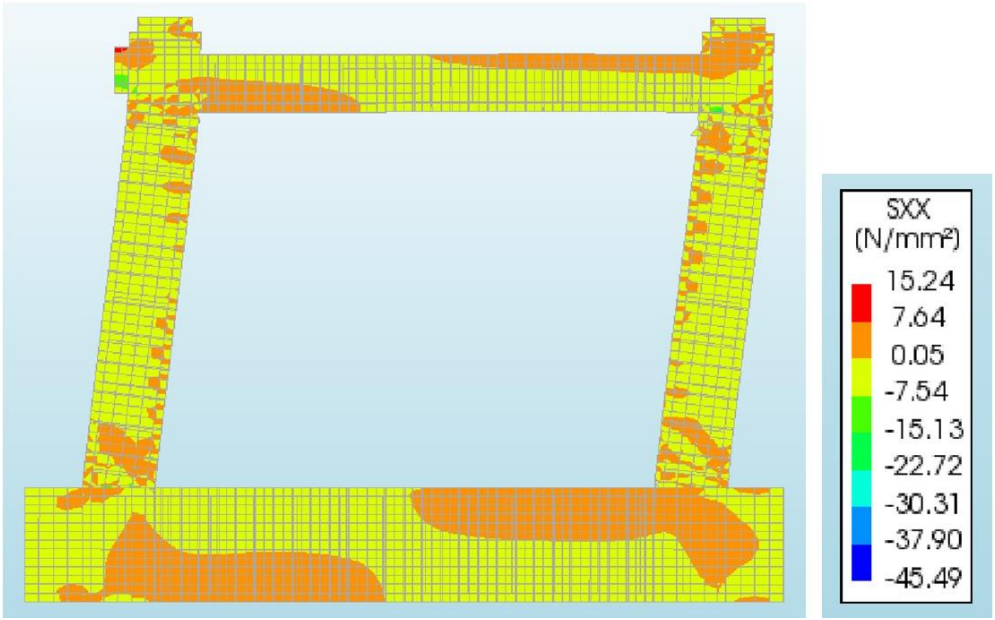

Figure 5.3.5. Response of RC Bare Frame model M1-B1 under axial load N1=125.0 kN and monotonic loading: Computed Cauchy total stresses SXX for loading step 130.

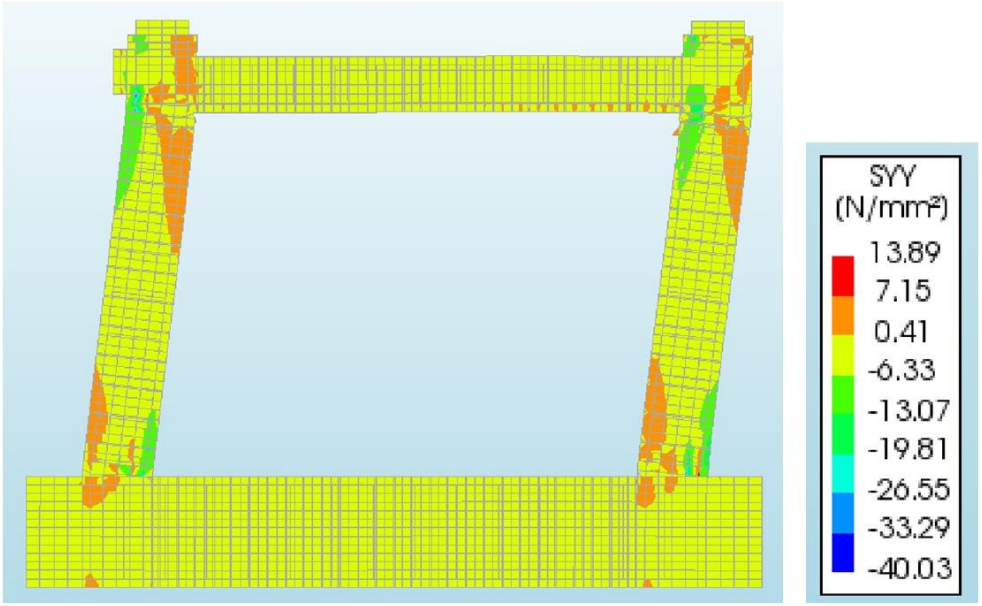

Figure 5.3.6. Response of RC Bare Frame model M1-B1 under axial load N1=125.0 kN and monotonic loading: Computed Cauchy total stresses SYY for loading step 130.

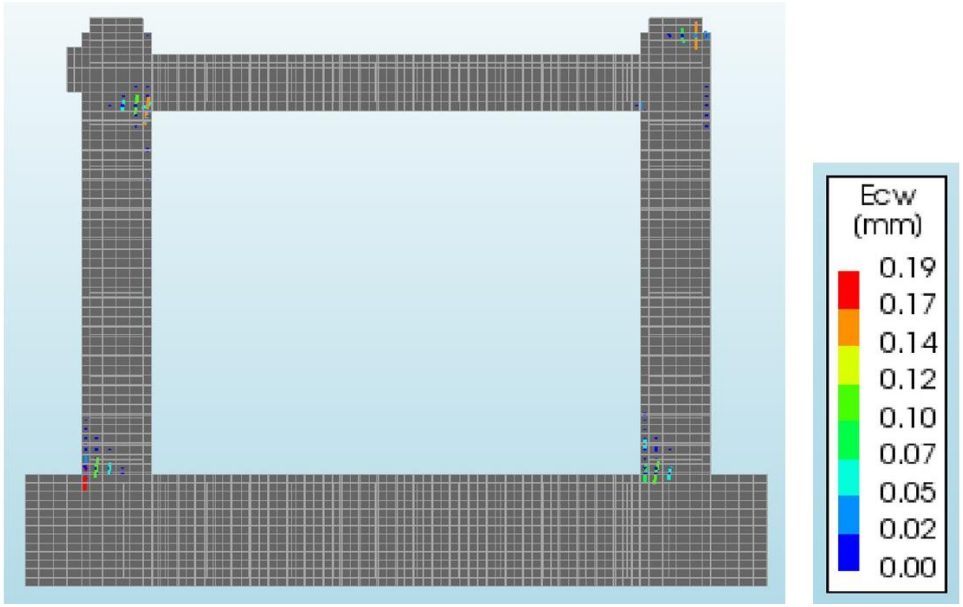

Figure 5.3.7. Response of RC Bare Frame model M1-B1 under axial load N1=125.0 kN and monotonic loading: Computed crack distribution for loading step 30.

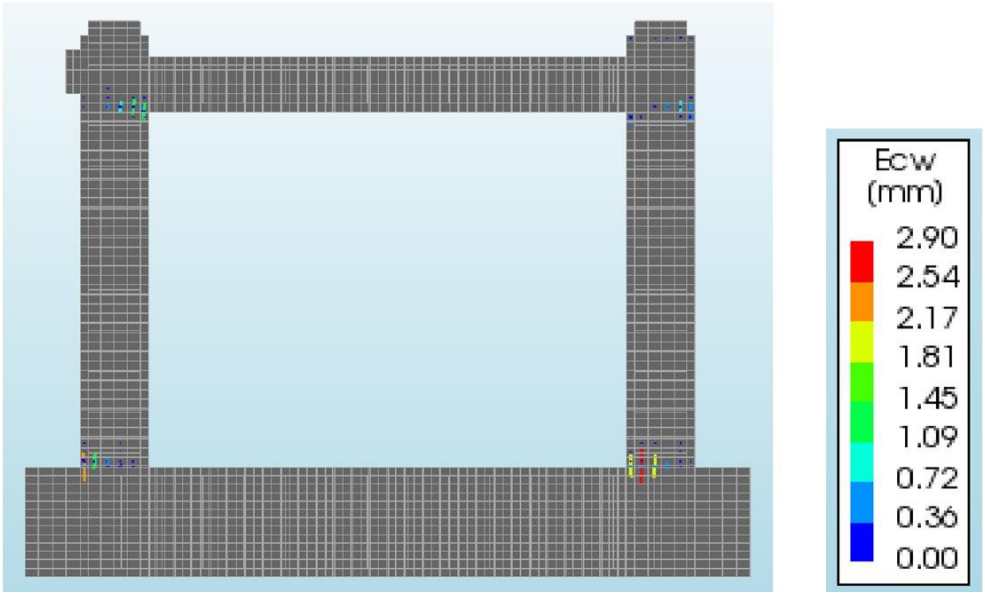

Figure 5.3.8. Response of RC Bare Frame model M1-B1 under axial load N1=125.0 kN and monotonic loading: Computed crack distribution for loading step 130.

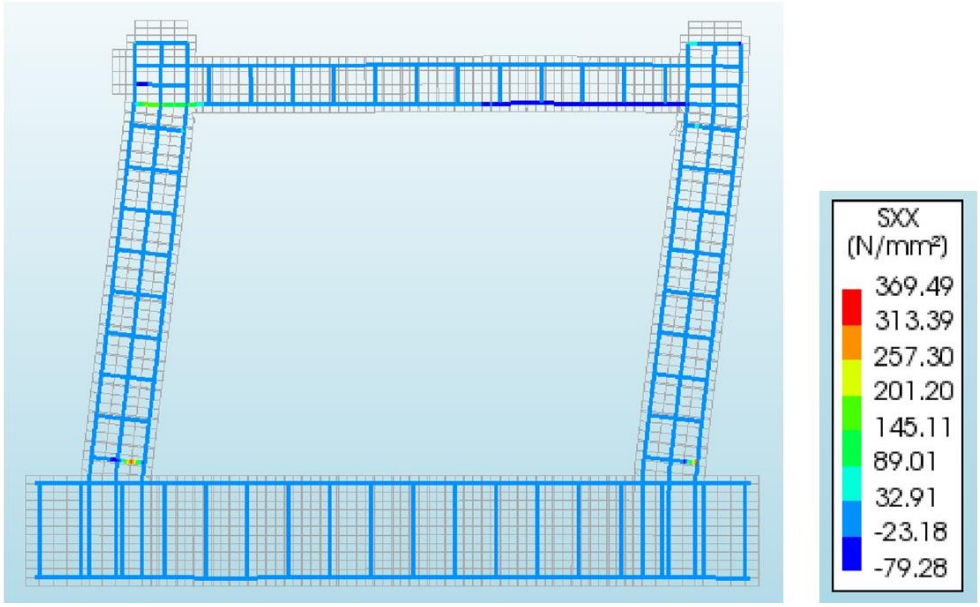

Figure 5.3.9. Response of RC Bare Frame model M1-B1 under axial load N1=125.0 kN and monotonic loading: Computed reinforcement stresses SXX for loading step 130.

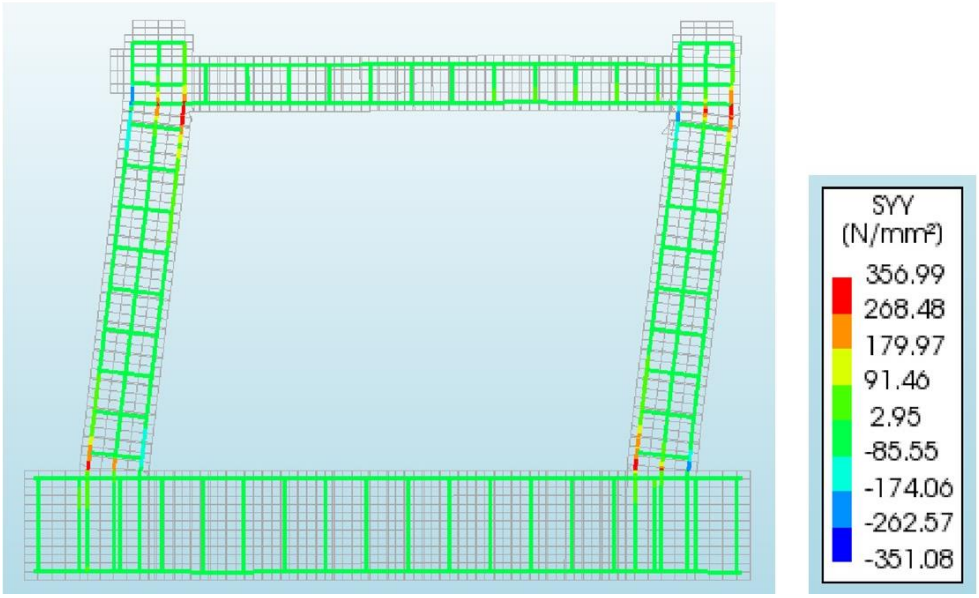

Figure 5.3.10. Response of RC Bare Frame model M1-B1 under axial load N1=125.0 kN and monotonic loading: Computed reinforcement stresses SYY for loading step 130.

5.4 High Axial Load N3: Modelling and Nonlinear Response of RC Bare Frame, model (M1-B2)

This part of the study is also of particular importance since the level of vertical loads increased even more to the amount of N3 = 280.0 kN.

Fig. 5.4.1 shows the formulated nonlinear micro-model as well as the applied loading conditions.

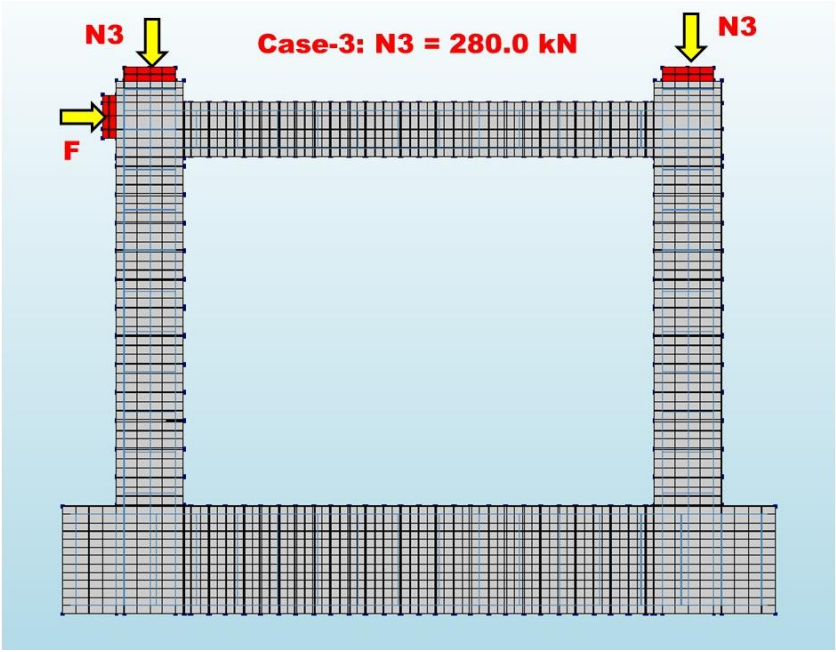

Figure 5.4.1 FE model of RC bare frame with axial load N1=280.0 kN and monotonic loading.

The review of the results obtained in this analytical phase indicated as A1-3 is given in the analog Table 5.4.1. From the table, it is evident that the analysis finishes with a smaller number of solution steps, i.e., at smaller values of displacements, there follows the critical phase of the nonlinear response. Analogously, Fig. 5.4.2, Fig. 5.4.3 and Fig. 5.4.4 respectively show the distributions of DXX, DYY and DXY. In all three cases, considerable changes are evident since the final solution (loading) step is smaller, amounting to 45.

Fig. 5.4.5 and Fig. 5.4.6 respectively show the Cauchy total stresses SXX and SYY. Due to the increased amount of vertical compressive loads, a considerable difference in stresses in concrete SYY is evident. Fig. 5.4.7 and Fig. 5.4.8 comparatively show the distributions of the cracks in concrete at solution step 30 and solution step 45. Although at both times, they are not very different, the change in the development and enlargement of cracks is considerable. Fig. 5.4.9 and Fig. 5.4.10 respectively show the reinforcement stresses SXX and SYY. It is evident that there is a considerable increase of stresses SYY in critical localized zones.

Table 5.4.1. Analytical phase A1-3: Computed nonlinear response of the tested RC bare frame model (M1-B2) simulating vertical load N1=280.0 kN and monotonic loading (Ch. 5.3)

ANALYTICAL PHASE A1-3: Details of the RC bare frame model (M1-B2) under vertical load N2=280.0 kN and monotonic loading (Ch. 5.3)					
File	Presented FEM parameter	Notation	Load step	E-Plotted	Shown
0	Mesh of micro-model	Geometry	-	yes	+ / 5.3.0.
1	Displacement-x (mm)	TDtX	30	yes	
2	Displacement-x (mm)	TDtX	45	yes	+ / 5.3.1.
3	Displacement-y (mm)	TDtY	30	yes	
4	Displacement-y (mm)	TDtY	45	yes	+ / 5.3.2.
5	Displacement-xy (mm)	TDtXY	30	yes	
6	Displacement-xy (mm)	TDtXY	45	yes	+ / 5.3.3.
7	Cauchy total stresses-x (N/mm2)	SXX	30	yes	
8	Cauchy total stresses-x (N/mm2)	SXX	45	yes	+ / 5.3.4.
9	Cauchy total stresses-y (N/mm2)	SYY	30	yes	
10	Cauchy total stresses-y (N/mm2)	SYY	45	yes	+ / 5.3.5.
11	Cauchy total stresses-xy (N/mm2)	SXY	30	yes	
12	Cauchy total stresses-xy (N/mm2)	SXY	45	yes	
13	Total strains-x (mm/mm)	EXX	30	yes	
14	Total strains-x (mm/mm)	EXX	45	yes	
15	Total strains-y (mm/mm)	EYY	30	yes	
16	Total strains-y (mm/mm)	EYY	45	yes	
17	Total strains-xy (mm/mm)	EXY	30	yes	
18	Total strains-xy (mm/mm)	EXY	45	yes	
19	Crack widths: plane princ./comp. (mm)	Ecw	30	yes	+ / 5.3.6.
20	Crack widths: plane princ./comp. (mm)	Ecw	45	yes	+ / 5.3.7.
21	Reinforcement CT stresses-x (N/mm2)	SXX	30	yes	
22	Reinforcement CT stresses-x (N/mm2)	SXX	45	yes	+ / 5.3.8.
23	Reinforcement CT stresses-y (N/mm2)	SYY	30	yes	
24	Reinforcement CT stresses-y (N/mm2)	SYY	45	yes	+ / 5.3.9.
25	Reinforcement CT stresses-xy (N/mm2)	SXY	30	yes	
26	Reinforcement CT stresses-xy (N/mm2)	SXY	45	yes	
27	Reinforcement total strain-x (mm/mm)	EXX	30	yes	
28	Reinforcement total strain-x (mm/mm)	EXX	45	yes	
29	Reinforcement total strain-y (mm/mm)	EYY	30	yes	
30	Reinforcement total strain-y (mm/mm)	EYY	45	yes	
31	Reinforcement total strain-xy (mm/mm)	EXY	30	yes	
32	Reinforcement total strain-xy (mm/mm)	EXY	45	yes	
Number of plotted figures from analytical study using formulated micro-model					32
Number of presented figures showing representative results					10

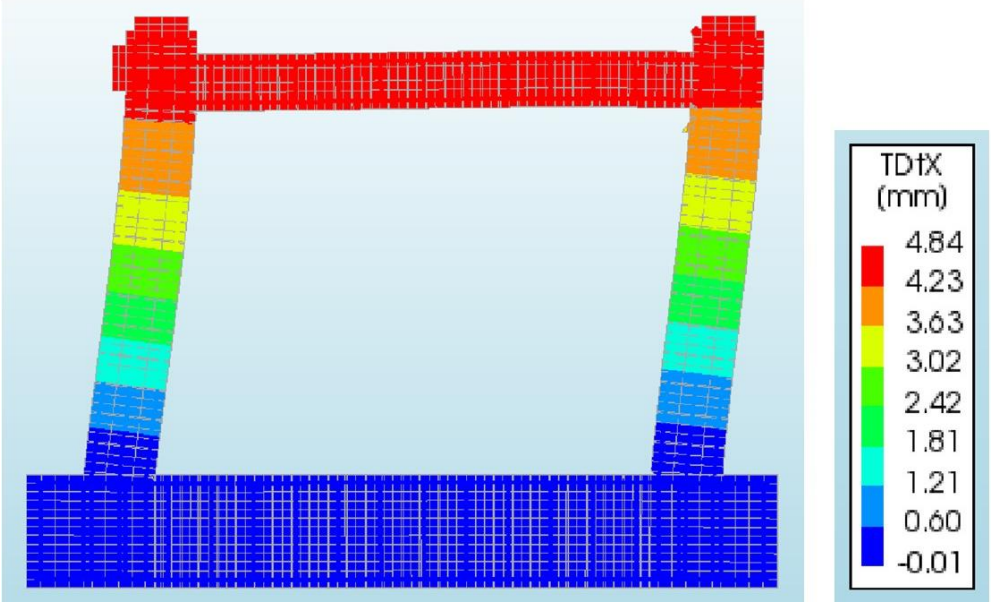

Figure 5.4.2. Response of RC bare Frame model M1-B2 under axial load N1=280.0 kN and monotonic loading: Computed displacements DX for loading step 45.

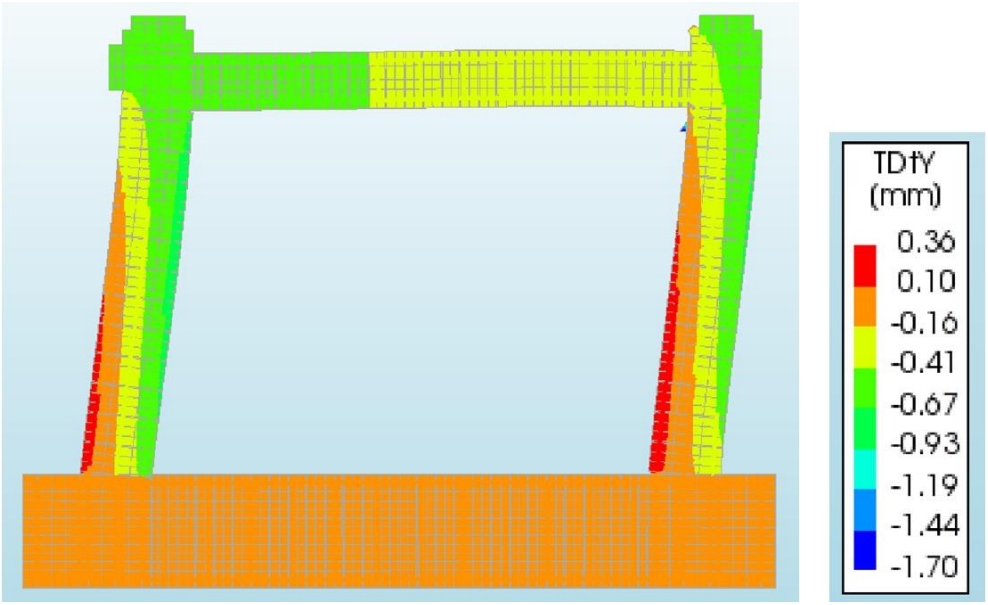

Figure 5.4.3. Response of RC bare Frame model M1-B2 under axial load N1=280.0 kN and monotonic loading: Computed displacements DY for loading step 45.

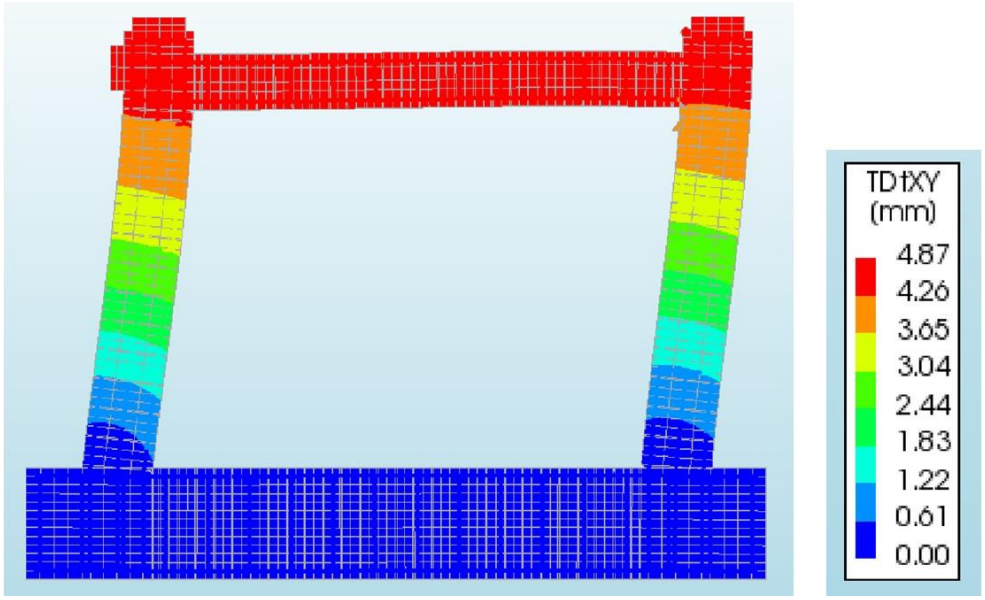

Figure 5.4.4. Response of RC bare Frame model M1-B2 under axial load N1=280.0 kN and monotonic loading: Computed displacements DXY for loading step 45.

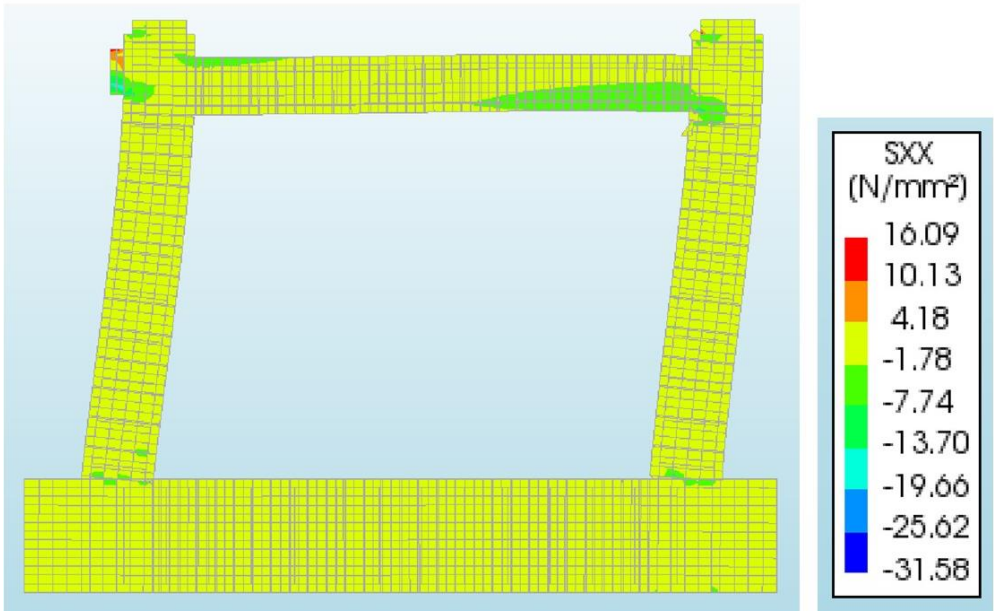

Figure 5.4.5. Response of RC bare Frame model M1-B2 under axial load N1=280.0 kN and monotonic loading: Computed Cauchy total stresses SXX for loading step 45.

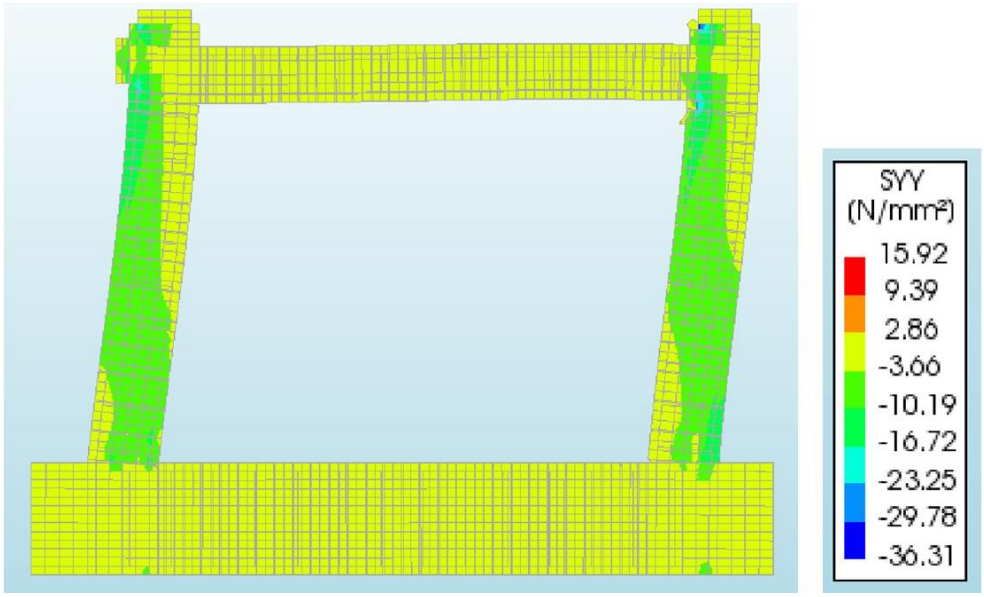

Figure 5.4.6. Response of RC bare Frame model M1-B2 under axial load N1=280.0 kN and monotonic loading: Computed Cauchy total stresses SYY for loading step 45.

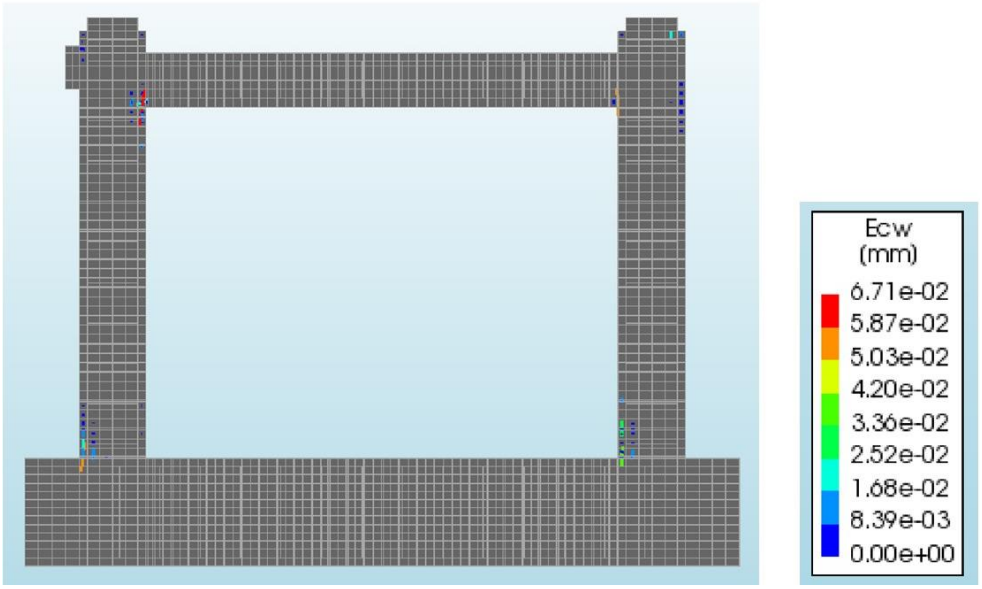

Figure 5.4.7. Response of RC bare Frame model M1-B2 under axial load N1=280.0 kN and monotonic loading: Computed crack distribution for loading step 30.

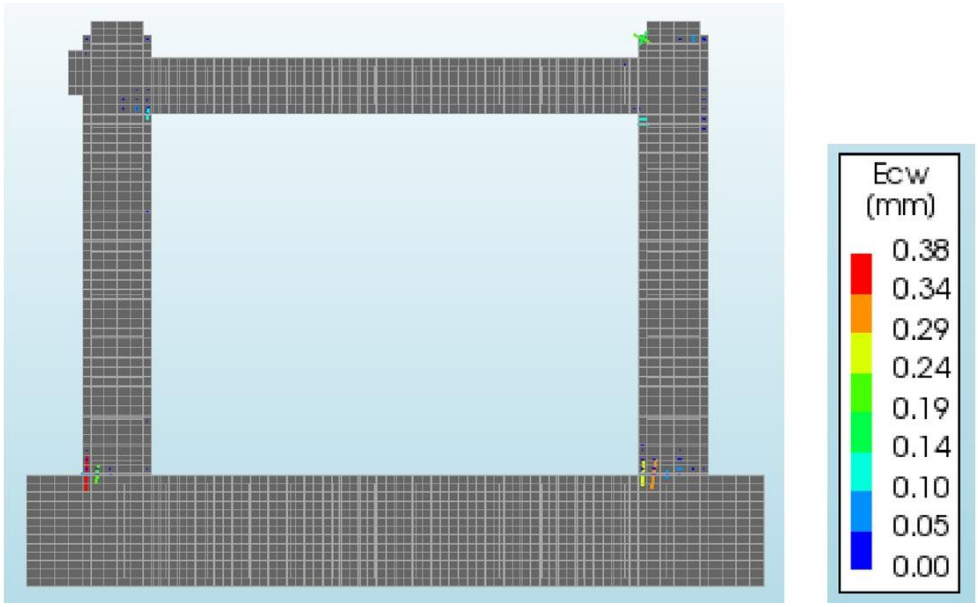

Figure 5.4.8. Response of RC bare Frame model M1-B2 under axial load N1=280.0 kN and monotonic loading: Computed crack distribution for loading step 45.

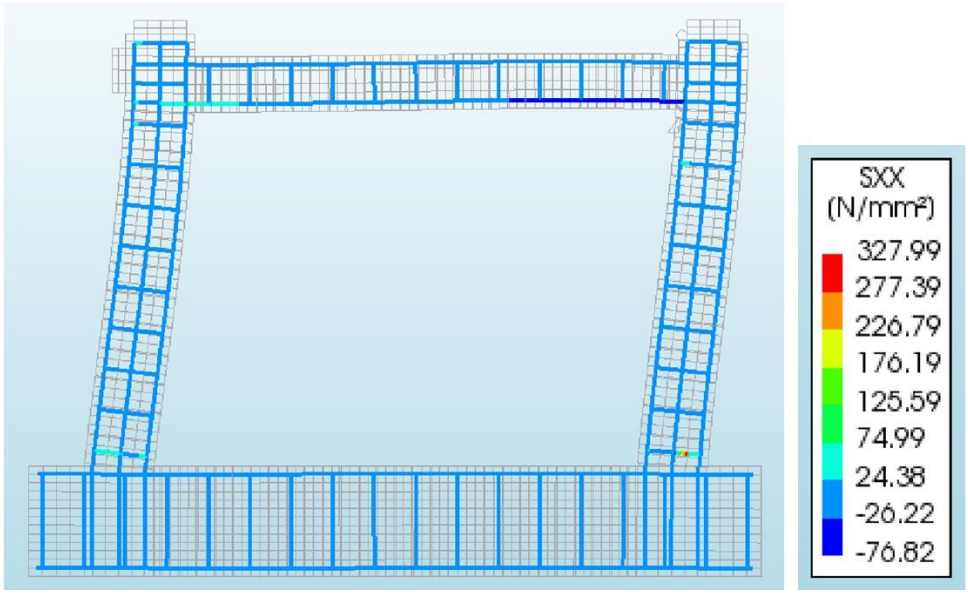

Figure 5.4.9. Response of RC bare Frame model M1-B2 under axial load N1=280.0 kN and monotonic loading: Computed reinforcement stresses SXX for loading step 45.

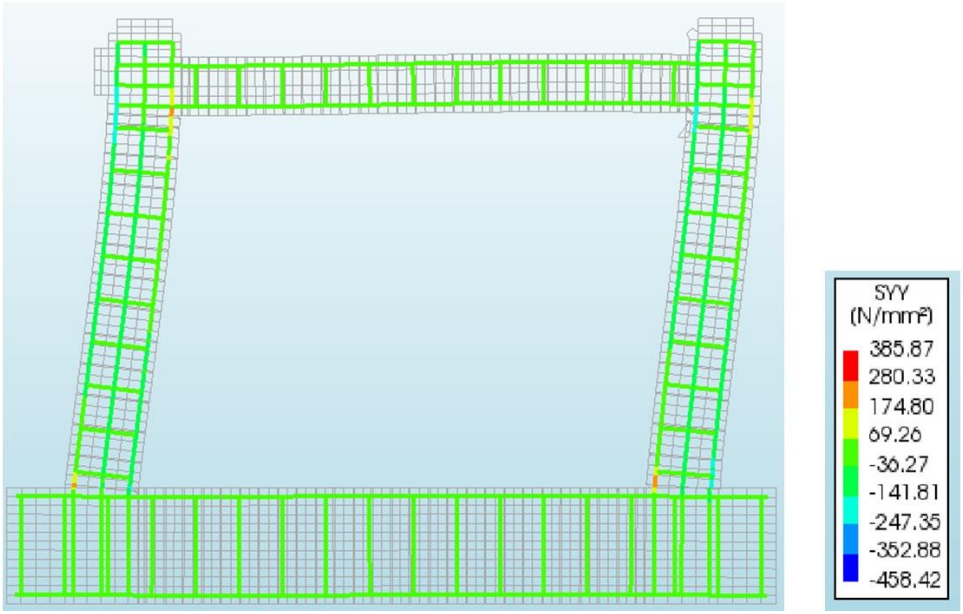

Figure 5.4.10. Response of RC bare Frame model M1-B2 under axial load N1=280.0 kN and monotonic loading: Computed reinforcement stresses SYY for loading step 45.

5.5 Graphical and Quantitative Comparison of Results

Figure 5.5.1 shows the force-displacement relationships obtained from the nonlinear pushover analyses of the RC bare frame under three different axial load levels (N_1 = 62.5 kN, N_2 = 125 kN, N_3 = 280 kN). The results demonstrate a clear influence of the applied axial load on the overall stiffness, strength, and deformation capacity of the frame.

At the lowest axial load (N_1 = 62.5 kN), the frame reached a maximum horizontal load of 53.5 kN. When the axial load increased to 125 kN, the peak lateral force rose to 69.0 kN, corresponding to an increase of 28.9 %. At the highest compression level (N_3 = 280 kN), the maximum lateral resistance reached 89.9 kN, representing an overall increase of 68 % relative to the reference case.

It is evident that higher axial compression enhances the initial stiffness and the lateral strength of the frame but simultaneously reduces its deformation and energy-dissipation capacity. The curve for N_3 becomes steeper and terminates earlier, indicating a stiffer yet more brittle response. Conversely, the curve for N_1 exhibits gradual strength degradation, typical of a ductile behavior.

This confirms that the axial load has a dual effect: it improves strength due to confinement and compression of the concrete column, but limits ductility through early crushing in the plastic-hinge regions. The identified trend provides quantitative evidence of the interdependence between axial compression and lateral response in RC frames.

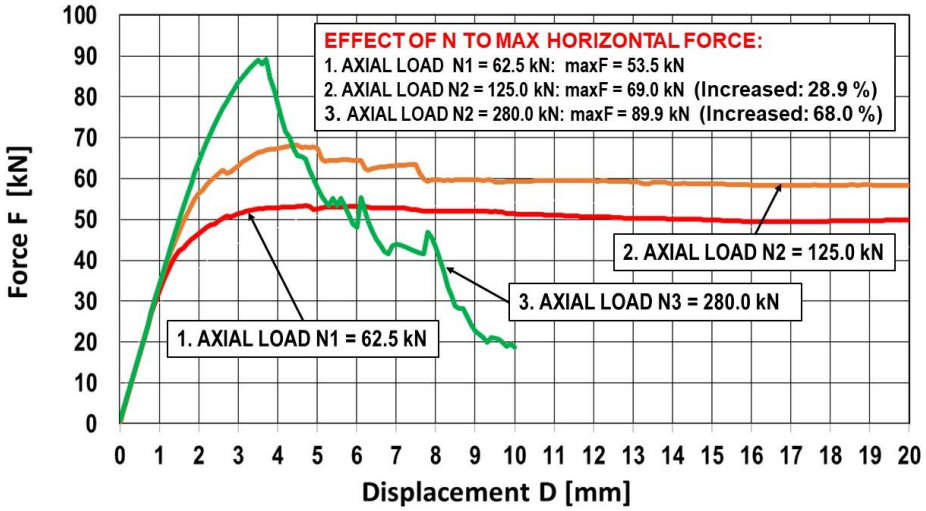

Figure 5.5.1. Comparison of Force-Displacement curves of RC bare frames M1-B, M1-B1, M1-B2 with different axial loads and monotonic loading

The numerical values presented in Table 5.5.1 were obtained directly from the pushover analysis results performed in DIANA FEA. The peak, yield, and ultimate points were identified from the force displacement curves for each axial load level (62.5 kN, 125 kN, and 280 kN). The yield point corresponds to the first deviation from linearity on the curve, the peak load represents the maximum recorded lateral resistance, and the ultimate displacement was defined at a 20 % reduction of the peak load capacity. The ductility ratios were calculated as the ratio between ultimate and yield displacements.

Table 5.5.1. Summary of Key Parameters from Nonlinear Analyses under Different Axial Loads

Axial Load (kN)	**Initial Stiffness Ko (kN/mm)**	**Yield Load Fy (kN)**	**Yield Disp. δy (mm)**	**Peak Load Fm (kN)**	**Peak Disp. δm (mm)**	**Ultimate Disp. δu (mm)**	**Ductility Ratio μ**	**Percentage Change Relative to Reference Case (62.5 kN)***
62.5 (Ref.)	20.0	40.0	2.0	53.5	4.5	11.0	5.5	–
125	32.2	58.0	1.8	69.0	3.5	9.6	5.3	+61 % Ko, +45 % Fy, +29 % Fm, −13 % δu, −4 % μ
280	40.6	65.0	1.6	89.9	2.8	7.5	4.7	+103 % Ko, +63 % Fy, +68 % Fm, −32 % δu, −15 % μ

5.5.1 Parametric analysis Discussion

- **Initial Stiffness**

The initial stiffness of the bare RC frame increases progressively with the applied axial load, as shown in Table 5.4.1. At the lowest axial load level (N_1 = 62.5 kN), the frame exhibits a moderate initial stiffness of approximately 20 kN/mm, primarily governed by the flexural rigidity of the columns and the elastic behavior of the concrete before cracking. When the axial load increases to N_2 = 125 kN, the stiffness rises to about 32 kN/mm, representing an increase of nearly 60 % compared to the reference case. At the highest axial load level (N_3 = 280 kN), the initial stiffness reaches approximately 41 kN/mm, which corresponds to an overall increase of around 105 % relative to the lowest axial load case.

This trend clearly indicates that axial compression enhances the effective stiffness of the columns by reducing tensile strain, closing pre-existing micro-cracks, and increasing confinement in the concrete core. The values of the initial stiffness were determined directly from the pushover force-displacement curves by applying the relationship:

$$K_0 = \frac{F_y}{\boldsymbol{\delta}_y}$$

where Fy is the yield load and $\boldsymbol{\delta}_\gamma$ is the corresponding yield displacement. This approach provides a reliable measure of the elastic slope of the curve before the onset of cracking. Consequently, the increase of K_0 with axial compression reflects a stiffer and less deformable structural response under higher vertical loading.

- **Peak Lateral Load Capacity**

The lateral strength of the RC bare frame improves consistently with higher axial compression. The peak lateral force rises from 53.5 kN at N_1 to 69.0 kN at N_2, and further to 89.9 kN at N_3, corresponding to an overall increase of approximately 68 % compared to the reference case. This trend confirms that moderate axial compression enhances shear and flexural resistance through additional confinement, but excessive compression may bring the frame closer to a brittle limit state [59].

- **Yield Characteristics**

The yield point shifts to smaller displacements with increasing axial load. The displacement at first yielding decreases from 2.5 mm at N_1 to about 2.0 mm at N_3. This indicates that the frame becomes stiffer and yields earlier under compression, as axial load restricts tensile cracking and delays flexural softening.

- **Ductility**

As per Eurocode 8 and displacement-based design principles [59], [60], ductility is defined as:

$$\mu = \frac{\delta_u}{\delta_y}$$

Where:

δ_y – is the yield displacement (start of inelastic response)

δ_u – is the ultimate displacement (where significant strength degradation occurs)

The ductility ratio (μ) decreases gradually with higher axial load, from 5.5 at N_1 = 62.5 kN to 5.3 at N_2 = 125 kN, and further to 4.7 at N_3 = 280 kN. Although the RC frame remains ductile throughout the investigated range, this gradual reduction clearly indicates a transition from a highly deformable response to stiffer, strength-dominated behavior. The decrease in ductility is primarily attributed to the reduced rotational capacity in the plastic hinge zones and the earlier onset of concrete crushing at the column bases under higher axial compression. Increased vertical load confines the core concrete and delays tensile cracking but simultaneously limits curvature development and energy dissipation capacity.

- **Post-Peak and Ultimate Behavior**

The post-peak response of the bare frame is characterized by gradual strength degradation and softening. At low axial load, the force-displacement curve shows stable post-yield behavior with considerable deformation capacity [59], [60]. With higher compression, the softening branch becomes steeper, and ultimate displacement reduces by roughly 30 %. The failure mechanism evolves from flexural cracking and bar yielding (ductile mode) to partial concrete crushing at the base of the columns (semi-brittle mode).

5.5.2 Interaction Effects

- **Frame Behavior under Axial Compression**

The frame shows a strong dependence of both stiffness and ultimate strength on the applied axial compression. The increase in axial load enhances confinement, improving shear resistance and reducing the curvature demands in the columns. However, it also reduces the margin for ductile energy dissipation. Under moderate axial ratios (5-10 %), the behavior remains stable, but when the ratio exceeds 25 %, the stiffness gain no longer compensates for the ductility loss.

- **Axial Load Sensitivity**

The parametric results demonstrate that even small variations in axial load can produce significant differences in the lateral response of the bare frame. This sensitivity highlights the importance of accurate consideration of realistic axial load ratios in performance-based analysis, especially for lower-story columns in multi-story structures where axial compression is the highest.

5.6 Findings from Modeling Study of RC bare frame with different axial load levels

Based on the results obtained from the conducted extensive analytical micro-modeling study of the tested RC bare frame model M1-B, the following major findings are derived:

1. The advanced capability of the formulated nonlinear micro-model to realistically simulate the nonlinear response of RC frames exposed to interactive effects of vertical and horizontal loads was experimentally confirmed. The comparison between the analytical and experimental results showed an excellent match in stiffness, strength, and overall shape of the envelope curve, confirming that the model can accurately reproduce the force-displacement behavior under combined axial and lateral actions.
2. The variation of the axial load levels largely affects the nonlinear response of the RC bare frames and cannot be disregarded in the seismic design of RC-framed structures located in seismic regions. The parametric analyses demonstrated that higher axial compression leads to increased initial stiffness and lateral strength but simultaneously reduces ductility. Moderate axial ratios (around 10 % of column capacity) produced optimal performance, whereas high compression (around 25 %) shifted the behavior toward brittle response.
3. The structures exposed to considerably high levels of axial loads possess much lower ductility and are susceptible to very critical damaging states or total failures. The results indicated that, although the ultimate load capacity rises with higher compression, the corresponding deformation capacity decreases by approximately 25 - 30 %. This trend highlights the trade-off between strength enhancement and loss of deformability, which is a key parameter in performance-based seismic assessment.
4. The formulated nonlinear micro-model for an RC bare frame was created as fully compatible to be upgraded with the corresponding nonlinear AAC infill finite elements, joint finite elements and other related interface finite elements. Such compatibility enables direct extension of the verified frame model toward complex simulations involving frame-infill interaction, allowing for consistent calibration of interface behavior and validation against future experimental campaigns.
5. Following full experimental verification, the created complete nonlinear micro-model of an RC frame with incorporated AAC infill can be creatively applied in investigating the nonlinear response characteristics of an RC bare frame with an AAC infill under simulated interactive effects of vertical and horizontal loads. The verified bare-frame model therefore serves as a fundamental reference case, ensuring that any subsequent modifications related to infill addition or interface definition can be quantitatively evaluated with respect to a reliable baseline.

6 CHAPTER 6 - NUMERICAL SIMULATION OF THE EXPERIMENTAL RESULTS FOR RC FRAME WITH AAC INFILL

This Chapter 6 contains the results from the realized analytical studies carried out based on experimental results recorded during the testing of the experimental models M2-A and M2-B, representing an RC frame with AAC infill. With experimental tests of RC frame model with infill confirmed that the nonlinear envelope curves obtained by cyclic horizontal loading or by monotonic loading are very similar. To provide conditions for specifically targeted analytical studies, the monotonic loading type was adopted as the representative loading case. Specifically, the experimental test of the prototype model M2-B tested under the effect of vertical loads and monotonic loading was used for the analytical studies presented in this chapter. The results from the realized numerical studies carried out are presented in five successive sub-chapters. Respective details regarding application of advanced micro-modeling concept are included. Part 6.1 shows the introduction of parametric study while part 6.2 shows material parameter used. Part 6.3 shows the analytical studies directed to experimental validation of the developed simplified micro-model since an identical vertical load of N1 = 62.5 kN was simulated during both experimental and analytical studies. Part 6.4 and part 6.5 show the analytical results obtained under increased vertical loads to N2 = 125.0 kN and to N3 = 280.0 kN, based on implementation of experimentally verified analytical model. The two additional analytical studies represent the two specific and very successful "analytical experiments" since the applied detailed analytical model was fully verified with the results from the performed experimental tests. The formulated experimentally verified analytical models are of high importance because numerous innovative projects and other specific studies can be successfully realized with their application. Finally, in part 6.7 briefly the major findings are summarized from the conducted micro-modeling study of the tested model M2-B representing RC frame with AAC infill.

6.1 Parametric study - RC Frame Model with AAC Infill (M2-B)

6.1.1 Importance of the Conducted Analytical Study

Many studies were dedicated in the past to investigations of the effect of infill on nonlinear behavior of RC framed buildings. Mostly, they performed investigations that considered brick masonry infill or hollow ceramic blocks masonry infill. However, during recent years, the AAC infill has been intensively applied in frame structures in the form of constructed masonry with AAC elements of different sizes.

Regarding the confirmed quite different mechanical behavior of the masonry constructed of AAC elements, there is an evident need to address the interactive effects.

The present experimental and analytical studies were targeted to provide research contributions in two important research domains: (1) To obtain reliable experimental results with the experimental tests on large-scale prototype models of RC frames without and with AAC infill,

and (2) To use the obtained experimental results for experimental verification of the simplified micro-models.

The studies presented in this chapter were dedicated to formulation, verification and advanced research application of the developed simplified micro-model of the tested RC frame with AAC infill (M2-B).

6.1.2 Introduction to a parametric study

The numerical parametric study was conducted to examine the influence of different axial load levels on the nonlinear lateral behavior of the RC frame with AAC infill (model M2-B). The main objective of this study was to evaluate how varying axial compression in the columns affects the overall stiffness, strength, and ductility of the infilled frame system. This analysis is particularly important because, in real multistory buildings, the magnitude of the axial load in columns increases significantly toward the lower stories, directly influencing the global seismic response and the contribution of the infill walls.

The study aimed to identify how the interaction between the RC frame and the AAC infill evolves under different vertical load levels, especially in terms of stiffness enhancement, strength gain, and potential reduction in deformation capacity. All other parameters, including the geometry, material properties, and boundary conditions, were kept constant to ensure that the axial load remained the only variable influencing the response.

The nonlinear static analyses were performed using DIANA FEA, employing the same detailed micro-modeling approach described in previous sections, including contact-interface elements between the RC frame and the AAC infill. This ensured full consistency between the experimental calibration and the numerical evaluation, allowing direct comparison of the results obtained under different axial load ratios.

6.1.3 Simulation of RC Frame M2-B under Three Axial Load Levels

In the past, research was not sufficiently targeted to deep study of the effect of dynamically induced different (varying) levels of axial forces in RC columns, producing during vibrations important modifications of their nonlinear seismic response.

For example, during intensive seismic response, variations of axial forces are possible in many cases. Such variations may reach quite big differences of 80% to 100% or more. The variation of the axial forces induces important fluctuation (change) of the moment bearing capacity of the affected RC cross-sections.

To investigate the effect of the changed axial forces on the nonlinear behavior of RC frames with AAC infill, a corresponding combined experimental and analytical research was realized as follows:

1) Firstly, conducted was targeted experimental testing of the constructed large-scale RC frame model with AAC infill under simulated interactive effects of vertical loads of N1 = 62.5 kN in both columns and gradually increased monotonic loading (M2-B).
2) Using the experimental results obtained, numerical models were formulated. The performed analytical simulation of the experimental test verified that the numerical model simulated very successfully the nonlinear behavior of the tested RC frame with AAC infill (M2-B).
3) To study the effect of different axial load levels on nonlinear behavior of the RC frame with AAC infill, the analytical study was performed for two additional levels of axial loads defined as N2 = 125.0 kN and N3 = 280.0 kN. These studies were only possible by application of the previously formulated and experimentally verified numerical micro-model. The complete study of nonlinear behavior of the RC frame with AAC infill under three levels of axial loads, N1, N2 and N3, were of great importance for study of the effects of the AAC infill.

Based on the research results obtained from deeply studied identical RC frames without and with an AAC infill and consequently for three identical levels of axial loads, the effects of the AAC infill on the nonlinear behavior of RC frames were very successfully identified, evaluated and presented. he selected axial load levels of 62.5 kN, 125 kN, and 280 kN correspond approximately to 5%, 10%, and 25% of the total axial load-bearing capacity of the column section, which was calculated as 1.22 MN for a 25×25 cm column reinforced with 4Ø12 + 4Ø10 longitudinal bars and concrete of class C25/30. The axial load-bearing capacity of the column was determined through a standard analytical approach based on the material properties and cross-sectional characteristics. The calculation considered the combined contribution of concrete and longitudinal reinforcement to axial resistance, following the fundamental design expressions prescribed in Eurocode 2. This provided a closely estimation of the total column capacity, which served as a reference for defining the three representative axial load levels used in the parametric analysis of the RC frame with AAC infill (model M2-These load levels were intentionally chosen to represent typical ranges of axial load ratios in RC frames with infill walls and are summarized in Table 6.1.1, which presents the corresponding values expressed as a percentage of the total column capacity.

Table 6.1.1. Axial load levels used in parametric study

Axial Load Level	**Axial Load (kN)**	**Percentage of Column Axial Capacity (1.22 MN)**
N_1	62.5	≈ 5 %
N_2	125	≈ 10 %
N_3	280	≈ 23-25 %

This range allows the assessment of both beneficial and adverse effects of axial compression on the global behavior of the RC frame AAC infill system, particularly in terms of stiffness increase, strength enhancement, and ductility reduction. All other mechanical parameters,

modeling assumptions, and loading conditions were kept unchanged to ensure that the obtained differences in structural performance are solely attributed to the variation in axial load.

6.1.4 Geometry of the RC Frame with AAC Infill (M2-B)

A detailed description of the geometrical characteristics of the prototype models M2-A and M2-B is given in Chapter 4, specifically in part 4.3.1.

Considering the presented geometrical characteristics, the loading concept for the realized experimental test, the applied loading procedure with interactive vertical and monotonic loading as well as using data on the defined characteristics of the built-in materials, formulated was or responding advanced nonlinear micro-model. The formulated nonlinear micro-model was very successfully applied for realization of the analytical studies presented in this chapter (Chapter 6).

6.1.5 Simplified Micro-Model of RC Frame with AAC Infill (M2-B)

To create optimal conditions for formulation of representative simplified micro-model for the tested RC frame with AAC infill, some practical modeling assumptions were identified and introduced. The important conceptual details used as the basis during formulation of simplified micro-analytical model are briefly explained to enable an adequate interpretation of the results obtained from the analytical studies.

i. ***Concept of simplified micro-model of RC frame with AAC infill:*** Simplified micro-model of RC Frame with AAC Infill was formulated based on considered concept of rational simplification with assured conditions for realistic simulation of the experimentally recorded complex response characteristics. To improve the accuracy, advanced analytical approach based on the application of the modern finite element method (FE method) was selected. In that way, the general conditions were created for improved accuracy through the increase of the number of finite elements and reduction of their dimensions. To provide conditions for simulation of the behavior of the tested model, introduced were finite elements adapted for successful simulation of the nonlinear behavior of the corresponding materials and other specific nonlinear phenomena. Conditions for detailed simulation of nonlinear behavior of different materials were provided considering finite elements for nonlinear analyze formulated based on the fundamental nonlinear stress-strain relationships. To provide conditions for the application of the intended simplified micro-modeling concept, the same advanced software DIANA [40] was used. This software is developed for solving various complex problems of similar types and represents one of the most powerful software worldwide today. The numerical simulations were carried out with applied interactive loads completely spaced in two-dimensional (2D) plane. For these reasons and particularly to reduce the complexity of the model and necessary computation time, the representative 2D simplified micro-model was formulated. The formulated 2D simplified micro-model was provided with advanced capability to simulate complex

nonlinear interactive effects with considered in modeling representative effects of all the existing materials, elements and components.

ii. ***Modeling of concrete elements in the 2D micro-model:*** Contribution of the various concrete elements included in tested RC model, Fig. 6.1.1, considered are in the formulated 2D micro-model all constituent structural components with their respective thicknesses as follows: (1) RC Foundation segment with a thickness of 550 mm; (2) RC columns with a thickness of 250 mm; (3) RC beam with a thickness of 150 mm; (4) RC plate with a thickness of 550 mm; (5) Steel plate with RC bottom layer with a thickness of 150 mm; (6) AAC infill with a thickness of 125 mm; (7) AAC infill joints with a thickness of 125 mm.

iii. ***Modeling of reinforcing bars in the 2D micro model:*** (1) The reinforcing bars in the RC footing were modeled with upper and lower single bar-lines including also the existing steel hoops. The cross-section area of the modeled, representative "single" reinforcing bar was calculated as the sum of the cross-section areas of all the projected reinforcing bars along the respective single line; (2) The reinforcing bars in both RC columns were modeled with three parallel representative reinforcement lines. In the cross-section, the columns were reinforced by a regularly distributed total of 8ϕ10 mm longitudinal bars. Accordingly, the alternative reinforcement on the left and the right side included an equivalent total area corresponding to 3ϕ10 mm, whereas the modeled reinforcement in the middle of the cross-section included an area of 2ϕ10 mm. The existing stirrups were modeled in compliance with their number and position. (3) The reinforcing bars in the RC floor beam were modeled by respective reinforcement in the upper and the lower zone, with a cross-section defined in accordance with the reinforcement. In addition, the stirrups were modeled at the actual locations and with the actual cross-sections.

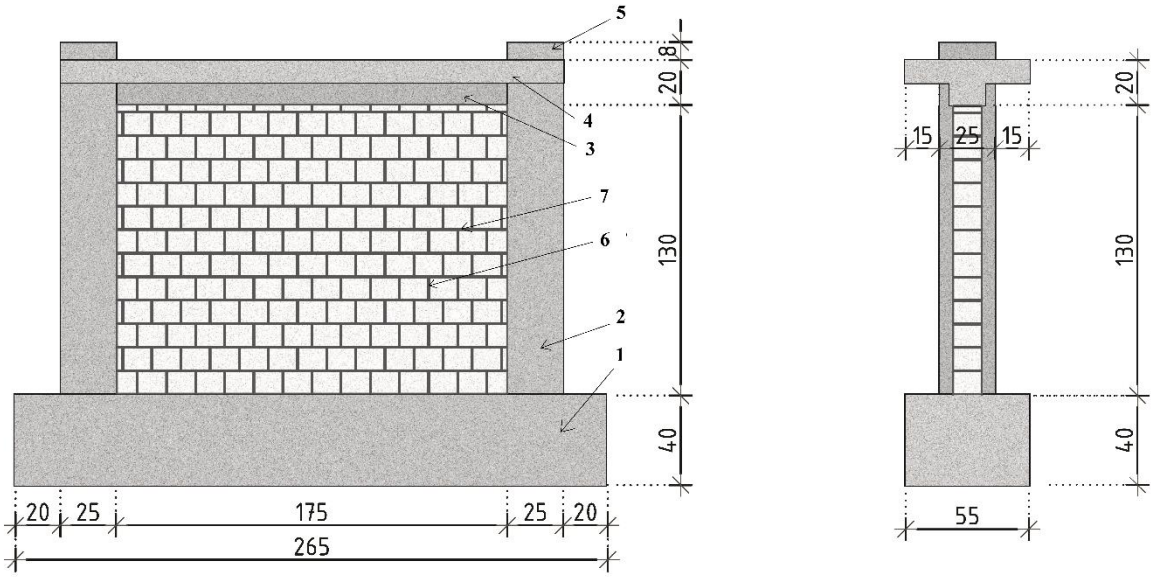

Figure 6.1.1. Concept of formulated nonlinear analytical model of the tested large-scale prototype model (M2-B) representing RC Frame with AAC infill.

iv. ***Modeling of vertical and horizontal loading segments:*** To provide conditions for correct simulation of the applied vertical loads, corresponding RC segments with end steel plates were included over the columns of the simplified micro- model. In that way, the applied loads were realistically distributed analogously to the system applied in the experimental test. Analogously, to provide conditions for simulation of the distributed horizontal load, an RC segment with end steel plate was included in the analytical model.

v. ***The concept of the created FEM mesh:*** While creating the applied FEM mesh, special attention was paid to enabling the accuracy needed and on achieving execution economy by shortening the computer time to acceptable frames. As is evident from the formulated analytical model, the size of the finite elements by which the concrete material is modeled is quite small and is of the order of 4 x 4 cm. With the adopted quite small finite elements also for AA infill, joints and interfaces, satisfying accuracy of the developed model of RC Frame with AAC Infill was provided.

vi. ***Modeling of boundary conditions:*** In the formulation of the FE model, the boundary conditions were specified in compliance with the real fixed support of the RC footing of the model on the rigid laboratory experimental frame. Therefore, fixed boundary conditions were modeled for all nodal points in the base of the formulated model.

vii. ***Concept of the analytically simulated loading pattern:*** Analogously to the experimental test of model M2-B, in the first phase, vertical load to the specified amount of N1 = 62.5 kN was gradually applied on each of both RC columns. This process was realized by an incremental increase of the loads. In the second phase, loading with horizontal load was carried out. The loading process was realized by application of small incremental deformations to provide conditions for required convergence of the final solutions.

viii. ***Micro-modeling of AAC infill:*** During the formulation of the analytical model for simulation of the behavior for the tested model M1-B representing an RC bare frame, the necessary conditions were created for its upgrading and simulation of the behavior of the tested model M2-B representing the RC frame with AAC infill. To provide the necessary accuracy during the modeling of the AAC infill, corresponding finite elements to model the material of the AAC elements and separately the material of the formed joints were applied. In addition, formulated were the corresponding separate nonlinear interface elements used to model the contacts between the joint material and the AAC element material as well as the contact between the joint material and the contact face of concrete built-in the corresponding RC elements, the footing beam, the two columns and the existing floor beam.

ix. ***Material FEM model and modeling parameters:*** Selection of the appropriate FEM models of different materials and/or other, present, specific nonlinear behavior sources was adapted to the available modeling options in the DIANA computer software [40], selected as an appropriate and advanced option for solving complex problems of this type. During analytical modeling of the model M2-B that represents an RC frame with AAC infill, representative options of finite elements defined with a corresponding set of representative input parameters were selected. Nonlinear behavior modelling of the

materials used in the formulated analytical model of RC frame with AAC infill, was provided with implementation of some input parameters defined by the conducted respective testing, while some additional input parameters were adopted from the available literature:

(1) FE type for concrete: For modeling of concrete used the same finite element Q8MEM, defined as four-node quadrilateral isoparametric element having 8 degrees-of-freedom representing translational displacements Ux and Uy of each node. It includes linear interpolation functions and 2 x 2 Gauss integration points.

In the model concrete material was represented with the following representative input parameters: Young's modulus 21000 N/mm^2; Poisson's ratio 0.2; Tensile strength 2.0 N/mm^2; Mode-I tensile fracture energy 0.169 N/mm; Compressive strength 25 N/mm^2. The quality of the concrete was verified by testing sample cubes proportioned 15x15x15 cm.

(2) FE type for steel: For modeling of steel, the same option simulating longitudinal bars connected to the mother concrete elements was provided in the DIANA computer software. The same representative input parameters were considered: Young's modulus 200000 N/mm^2; plastic hardening total strain-yield stress; and total strain-yield stress defined with four (strain, stress N/mm^2) points: P_0: 0., 0.; P_1: 0.00119, 240; P_2: 0.01, 280; P_3: 0.1, 280.

(3) Modeling of steel plates: Adopted parameters for micro-modeling of loading steel plates: (1) Linear elastic material; (2) Young's modulus = 200000 N/mm^2; (3) Poisson's ratio = 0.15.

(4) Micro-modeling of AAC infill elements: Adopted parameters for micro-modeling of AAC infill elements: (1) Young's modulus = 2000 N/mm^2; (2) Shear modulus = 1000 N/mm^2; (3) Mass density = 4e-10 T/mm^3; (4) Tensile strength = 0.25 N/mm^2; (5) Fracture energy in tension = 0.05 N/mm; (6) Residual tensile strength = 0.1 N/mm^2; (7) Angle between stepped diagonal crack and bed-joint = 12.5 °; (8) Compressive strength = 2.5 N/mm^2; (9) Fracture energy in compression = 40 N/mm; (10) Factor to strain at compressive strength = 1.8; (11) Unloading factor, 1=secant, 0=linear = 0.25; (12) Friction angle = 0.25; (13) Cohesion = 0.3 N/mm^2; (14) Fracture energy in shear = 0.0001 N/mm.

(5) Micro-modeling of joint material: (1) Material model = Total strain based crack model; (2) Young's modulus = 2000 N/mm^2; (3) Poisson's ratio = 0.2; (4) Crack orientation = Rotating; (5) Tensile strength = 0.25 N/mm^2; (6) Mode-I tensile fracture energy = 0.169 N/mm; (7) Compression curve = 0.169 N/mm; (8) Compressive strength = 2.5 N/mm2.

(6) Micro-modeling of interface elements: (1) Material model = Coulomb friction; (2) Type = 2D line interface; (3) Normal stiffness modulus-y = 6000 N/mm^3; (4) Shear stiffness modulus-x = 3000 N/mm^3; (5) Cohesion = 0.35 N/mm^2; (6) Friction angle = 30 °; (7) Dilatancy angle = 0 °; (8) Interface opening model = Gapping model; (9) Tensile strength = 0.25 N/mm^2; (10) Model for gap appearance = Brittle.

Considering the presented modeling assumptions, material representation and representative software options, a nonlinear analytical micro-model of the tested model M2-B representing RC frame with AAC infill was formulated and used for realization of the extended analytical study presented in this Chapter 6.

6.2 Material parameters used

Material parameters needed can be calculated from simple material tests, but for some parameters it will be not always possible. This is the main problem during model calibration for parameters. Material parameters were taken from test data whenever possible. And other material properties were taken from literature and DIANA guide.

The modulus of elasticity of concrete depends on the elastic properties of its components (aggregates and cementitious matrix) and the proportions of these components. According to EN 1992-1-1, the secant modulus of elasticity of concrete at 28 days, E_{cm}can be estimated using the following empirical expression:

$$E_{cm} = 22 * \left[\frac{f_{cm}}{10}\right]^{0.3} GPa$$

Where:

$$\mathrm{f_{cm}} = \mathrm{f_{ck}} + 8\mathrm{MPa\ is\ thr\ mean\ compressive\ strength\ of\ concrete}$$

$$\mathrm{f_{ck}\ is\ the\ characteristic\ compressive\ strength\ of\ concrete\ (MPa)}$$

The modulus of elasticity of the masonry (AAC units, mortar, and plaster) is generally evaluated from prism compression tests following EN 1052-1. In this work, the parameter was adopted based on standard experimental practice and literature references.

6.2.1 Tensile Strength and Fracture Energy of AAC Masonry

The tensile strength and fracture energy are fundamental mechanical parameters required to describe the cracking behavior and post-peak response of AAC masonry under lateral and dynamic actions. These parameters govern the initiation and propagation of cracks, energy dissipation capacity, and overall ductility of the masonry system, which are essential inputs for nonlinear analyses and for defining appropriate constitutive laws in numerical simulations. Understanding these properties is crucial for accurately modeling the load-transfer mechanisms between AAC units and mortar joints, and for assessing the seismic performance of AAC infilled frames.

Direct tensile tests are theoretically the most accurate method for determining the tensile strength of AAC masonry units. However, due to the complexity and sensitivity of direct tension setups, indirect methods are commonly adopted. Two practical alternatives are the

flexural tensile strength test (modulus of rupture) and the split-cylinder test [54]. According to empirical relationships reported in the literature and partially referenced in EN 12602 for prefabricated AAC elements, the tensile strength of AAC elements can be approximated as 5-10% of their compressive strength, depending on the density class and moisture condition [47].

Specifically, for AAC elements:

- If f_c is between 3 MPa and 6 MPa (typical for AAC densities 400-600 kg/m³), then f_t generally ranges between 0.15 MPa and 0.60 MPa.

Fracture behavior of AAC has been experimentally investigated by Wittmann (2002), showing that the mode-I fracture energy (G_f)of AAC materials is significantly lower compared to normal-weight concrete. For AAC materials with tensile strengths ranging between 0.2 MPa and 0.6 MPa, the corresponding fracture energy typically ranges from 20 N/m to 60 N/m, depending on porosity and curing conditions.

Further research by Bazant and Planas (1998) and Müller et al. (2017) confirmed that fracture energy is a critical parameter influencing the crack propagation and failure behavior of AAC masonry under tensile and flexural loads.

The CEB-FIP Model Code 1990 also provides empirical relationships to estimate the mechanical properties of materials based on their compressive strength. According to the Model Code, the tensile strength f_t, modulus of elasticity E_c, and fracture energy G_f can be related to the compressive strength f_c by the following expressions:

Tensile strength:

$$f_t = 0.30 * f_c^{2/3}$$

$f_c - comperssive\ strength\ in\ MPa$

$f_t - Tensile\ strength\ in\ MPa$

Modules of elasticity:

$$E_c = 21500 * (\frac{f_c}{10})^{1/3}$$

Fracture energy:

$$G_f = G_{f0} * (\frac{f_c}{f_{c0}})^{0.7}$$

$G_{f0} -$ Fracture energy

f_{c0} − Compresive strength

In CEB-FIP Model Code 1990, the reference fracture energy G_{f0} depends on d_{max} (maximum aggregate size) for concrete.

Value of G_{f0} is obtained from Table 6.2.1:

Table 6.2.1. Value of G_{f0}

	$d_{max}(mm)$		
	8	16	32
Fracture Energy (J/m^2)	25	30	58

Typical fracture energy for AAC elements based on density:

- For low-density AAC (400-600 kg/m³): G_f ≈ 20-60 N/m.
- In terms of J/m² (since 1 N/m = 1 J/m²): G_f≈ 20-60 J/m².

The compressive fracture energy (G_{f0} is typically estimated to be about 50 to 100 times greater than the tensile fracture energy G_f [41]. For AAC elements, considering that the tensile fracture energy G_f typically ranges between 20-60 J/m², the corresponding compressive fracture energy G_{fc} can be estimated between approximately 1000 J/m² and 6000 J/m², depending on the material density and microstructure. Parameters needed to define concrete and brick for smeared crack model in DIANA are listed below in Table 6.2.2:

Table 6.2.2. Parameters needed to define concrete and brick for smeared crack model in DIANA

Parameter	**Parameter Definition**	**Source**
f_c	Compressive Strength	Experiment, [45]
f_t	Tensile Strength	Estimated, Literature
E	Modulus of Elasticity	EN 12602 / CEB-FIP Model Code 1990
ν	Poisson's Ratio	Literature
G_f^I	First Mode Fracture Energy (Tension)	DIANNA Manual (2014) [40]
G_{fc}	Fracture Energy in Compression	DIANA Manual (2014) [40]
Tension Curve	Shape of tensile stress-strain curve	DIANA Manual (Exponential Softening) [40]
Compression Curve	Shape of compression stress-strain curve	DIANA Manual (Parabolic Hardening-Softening) [40]

6.2.2 Properties for Interface

In masonry structures, and particularly in AAC block masonry, the bond between mortar and masonry units represents one of the most critical and weakest zones. Numerous studies have shown that the mechanical behavior of masonry assemblies under loading, especially nonlinear and seismic actions, is heavily influenced by the performance of mortar joints and the AAC element-mortar interface [15], [28].

To accurately represent this behavior in numerical models, the interface between the AAC elements and mortar was modelled using special interface elements. These elements allow independent definition of normal and shear behaviors, enabling the simulation of two major failure mechanisms:

- Tensile failure (mode-I opening and loss of adhesion), and
- Shear failure (mode-II slide at the interface).
- The mechanical properties assigned to the interface elements include:
- Normal stiffness and shear stiffness, to prevent unrealistic deformations at the interface,
- Tensile strength and cohesion, to control crack initiation,
- Friction angle, to govern post-cracking sliding behavior.

For AAC masonry, tensile strength at the interface is significantly lower than the tensile strength of the blocks themselves. Based on literature, the tensile strength of the AAC element-mortar interface typically ranges between 0.05 MPa and 0.15 MPa, while the cohesion is generally between 0.05 MPa and 0.20 MPa [47], [48]. The friction angle usually varies between 30° and 40°, depending on surface characteristics and mortar properties. The values used for normal and shear stiffness were selected to be sufficiently high (typically around 10^7 N/m³) to ensure accurate simulation of elastic behavior before cracking initiates [41].

This modelling strategy ensures that both tensile deboning and shear sliding phenomena at the mortar-block interfaces are closely captured, thereby providing a reliable prediction of masonry behavior under various loading conditions.

To define the interface behavior for AAC masonry, the normal and shear elastic stiffnesses were calculated based on the formulations provided by [28]. The normal stiffness k_n and shear stiffness k_t are functions of the elastic and shear moduli of both the AAC unit and the mortar, and the joint thickness, according to the following relationships:

$$k_n = \frac{E_u E_j}{h_j(E_u - E_j)} \ , \ k_t = \frac{G_u G_j}{h_j(G_u - G_j)}$$

E_u and E_j are the elastic module of AAC element and mortar

$G_u$and G_j are their shear module, and h_j is the joint thicknes

For modelling the tension mode failure at the AAC element-mortar interface, the tensile bond strength (f_t) and the first mode fracture energy (G_f^I) were assigned based on recommendations from Lourenço (1996), [15]. These parameters are strongly influenced by the surface characteristics of the AAC element, mortar properties, and workmanship quality. The relationship between stress and displacement under tension was modelled using an exponential decay curve, where f_t represents the peak stress and the area under the curve corresponds to G_f^I.

6.2.3 Tension mode

The tensile strength of the bond (f_t) and the first mode fracture energy (G_f^I) are required as parameters to define the behavior of the interface under tension Fig 6.2.1. The bond properties are primarily influenced by the characteristics of the AAC element surface, the mortar properties, and the quality of workmanship during construction [15].

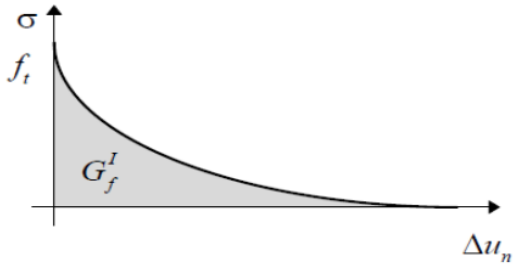

Figure 6.2.1. Stress-strain relations of AAC prisms of different grade under uniaxial compression.

Although a value of 0.012 Nmm/mm² is sometimes recommended for the first mode fracture energy of very weak bond interfaces [28], this value is considered too low for AAC masonry. In this study, a higher fracture energy value (typically between 20-50 J/m²) was adopted, based on the material properties of AAC elements and thin-joint mortar systems [48], [49].

6.2.4 Shear mode for interface behavior

In addition to tension failure, shear failure at the AAC element-mortar interface must also be considered. To model shear behavior accurately, several parameters are required:

- Bond strength (c),
- Friction angle (tanϕ),
- Dilatancy angle (tanψ),
- Mode II fracture energy (G_f^{II}).

According to Lotti and Shing (1994) and Rots (1997), Mode II fracture energy G_f^{II} can be estimated as approximately 10 times the Mode I fracture energy G_f^I. Alternatively, it can be approximated as 1/10 of the bond strength c, Fig 6.2.2.

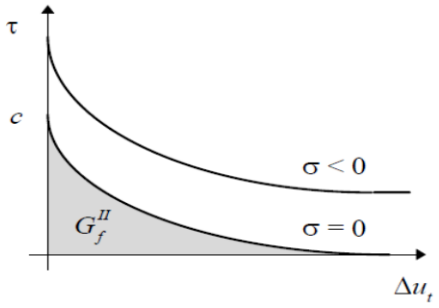

Figure 6.2.2. Stress-strain relations of AAC prisms of different grade under uniaxial compression

The friction angle ϕ represents the interface resistance after the initial bond failure and largely depends on the material surface roughness and mortar properties. Based on experimental studies [50], the friction angle for masonry interfaces can be reasonably assumed as 0.75 (in tangent form) unless specific testing data is available. For AAC masonry, a friction angle between 30° and 40° is typically appropriate, considering the smoother surfaces compared to natural bricks.

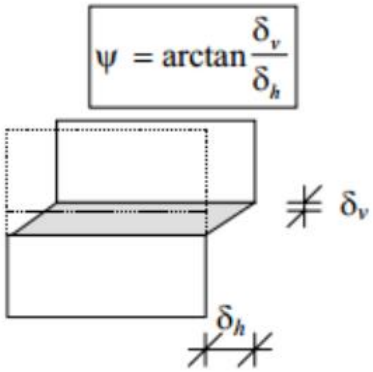

Figure 6.2.3. Stress-strain relations of AAC prisms of different grade under uniaxial compression

Similarly, dilatancy angle ψ describes the volumetric expansion (uplift) of the interface during shearing. As observed by Roca et al. (1998) and Lourenço (1996), the dilatancy angle depends strongly on confining pressure:

- At low confinement, the dilatancy angle is typically between 0.2-0.7 (in tangent value).
- At high confinement, dilatancy tends to 0 because surface sliding dominates and roughness effects vanish.

For AAC element interfaces, due to their relatively smooth surfaces, a zero dilatancy angle (ψ=0) was adopted in this study [28].

6.2.5 Cap Mode for Compression Behavior

To simulate the nonlinear behavior of AAC masonry under compression, a cap model was adopted. The cap mode requires the definition of four key parameters:

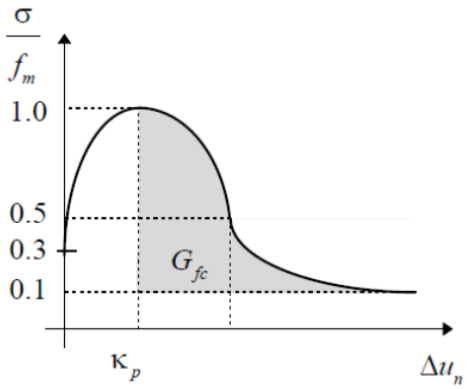

Figure 6.2.4. Stress-strain relations of AAC prisms of different grade under uniaxial compression

f_m: Uniaxial compressive strength of masonry

C_c: A shape parameter for the elliptical cap

G_{fc}: Compressive fracture energy

k_p: Equivalent relative displacement corresponding to 0.02% peak strain

According to the model Code 90(CEB-FIP,19910, the compressive fracture energy G_{fc} and equivalent relative displacement k_p can be estimated using the following expressions:

Compressive fracture energy:

$$G_{fc} = 15 + 0.43f_m - 0.0036f_m^2$$

Equivalent relative displacement:

$$k_p = \left(0.002 - \frac{f_m}{E_u}\left[1 + \frac{1}{k_n(h_u + h_j}\right]\right) f_m$$

f_m: Compressive strength of material

E_u: Elastic modulus of AAC element (MPa)

k_n: Normal stiffnes of the interface (N/mm^3)

h_u: thickness of AAC unit (mm)

h_j: thickness of the mortar joint (mm)

Additionally, an alternative empirical estimation for compressive fracture energy is given by Nakamura & Higai (2001), [51]:

$$G_{fc} = 8.8\sqrt{f_m}\ \ (MPa)$$

For the shape of compression cup, a value of C_c=9 was adopted [15].

In this study, based on the experimental values for AAC masonry compressive strength and modulus of elasticity, the compressive fracture energy G_{fc} and equivalent displacement k_p are calculated according to the expressions provided by the Model Code 90. A cap shape parameter C_c=9 was adopted, consistent with values recommended in literature for masonry materials [15].

Table 6.2.3. Parameter definition table

Parameter	**Parameter Definition**	**Source**
f_m	Compressive Strength of AAC Masonry	Experiment (This Study) + EN 12602
f_t	Tensile Strength of AAC element-Mortar Interface	Estimated (5-10% of f_m) + Literature
c	Cohesion (Shear Strength of Interface)	Experiment (Interface Tests) or Literature
K_n& K_s	Normal and Shear Stiffness of Interface	Relation (CUR 1994)
tanφ	Tangent of Initial Friction Angle	Experiment (Interface Tests) or Literature
G_f^I	First Mode Fracture Energy (Tension Mode)	Literature (Wittmann, 2002; DIANA Guide)
G_f^{II}	Second Mode Fracture Energy (Shear Mode)	Relation (G_f^{II}≈10×G_f^I
G_{fc}	Fracture Energy in Compression	Model Code 90 (CEB-FIP, 1991)
tan ψ	Dilatancy Angle (Tangent)	Assumed 0.0 (Roca et al., 1998)
tan φ_r	Tangent of Residual Friction Angle	Literature (Roca et al., 1998)
δ	Softening Parameter (Post-Peak Behavior)	DIANA Guide
C_c	Cap Shape Parameter	Lourenço (1996a) (Adopted C_c=9)
б$_u$	Confining Normal Stress	DIANA Guide
k_p	Equivalent Relative Displacement at Peak	Relation (Model Code 90 Formulas)

6.3 Low Axial Loads N1: Validation of Nonlinear Model based on experimental tests of RC Frame Models with AAC Infill

In Fig. 6.3.1 show is the developed nonlinear micro-model of the tested RC frame model M2-B with AAC infill used for its response analysis under axial load N1 = 62.5 kN and monotonic loading.

From the performed nonlinear analysis with application of the sleeted DIANA computer software, provided with installed corresponding input data, a complete solution output was obtained in the form of various types of large files.

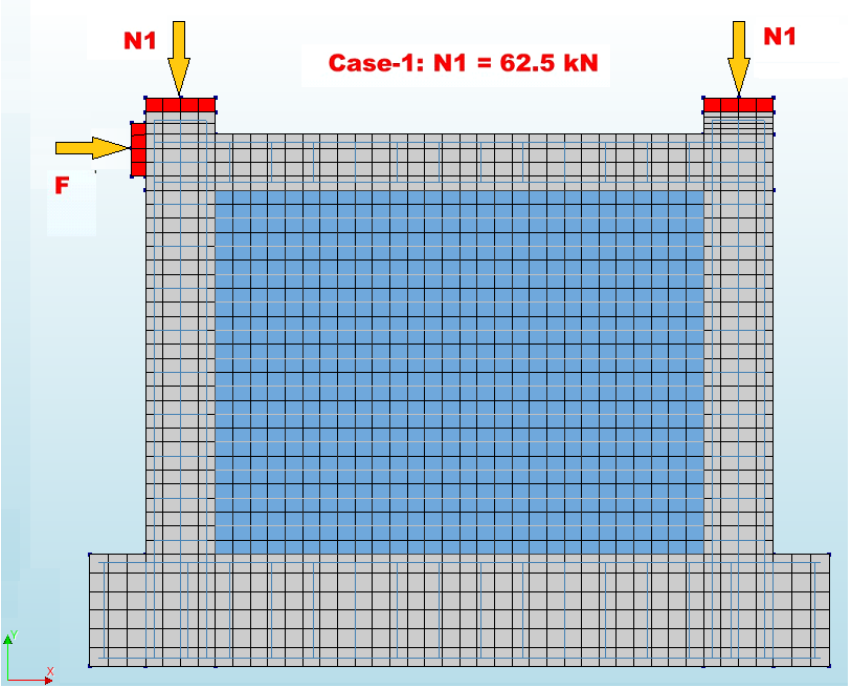

Figure 6.3.1. FE model of RC Frame M2-B with AAC infill used for its response analysis under axial load N1=62.5 kN and monotonic loading.

One part of the files contains the results from the solution in the form of numerical values. The second part of the files contains presentations of the corresponding results in the form of individual video presentations of the corresponding parameters, whose values are marked with a corresponding colour.

The video presentations were made to enable monitoring of the change of the computed physical quantities of the nonlinear response.

In the case of this specific analysis, a selection of the characteristic time from the video presentations was made and the representative states (images) were presented in a total of 32 electronic files, Table 6.3.1.

The stated table presents the obtained results from analytical phase A2-1, including the computed nonlinear response of the tested RC frame model with AAC infill (M2-B) under vertical load N1 = 62.5 kN and monotonic loading (Chapter 6.1).

In Table 6.1.1. given is list of included relevant data like for example: (1) mesh of the micro-model (file - 0); (2) six characteristic distributions of displacements (files 1 - 6); (3) six characteristic distributions of Cauchy total stresses (files 7 - 12); (4) six characteristic distributions of total strains (file 13 - 18); (5) two characteristic distributions of propagation of cracks in concrete (files 19 - 20); (6) six characteristic distributions of stresses in reinforcement (files 21 - 26) and (7) six characteristic distributions of total strains in reinforcement (files 27 - 32). To make closer evidence into the most characteristic results, presented in this text that refers to part 6.1, there are a total of 10 selected characteristic figures indicated as Fig. 6.3.1, Fig. 6.3.2 through Fig. 6.3.10. in the stated basic Table 6.3.1 showing the analytical phase A2-1. In all the figures included, the characteristic results obtained are clearly presented in color. For example, Fig. 6.3.2, Fig. 6.3.3 and Fig. 6.3.4 show the distributions of displacements DX(mm), DY(mm) and DXY(mm) for the respective computation time steps. From the stated figures, displacement DX is the most pronounced (Fig. 6.1.1), displacement DY is smaller (Fig. 6.1.2), while displacement DXY is quite expressed, Fig. 6.1.3.

Fig. 6.1.4 and Fig. 6.1.5 show the computed Cauchy total stresses SXX and SYY, respectively, in RC elements and in AAC infill. The values of both total stresses are characterized by the occurrence of two different zones (compression and tension), however, in both cases, compressive stresses dominate. Fig. 6.1.6 and Fig. 6.1.7 show the predicted distributions of cracks in concrete elements and in AAC infill for the solution steps 20 and 55, respectively. In Fig. 6.1.8, the zones of occurred cracks are enlarged since they correspond to higher values of induced displacements. However, the occurred distributions of cracks in concrete are generally of a local character while cracks in AAC infill are logically distributed in wider area, similarly as it was observed in the use of conducted experimental test. Fig. 6.1.9 and Fig. 6.1.10 show the computed distributions of reinforcement stresses SXX and SYY, respectively for the same solution step 55.

From the stated figures, it is evident that pronounced compressive and tensile stresses occur in the reinforcement. At segments where cracks occur in concrete, the tensile stresses are transferred to the reinforcement bars. Fig. 6.1.11 comparatively shows the nonlinear force - deformation relationships obtained by experimental test and FE simulation by application of the formulated nonlineaefficient technical conditionsr micro-model. Considering the great complexity of the analytical simulation, it can be concluded that the analytical and the experimental curves show a very good correlation. Only in limited zones observed was small mutual deviation. However, the occurred difference between the values of the maximum restoring force obtained experimentally and analytically is minimal and amounts to only 2.5%. The value of the maximum resisting force, i.e., the bearing capacity of the RC frame under horizontal loads represents one of the most important parameters. Besides this, the nonlinear force-deformation relationship obtained by applying the developed model is generally in good correlation with the experimentally defined envelope curve by means of the experimental test

on the model M2-B. The obtained results from the realized analytical study enabled full validation of the developed model of a reinforced concrete frame with AAC infill under vertical and horizontal loads. Considering the gained simulation benefits from the developed detailed and verified micro-model, an opportunity is opened for realization of new analytical research activity that is of the highest scientific importance. Further in this chapter presented are the results obtained from the two performed specific additional analytical studies of nonlinear response of RC frame with AAC infill under higher levels (N2 and N3) of vertical loads. The results obtained from the conducted extended analytical study, presented in parts 6.2 and 6.3, are generally of the highest importance for modern seismic engineering.

Table 6.3.1. Analytical phase A2-1: Computed nonlinear response of the tested RC frame model with AAC infill (M2-B) under vertical load N1=62.5 kN and monotonic loading (Ch. 6.1)

ANALYTICAL PHASE A2-1: Details of the RC frame with AAC infill (M2-B) under vertical load N1=62.5 kN and monotonic-loading (Ch. 6.1)					
File	Presented FEM parameter	Notation	Load step	E-Plotted	Shown/Fig.
0	Mesh of micro-model	Geometry	-	yes	+ / 6.1.0.
1	Displacement-x (mm)	TDtX	20	yes	
2	Displacement-x (mm)	TDtX	55	yes	+ / 6.1.1.
3	Displacement-y (mm)	TDtY	20	yes	
4	Displacement-y (mm)	TDtY	55	yes	+ / 6.1.2.
5	Displacement-xy (mm)	TDtXY	20	yes	
6	Displacement-xy (mm)	TDtXY	55	yes	+ / 6.1.3.
7	Cauchy total stresses-x (N/mm2)	SXX	20	yes	
8	Cauchy total stresses-x (N/mm2)	SXX	55	yes	+ / 6.1.4.
9	Cauchy total stresses-y (N/mm2)	SYY	20	yes	
10	Cauchy total stresses-y (N/mm2)	SYY	55	yes	+ / 6.1.5.
11	Cauchy total stresses-xy (N/mm2)	SXY	20	yes	
12	Cauchy total stresses-xy (N/mm2)	SXY	55	yes	
13	Total strains-x (mm/mm)	EXX	20	yes	
14	Total strains-x (mm/mm)	EXX	55	yes	
15	Total strains-y (mm/mm)	EYY	20	yes	
16	Total strains-y (mm/mm)	EYY	55	yes	
17	Total strains-xy (mm/mm)	EXY	20	yes	
18	Total strains-xy (mm/mm)	EXY	55	yes	
19	Crack widths: plane princ./comp. (mm)	Ecw	20	yes	+ / 6.1.6.
20	Crack widths: plane princ./comp. (mm)	Ecw	55	yes	+ / 6.1.7.
21	Reinforcement CT stresses-x (N/mm2)	SXX	20	yes	
22	Reinforcement CT stresses-x (N/mm2)	SXX	55	yes	+ / 6.1.8.
23	Reinforcement CT stresses-y (N/mm2)	SYY	20	yes	
24	Reinforcement CT stresses-y (N/mm2)	SYY	55	yes	+ / 6.1.9.
25	Reinforcement CT stresses-xy (N/mm2)	SXY	20	yes	
26	Reinforcement CT stresses-xy (N/mm2)	SXY	55	yes	
27	Reinforcement of total strain-x (mm/mm)	EXX	20	yes	
28	Reinforcement of total strain-x (mm/mm)	EXX	55	yes	
29	Reinforcement total strain-y (mm/mm)	EYY	20	yes	
30	Reinforcement total strain-y (mm/mm)	EYY	55	yes	
31	Reinforcement total strain-xy (mm/mm)	EXY	20	yes	
32	Reinforcement total strain-xy (mm/mm)	EXY	55	yes	
Number of plotted figures from analytical study using formulated micro-model					32
Number of figures presented showing representative results					10

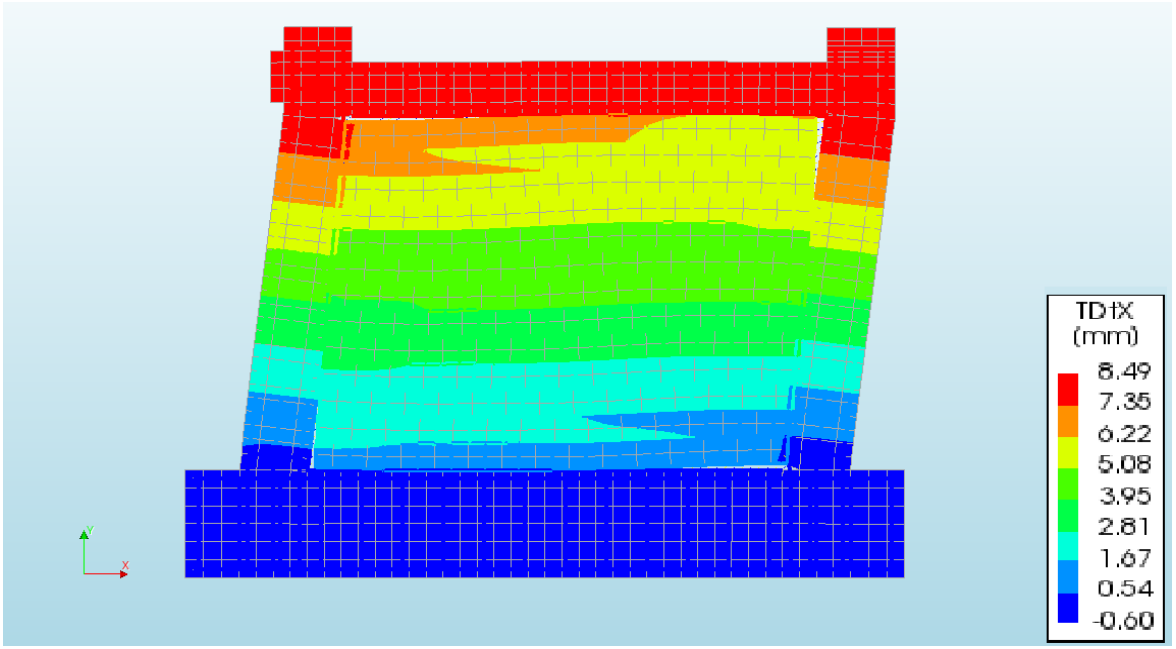

Figure 6.3.2. RC Frame model M2-B with AAC infill under axial load N1=62.5 kN and monotonic loading: Computed displacements DX for loading step 55.

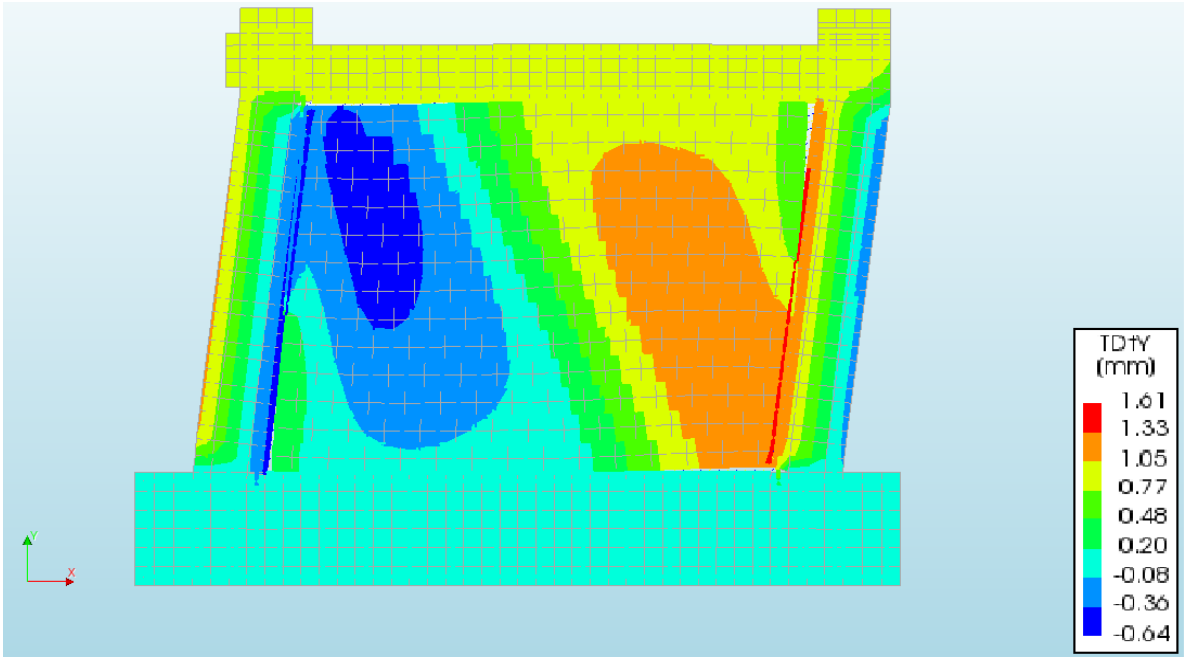

Figure 6.3.3. RC Frame model M2-B with AAC infill under axial load N1=62.5 kN and monotonic loading: Computed displacements DY for loading step 55.

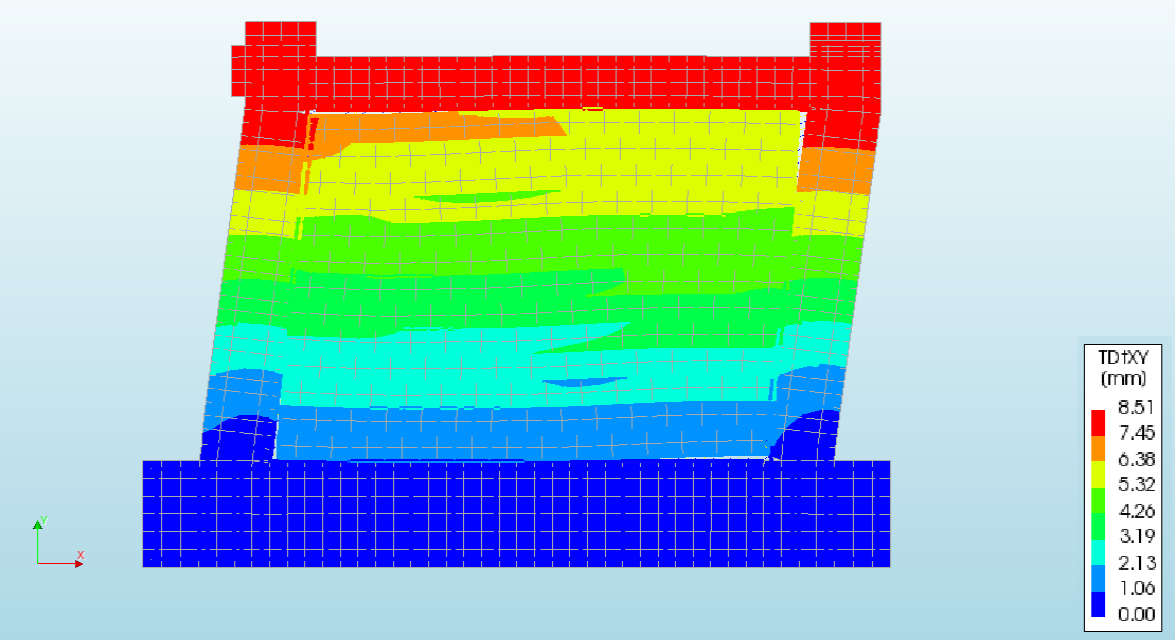

Figure 6.3.4. RC Frame model M2-B with AAC infill under axial load N1=62.5 kN and monotonic loading: Computed displacements DXY for loading step 55.

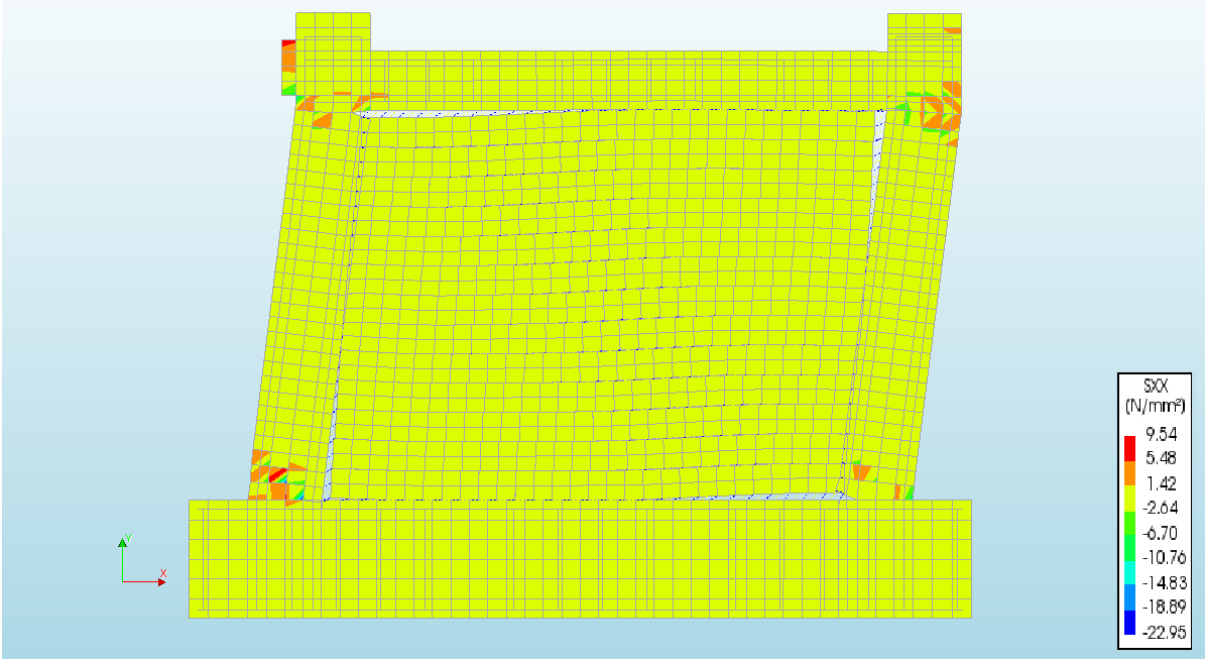

Figure 6.3.5. RC Frame model M2-B with AAC infill under axial load N1=62.5 kN and monotonic loading: Computed Cauchy total stresses SXX for loading step 55.

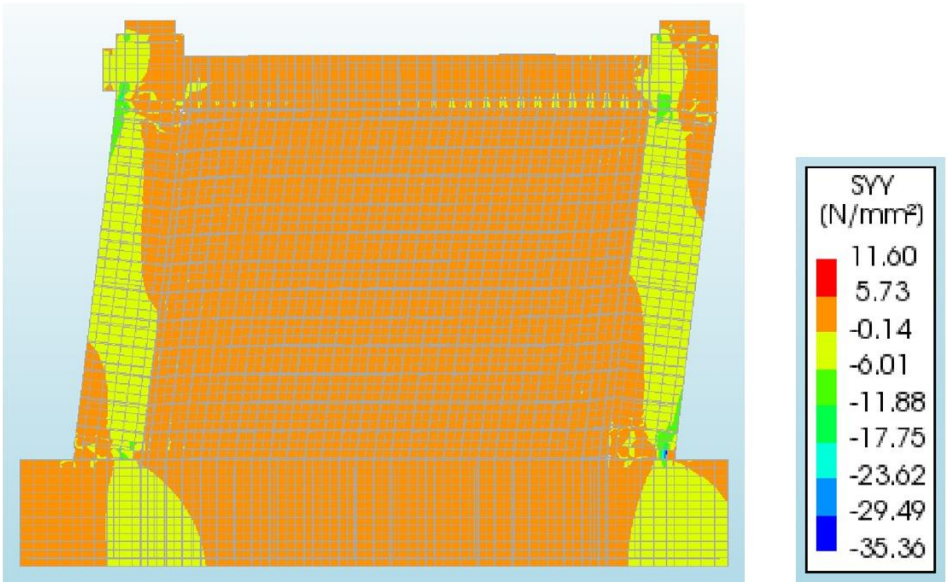

Figure 6.3.6. RC Frame model M2-B with AAC infill under axial load N1=62.5 kN and monotonic loading: Computed Cauchy total stresses SYY for loading step 55.

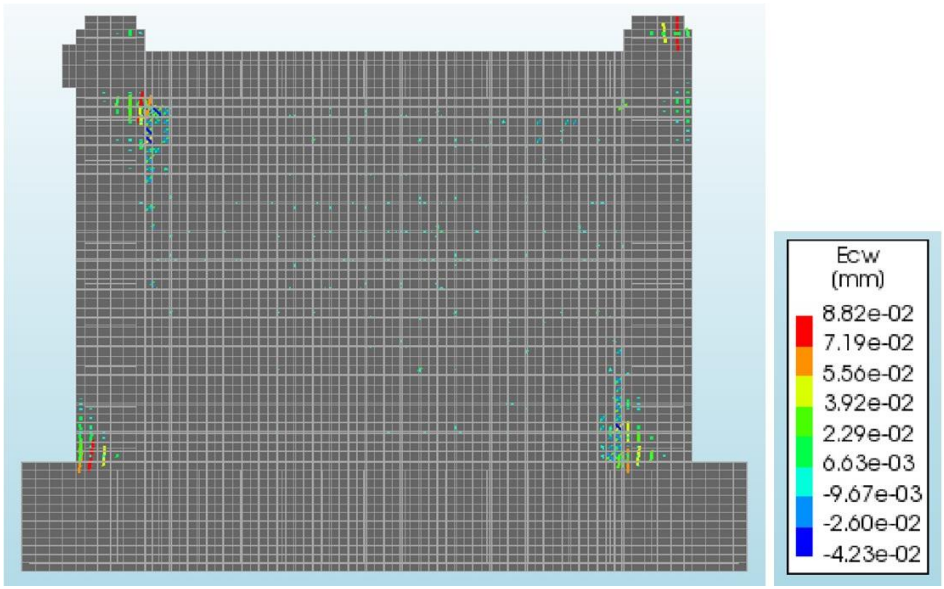

Figure 6.3.7. RC Frame model M2-B with AAC infill under axial load N1=62.5 kN and monotonic loading: Computed crack distribution for loading step 20.

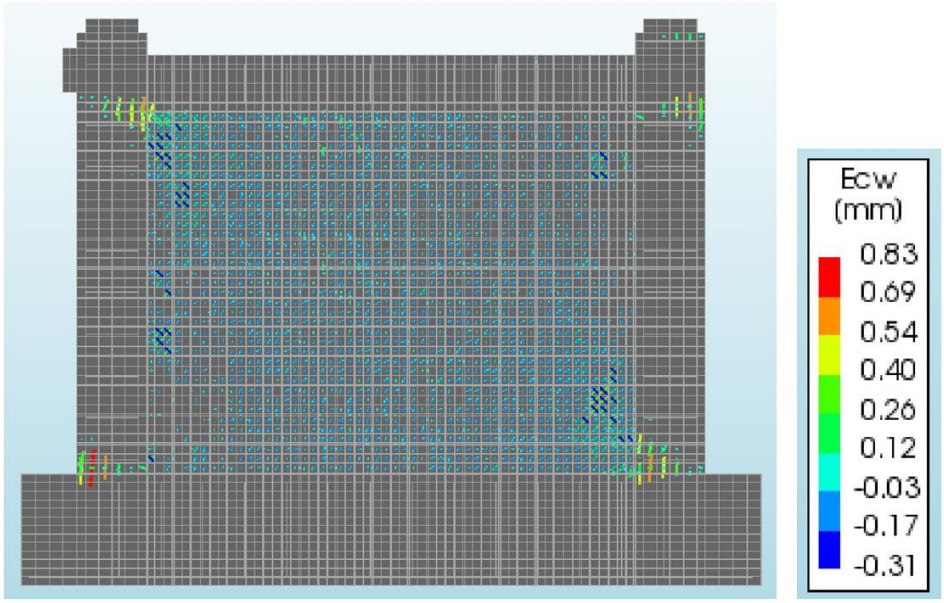

Figure 6.3.8. RC Frame model M2-B with AAC infill under axial load N1=62.5 kN and monotonic loading: Computed crack distribution for loading step 55.

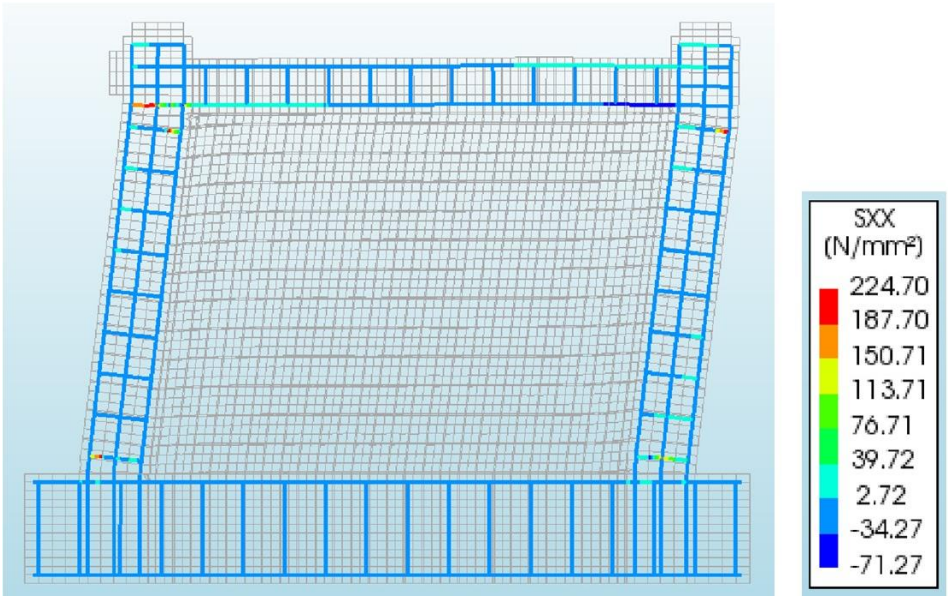

Figure 6.3.9. RC Frame model M2-B with AAC infill under axial load N1=62.5 kN and monotonic loading: Computed reinforcement stresses SXX for loading step 55.

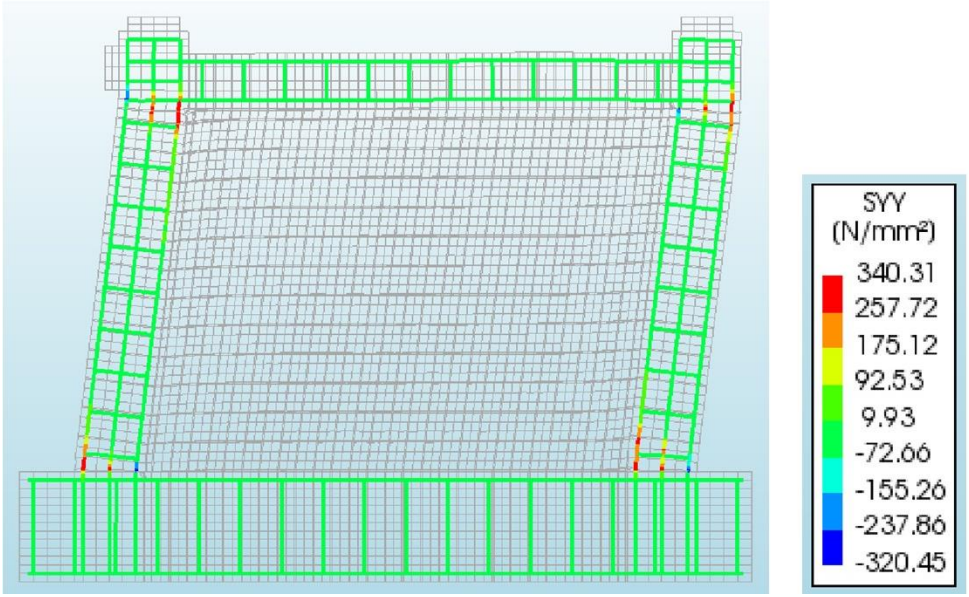

Figure 6.3.10. RC Frame model M2-B with AAC infill under axial load N1=62.5 kN and monotonic loading: Computed reinforcement stresses SYY for loading step 55.

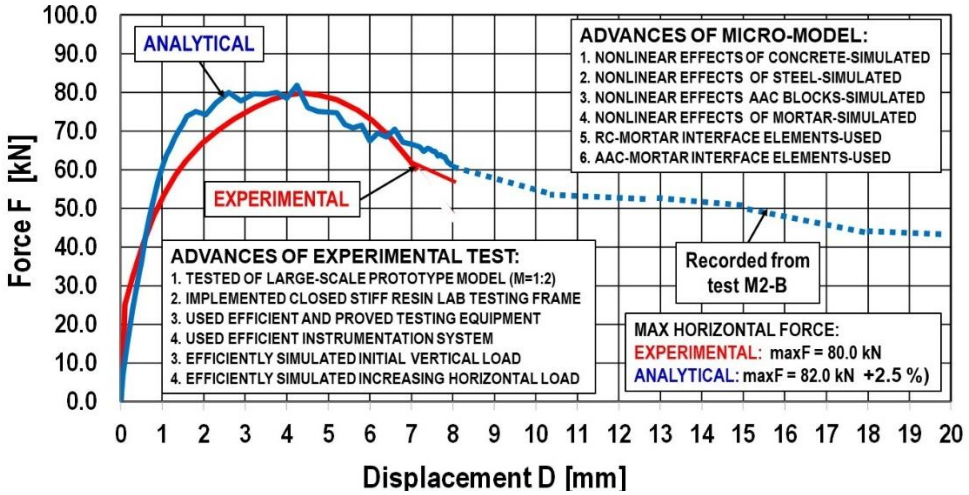

Figure 6.3.11. Comparison of experimental and numerical Force-Displacement curves of RC Frame model M2-B tested with AAC infill under axial load N1=62.5 kN and monotonic loading.

6.4 Medium Axial Loads N2: Nonlinear Response of RC Frame Model with AAC Infill M2-B1

This part of specific analytical study was conducted considering the formulated experimentally verified nonlinear micro-model and modified pattern of vertical and horizontal loads. In this case, on both RC columns the axial force was increased to N2 = 125.0 kN as shown in Fig. 6.4.1. The results obtained from the performed study are analogously presented and analyzed in an identical way due to their extensiveness.

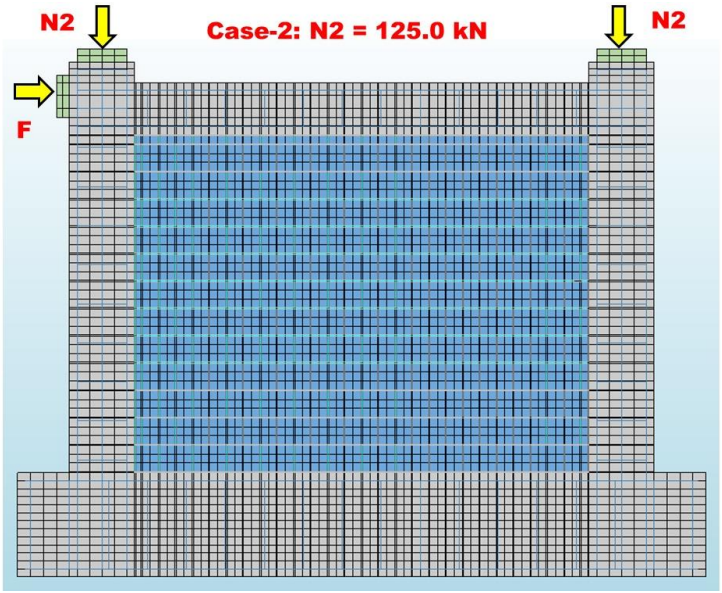

Figure 6.4.1. FE model of RC Frame model M2-B1 with AAC infill, under axial load N2=125.0 kN and monotonic loading.

Summarized in Table 6.4.1 are the results obtained from the analytical phase A2-2 representing the computed nonlinear response of the tested RC frame model with AAC infill (M2-B1) under vertical load N2 = 125.0 kN and monotonic loading (Chapter 6.2). For the selected characteristic solution step 43, Fig. 6.4.2, Fig. 6.4.3 and Fig. 6.4.4 show the distributions of displacements DX, DY and DXY, respectively. Although these distributions generally show similarities with the previous solution, there are certain differences due to the increased level of vertical loads. Fig. 6.4.5 and Fig. 6.4.6 show respectively the distributions of the computed total Cauchy stresses SXX and SYY, in concrete and in AAC infill, for the same solution, step 43. Due to the presence of reinforcement, the distribution of stresses in concrete is considerably changed. In the tensile zones, the tensile stresses are transferred to the built-in reinforcement to a dominant amount. In the AAC infill, the predated total Cauchy stresses show specific zones exposed to tension and compression. Fig. 6.4.7 and Fig. 6.4.8 comparatively show the distributions of cracks in concrete and in the AAC infill for two solution steps, 20 and 43, respectively. Although the zones of occurred cracks are approximately similar, the propagation of the zones and cracks is considerably larger for the solution step 43 which represents the state with increased displacements DXY. In the last two figures, Fig. 6.4.9 and Fig. 6.4.10, respectively, the reinforcement stresses SXX and SYY are presented. It is evident that stresses SYY are dominant in the critical zones since reinforcement dominantly sustains the tensile

stresses. To demonstrate the occurred difference in the model responses, comparatively are presented the computed envelope curves for axial load amounting to N1 = 62.5 kN and for an increased amount of axial load to the value of N2 = 125.0 kN, Fig. 6.2.10. From the results obtained, it is evident that the difference in the values of the computed maximum forces is considerable and amounts to 12.4%. With the conducted study it was verified that the increased axial force during seismic response can greatly affect nonlinear response followed by reduction of ductility and could not be neglected in the process of modern seismic resistant design.

Table 6.4.1. Analytical phase A2-2: Computed nonlinear response of the tested RC frame model with AAC infill (M2-B1) under vertical load N2=125.0 kN and monotonic loading (Ch. 6.2)

ANALYTICAL PHASE A2-2: Details of the RC frame with infill model (M2-B1) under vertical load N2=125.0 kN and monotonic loading (Ch. 6.2)					
File	Presented FEM parameter	Notation	Load step	E-Plotted	Shown
0	Mesh of micro-model	Geometry	-	yes	+ / 6.2.0.
1	Displacement-x (mm)	TDtX	20	yes	
2	Displacement-x (mm)	TDtX	43	yes	+ / 6.2.1.
3	Displacement-y (mm)	TDtY	20	yes	
4	Displacement-y (mm)	TDtY	43	yes	+ / 6.2.2.
5	Displacement-xy (mm)	TDtXY	20	yes	
6	Displacement-xy (mm)	TDtXY	43	yes	+ / 6.2.3.
7	Cauchy total stresses-x (N/mm^2)	SXX	20	yes	
8	Cauchy total stresses-x (N/mm^2)	SXX	43	yes	+ / 6.2.4.
9	Cauchy total stresses-y (N/mm^2)	SYY	20	yes	
10	Cauchy total stresses-y (N/mm^2)	SYY	43	yes	+ / 6.2.5.
11	Cauchy total stresses-xy (N/mm^2)	SXY	20	yes	
12	Cauchy total stresses-xy (N/mm^2)	SXY	43	yes	
13	Total strains-x (mm/mm)	EXX	20	yes	
14	Total strains-x (mm/mm)	EXX	43	yes	
15	Total strains-y (mm/mm)	EYY	20	yes	
16	Total strains-y (mm/mm)	EYY	43	yes	
17	Total strains-xy (mm/mm)	EXY	20	yes	
18	Total strains-xy (mm/mm)	EXY	43	yes	
19	Crack widths: plane princ./comp. (mm)	Ecw	20	yes	+ / 6.2.6.
20	Crack widths: plane princ./comp. (mm)	Ecw	43	yes	+ / 6.2.7.
21	Reinforcement CT stresses-x (N/mm^2)	SXX	20	yes	
22	Reinforcement CT stresses-x (N/mm^2)	SXX	43	yes	+ / 6.2.8.
23	Reinforcement CT stresses-y (N/mm^2)	SYY	20	yes	
24	Reinforcement CT stresses-y (N/mm^2)	SYY	43	yes	+ / 6.2.9.
25	Reinforcement CT stresses-xy (N/mm^2)	SXY	20	yes	
26	Reinforcement CT stresses-xy (N/mm^2)	SXY	43	yes	
27	Reinforcement of total strain-x (mm/mm)	EXX	20	yes	
28	Reinforcement of total strain-x (mm/mm)	EXX	43	yes	
29	Reinforcement total strain-y (mm/mm)	EYY	20	yes	
30	Reinforcement total strain-y (mm/mm)	EYY	43	yes	
31	Reinforcement total strain-xy (mm/mm)	EXY	20	yes	
32	Reinforcement total strain-xy (mm/mm)	EXY	43	yes	
Number of plotted figures from analytical study using formulated micro-model					32
Number of figures presented showing representative results					10

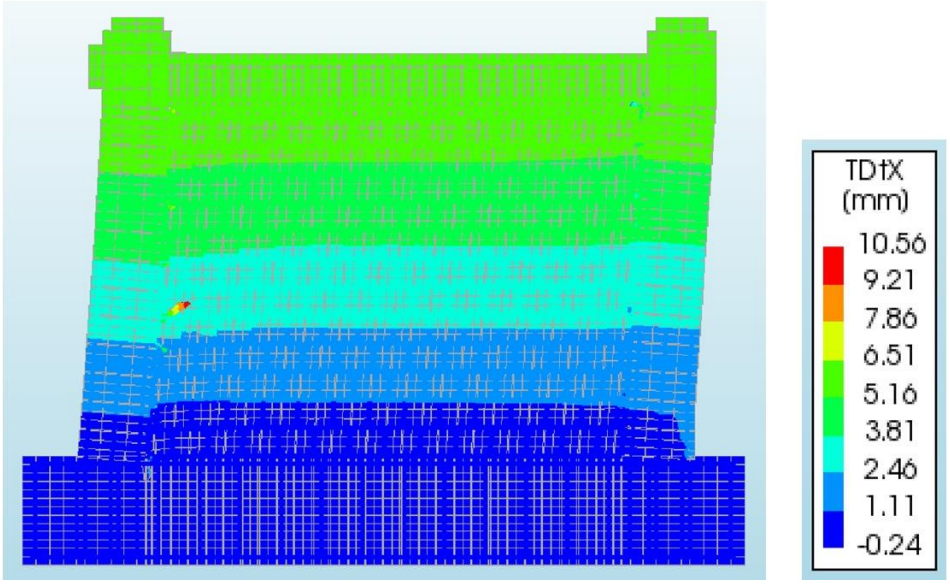

Figure 6.4.2. RC Frame model M2-B1 with AAC infill under axial load N2=125.0 kN and monotonic loading: Computed displacements DX for loading step 43.

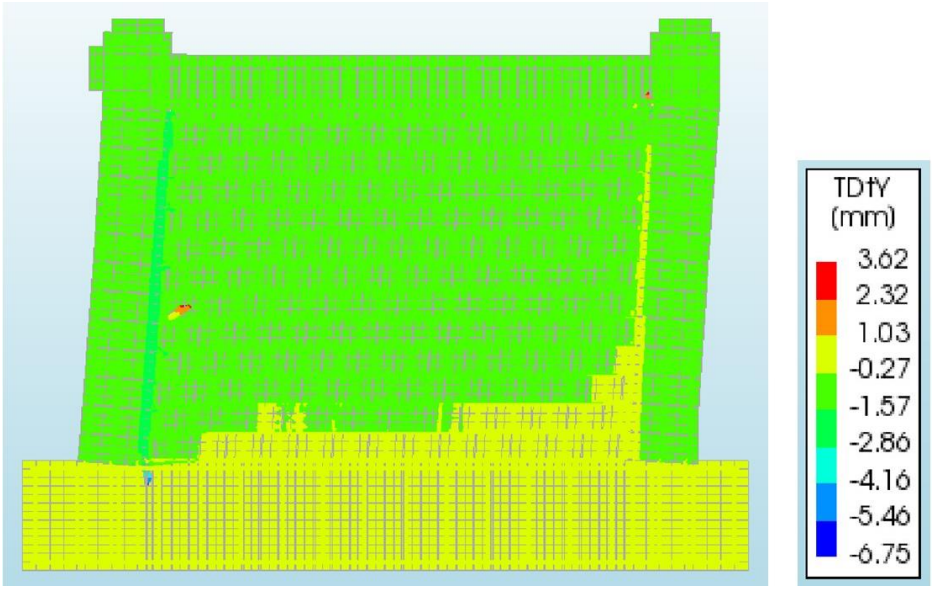

Figure 6.4.3. RC Frame model M2-B1 with AAC infill under axial load N2=125.0 kN and monotonic loading: Computed displacements DY for loading step 43.

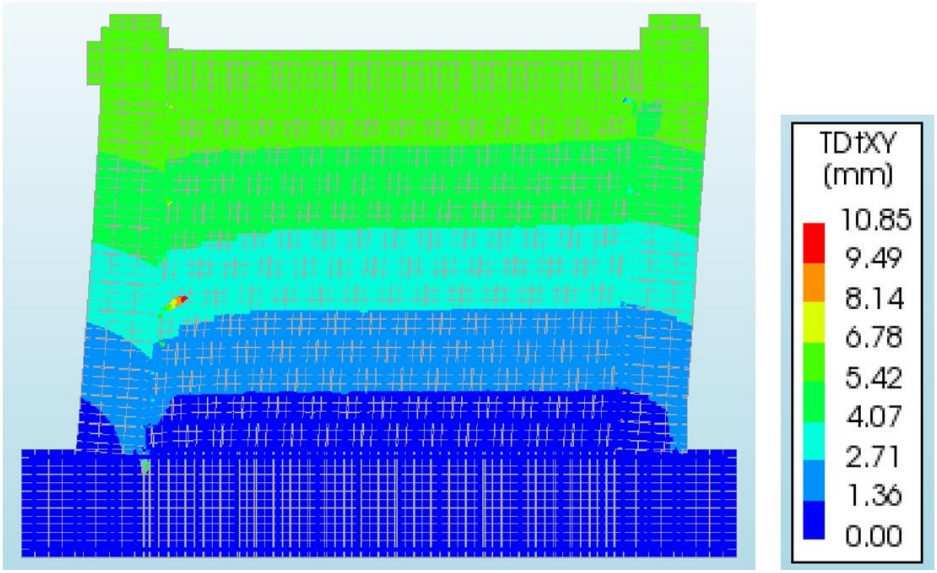

Figure 6.4.4. RC Frame model M2-B1 with AAC infill under axial load N2=125.0 kN and monotonic loading: Computed displacements DXY for loading step 43.

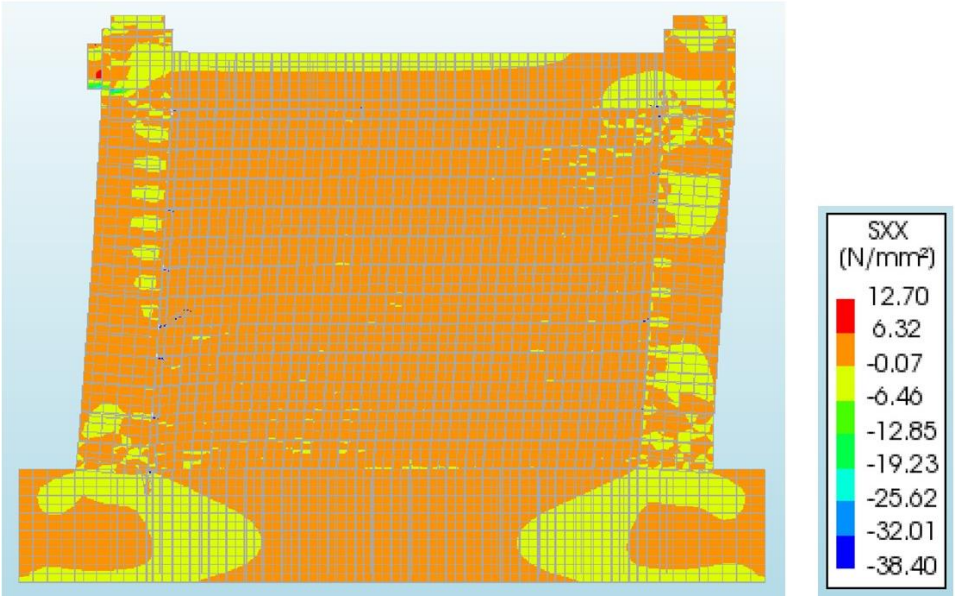

Figure 6.4.5. RC Frame model M2-B1 with AAC infill under axial load N2=125.0 kN and monotonic loading: Computed Cauchy total stresses SXX for loading step 43.

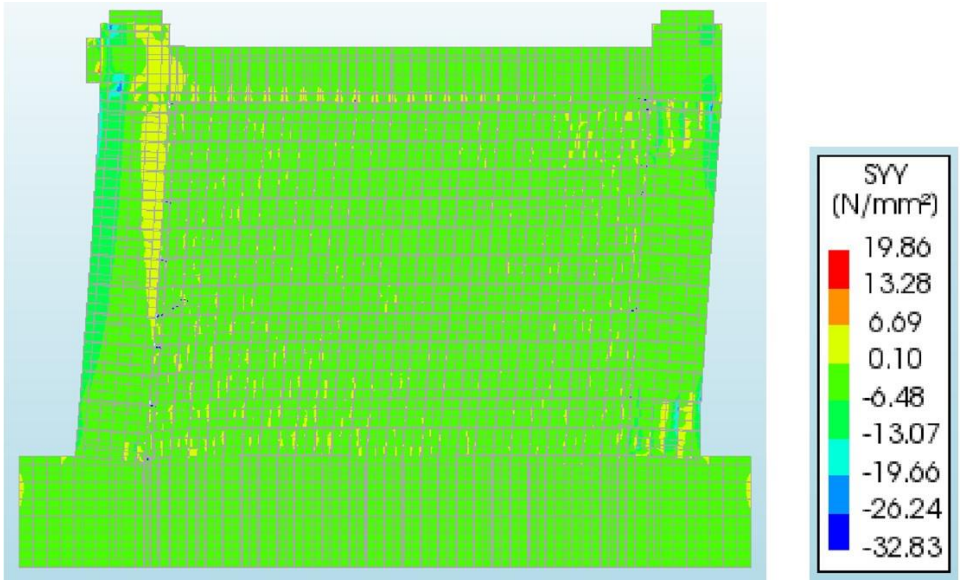

Figure 6.4.6. RC Frame model M2-B1 with AAC infill under axial load N2=125.0 kN and monotonic loading: Computed Cauchy total stresses SYY for loading step 43.

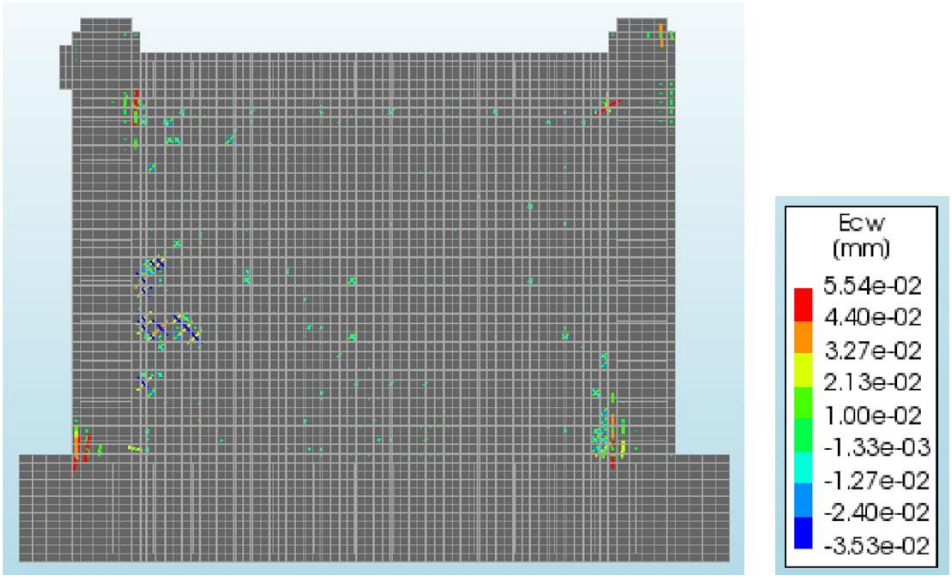

Figure 6.4.7. RC Frame model M2-B1 with AAC infill under axial load N2=125.0 kN and monotonic loading: Computed crack distribution for loading step 20.

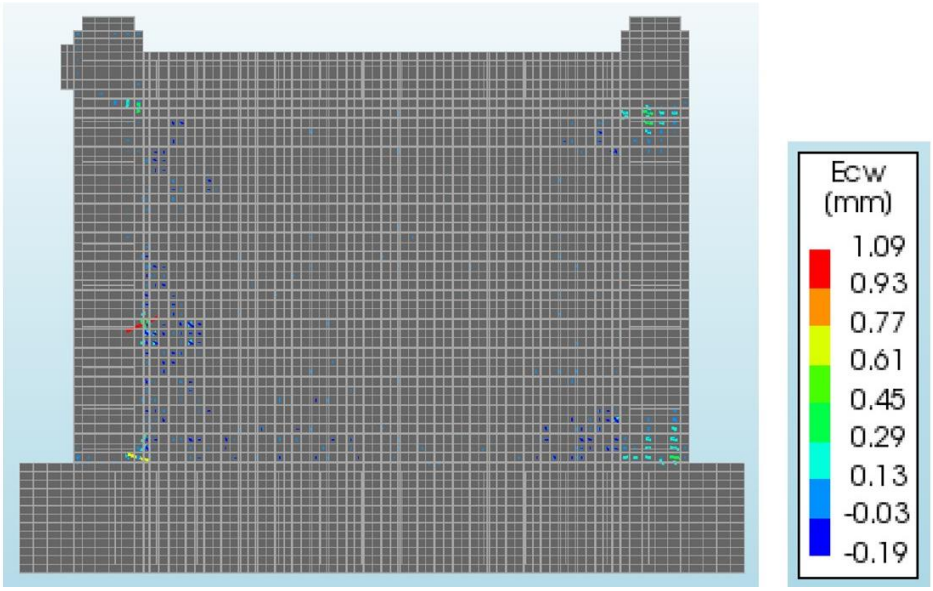

Figure 6.4.8. RC Frame model M2-B1 with AAC infill under axial load N2=125.0 kN and monotonic loading: Computed crack distribution for loading step 43.

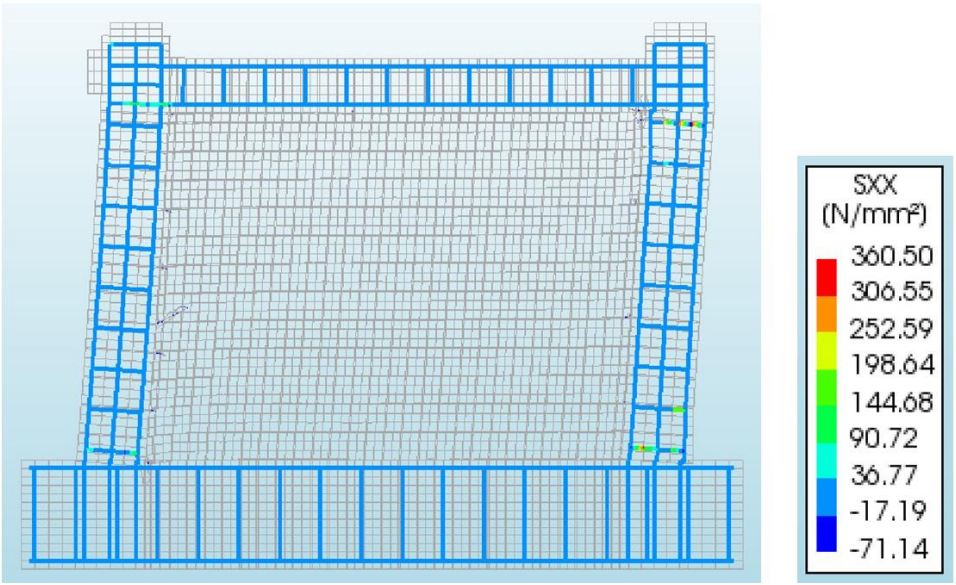

Figure 6.4.9. RC Frame model M2-B1 with AAC infill under axial load N2=125.0 kN and monotonic loading: Computed reinforcement stresses SXX for loading step 43.

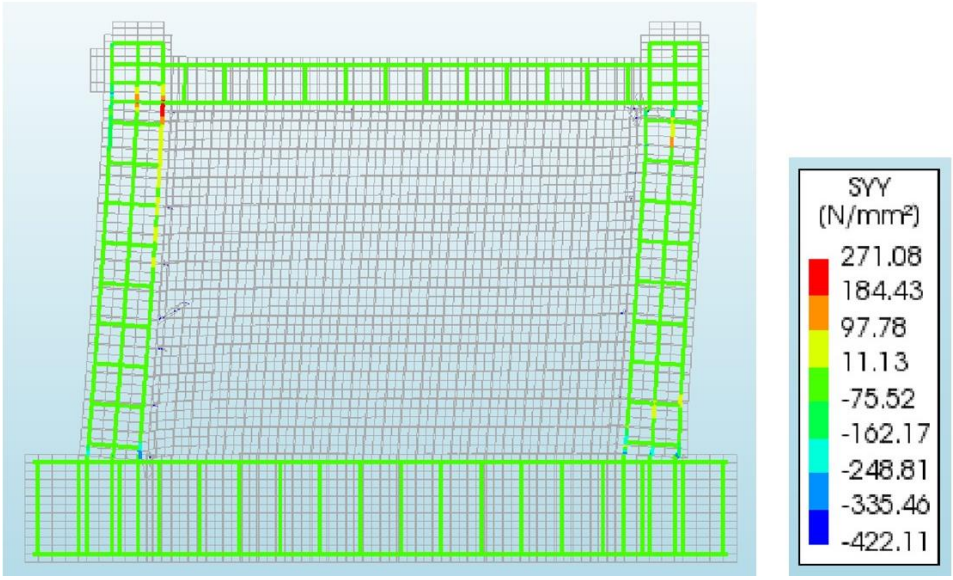

Figure 6.4.10. RC Frame model M2-B1 with AAC infill under axial load N2=125.0 kN and monotonic loading: Computed reinforcement stresses SYY for loading step 43.

6.5 High Axial Loads N3: Nonlinear Response of RC Frame Model with AAC Infill Using developed Analytical Model M2-B2

This third part of the study is also of particular importance since the level of vertical loads was increased even more to the amount of N3 = 280.0 kN. Fig. 6.5.1 shows the formulated nonlinear micro-model as well as the applied loading conditions.

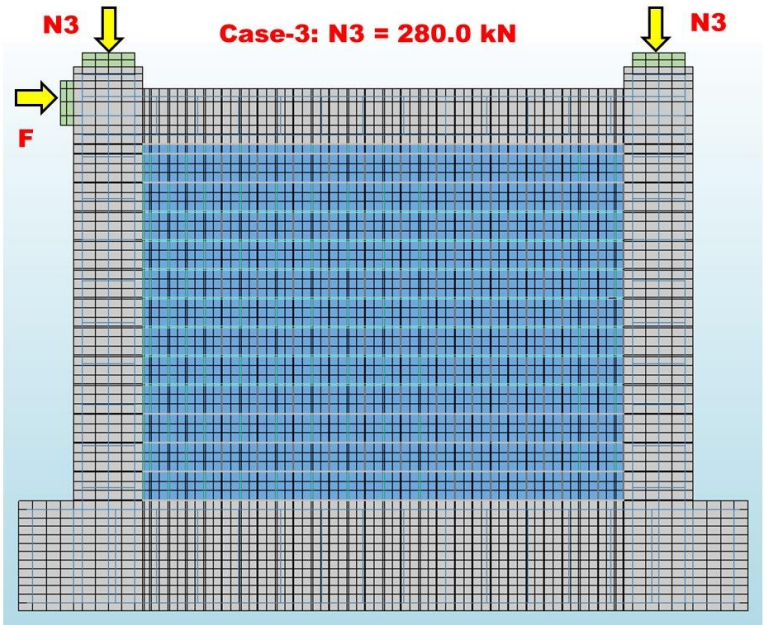

Figure 6.5.1. FE model of RC Frame model M2-B2 with AAC infill, under axial load N3=280.0 kN and monotonic loading.

The review of the results obtained in this analytical phase indicated as A2-3 is given in the analog Table 6.5.1. From the table, it is evident that the analysis finishes with a smaller number

of solution steps, i.e., at smaller values of displacements, there follows the critical phase of the nonlinear response.

Analogously, Fig. 6.5.2, Fig. 6.5.3 and Fig. 6.5.4 respectively show the distributions of displacements DXX, DYY and DXY. In all three cases, considerable changes are evident since the final solution (loading) step is smaller, amounting to 47.

Fig. 6.5.4 and Fig. 6.5.5 respectively show the Cauchy total stresses SXX and SYY. Due to the increased amount of vertical compressive loads, a considerable difference in stresses in concrete SYY is evident.

Fig. 6.5.6 and Fig. 6.5.7 comparatively show the distributions of the cracks in concrete and in AAC infill at solution step 20 and solution step 47. Although at both moments, locations of cracks are similar, for the solution step 47 the recorded rakes are largely changed. Very considerable enlargement of the area with cracks was recorded followed by significant enlargement of the width of cracks in critical zones.

Fig. 6.5.8 and Fig. 6.5.9 respectively show the reinforcement stresses SXX and SYY. It is evident that there is a considerable increase of stresses SYY in critical localized zones.

In the last Fig. 6.5.10, for the purpose of a clearer insight into response differences, the most important force-displacement relations obtained from the performed analytical studies presented in this chapter (Chapter 6) are comparatively shown.

As evident, the performed analysis verified the capability of the formulated micro-model to successfully predict the nonlinear response of the RC frame model M2-B with an AAC infill under the axial load of N3 = 280.0 kN and monotonic loading. In this case, the obtained maximum resisting force was greater for even 33.9% of the maximum force defined for the vertical load N1 = 62.5 kN. Consequently, the ductility of the analyzed RC frame model M2-B with AAC infill was dramatically decreased producing very critical response ending with collapse state.

Finally, the performed analysis directly confirms that the high level of axial forces leads to rapid reduction of the resisting force up to complete failure. The obtained results also point out that, in seismically active regions, the high levels of induced axial forces lead to critical situations and should be eliminated in the process of design of RC frame systems.

Table 6.5.1. Analytical phase A2-3: Computed nonlinear response of the tested RC frame model with AAC infill (M2-B2) under vertical load N1=280.0 kN and monotonic loading (Ch. 6.3)

ANALYTICAL PHASE A2-3: **Details of the RC frame with infille model (M2-B2) under vertical load N3=280.0 kN and monotonic loading (Ch. 6.3)**					
File	Presented FEM parameter	Notation	Load step	E-Plotted	Shown
0	Mesh of micro-model	Geometry	-	yes	+ / 6.3.0.
1	Displacement-x (mm)	TDtX	20	yes	
2	Displacement-x (mm)	TDtX	47	yes	+ / 6.3.1.
3	Displacement-y (mm)	TDtY	20	yes	
4	Displacement-y (mm)	TDtY	47	yes	+ / 6.3.2.
5	Displacement-xy (mm)	TDtXY	20	yes	
6	Displacement-xy (mm)	TDtXY	47	yes	+ / 6.3.3.
7	Cauchy total stresses-x (N/mm^2)	SXX	20	yes	
8	Cauchy total stresses-x (N/mm^2)	SXX	47	yes	+ / 6.3.4.
9	Cauchy total stresses-y (N/mm^2)	SYY	20	yes	
10	Cauchy total stresses-y (N/mm^2)	SYY	47	yes	+ / 6.3.5.
11	Cauchy total stresses-xy (N/mm^2)	SXY	20	yes	
12	Cauchy total stresses-xy (N/mm^2)	SXY	47	yes	
13	Total strains-x (mm/mm)	EXX	20	yes	
14	Total strains-x (mm/mm)	EXX	47	yes	
15	Total strains-y (mm/mm)	EYY	20	yes	
16	Total strains-y (mm/mm)	EYY	47	yes	
17	Total strains-xy (mm/mm)	EXY	20	yes	
18	Total strains-xy (mm/mm)	EXY	47	yes	
19	Crack widths: plane princ./comp. (mm)	Ecw	20	yes	+ / 6.3.6.
20	Crack widths: plane princ./comp. (mm)	Ecw	47	yes	+ / 6.3.7.
21	Reinforcement CT stresses-x (N/mm^2)	SXX	20	yes	
22	Reinforcement CT stresses-x (N/mm^2)	SXX	47	yes	+ / 6.3.8.
23	Reinforcement CT stresses-y (N/mm^2)	SYY	20	yes	
24	Reinforcement CT stresses-y (N/mm^2)	SYY	47	yes	+ / 6.3.9.
25	Reinforcement CT stresses-xy (N/mm^2)	SXY	20	yes	
26	Reinforcement CT stresses-xy (N/mm^2)	SXY	47	yes	
27	Reinforcement of total strain-x (mm/mm)	EXX	20	yes	
28	Reinforcement of total strain-x (mm/mm)	EXX	47	yes	
29	Reinforcement total strain-y (mm/mm)	EYY	20	yes	
30	Reinforcement total strain-y (mm/mm)	EYY	47	yes	
31	Reinforcement total strain-xy (mm/mm)	EXY	20	yes	
32	Reinforcement total strain-xy (mm/mm)	EXY	47	yes	
Number of plotted figures from analytical study using formulated micro-model					32
Number of figures presented showing representative results					10

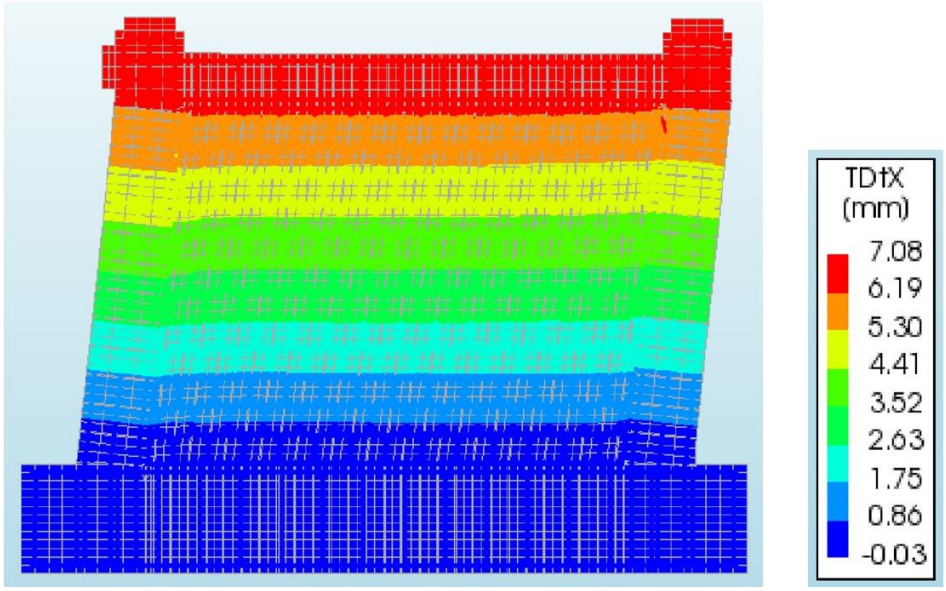

Figure 6.5.2. RC Frame model M2-B2 with AAC infill under axial load N3=280.0 kN and monotonic loading: Computed displacements DX for loading step 47.

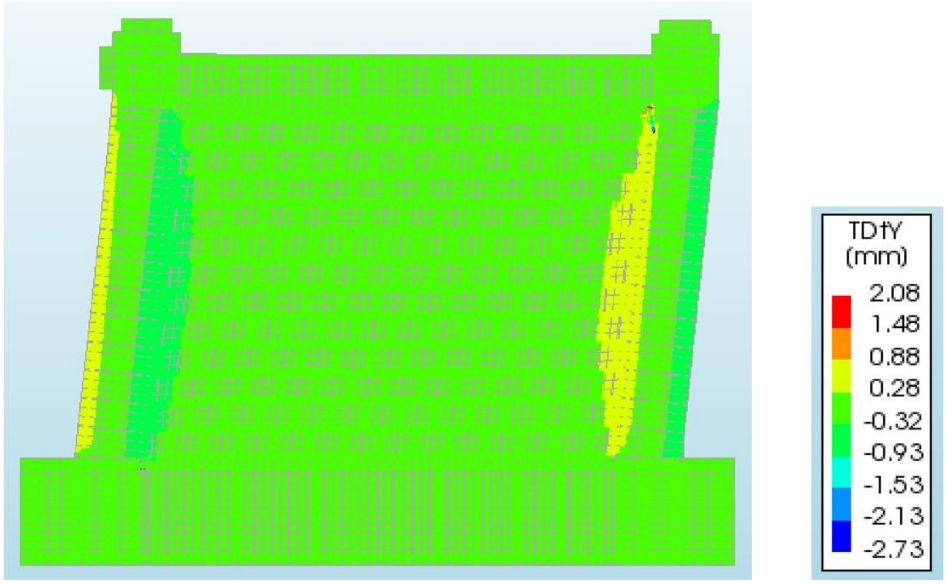

Figure 6.5.3. RC Frame model M2-B2 with AAC infill under axial load N3=280.0 kN and monotonic loading: Computed displacements DY for loading step 47.

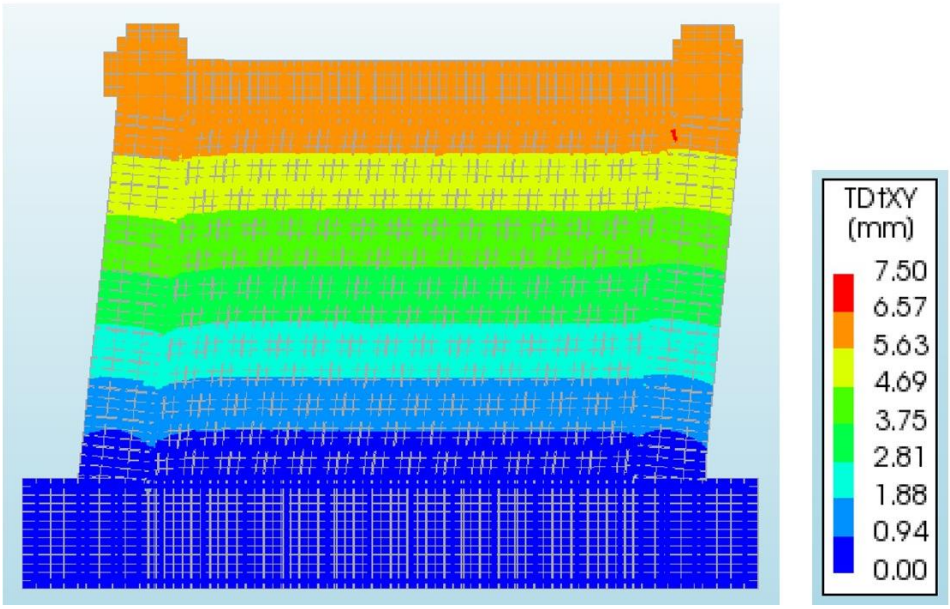

Figure 6.5.4. RC Frame model M2-B2 with AAC infill under axial load N3=280.0 kN and monotonic loading: Computed displacements DXY for loading step 47.

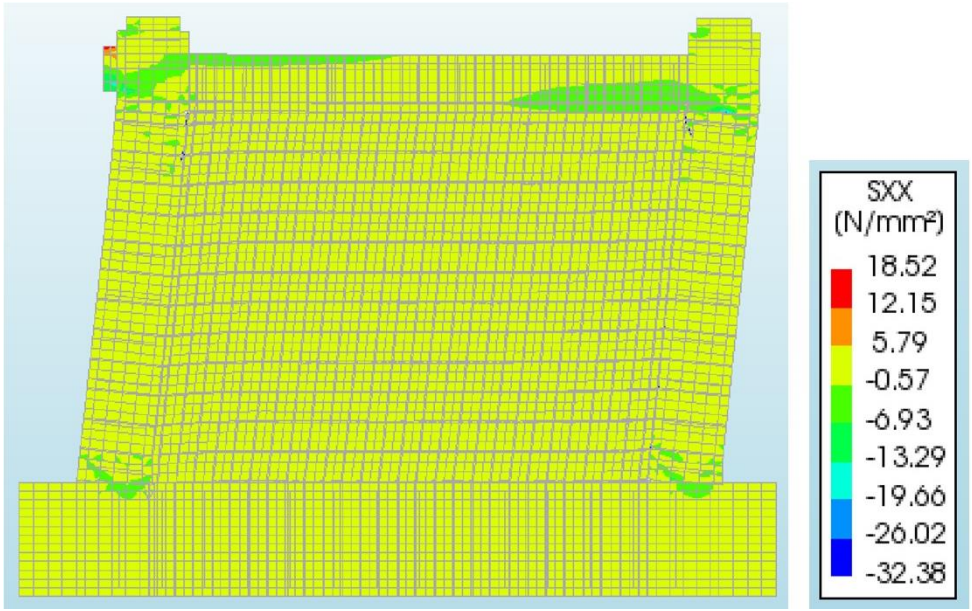

Figure 6.5.5. RC Frame model M2-B2 with AAC infill under axial load N3=280.0 kN and monotonic loading: Computed Cauchy total stresses SXX for loading step 47.

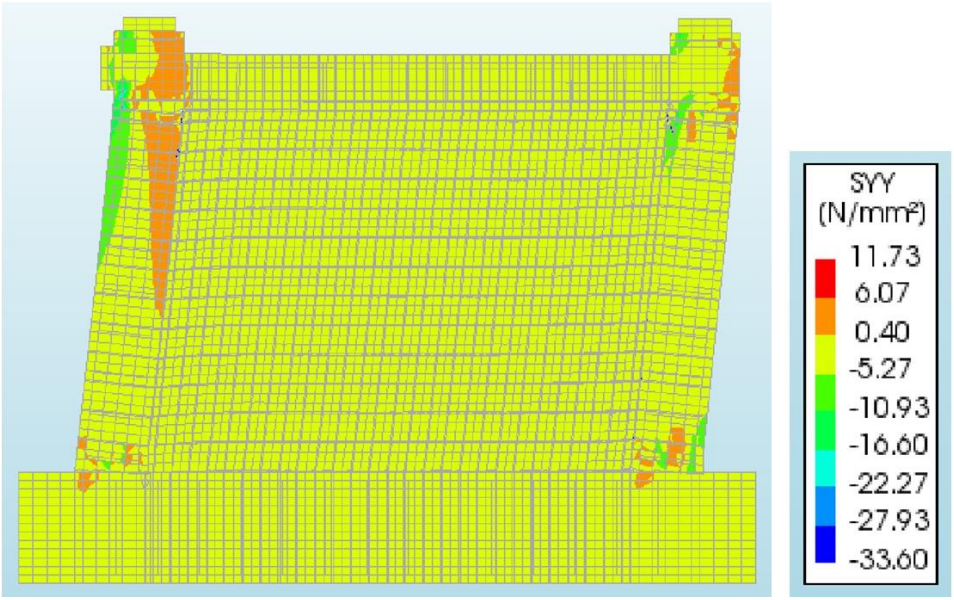

Figure 6.5.6. RC Frame model M2-B2 with AAC infill under axial load N3=280.0 kN and monotonic loading: Computed Cauchy total stresses SYY for loading step 47.

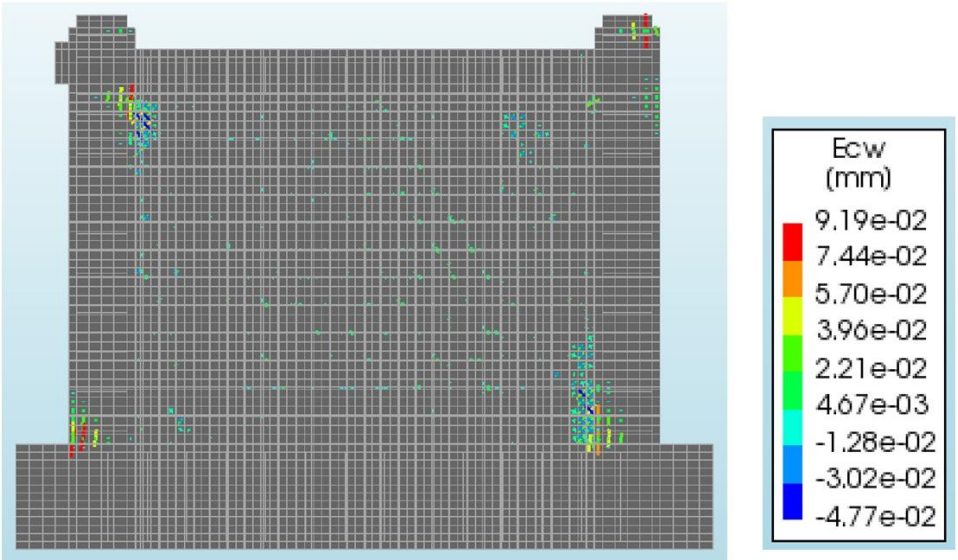

Figure 6.5.7. RC Frame model M2-B2 with AAC infill under axial load N3=280.0 kN and monotonic loading: Computed crack distribution for loading step 20.

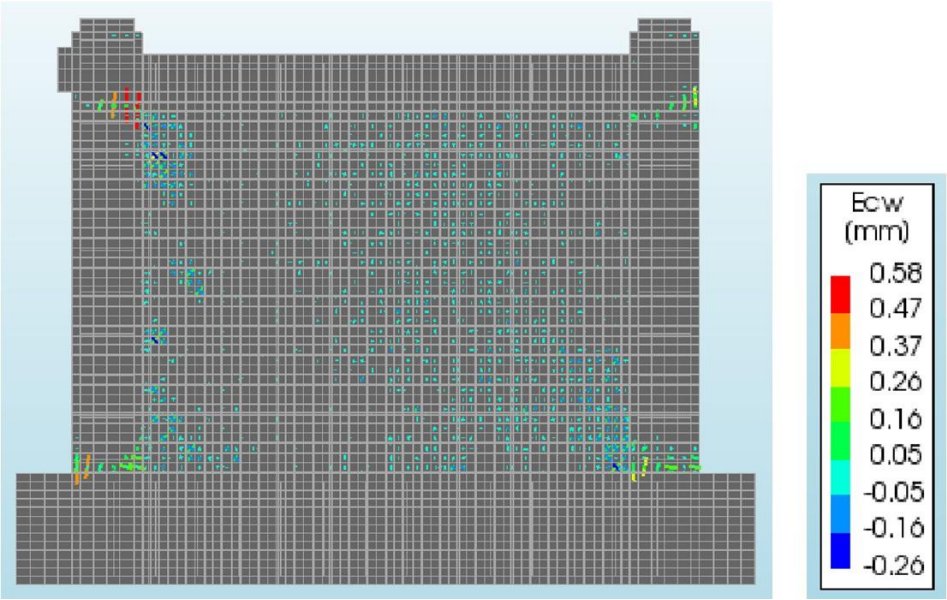

Figure 6.5.8. RC Frame model M2-B2 with AAC infill under axial load N3=280.0 kN and monotonic loading: Computed crack distribution for loading step 47.

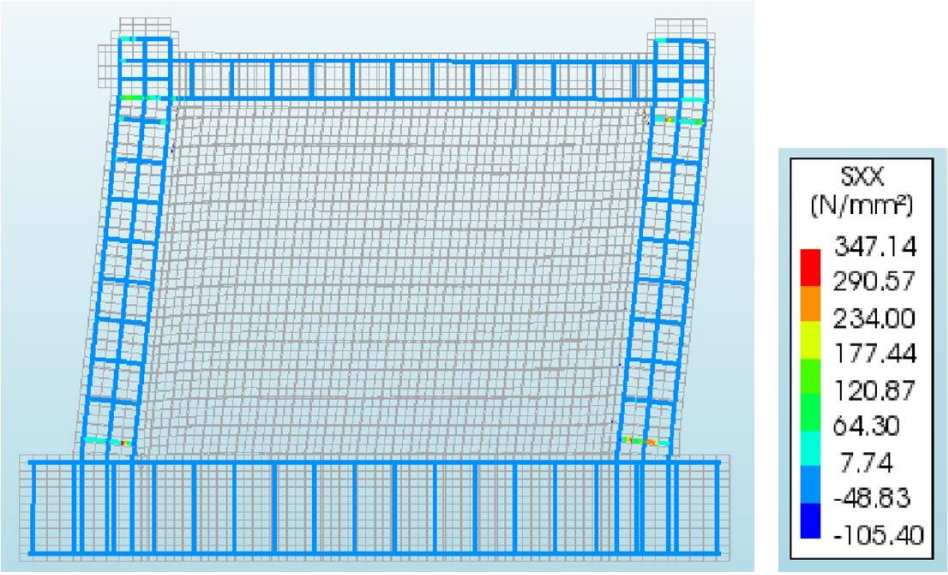

Figure 6.5.9. RC Frame model M2-B2 with AAC infill under axial load N3=280.0 kN and monotonic loading: Computed reinforcement stresses SXX for loading step 47.

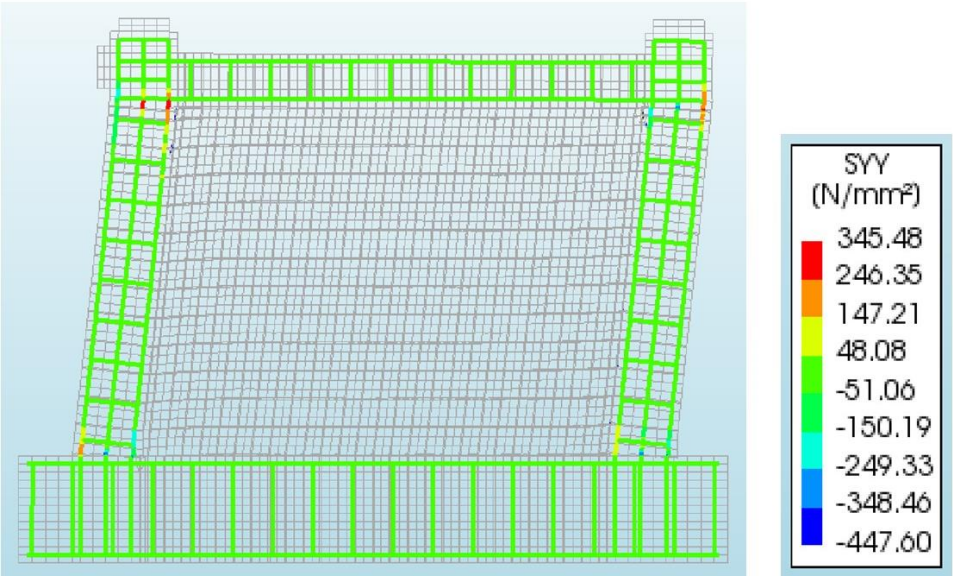

Figure 6.5.10. RC Frame model M2-B2 with AAC infill under axial load N3=280.0 kN and monotonic loading: Computed reinforcement stresses SYY for loading step 47.

6.6 Graphical and Quantitative Comparison of Results

Figure 6.6.1 shows the force-displacement relationships obtained from the nonlinear pushover analyses of the RC frame with AAC infill under three different axial load levels (N_1 = 62.5 kN, N_2 = 125 kN, N_3 = 280 kN). The results demonstrate a clear influence of the applied axial load on the overall stiffness, strength, and deformation capacity of the infilled frame.

At the lowest axial load (N_1 = 62.5 kN), the frame reached a maximum horizontal load of 82.0 kN. When the axial load increased to 125 kN, the peak lateral resistance rose to 92.2 kN, corresponding to an increase of 12.4 %. At the highest compression level (N_3 = 280 kN), the maximum lateral load reached 109.8 kN, representing an overall increase of 33.9 % relative to the reference case.

It is evident that higher axial compression enhances the initial stiffness and peak strength of the RC frame with AAC infill but simultaneously reduces its deformation and energy-dissipation capacity. The curve for N_3 becomes significantly steeper and terminates earlier, indicating a stiffer yet more brittle response. Conversely, the curve for N_1 exhibits gradual strength degradation and larger post-peak deformations, typical of a more ductile behavior.

This confirms that the axial load has a dual effect on the seismic performance of the RC frame with AAC infill: it increases the lateral load-carrying capacity due to confinement and diagonal compression of the infill but decreases ductility because of premature crushing and shear cracking within the AAC elements and the interface zones. The identified trend quantitatively illustrates the interdependence between axial compression, stiffness enhancement, and loss of deformability in infilled RC frames. The initial stiffness of the infilled frame is significantly

higher than that of the bare frame due to the presence of the AAC infill, which provides an additional diagonal compression path. However, as the axial load increases, the stiffness enhancement effect becomes less pronounced because the infill undergoes early micro-cracking and partial separation from the RC frame.

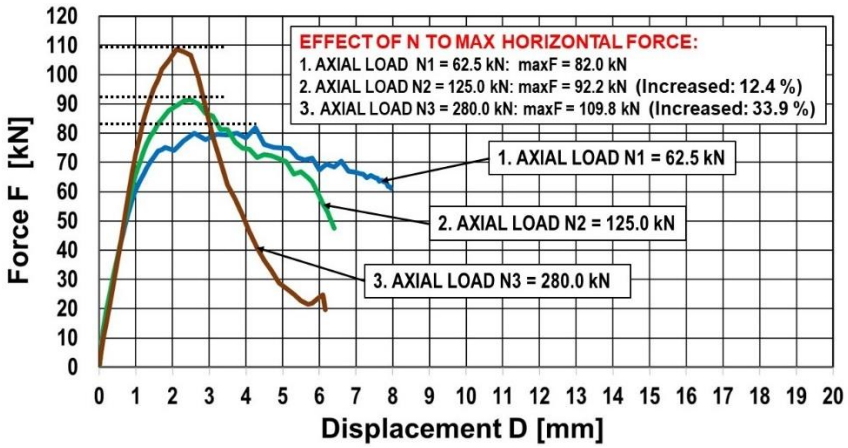

Figure 6.6.1. Comparison of Force-Displacement curves of RC Frame with AAC infill, models M2-B, M2-B1, M2-B2, with different axial loads and monotonic loading.

The numerical values presented in Table 6.6.1 were obtained directly from the pushover analysis results performed in DIANA FEA. The yield, peak, and ultimate points were identified from the force-displacement curves for each axial load level (62.5 kN, 125 kN, and 280 kN). The yield point corresponds to the first deviation from linearity on the curve, the peak load represents the maximum recorded lateral resistance, and the ultimate displacement was defined at a 20 % reduction of the peak load capacity. The ductility ratios were calculated as the ratio between ultimate and yield displacements.

Table 6.6.1. Summary of Key Parameters from Nonlinear Analyses under Different Axial Load

Axial Load (kN)	**Initial Stiffness Ko (kN/mm)**	**Yield Load Fy (kN)**	**Yield Disp. δy (mm)**	**Peak Load Fm (kN)**	**Peak Disp. δm (mm)**	**Ultimate Disp. δu (mm)**	**Ductility Ratio μ**	**Percentage Change Relative to Reference Case***
62.5 (Ref.)	17.6	44.0	2.5	82.0	2.3	11.0	4.4	–
125	20.4	47.0	2.3	92.2	2.4	9.6	4.2	+16 % Ko, +7 % Fy, +12 % Fm, −13 % δu, −5 % μ
280	26.0	52.0	2.0	109.8	–	7.5	3.8	+48 % Ko, +18 % Fy, +34 % Fm, −32 % δu, −14 % μ

6.6.1 Parametric Analysis Discussion

- Initial Stiffness

The initial stiffness of the AAC infilled frame increases progressively with the applied axial load, as presented in Table 6.5.1. At the lowest axial load level (N_1 = 62.5 kN), the frame exhibits an initial stiffness of approximately 17.6 kN/mm, mainly governed by the composite interaction between the RC frame and the AAC infill through diagonal compression struts. When the axial load increases to N_2 = 125 kN, the stiffness rises to about 20.4 kN/mm, representing an increase of nearly 16 % compared to the reference case. At the highest axial load level (N_3 = 280 kN), the initial stiffness reaches approximately 26.0 kN/mm, corresponding to an overall increase of about 48 % relative to the lowest axial load case.

This trend clearly indicates that axial compression enhances the effective stiffness of the infilled frame by reducing tensile strain in the columns, closing micro-cracks in the AAC wall, and improving confinement along the frame-infill interface. The initial stiffness values were determined directly from the pushover force-displacement curves using the relationship:

$$K_0 = \frac{F_y}{\delta_y}$$

where F_y is the yield load and δ_y is the corresponding yield displacement. This approach provides a reliable measure of the elastic slope of the curve before the onset of cracking. Consequently, the increase of $K_0$with axial compression reflects a stiffer and less deformable composite response of the infilled frame under higher vertical loading.

- **Peak Lateral Load Capacity**

The peak load increases steadily with axial compression, mainly due to the confinement effect in the columns and higher normal pressure at the contact zones. The AAC infill remains effective until crushing initiates at the corners. At N_3 = 280 kN, the maximum lateral force rises to about 110 kN (an increase of 33.9 %), confirming that the axial load can significantly enhance strength when within moderate limits.

- **Yield Characteristics**

The yield point shifts toward smaller displacements with higher axial load (from 2.3 mm to 1.9 mm). This reflects a stiffer pre-yield response and earlier onset of nonlinearity, showing that the system becomes more resistant but less deformable under increased compression.

- **Ductility**

As per Eurocode 8 and displacement-based design principles [59], [60], ductility is defined as:

$$\mu = \frac{\delta_u}{\delta_y}$$

Where:

δ_y – is the yield displacement (start of inelastic response)

δ_u – is the ultimate displacement (where significant strength degradation occurs)

The ductility ratio (μ) decreases progressively with increasing axial load from 4.4 at N_1 = 62.5 kN to 4.2 at N_2 = 125 kN, and further to 3.8 at N_3 = 280 kN. Although the AAC infilled frame remains ductile across all load levels, this gradual reduction clearly indicates a transition from a highly deformable response to a stiffer, strength-controlled behavior. The decrease in ductility is primarily attributed to the reduced rotational capacity within the plastic hinge regions and the earlier onset of crushing in the AAC elements and concrete at the column-infill interfaces under higher axial compression. While the increased vertical load enhances confinement and delays tensile cracking in both the frame and the infill, it simultaneously restricts curvature development and limits the overall energy dissipation capacity of the system.

- **Post-Peak and Ultimate Behavior**

At low axial load, the post-peak curve shows gradual strength degradation typical of ductile behavior. With increased axial load, the degradation becomes steeper, and ultimate displacement is significantly reduced [59], [60]. The failure mechanism transitions from diagonal tension cracking to local crushing and partial sliding at the interface, confirming the brittle nature of the AAC infill under high compression.

6.4.2 Infill-Specific Parameters

- **Infill Contribution to Total Resistance**

The AAC infill contributes approximately 40 % of the total lateral strength at N_1, 30 % at N_2, and 25 % at N_3. As the vertical compression increases, the infill's effective participation decreases due to progressive crushing and loss of shear transfer capacity.

- **Failure Modes**

Failure transitions from diagonal cracking at low load to corner crushing and interface sliding at high load. At high compression, the interaction between the column and infill intensifies, leading to localized crushing and eventual detachment along the contact zones.

- **Stiffness Degradation Patterns**

Stiffness degradation occurs more rapidly in the infilled frame after initial cracking. The residual stiffness at failure is around 25-30 % of the initial value, governed by frictional resistance along the cracked interfaces.

6.4.3 Interaction Effects

- **Frame-Infill Interaction**

Higher axial load increases the normal stress along the contact interface, reducing early sliding but promoting crushing at corners. The interface stress distribution becomes nonuniform, concentrating in the compression diagonal, which accelerates the formation of brittle failure zones.

- **Axial Load Sensitivity**

The infilled system is more sensitive to axial load variations than the bare frame because the AAC infill's nonlinear behavior strongly depends on compressive confinement. Small changes in vertical load significantly modify both the stiffness and the mode of interaction between the frame and the infill.

6.7 Findings from the Conducted Study of RC Frame Model with AAC Infill (M2-B)

Based on the new research results obtained from the study of the nonlinear behavior of RC frame structures with infill of AAC elements, these conclusions were summarized as follows:

1. The nonlinear horizontal resisting force-deformation relationship obtained by application of the formulated detailed nonlinear micro-model is in very good correlation with the experimentally verified nonlinear envelope curve. The difference between the experimentally defined maximum resisting force (maxF = 80.0 kN) and the analytically obtained maximum resisting force (maxF = 82.0 kN) is minimal and amounts to only 2.5%. This confirms the reliability of the adopted numerical procedure and its capability to predict closely load-deformation characteristics of infilled RC frames.
2. Summarizing the results obtained from the model verification study, it can be concluded that the formulated experimentally verified detailed nonlinear micro-model represents a very important research contribution, providing conditions for solving related complex problems. The formulated micro-model can therefore be successfully applied for realization of other specific research projects and for calibration of different infill materials and interface parameters under combined axial and lateral loading.
3. Based on the results obtained from the performed study of the nonlinear behavior of the RC frame with AAC infill, by application of the simulated effect of three different levels of axial forces on the columns, it is confirmed that axial forces have a significant

influence on the global behavior of the infilled frame. Therefore, their variation during intensive seismic excitations cannot be neglected. The axial load affects all key mechanical parameters stiffness, strength, and ductility and governs the transition from ductile to brittle response modes.

4. The increase of axial forces in the columns causes a significant increase of the maximum resisting forces in the RC frames with infill of AAC elements. This evidence was confirmed with the extended analytical studies, considering three different axial load levels, in specific studies realized with application of the experimentally verified nonlinear micro-model. At moderate axial compression (around 10% of column capacity), both stiffness and strength reach optimal values, while further increase of axial load (around 25%) no longer provides benefits and rather promotes earlier crushing of the infill. This observation defines an important design implication regarding the acceptable range of axial load ratios for infilled systems.
5. On the contrary, the increase of axial forces in the columns leads to a considerable reduction in ductility. This phenomenon represents the source of a very critical state, since stronger earthquakes may induce heavy damage or complete failure of the RC frames. The ductility reduction observed in the analyses corresponds to a 20-25% decrease in ultimate displacement when axial load increases from low to high levels. Such behavior emphasizes that stiffness and strength enhancement factors must always be balanced against ductility losses in performance-based design.
6. The cracks in the RC columns are generally of a local character and occur exactly in zones where they are expected close to the column-beam joints and at the base, representing locations of extreme compressive and tensile stresses. To solve this problem, the RC columns should be adequately designed for seismic zones of pronounced intensity. The obtained results also indicate that higher axial load increases local stress concentration and shear demand at the beam-column interfaces, making proper confinement and detailing of critical regions essential.
7. The cracks that occur in the AAC infill are generally dispersive. Larger cracks take place in diagonally oriented extended zones, while at the corners, more extensive local damage to the AAC infill occurs. One of the most important evidences about the behavior of the AAC infill is the confirmed complexity of the nonlinear response: (1) the AAC infill initially acts positively by increasing the system stiffness; (2) it also contributes positively to the increase of the resisting force of the system; (3) however, initial and extended cracks in AAC infill occur very early for relatively small deformations, representing an unwanted characteristic; and (4) extensive damage or complete failure of the AAC infill occurs even at relatively small lateral deformations. Following such extended damage and failures of AAC infill, the system can remain stable if adequate ductility of the RC columns is provided. These findings underline the interaction mechanism between frame and infill: as axial load increases, contact stress at the interface initially delays sliding, but later accelerates crushing and debonding. Therefore, the axial load not only modifies stiffness but also shifts the infill participation in total resistance from about 40% at low load to nearly 25% at high load.

8. The large vulnerability of the infill of AAC elements in zones with higher earthquake intensities cannot be allowed, but at the same time, it is difficult to reduce it successfully. Therefore, innovative and efficient technical solutions are necessary. To define efficient technological solutions, further research should continue in this direction. To reduce damage to the AAC infill, various options should be investigated, including:
    i. development of innovative concepts for adequate design of RC frame systems.
    ii. development of local isolation or sliding mechanisms between frame and infill; and
    iii. development of efficient base isolation systems for the integral building structures. From a practical design standpoint, it is recommended that axial load levels not exceed approximately 20-25% of the column's axial capacity when AAC infill is used as a nonstructural wall. This limit ensures that beneficial stiffness and strength contributions are utilized without compromising overall ductility. Ignoring the interaction between infill presence and axial load effects may lead to unsafe seismic performance predictions or uneconomical retrofitting decisions.

7 CHAPTER 7 - NUMERICAL SIMULATION OF RC FRAME WITH HALF-SPAN AAC INFILL

7.1 Nonlinear Analysis of RC Frame with Half-span AAC infill (M3-B)

In this Chapter 7 presented are new results obtained from the realized two specific complementary nonlinear response studies of two identical nonsymmetrical RC frames (M3-A and M3-B) designed with half-span AAC infill, analyzed under horizontal loading firstly in positive direction (M3-A) and then in negative direction (M3-B). However, in the case of both numerical studies, identical vertical load of N1 = 62.5 kN was. The performed numerical studies represent two specific ***"numerical experiments"*** since the applied analytical micro-model was verified with the obtained results from the experimental tests. The developed experimentally verified analytical models are of high importance because numerous innovative projects and other specific investigations can be successfully realized with their application. The results obtained from the two numerical studies carried out are presented in two successive sub-chapters 7.1 and 7.2. Finally, part 7.3 briefly the major findings are summarized from the conducted study using developed models of the considered M3-A and M3-B prototype models, representing RC frame with half-span AAC infill.

7.1.1 Importance of the Conducted Analytical Study

Regarding the achieved and confirmed success in micro-modelling of RC frames with masonry constructed of AAC elements in full frame-span, identified was the more specific research gap involving need for quantification of related nonlinear response of RC frames with the same masonry, but constructed in reduced extent, equal to only half of frame-span.

The analytical studies presented in this Chapter 7 were specifically targeted to provide research contribution in two important domains: (1) To evaluate response characteristics of nonsymmetrical RC frame with half-span AAC infill under horizontal monotonic loading in positive direction, and (2) To evaluate response characteristics of nonsymmetrical RC frame with half-span AAC infill under horizontal loading in negative direction.

7.1.2 Simulation of RC frame with half-span AAC infill (M3-A and M3-B)

The implemented advanced representative nonlinear micro-model of the selected specific example of RC frame with half-span AAC infill, presently analyzed under identical vertical and bi-directional horizontal loading (M3-A and M3-B), was formulated considering the same, previously presented, micro-modeling assumptions. Geometrical characteristics of the example frame and other related conceptual details used as the basis during formulation of respective nonlinear micro-model were presented in all necessary details in Chapter 6, enabling correct understanding and interpretation of the results obtained from the conducted specific analytical studies.

7.2 Introduction to parametric study

The purpose of this parametric comparison is to isolate and evaluate the influence of loading direction on the global response of the frame–infill system. The half-span infill configuration inherently introduces geometric asymmetry, and therefore it is reasonable to expect that loading direction could influence the stiffness, strength, crack development, and the distribution of internal forces. Chapter 7 emphasizes that all other parameters boundary conditions, material properties, reinforcement, and modelling assumptions were strictly kept constant, ensuring that the analysis compares only the effect of reversing the horizontal load.

7.2.1 Nonlinear Response of RC Frame model M3-A with Half-Span AAC Infill under Axial Load N1=62.5 kN and positive monotonic loading

In Fig. 7.2.1 shown is the formulated detailed nonlinear micro-model of the RC frame prototype model M3-A with half-span AAC infill used for its response analysis under axial load N1 = 62.5 kN and monotonic loading in ***positive*** direction.

From the performed nonlinear analysis with application of DIANA computer software and with provided respective input data, a complete solution output was obtained in the form of analogous types of different files.

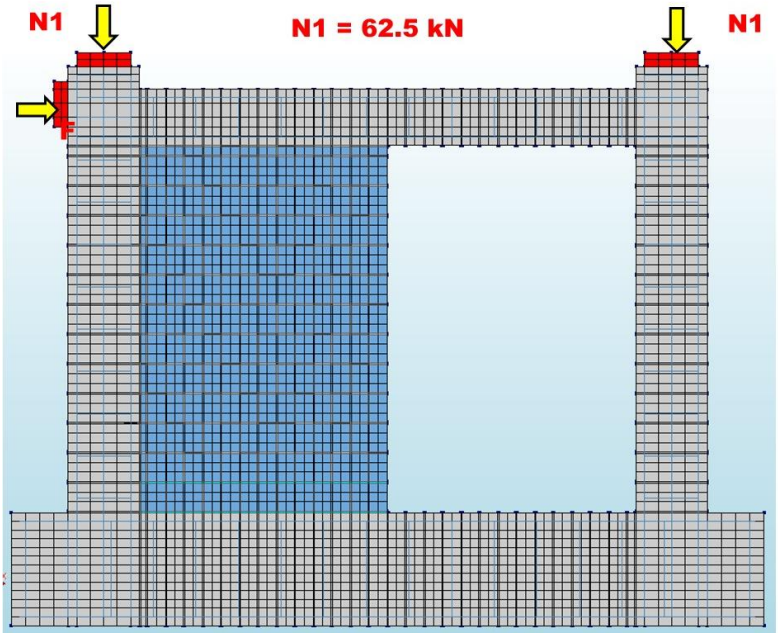

Figure 7.2.1. Developed nonlinear model of RC Frame model M3-A with half-span AAC infill under axial load N1=62.5 kN and positive monotonic loading.

In the case of this specific analysis, from the output video presentations selected were characteristic solution steps showing the representative solution states, in total 32 electronic files, Table 7.2.1. To make closer evidence into the most characteristic results, presented in this

text are a total of 10 selected characteristic figures indicated as Fig. 7.2.1, and Fig. 7.2.2 through Fig. 7.2.10. In all figures, the respective characteristic results are presented in color.

For example, Fig. 7.2.2, Fig. 7.2.3 and Fig. 7.2.4 show the distributions of displacements DX(mm), DY(mm) and DXY(mm) for the respective computation time steps. From the stated figures, displacement DX is the most pronounced (Fig. 7.2.2), displacement DY is smaller (Fig. 7.2.3), while displacement DXY is quite expressed, Fig. 7.2.4.

Fig. 7.2.5 and Fig. 7.2.6 show the computed Cauchy total stresses SXX and SYY, respectively, in RC elements and in AAC infill. The values of both total stresses are characterized by the occurrence of two different zones (compression and tension), however, in both cases, compressive stresses dominate.

Fig. 7.2.7 and Fig. 7.2.8 show the predicted distributions of cracks in concrete elements and in AAC infill for the solution steps 20 and 46, respectively. In Fig. 7.2.9, the zones of occurred cracks are enlarged since they correspond to higher values of induced displacements. However, the occurred distributions of cracks in concrete are generally of a local character while cracks in AAC infill are logically distributed in wider area.

Fig. 7.2.9 and Fig. 7.2.10 show the computed distributions of reinforcement stresses SXX and SYY, respectively for the same solution step 45.

From the stated figures, it is evident that pronounced compressive and tensile stresses occur. At segments where cracks occur in concrete, the tensile stresses are transferred to the reinforcement bars.

Fig. 7.2.11 shows the force - deformation curves, response of RC Frame model M3-A with half-span AAC infill under axial load N1=62.5 kN and monotonic loading positive direction. The maximum computed restoring force amounts to max F1(+) = 70.2 kN. Then, in the same figure shown is nonlinear fore - deformation response of only RC Frame represented with maximum restoring force amounting to max F2(+) = 45.0 kN, or 64.1%. Finally, to improve evidence of AAC effects, comparatively is shown in the figure the actual (extracted) nonlinear fore - deformation response of only AAC infill, represented with maximum restoring force of max F3(+) = 25.2 kN, or 35.9%.

The results obtained from the numerical study, presented in part 7.2, are of the highest importance for improved understanding of the effects of partially constructed AAC infill in modern RC frame systems.

Table 7.2.1. Analytical phase A3-1: Computed nonlinear response of the RC frame model with half-span AAC infill (M3-A1) under vertical load N1=62.5 kN and positive monotonic loading (Ch. 7.1)

ANALYTICAL PHASE A3-1: **Capability of formulated model: RC frame with half span AAC infill (M3-A1) under vertical load N1=62.5 kN and (+) monotonic loading (Ch. 7.1)**					
File	Presented FEM parameter	Notation	Load step	E-Plotted	Shown/Fig.
0	Mesh of micro-model	Geometry	-	yes	+ / 7.1.0.
1	Displacement-x (mm)	TDtX	20	yes	
2	Displacement-x (mm)	TDtX	47	yes	+ / 7.1.1.
3	Displacement-y (mm)	TDtY	20	yes	
4	Displacement-y (mm)	TDtY	47	yes	+ / 7.1.2.
5	Displacement-xy (mm)	TDtXY	20	yes	
6	Displacement-xy (mm)	TDtXY	47	yes	+ /7.1.3.
7	Cauchy total stresses-x (N/mm^2)	SXX	20	yes	
8	Cauchy total stresses-x (N/mm^2)	SXX	47	yes	+ / 7.1.4.
9	Cauchy total stresses-y (N/mm^2)	SYY	20	yes	
10	Cauchy total stresses-y (N/mm^2)	SYY	47	yes	+ / 7.1.5.
11	Cauchy total stresses-xy (N/mm^2)	SXY	20	yes	
12	Cauchy total stresses-xy (N/mm^2)	SXY	47	yes	
13	Total strains-x (mm/mm)	EXX	20	yes	
14	Total strains-x (mm/mm)	EXX	47	yes	
15	Total strains-y (mm/mm)	EYY	20	yes	
16	Total strains-y (mm/mm)	EYY	47	yes	
17	Total strains-xy (mm/mm)	EXY	20	yes	
18	Total strains-xy (mm/mm)	EXY	47	yes	
19	Crack widths: plane princ./comp. (mm)	Ecw	20	yes	+ / 7.1.6.
20	Crack widths: plane princ./comp. (mm)	Ecw	47	yes	+ / 7.1.7.
21	Reinforcement CT stresses-x (N/mm^2)	SXX	20	yes	
22	Reinforcement CT stresses-x (N/mm^2)	SXX	47	yes	+ / 7.1.8.
23	Reinforcement CT stresses-y (N/mm^2)	SYY	20	yes	
24	Reinforcement CT stresses-y (N/mm^2)	SYY	47	yes	+ / 7.1.9.
25	Reinforcement CT stresses-xy (N/mm^2)	SXY	20	yes	
26	Reinforcement CT stresses-xy (N/mm^2)	SXY	47	yes	
27	Reinforcement of total strain-x (mm/mm)	EXX	20	yes	
28	Reinforcement of total strain-x (mm/mm)	EXX	47	yes	
29	Reinforcement total strain-y (mm/mm)	EYY	20	yes	
30	Reinforcement total strain-y (mm/mm)	EYY	47	yes	
31	Reinforcement total strain-xy (mm/mm)	EXY	20	yes	
32	Reinforcement total strain-xy (mm/mm)	EXY	47	yes	
Number of plotted figures from analytical study using formulated micro-model					32
Number of figures presented showing representative results					10

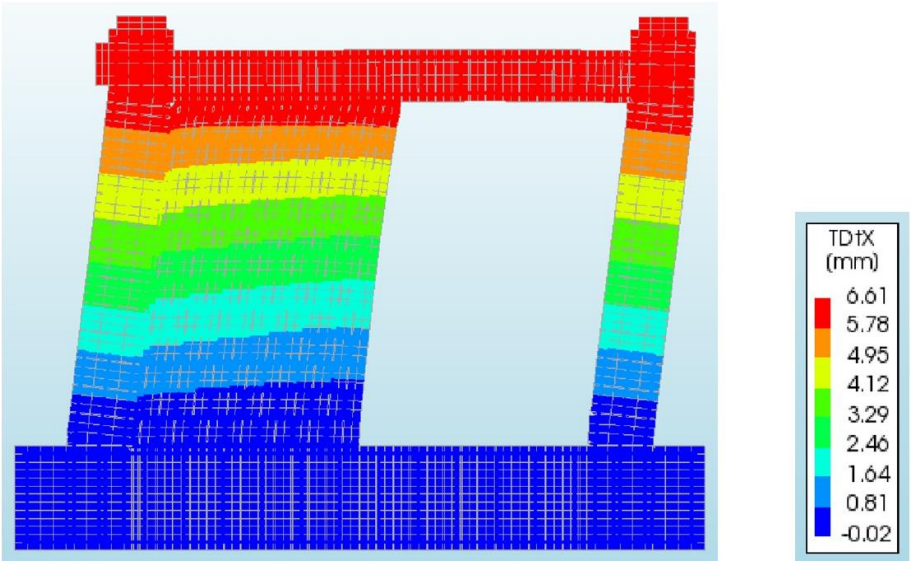

Figure 7.2.2. RC Frame model M3-A with half-span AAC infill under axial load N1=62.5 kN and positive monotonic loading: Computed displacements DX for loading step 46.

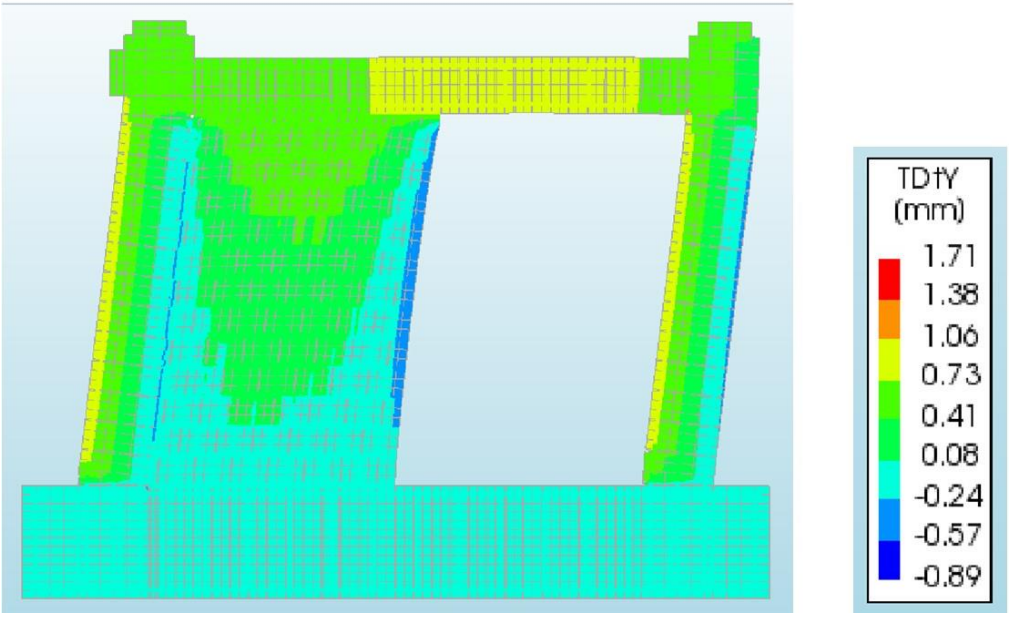

Figure 7.2.3. RC Frame model M3-A with half-span AAC infill under axial load N1=62.5 kN and positive monotonic loading: Computed displacements DY for loading step 46.

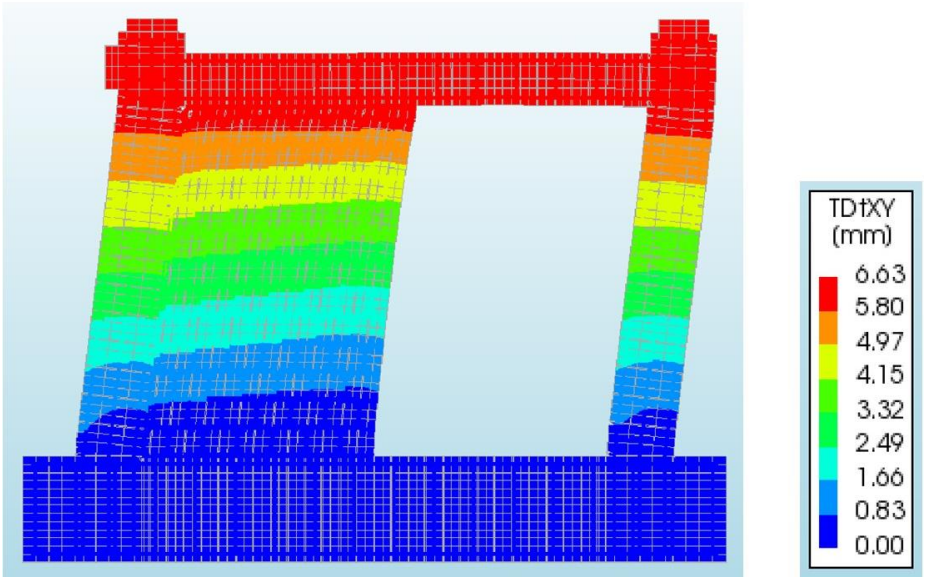

Figure 7.2.4. RC Frame model M3-A with half-span AAC infill under axial load N1=62.5 kN and positive monotonic loading: Computed displacements DXY for loading step 46.

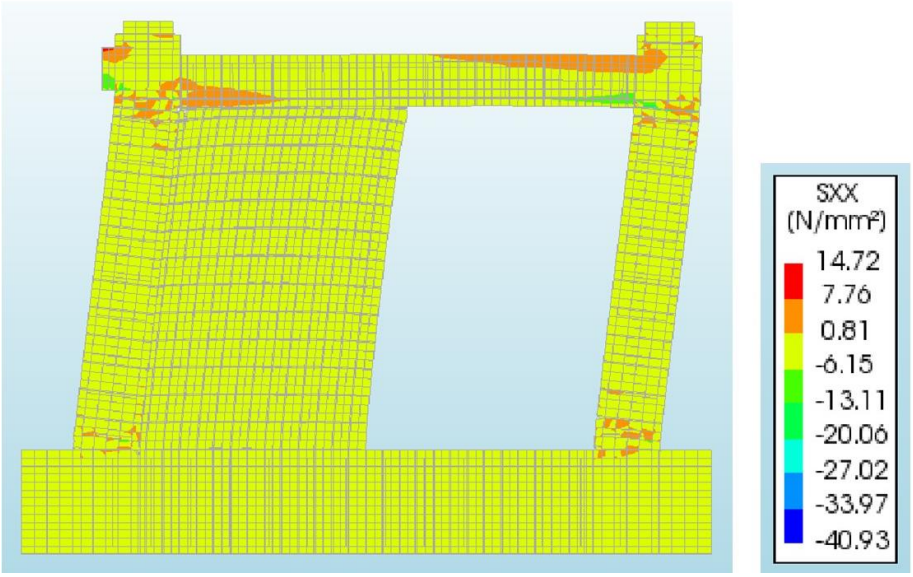

Figure 7.2.5. RC Frame model M3-A with half-span AAC infill under axial load N1=62.5 kN and positive monotonic loading: Cauchy total stresses SXX for loading step 46.

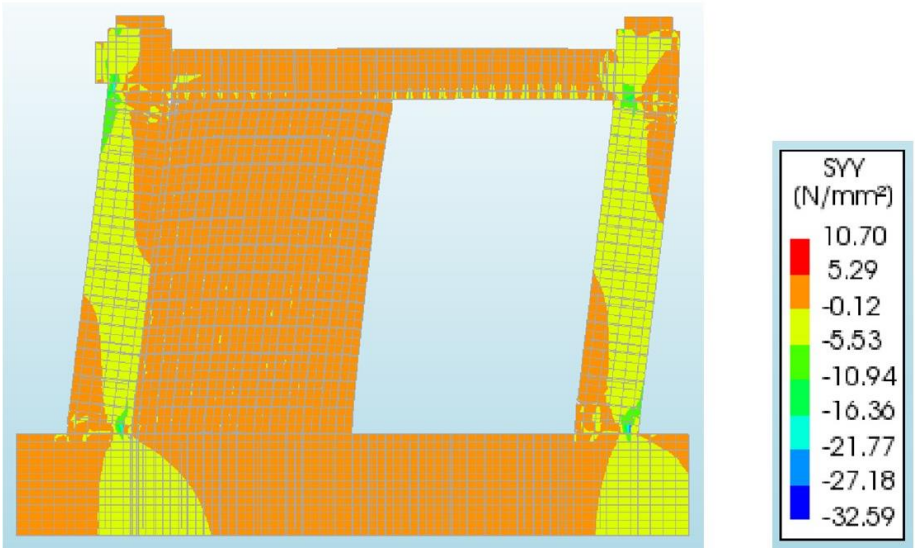

Figure 7.2.6. RC Frame model M3-A with half-span AAC infill under axial load N1=62.5 kN and positive monotonic loading: Cauchy total stresses SYY for loading step 46.

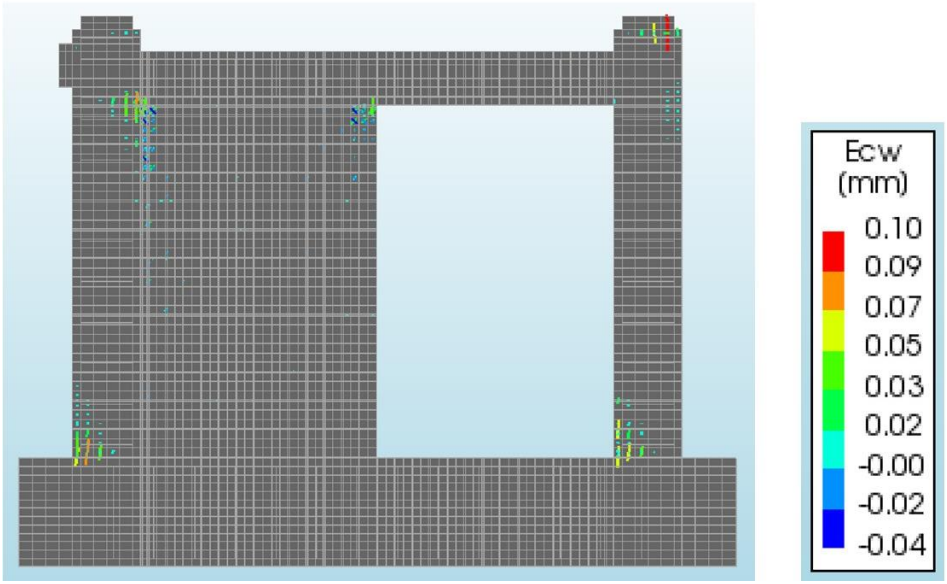

Figure 7.2.7. RC Frame model M3-A with half-span AAC infill under axial load N1=62.5 kN and positive monotonic loading: Computed crack distribution for loading step 20.

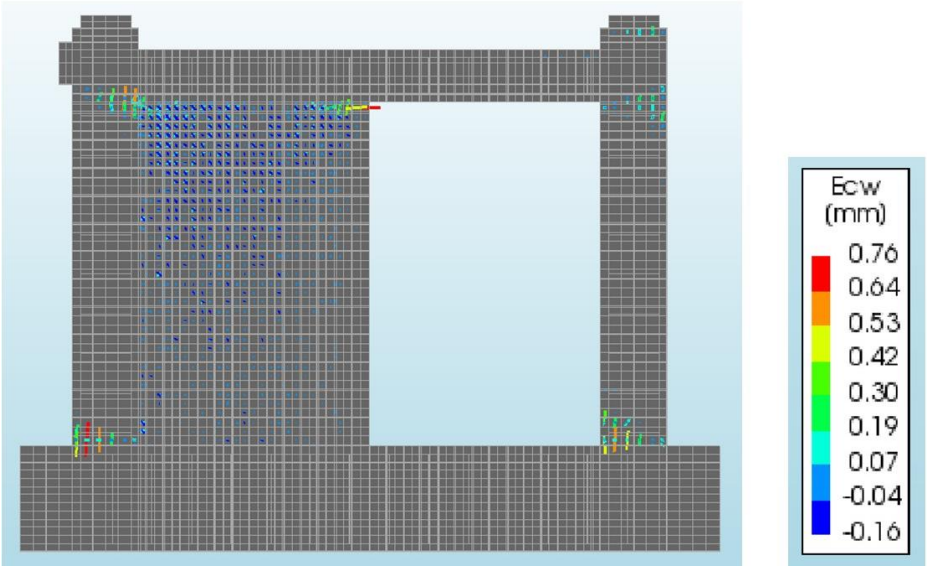

Figure 7.2.8. RC Frame model M3-A with half-span AAC infill under axial load N1=62.5 kN and positive monotonic loading: Computed crack distribution for loading step 46.

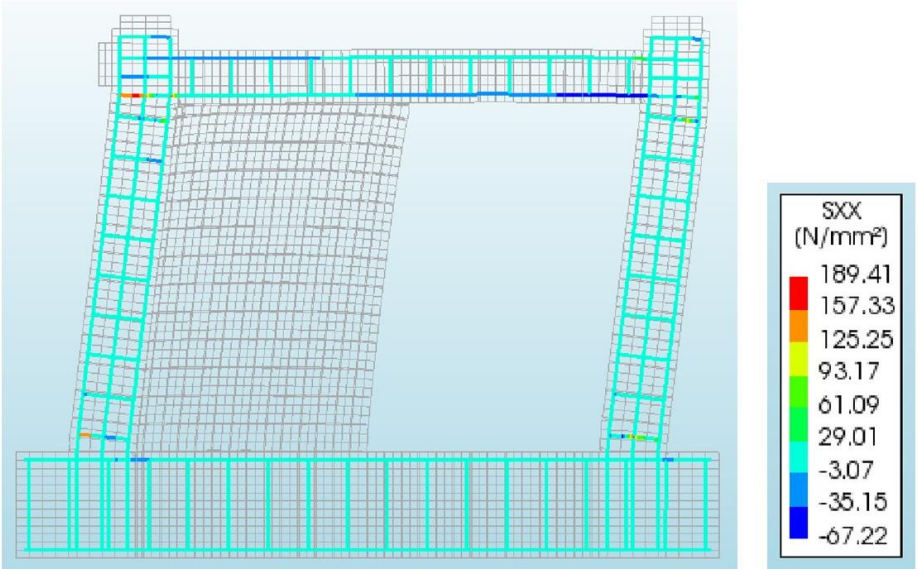

Figure 7.2.9. RC Frame model M3-A with half-span AAC infill under axial load N1=62.5 kN and positive monotonic loading: Reinforcement stresses SXX for loading step 46.

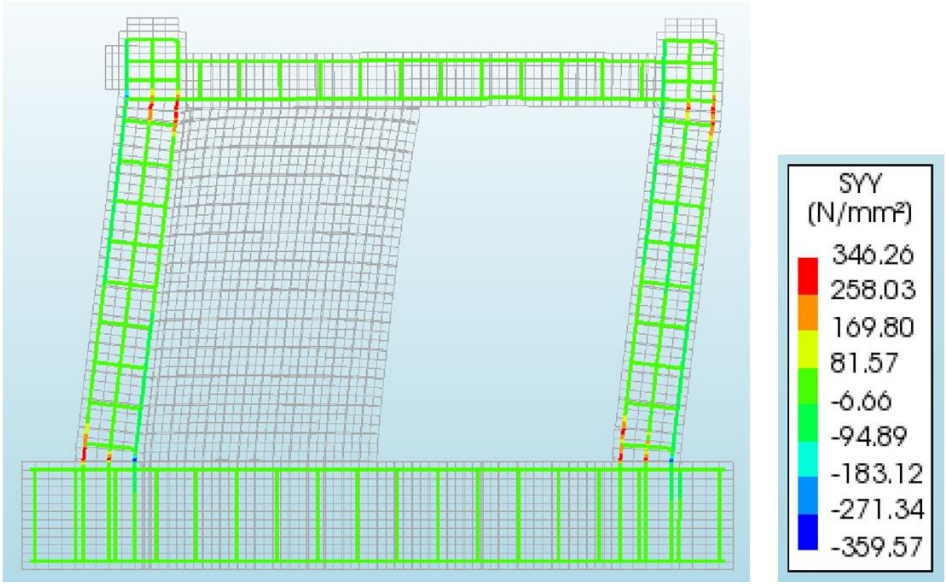

Figure 7.2.10. RC Frame model M3-A with half-span AAC infill under axial load N1=62.5 kN and positive monotonic loading: Computed reinforcement stresses SYY for loading step 46.

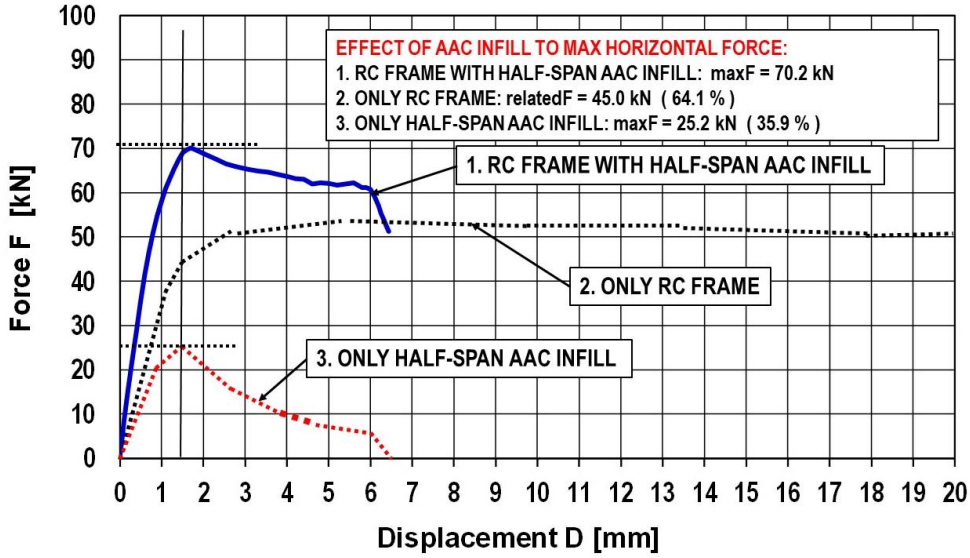

Figure 7.2.11. F-D curves, RC Frame model M3-A with half-span AAC infill under axial load N1=62.5 kN and positive monotonic loading.

7.3 Nonlinear response of RC frame model M3-B with half-span AAC infill under axial load N1=62.5 kN and negative monotonic loading

In Fig. 7.2.1 shown is the formulated nonlinear micro-model of the same RC frame prototype model M3-B with half-span AAC infill used for new response analysis under the same axial load N1 = 62.5 kN and monotonic loading in ***negative*** direction.

From the performed nonlinear analysis with application of DIANA computer software and with provided respective input data, a complete solution output was obtained in the identical form stored in different files.

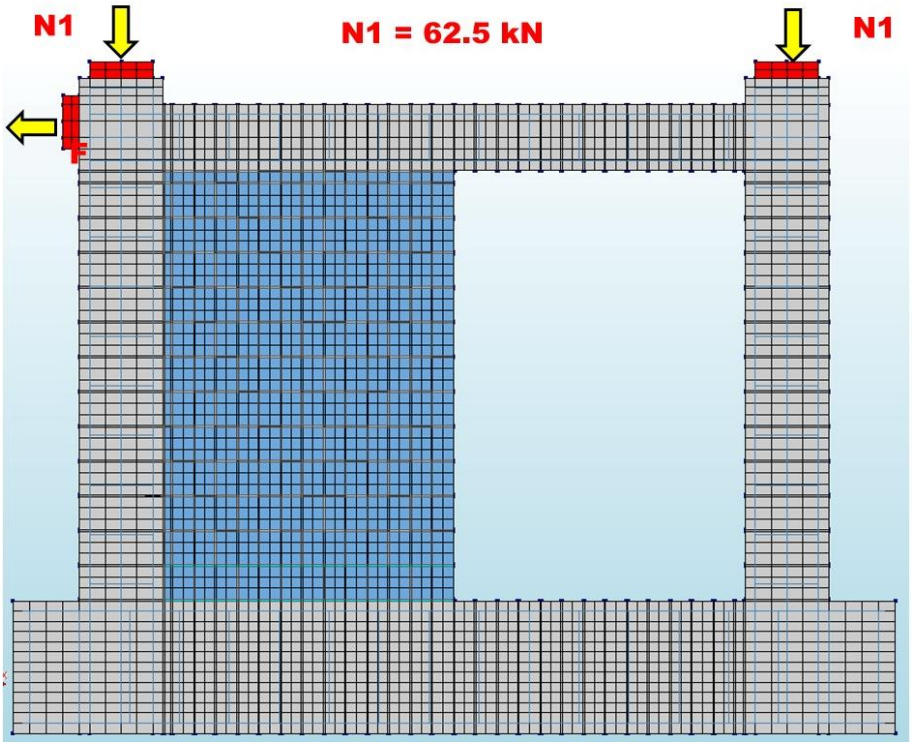

Figure 7.3.1. Developed nonlinear model of RC Frame model M3-B with half-span AAC infill under axial load N1=62.5 kN and negative monotonic loading.

In the case of this specific analysis, from the output video presentations selected were the characteristic solution steps showing the representative solution states, in total 32 electronic files, Table 7.3.1. To make closer evidence of the most characteristic results, presented in this text are 10 selected characteristic figures indicated as Fig. 7.3.1, and Fig. 7.3.2 through Fig. 7.3.10. In all figures, the respective characteristic results are presented in color.

For example, Fig. 7.3.2, Fig. 7.3.3 and Fig. 7.3.4 show the distributions of displacements DX(mm), DY(mm) and DXY(mm) for the respective computation time steps. From the figures is clear that displacement DX is the most pronounced (Fig. 7.3.2), displacement DY is smaller (Fig. 7.3.3), while displacement DXY is quite expressed, Fig. 7.3.4.

Fig. 7.3.5 and Fig. 7.3.6 show the computed Cauchy total stresses SXX and SYY, respectively, in RC elements and in AAC infill. The values of both total stresses are characterized by the occurrence of two different zones (compression and tension), however, in both cases, compressive stresses dominate.

Fig. 7.3.7 and Fig. 7.3.8 show the predicted distributions of cracks in concrete elements and in AAC infill for the solution steps 20 and 46, respectively. In Fig. 7.3.8, the zones of occurred cracks are enlarged since they correspond to higher values of induced displacements. However, the occurred distributions of cracks in concrete are generally of a local character while cracks in AAC infill are logically distributed in wider area.

Fig. 7.3.9 and Fig. 7.3.10 show the computed distributions of reinforcement stresses SXX and SYY, respectively for the same solution step 45.

From the stated figures, it is evident that pronounced compressive and tensile stresses occur. At segments where cracks occur in concrete, the tensile stresses are transferred to the reinforcement bars.

Fig. 7.3.11 shows the computed nonlinear fore - deformation response of RC Frame model M3-B with half-span AAC infill under axial load N1=62.5 kN and monotonic loading negative direction. The maximum computed restoring force amounts to max F1(-) = 73.5 kN.

Before, for the case of monotonic loading in positive direction, the computed maximum restoring force amounted to max F1(+) = 72.5 kN. The recorded difference is very small and amounts only to 1.4%.

The results obtained from the conducted this specific extended analytical study, presented in part 7.3, provide new facts for improved understanding the effects of partially constructed AAC infill in RC frame systems.

Table 7.3.1. Analytical phase A3-2: Computed nonlinear response of the RC frame model with half-span AAC infill (M3-A2) simulating vertical load N1=62.5 kN and negative monotonic loading (Ch. 7.2)

ANALYTICAL PHASE A3-2: **Capability of developed model: nonlinear response of RC frame with half span AAC infill (M3-A2) under vertical load N1=62.5 kN and (-) monotonic loading (Ch. 7.2)**					
File	Presented FEM parameter	Notation	Load step	E-Plotted	Shown/Fig.
0	Mesh of micro-model	Geometry	-	yes	+ / 7.2.0.
1	Displacement-x (mm)	TDtX	20	yes	
2	Displacement-x (mm)	TDtX	46	yes	+ / 7.2.1.
3	Displacement-y (mm)	TDtY	20	yes	
4	Displacement-y (mm)	TDtY	46	yes	+ / 7.2.2.
5	Displacement-xy (mm)	TDtXY	20	yes	
6	Displacement-xy (mm)	TDtXY	46	yes	+ /7.2.3.
7	Cauchy total stresses-x (N/mm^2)	SXX	20	yes	
8	Cauchy total stresses-x (N/mm^2)	SXX	46	yes	+ / 7.2.4.
9	Cauchy total stresses-y (N/mm^2)	SYY	20	yes	
10	Cauchy total stresses-y (N/mm^2)	SYY	46	yes	+ / 7.2.5.
11	Cauchy total stresses-xy (N/mm^2)	SXY	20	yes	
12	Cauchy total stresses-xy (N/mm^2)	SXY	46	yes	
13	Total strains-x (mm/mm)	EXX	20	yes	
14	Total strains-x (mm/mm)	EXX	46	yes	
15	Total strains-y (mm/mm)	EYY	20	yes	
16	Total strains-y (mm/mm)	EYY	46	yes	
17	Total strains-xy (mm/mm)	EXY	20	yes	
18	Total strains-xy (mm/mm)	EXY	46	yes	
19	Crack widths: plane princ./comp. (mm)	Ecw	20	yes	+ / 7.2.6.
20	Crack widths: plane princ./comp. (mm)	Ecw	46	yes	+ / 7.2.7.
21	Reinforcement CT stresses-x (N/mm^2)	SXX	20	yes	
22	Reinforcement CT stresses-x (N/mm^2)	SXX	46	yes	+ / 7.2.8.
23	Reinforcement CT stresses-y (N/mm^2)	SYY	20	yes	
24	Reinforcement CT stresses-y (N/mm^2)	SYY	46	yes	+ / 7.2.9.
25	Reinforcement CT stresses-xy (N/mm^2)	SXY	20	yes	
26	Reinforcement CT stresses-xy (N/mm^2)	SXY	46	yes	
27	Reinforcement of total strain-x (mm/mm)	EXX	20	yes	
28	Reinforcement of total strain-x (mm/mm)	EXX	46	yes	
29	Reinforcement total strain-y (mm/mm)	EYY	20	yes	
30	Reinforcement total strain-y (mm/mm)	EYY	46	yes	
31	Reinforcement total strain-xy (mm/mm)	EXY	20	yes	
32	Reinforcement total strain-xy (mm/mm)	EXY	46	yes	
Number of plotted figures from analytical study using formulated micro-model					32
Number of figures presented showing representative results					10

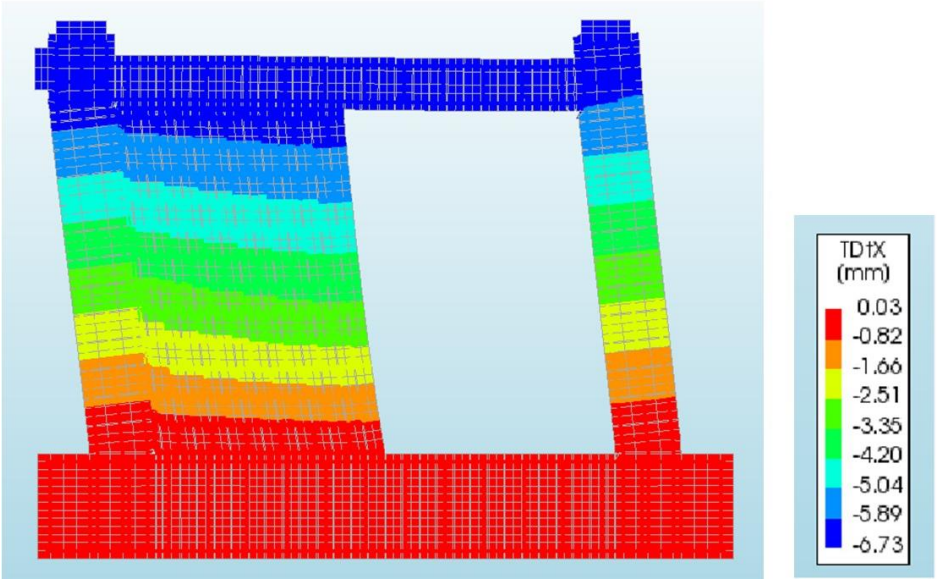

Figure 7.3.2. RC Frame model M3-B with half-span AAC infill under axial load N1=62.5 kN and negative monotonic loading: Computed displacements DX for loading step 46.

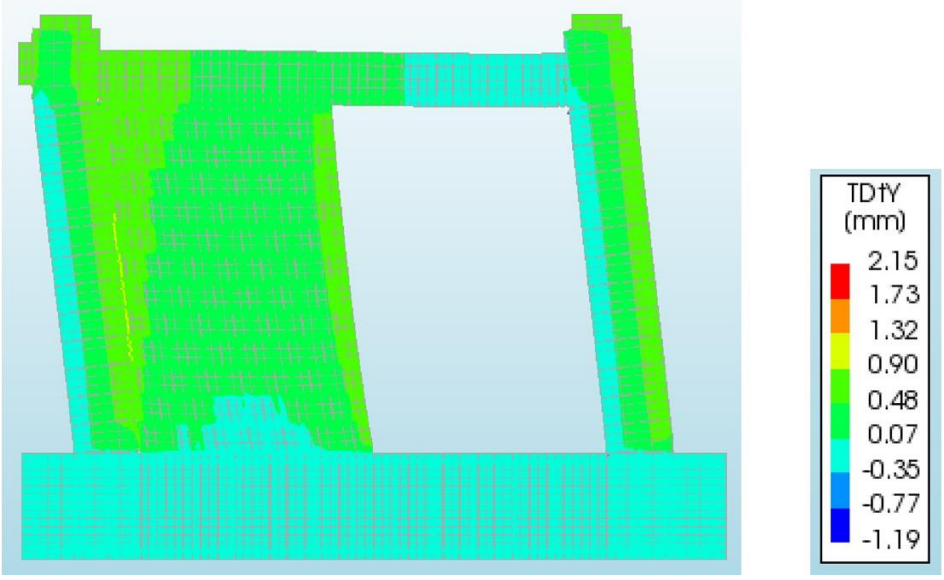

Figure 7.3.3. RC Frame model M3-B with half-span AAC infill under axial load N1=62.5 kN and negative monotonic loading: Computed displacements DY for loading step 46.

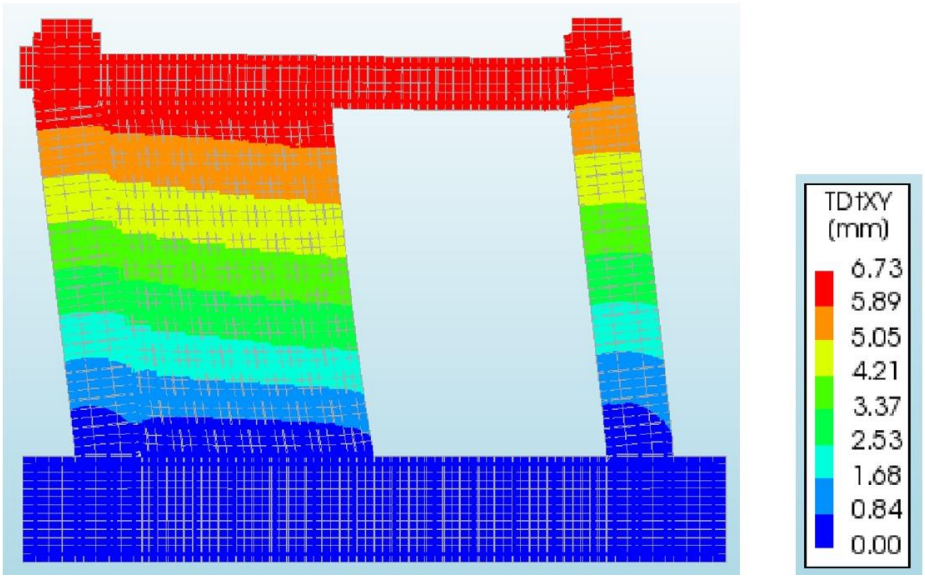

Figure 7.3.4. RC Frame model M3-B with half-span AAC infill under axial load N1=62.5 kN and negative monotonic loading: Computed displacements DXY for loading step 46.

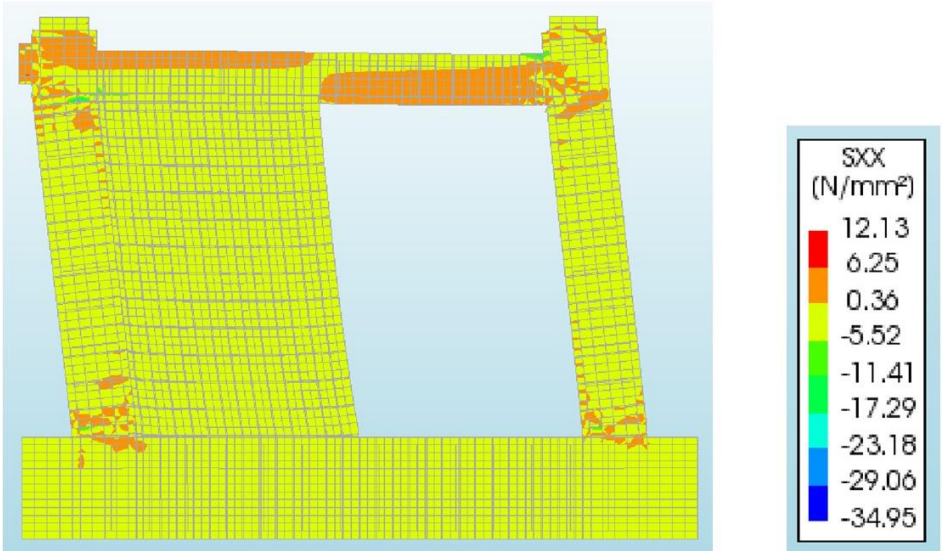

Figure 7.3.5. RC Frame model M3-B with half-span AAC infill under axial load N1=62.5 kN and negative monotonic loading: Computed Cauchy total stresses SXX for loading step 46.

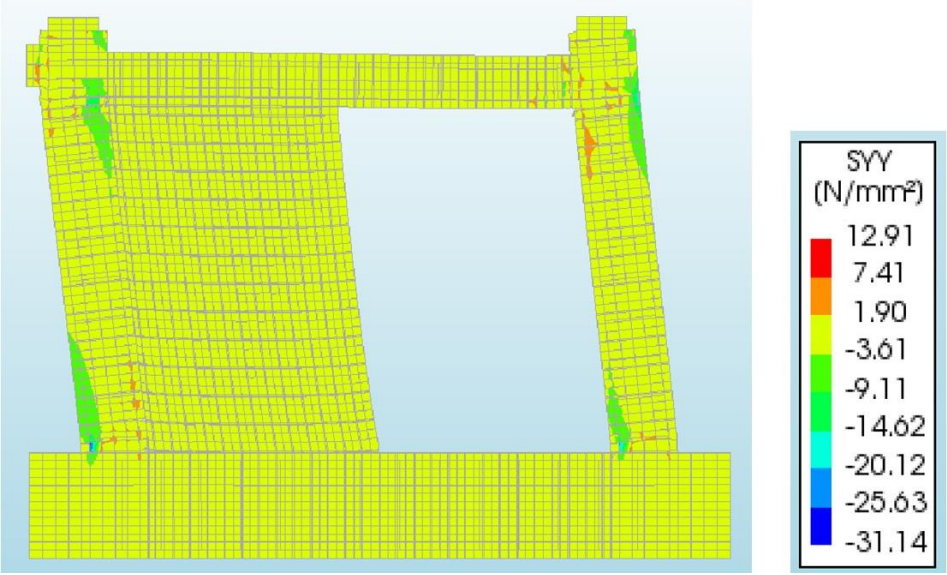

Figure 7.3.6. RC Frame model M3-B with half-span AAC infill under axial load N1=62.5 kN and negative monotonic loading: Computed Cauchy total stresses SYY for loading step 46.

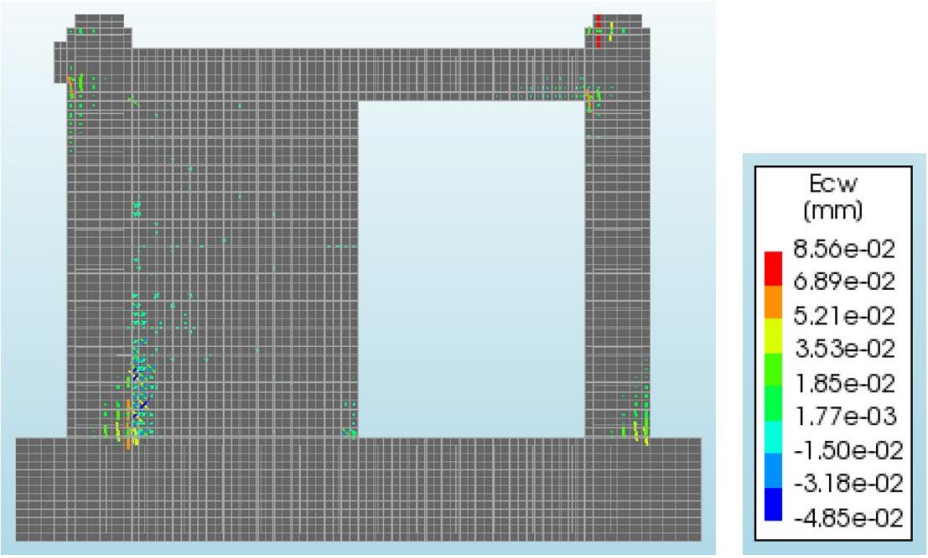

Figure 7.3.7. RC Frame model M3-B with half-span AAC infill under axial load N1=62.5 kN and negative monotonic loading: Computed crack distribution for loading step 20.

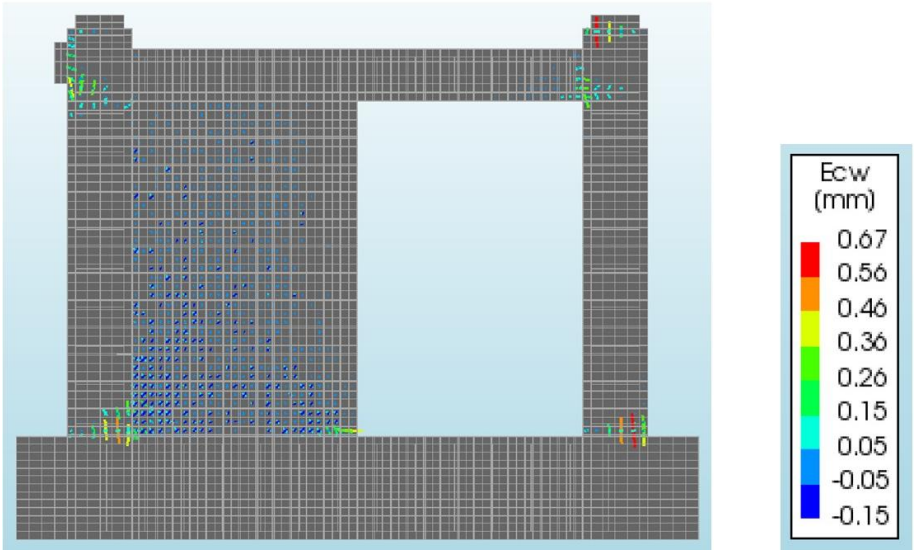

Figure 7.3.8. RC Frame model M3-B with half-span AAC infill under axial load N1=62.5 kN and negative monotonic loading: Computed crack distribution for loading step 46.

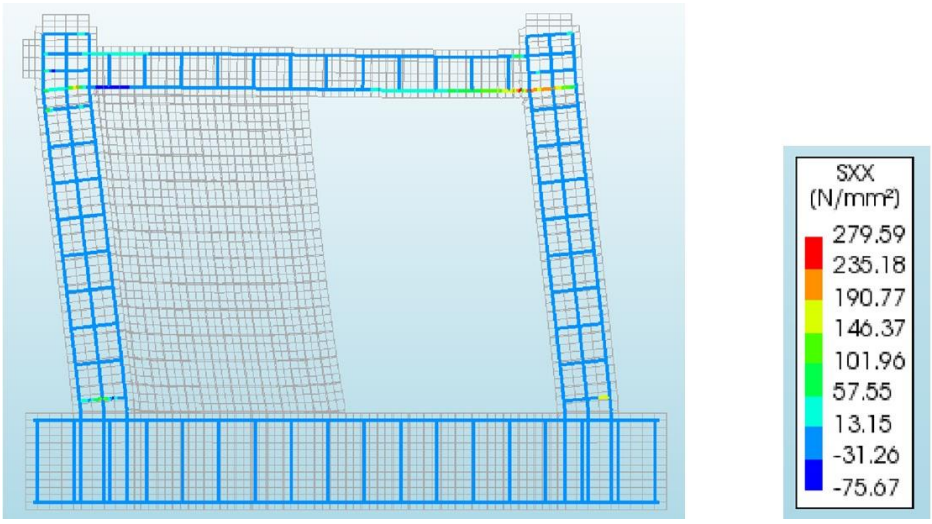

Figure 7.3.9. RC Frame model M3-B with half-span AAC infill under axial load N1=62.5 kN and negative monotonic loading: Computed reinforcement stresses SXX for loading step 46.

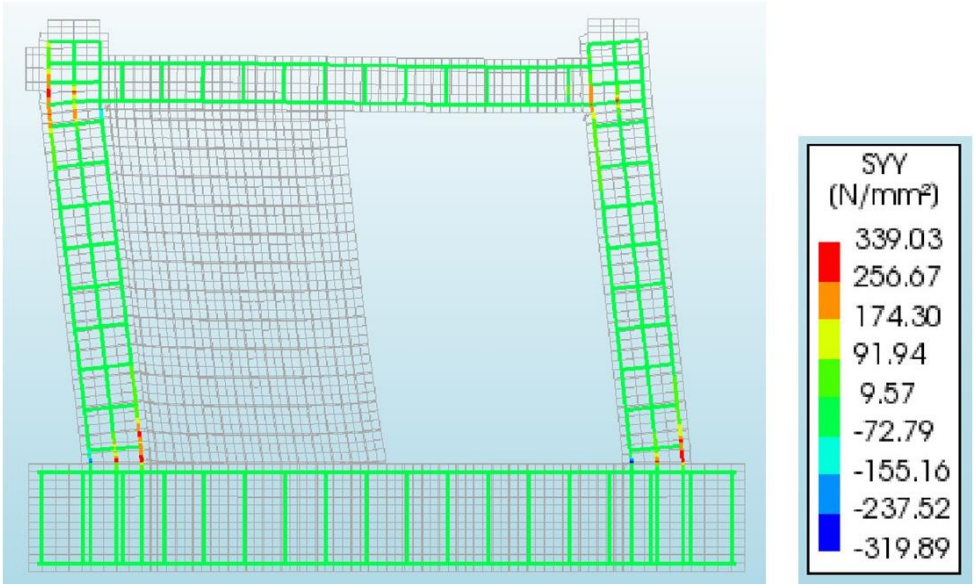

Figure 7.3.10. RC Frame model M3-B with half-span AAC infill under axial load N1=62.5 kN and negative monotonic loading: Computed reinforcement stresses SYY for loading step 46.

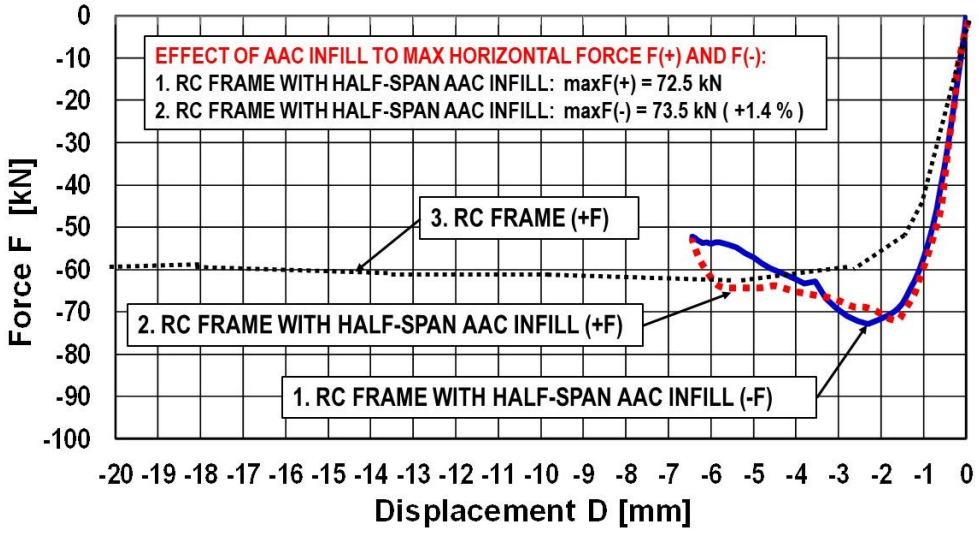

Figure 7.3.11. F-D curves, RC Frame model M3-B with half-span AAC infill under axial load N1=62.5 kN and negative monotonic loading.

7.4 Graphical Interpretation of Force-Displacement Curves

The force–displacement curves of M3-A and M3-B presented in Chapter 7 show an almost identical global response in both loading directions. The initial slopes of the curves, the shape leading up to peak load, and the descending post-peak branches follow nearly the same pattern. The text clearly notes that the peak loads differ by only about 1.4%, a small deviation considering the visible geometric asymmetry of the system.

Similarly, the displacements corresponding to peak load, as well as the ultimate displacements, show no significant divergence. This highlights that the nonlinear mechanisms activated in both directions are essentially the same, despite the infill being present only on one side of the frame. The graphical presentation supports this by showing overlapping or very closely aligned curve envelopes.

7.4.1 Quantitative Comparison

A strict summary of the numerical indicators given in Chapter 7 includes:

- The axial load is identical in both cases (62.5 kN).
- The difference in peak lateral resistance between M3-A and M3-B is very small (approximately 1.4%).
- The contribution of AAC and RC remains nearly unchanged in both loading directions, with reported values of: AAC ≈ 35.9% and RC ≈ 64.1%.

Maximum displacements and the general curvature of the response follow the same pattern in both directions.

Cracking in AAC is more distributed when compared to full-span infill, but the overall cracking sequence is similar between the two directions.

These observations are taken strictly from what is already written in the chapter.

7.4.2 Detailed Discussion

The symmetry in the nonlinear response of M3-A and M3-B, as emphasized in the chapter, arises from the deformation characteristics of the AAC panel. Although the infill occupies only part of the span, the diagonal deformation mechanism that develops under lateral loading is geometrically similar in both loading orientations. The AAC panel undergoes a comparable transformation from a rectangular shape into a “rhombus-shaped” distorted configuration in both directions, resulting in similar confinement, cracking, and compressive diagonal action.

The RC frame also exhibits nearly identical behavior in both loading cases. Chapter 7 explains that flexural cracking and joint rotations appear in the same regions and with comparable intensity. This indicates that the asymmetry of the infill does not significantly affect the global frame mechanism, at least for the loading level and configuration presented.

The chapter further notes that, when compared to the fully infilled frame, the half-span configuration results in approximately a 13.2% reduction in peak resistance. This reduction does not depend on loading direction but is instead related to the inherent geometric discontinuity introduced by the partial infill.

The damage patterns support the same conclusion: AAC cracking is wider and more scattered than in full-span infills, while RC cracking remains concentrated in similar zones as in symmetric models. Despite the infill occupying only half the span, the global lateral response remains almost unaffected by loading direction.

7.4.3 Conclusions from the Parametric Comparison

Based solely on the information in Chapter 7, the following strict conclusions can be drawn:

- The global nonlinear response of the half-span infilled frame is nearly identical for positive and negative directions of lateral loading.
- The small difference in peak resistance (~1.4%) confirms that loading direction has a negligible effect on stiffness, strength, and deformation capacity.
- The relative contribution of AAC and RC remains practically unchanged in both directions, reinforcing the symmetry of the nonlinear mechanisms.
- The reduction of strength compared to the fully infilled model (≈13.2%) is attributed to the partial infill configuration itself rather than the loading direction.
- Crack patterns in the AAC panel differ slightly in distribution but do not influence the global response.

7.4.4 Recommendations

Based on the conclusions drawn in the chapter:

- Half-span infills should not be assumed to behave like full-span infills, since they provide a noticeably lower lateral resistance.
- The nearly identical response in both loading directions suggests that, for this configuration and loading level, the model can be analyzed in either direction without introducing additional parameters or modifications.
- For practical assessments where half-span infills are present, attention should be given to the reduced global capacity and the more dispersed cracking observed in the AAC.

7.5 Main Findings from the Study of RC Frame with Half-Span AAC Infill

The performed specific study of the nonlinear behavior of an asymmetric RC frame with a spaced AAC infill in the left half-span resulted in new, i.e., knowledge from which very important conclusions were drawn:

1) Due to the asymmetrical position of the AAC infill in the frame, it was initially expected to obtain different nonlinear resisting force - deformation relationships under loading in a positive direction and alternatively, in a negative direction. However, almost identical resistance forces of max F(+) = 72.5 kN and max F (-) = 73.5 kN were obtained. The difference was very small, amounting to only 1.4%.

2) Regarding the recorded symmetry, rational engineering explanation of the phenomenon is made. Namely, the AAC infill panel with half-span possesses an ideally symmetric rectangular form. Therefore, during positive or negative deformations, dominant stresses were induced from the foundation RC beam and the floor RC beam. More concretely, deformations that can be both positive and negative give rise to a change of the initial panel geometry, namely, there is a forced transition from a rectangular form into an oblique rectangular form. Considering that the changes of form for positive and negative deformations were symmetrical, there arose the recorded symmetry of the resisting forces.

3) Due to the existence of the AAC infill over one half of the span, a smaller maximum resisting force amounting to max F* = 72.5 kN was recorded. Since the maximum resisting force in the case of the existence of an AAC infill over the entire span amounted to max F = 82.1 kN, a difference of 13.2% was recorded, indicating the necessity for appropriate consideration and study of the real geometrical forms of the AAC infill.

4) Regarding the total recorded maximum resisting force that, in this case, amounted to max F = 72.5 kN, it was very important to get an insight into the participation of the RC frame itself and the contribution of the AAC infill. In this case, the maximum resisting force of the RC frame amounted to max F = 45.0 kN or 64.1%, whereas the maximum resisting force of the AAC infill amounted to max F = 25.2 kN or 35.9%. Generally, depending on the specific structural characteristics of the RC frames as well as the applied types of an AAC infill, their individual participation in the total resisting force can be considerably different.

5) The cracks in the RC frame occurred due to the local concentration of compressive and tensile stresses. These concentrations of cracks occurred in the vicinity of the critical zones of fixation of the columns. Their size and distribution were very similar to those in the previous case of RC frames with AAC infill over the entire span.

6) The cracks in the AAC infill over half-span also generally occurred in the direction of the diagonal panel. However, their distribution was extended over a larger surface with a conditioned quite complex distribution form.

7) The research results presented in this chapter, related to considered change of infill geometry, pointed out that in such cases it is also necessary to introduce infill protection measures. It is necessary to develop and apply corresponding innovative solutions for reduction of the high vulnerability of the masonry of AAC elements with different geometrical forms and quite different mechanical nonlinear characteristics.

8 CHAPTER 8 - SUMMARY OF THE MAIN FINDINGS

This chapter summarizes the main experimental and numerical results obtained from the research program described in Chapters 3 to 7. The study addressed the nonlinear behaviour and seismic performance of reinforced concrete (RC) frame systems without infill, with full-span AAC infill, and with half-span AAC infill, under different axial load levels. The objective of this chapter is to synthesise the findings from the laboratory tests and parametric numerical analyses, highlighting the comparative responses, failure mechanisms, interaction effects, and sensitivities to the governing parameters.

The realization of the considered research activities provided knowledge referring to the nonlinear behaviour of RC frame structures of buildings with AAC infill. In accordance with the obtained and presented results from the realized four main research phases, the following important findings are briefly summarized in the subsequent text.

8.1 Testing of Large-Scale Models

The realized experimental testing of the constructed large-scale models of RC bare frames and RC frame with AAC infill provided very important results used as the basis for the creation of the essential prerequisites for continuation with the subsequent research activities. Specifically, the experimental investigations resulted in the following main findings: (1) provided was an insight into the real nonlinear behaviour of the constructed only basic RC bare frame under interactive effects of vertical loads and cyclic horizontal loads; (2) obtained are experimental results on the real nonlinear behaviour of an identical RC bare frame tested under the effect of monotonic loading and vertical loads; (3) comparatively obtained was an insight into the real nonlinear behaviour of the built upgraded model composed of an identical RC frame with AAC infill under the effect of cyclic horizontal loads and identical vertical loads, and finally, (4) obtained were comparative results for the identical RC frame with AAC infill under monotonic loading and identical vertical loads.

The obtained experimental results were used as the background starting evidence important for continueuing with the subsequent research activities.

8.2 Modelling of Bare Frame with Different Axial Loads

This specific research phase was presented in chapter 5. It was dedicated to the initial investigation of the nonlinear behaviour of the basic RC bare frame under effects of the considered three different of axial load levels, N1 = 62.5 kN, N2 = 125.0 kN and N3 = 280.0 kN.

Using the previously obtained experimental results on the nonlinear behaviour of the RC bare frame under axial loads N1 = 62.5 kN, a corresponding advanced nonlinear micro-model was successfully formulated and verified. Using then the experimentally verified nonlinear micro-

model, investigations of the nonlinear behaviour of the RC bare frame under effect of higher levels of axial loads N2 = 125.0 kN and N3 = 280.0 kN were also realized successfully.

These research activities clearly showed that the different levels of axial loads produced large changes in the nonlinear behaviour of the RC bare frames and should therefore be obligatorily considered in the design of buildings in seismically active regions.

8.3 Modelling of RC Frame with AAC Infill under Different Axial Loads

The numerical nonlinear micro-model that was used for the needs of the presented investigations in chapter 6 was formulated by adequate upgrading of the previous nonlinear model by including corresponding nonlinear finite elements to simulate the nonlinear behaviour of the AAC infill.

The formulated nonlinear micro-model of RC frame with infill of AAC elements was verified successfully for axial loads of N1 = 62.5 kN, based on obtained results from the performed experimental investigations. Following the performed analyses under effects of increased vertical loads to the level of N2 = 125.0 kN and N3 = 280.0 kN, it was confirmed that different levels of axial forces also had a great effect on the nonlinear behaviour and therefore could not be neglected.

With the obtained research results and confirmed success in formulation of experimentally verified model, provided were the basic conditions and new horizons for identification and continuation with the next ell targeted research activities.

8.4 Modelling of RC Frame with Half-Span AAC Infill

With introduced corresponding modification of the previous micro-model, the new nonlinear micro-model representing RC frame with AAC infill constructed over one half of the span was subsequently formulated. Due to the asymmetry of the masonry, analytical studies were realized for the two types of loading.

In the first case, the horizontal load was in a positive direction, whereas in the other case, the horizontal load was simulated in the opposite, negative direction. A new specific finding was confirmed from these studies. More concretely, in the specific case, although the location of the infill was asymmetric, the nonlinear envelope relationships for the loading in both opposite directions were very similar. However, due to the recorded big difference in the nonlinear behaviour of the RC bare frame and RC frame with infill gives rise to the need for an in-depth study of the problem related to the safe application of AAC infill in frame RC buildings located in seismically active regions.

8.5 Brief Summary of the Main Findings

The obtained research results are presented to details and integrally in the corresponding chapters of the text. However, for the need to point out the importance of certain new findings, the selected most important results are graphically presented in two separate figures. Fig. 8.1. shown is overview of recorded maximum resisting forces for different structural states of the studied experimental RC bare frame.

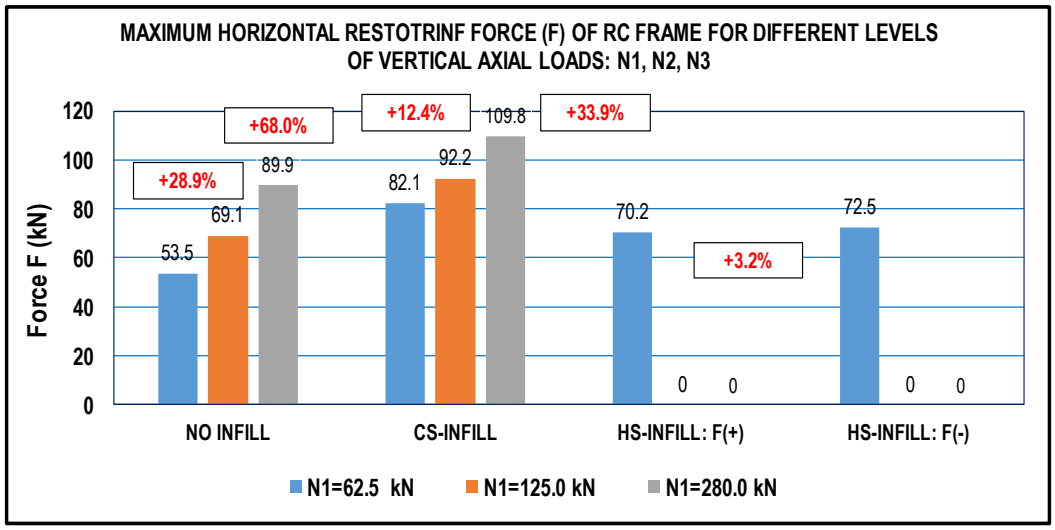

Figure 8.1. Maximum restoring forces for different structural states of the studied RC bare frame

In the case of a frame without an infill of AAC elements, the maximum resisting force is increased with the increase of the axial loads, but at the same time there is rapid reduction of the ductility capacity of the implemented RC bare frame.

In the case of a frame with an infill of AAC elements, the maximum resisting force is also increased with the increase of the axial loads. However, the amount of maximum resisting force is greater due to the contribution of the AAC infill. Analogously, with the increase of the axial load, there is the reduction of the ductility capacity leadiwng to critical states or failure of the bearing RC bare frame system.

In the case of a frame with an AAC infill over one half of the span, the direction of loading, whether positive or negative, does not cause considerable change in the nonlinear envelope relationship.

Fig. 8.2 shows graphically the values of the recorded maximum resisting forces for different states of the analysed frame with participations of RC bare frame and AAC infill.

For all three different levels of vertical loads shown is the participation of the maximal resisting forces of the RC frame and the AAC infill in the total amount of the resisting force. Analogously, a corresponding graphical presentation is given also for the case of an RC frame with AAC infill over half of the span (end right).

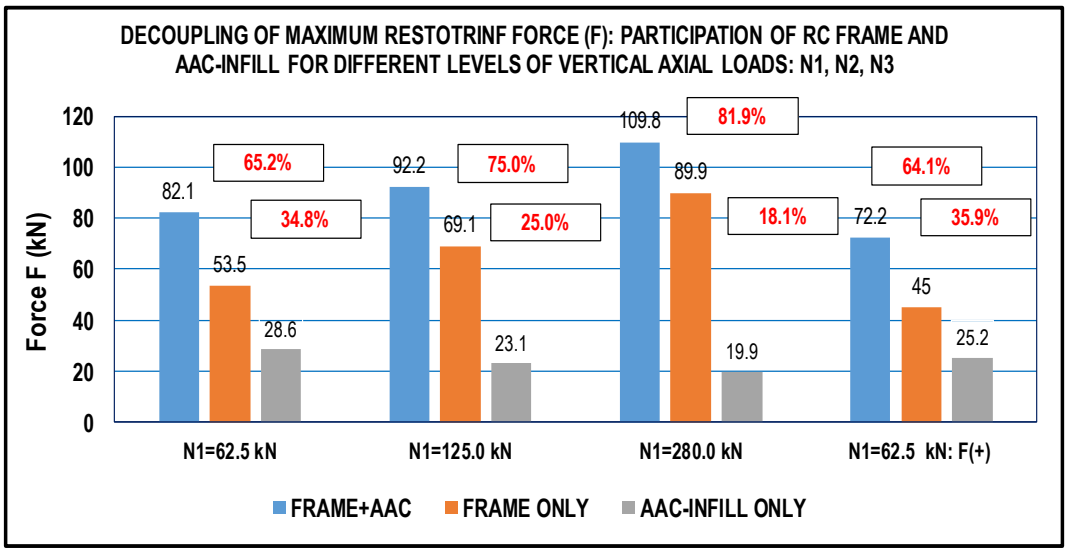

Figure 8.2. Maximum recorded resisting forces for different states of the analysed frame with shown participations of RC frame and AAC infill

These results point out that the effect of the RC frame with AAC elements is very important and cannot be neglected. More exactly, for the RC frame with AAC infill, it is necessary to define adequate conditions and measures for reduction of their high and intolerable vulnerability.

8.6 Summary of Key Findings

From the combined experimental and numerical investigations, the following main conclusions can be drawn: (1) AAC infill considerably increases the initial stiffness and lateral strength of RC frames but reduces ductility and energy-dissipation capacity; (2) higher axial load enhances stiffness and strength while limiting plastic rotations and accelerating post-peak strength degradation; (3) the frame-infill interface governs the initiation of cracking and stiffness degradation, making its accurate modelling essential for prediction of global behaviour; (4) the overall response is most sensitive to axial load and AAC compressive strength, whereas the influence of adhesive-joint thickness remains minor; (5) the close agreement between experimental and numerical results confirms the accuracy and reliability of the adopted nonlinear modelling approach for AAC-infilled RC frame systems.

9 CHAPTER 9 – PARAMETRIC ANALYSIS OF RC FRAMES WITH AAC INFILL CONFIGURATIONS

9.1 Introduction

In this Chapter 9 presented are important summary results obtained from the realized extensive parametric nonlinear response studies, including in total twenty-four characteristic prototype scaled models analyzed using formulated and experimentally validated nonlinear micro-models. The conducted parametric analyses aimed to evaluate the influence of key parameters such as the frame span length, the thickness, and the compressive strength of the AAC infill on the overall nonlinear behavior, stiffness, and strength of the RC frame with AAC masonry infill.

All analytical studies were performed under identical loading conditions, with a constant vertical load of 62.5 kN and simulated one-directional horizontal loading applied to each model. The numerical simulations were based on the geometry, reinforcement, and material characteristics of the experimentally tested frames, allowing for a consistent correlation between analytical and experimental results. Through these studies, reliable relationships between the stiffness, ultimate strength, and deformation capacity of the system were obtained.

For clarity, all models considered in the parametric study are summarized in Table 9.1.1, where the notation (M-L-G-D) represents the model type, the frame span (L), the AAC infill compressive strength (G), and the infill thickness (D). Each parameter variation was analyzed systematically to identify its contribution to the lateral load resistance and global nonlinear response of the system.

The performed analyses also represent a continuation of the “analytical experiments,” as the applied nonlinear micro-model was fully verified through experimental testing. The obtained results confirmed that the adopted modelling approach provides a reliable and basis for predicting the real behavior of RC frames with AAC infill.

Furthermore, the developed analytical framework enabled the formulation of a practical and consistent procedure for defining the complete set of nonlinear macro-modelling parameters of a decoupled AAC infill in RC frames. This procedure, presented in the subsequent sections of this chapter, was derived directly from the results of the parametric analyses and built upon the experimentally validated micro-models. It allows engineers to define the key parameters the maximum restoring force (FM) and the corresponding relative displacement (DM) for a wide range of frame spans, infill thicknesses, and AAC strengths, ensuring accurate scaling between model and prototype behavior.

The presented approach establishes the methodological foundation for transforming detailed analytical results into simplified and applicable design formulations, enabling the practical

implementation of AAC infill macro-models in seismic assessment and design of RC frame structures.

The results of the realized parametric studies and the formulation of the corresponding practical modelling procedure are presented and discussed in the subsequent sub-chapters (9.1-9.12), while the main conclusions and design recommendations are summarized at the end of the chapter.

Table 9.1.1 Scaled model M1-L1-G1-D1: Modelling parameters of decoupled AAC infill in

Model	Frame span (L)	Infill thickness (D)	Infill strength (G)
M1-L1-G1-D1	200 cm	125 mm	2.5 MPa
M1-L1-G1-D2	200 cm	200 mm	2.5 MPa
M1-L1-G1-D3	200 cm	250 mm	2.5 MPa
M2-L2-G1-D1	250 cm	125 mm	2.5 MPa
M2-L2-G1-D2	250 cm	200 mm	2.5 MPa
M2-L2-G1-D3	250 cm	250 mm	2.5 MPa
M3-L3-G1-D1	300 cm	125 mm	2.5 MPa
M3-L3-G1-D2	300 cm	200 mm	2.5 MPa
M3-L3-G1-D3	300 cm	250 mm	2.5 MPa
M4-L1-G1-D1	200 cm	125 mm	2.5 MPa
M4-L2-G1-D1	250 cm	125 mm	2.5 MPa
M4-L3-G1-D1	300 cm	125 mm	2.5 MPa
M5=M0-L1	200 cm	–	–
M5=M0-L2	250 cm	–	–
M5=M0-L3	300 cm	–	–
M6-L1-G1-D1	200 cm	125 mm	2.5 MPa
M6-L1-G2-D1	200 cm	125 mm	3.75 MPa
M6-L1-G3-D1	200 cm	125 mm	5.0 MPa
M7-L2-G1-D1	250 cm	125 mm	2.5 MPa
M7-L2-G2-D1	250 cm	125 mm	3.75 MPa
M7-L2-G3-D1	250 cm	125 mm	5.0 MPa
M8-L3-G1-D1	300 cm	125 mm	2.5 MPa
M8-L3-G2-D1	300 cm	125 mm	3.75 MPa
M8-L3-G3-D1	300 cm	125 mm	5.0 MPa

To derive practically valuable AAC infill modelling parameters, the selected RC frames were analyzed considering different frame spans and different AAC infill regarding thickens and strength, under simulated monotonic loading. To obtain uniform comparative results, in all analytical studies, identical vertical load of N1 = 62.5 kN was simulated.

For clarity, all models applied in parametric study are listed and explained in Table 9.1, where the notation (M, L, G, D) used in the study is described for each model.

The performed analytical studies, also represent very successful ***"analytical experiments"***, because the applied analytical micro-model was fully verified with the obtained results from the performed experimental tests.

From this study it is evident that the presently formulated experimentally verified analytical models are of high importance because many innovative projects and other specific investigations can be successfully realized with their application.

The results obtained from the realized analytical studies carried out are presented in successive sub-chapters 9.1 to 9.8. Then, in sub-chapter 9.9, shortly demonstrated the implemented uniform methodological data processing procedure. Finally, in part 9.9 briefly are summarized the major findings from the conducted parametric study using formulated micro-models of the considered prototype models, representing RC frame with AAC infill.

9.2 Influence of Infill Thickness on Response of Frame with Span L1 = 200 cm

9.2.1 Parametric Study of Frame with Span L1 = 200 cm and Computed Results

Parametric study of the selected frame with Span L1 = 200 cm was performed based on formulated and implemented three representative nonlinear micro-models considering the identically reinforced RC frames and three different AAC infill thicknesses:

D1 = 125 mm (Model M1-L1-G1-D1);

D2 = 200 mm (Model M1-L1-G1-D2);

D3 = 250 mm (Model M1-L1-G1-D3);

Compressive strength of AAC infill was considered identical G1 = 2.5 MPa. Geometrical characteristics of the analyzed frames and other related conceptual details used as the basis during formulation of related nonlinear micro-model were presented in all necessary details in the previous chapters. The computed results enabling understanding of nonlinear responses are comparatively presented in Fig. 9.2.1.

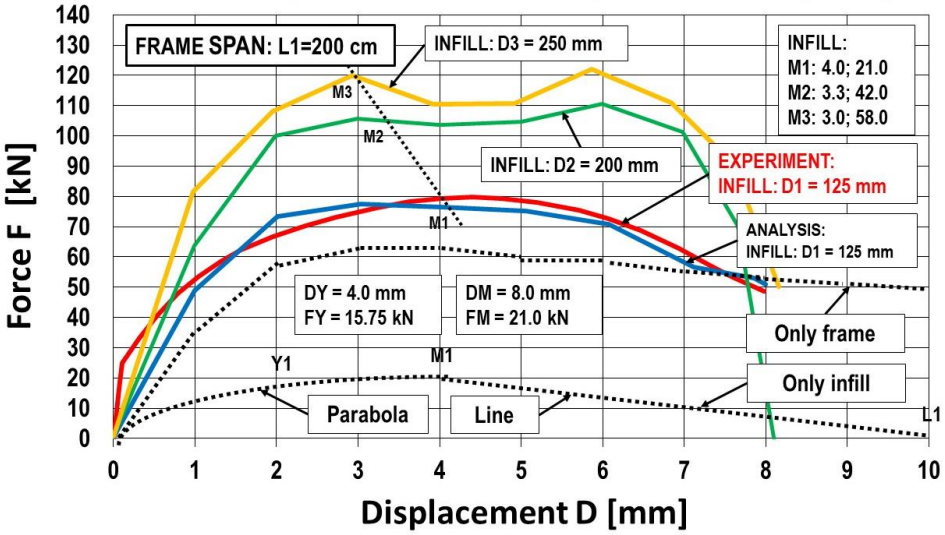

Fig. 9.2.1. Scaled model M1-L1-G1-3D: Computed nonlinear response of AAC infilled frame with span L1 = 200 cm and three infill thicknesses D1, D2 and D3

9.2.2 Frame span L1 = 200 cm and infill thickness D1=125 mm (Model M1-L1-G1-D1)

Decoupled response of frame and infill: For the selected representative scaled RC frame model (S=1:2) with span L1 = 200 cm, analysed was the effect of considered AAC infill with thickness D1 = 125 mm. Based on the computed nonlinear response of the frame with AAC infill and nonlinear response of non-infilled or only RC frame system, ***the decoupled infill nonlinear response was defined,*** Table 9.2.1**.** In the same table included are the resulting: (1) Modelling parameters of AAC infill for the scaled model, (2a) Modelling parameters of AAC infill for the respective prototype or real-scale system and (2b) Margins of estimated modelling parameters of AAC infill for practical design the real-scale prototype system.

Table 9.2.1. Scaled model M1-L1-G1-D1: Modelling parameters of decoupled AAC infill in frame with span L1 = 200 cm and thickness D1 = 125 mm and results for prototype.

1. SCALED MODEL: Modelling parameters (Micro-Modelling Results) SCALED MODEL: M1-L1-G1-D1: (L1 = 200 cm; G1 = 2.5 MPa; D1 = 125 mm)						
MODEL PARAMETERS OF DECOUPLED AAC INFILL						
K0 = 2.0*FM/DM	DY = 0.5*DM	FY = 0.75*FM	DM	FM	DL = 2.5*DM	FL
kN/mm	mm	kN	mm	kN	mm	kN
8.5	2.0	15.75	4.0	21.0	10.0	0.
2a. PROTOTYPE FRAME: Modelling parameters PROTOTYPE: P1-L1-G1-D1: (L1 = 400 cm; G1 = 2.5 MPa; D1 = 250 mm)						
PARAMETERS OF DECOUPLED AAC INFILL						
K0	DY	FY	DM	FM	DL	FL
kN/mm	mm	kN	mm	kN	mm	kN
17.0	4.0	51.0	8.0	68.0	20.0	0.
2b. PROTOTYPE FRAME: Margins of modelling parameters for practical design PROTOTYPE: P1-L1-G1-D1: (L1 = 400 cm; G1 = 2.5 MPa; D1 = 250 mm)						
1. Effective infill height H_0 = 260 cm = 2600 mm 2. Thickness D1 = 25 cm 3. Contact side area: $A_0 = H_0$ (cm) *D1(cm) = 260*25 = 6500 cm^2 4. Max side force: $N_0 = A_0$*G1 = 6500 0.25 = 1625 kN						
Story drift (‰) (model-**Dr** / H_0)	**1.53**		**3.07**		**7.69**	
H-Force (%) (Model-**F** / N_0		**3.13**		**4.18**		**0.**

9.2.3 Frame span L1 = 200 cm and infill thickness D2 = 200 mm (Model M1-L1-G1-D2)

Decoupled response of frame and infill: For the selected representative scaled RC frame model (S=1:2) with span L1 = 200 cm, analysed was the effect of considered AAC infill with thickness D2 = 200 mm. Based on the computed nonlinear response of the frame with AAC infill and nonlinear response of non-infilled or only RC frame system, ***the decoupled infill nonlinear response was defined,*** Table 9.2.2**.** In the same table included are the resulting: (1) Modelling parameters of AAC infill for the scaled model, (2a) Modelling parameters of AAC infill for the respective prototype or real-scale system and (2b) Margins of estimated modelling parameters of AAC infill for practical design the real-scale prototype system.

Table 9.2.2. Scaled model M1-L1-G1-D2: Modelling parameters of decoupled AAC infill in frame with span L1 = 200 cm and thickness D2 = 200 mm and results for prototype.

1. SCALED MODEL: Modelling parameters (Micro-Modelling Results) SCALED MODEL: M1-L1-G1-D2: (L1 = 200 cm; G1 = 2.5 MPa; D2 = 200 mm)						
MODEL PARAMETERS OF DECOUPLED AAC INFILL						
K0 = 2.0*FM/DM	DY = 0.5*DM	FY = 0.75*FM	DM	FM	DL = 2.5*DM	FL
kN/mm	mm	kN	mm	kN	mm	kN
25.45	1.65	31.5	3.3	42.0	8.25	0.
2a. PROTOTYPE FRAME: Modelling parameters PROTOTYPE: P1-L1-G1-D2: (L1 = 400 cm; G1 = 2.5 MPa; D2 = 400 mm)						
PARAMETERS OF DECOUPLED AAC INFILL						
K0	DY	FY	DM	FM	DL	FL
kN/mm	mm	kN	mm	kN	mm	kN
50.9	3.3	126.0	6.6	168.0	16.5	0.
2b. PROTOTYPE FRAME: Margins of modelling parameters for practical design PROTOTYPE: P1-L1-G1-D2: (L1 = 400 cm; G1 = 2.5 MPa; D2 = 400 mm)						
1. Effective infill height H_0 = 260 cm = 2600 mm 2. Thickness D2 = 40 cm 3. Contact side area: A_0 = H_0 (cm) *D2(cm) = 260*40 = 10400 cm^2 4. Max side force: N_0 = A_0*G1 = 10400 0.25 = 2600 kN						
Story drift (‰) (model-**Dr** / H_0)	**1.26**		**2.52**		**6.34**	
H-Force (%) (Model-**F** / N_0		**4.84**		**6.46**		**0.**

9.2.4 Frame span L1 = 200 cm and infill thickness D3 = 250 mm (Model M1-L1-G1-D3)

Decoupled response of frame and infill: For the selected representative scaled RC frame model (S=1:2) with span L1 = 200 cm, analysed was the effect of considered AAC infill with thickness D3 = 250 mm. Based on the computed nonlinear response of the frame with AAC infill and nonlinear response of non-infilled or only RC frame system, ***the decoupled infill nonlinear response was defined,*** Table 9.2.3***.*** In the same table included are the resulting: (1) Modelling parameters of AAC infill for the scaled model, (2a) Modelling parameters of AAC infill for the respective prototype or real-scale system and (2b) Margins of estimated modelling parameters of AAC infill for practical design the real-scale prototype system.

Table 9.2.3. Scaled model M1-L1-G1-D3: Modelling parameters of decoupled AAC infill in frame with span L1 = 200 cm and thickness D3 = 250 mm and results for prototype.

1. SCALED MODEL: Modelling parameters (Micro-Modelling Results) SCALED MODEL: M1-L1-G1-D3: (L1 = 200 cm; G1 = 2.5 MPa; D3 = 250 mm)						
MODEL PARAMETERS OF DECOUPLED AAC INFILL						
K0 = 2.0*FM/DM	DY = 0.5*DM	FY = 0.75*FM	DM	FM	DL = 2.5*DM	FL
kN/mm	mm	kN	mm	kN	mm	kN
38.66	1.5	43.5	3.0	58.0	7.5	0.
2a. PROTOTYPE FRAME: Modelling parameters PROTOTYPE: P1-L1-G1-D3: (L1 = 400 cm; G1 = 2.5 MPa; D3 = 500 mm)						
PARAMETERS OF DECOUPLED AAC INFILL						
K0	DY	FY	DM	FM	DL	FL
kN/mm	mm	kN	mm	kN	mm	kN
77.33	3.0	174.0	6.0	232.0	15.0	0.
2b. PROTOTYPE FRAME: Margins of modelling parameters for practical design PROTOTYPE: P1-L1-G1-D3: (L1 = 400 cm; G1 = 2.5 MPa; D3 = 500 mm)						
1. Effective infill height H_0 = 260 cm = 2600 mm 2. Thickness D3 = 50 cm 3. Contact side area: A_0 = H_0 (cm) *D3(cm) = 260*50 = 13000 cm^2 4. Max side force: N_0 = A_0*G1 = 13000 0.25 = 3250 kN						
Story drift (‰) (model-**Dr** / H_0**)**	**1.15**		**2.30**		**5.76**	
H-Force (%) (Model-**F** / N_0		**5.35**		**7.13**		**0.**

9.3 Effect of Infill Thickness on Response of Frame with Span L2 = 250 cm

9.3.1 Parametric Study of Frame with Span L2 = 250 cm and Computed Results

Parametric study of the selected frame with Span L2 = 250 cm was performed based on formulated and implemented three representative nonlinear micro-models considering the identically reinforced RC frames and three different AAC infill thicknesses:

D1 = 125 mm (Model M1-L2-G1-D1).

D2 = 200 mm (Model M1-L2-G1-D2).

D3 = 250 mm (Model M1-L2-G1-D3).

Compressive strength of AAC infill was considered identical G1 = 2.5 MPa. Geometrical characteristics of the analyzed frames and other related conceptual details used as the basis during formulation of related nonlinear micro-model were presented in all necessary details in the previous chapters. Computed results enabling understanding of nonlinear responses are comparatively presented in Fig. 9.3.1.

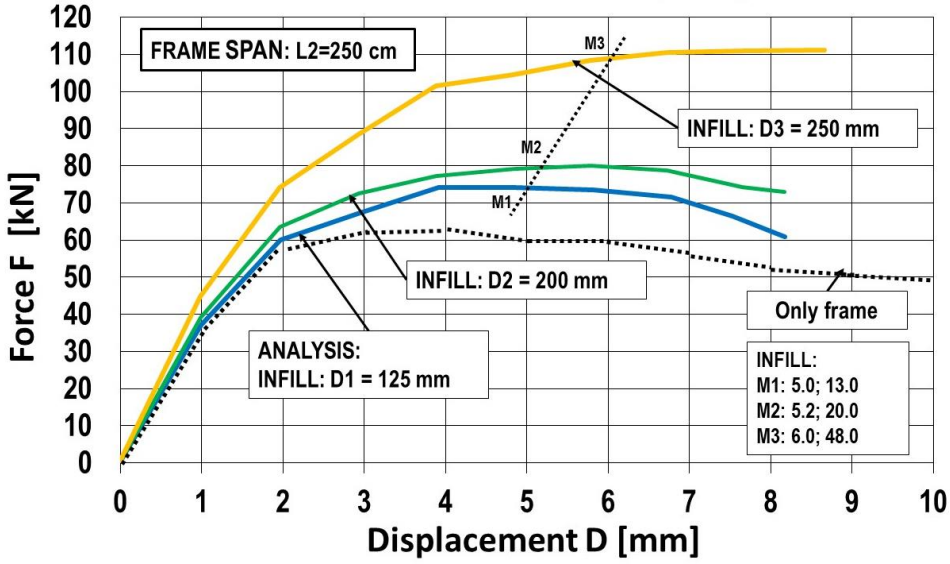

Fig. 9.3.1. Scaled model M2-L2-G1-3D: Computed nonlinear response of AAC infilled frame with span L2 = 250 cm and three infill thicknesses D1, D2 and D3

9.3.2 Frame span L1 = 250 cm and infill thickness D1=125 mm (Model M2-L2-G1-D1)

Decoupled response of frame and infill: For the selected representative scaled RC frame model (S=1:2) with span L2 = 250 cm, analysed was the effect of considered AAC infill with thickness D1 = 125 mm. Based on the computed nonlinear response of the frame with AAC infill and nonlinear response of non-infilled or only RC frame system, ***the decoupled infill nonlinear response was defined,*** Table 9.3.1**.** In the same table included are the resulting: (1) Modelling parameters of AAC infill for the scaled model, (2a) Modelling parameters of AAC infill for the respective prototype or real-scale system and (2b) Margins of estimated modelling parameters of AAC infill for practical design the real-scale prototype system.

Table 9.3.1. Scaled model M2-L2-G1-D1: Modelling parameters of decoupled AAC infill in frame with span L2 = 250 cm and thickness D1 = 125 mm and results for prototype.

1. SCALED MODEL: Modelling parameters (Micro-Modelling Results) SCALED MODEL: M2-L2-G1-D1: (L2 = 250 cm; G1 = 2.5 MPa; D1 = 125 mm)						
MODEL PARAMETERS OF DECOUPLED AAC INFILL						
K0 = 2.0*FM/DM	DY = 0.5*DM	FY = 0.75*FM	DM	FM	DL = 2.5*DM	FL
kN/mm	mm	kN	mm	kN	mm	kN
5.2	2.5	9.75	5.0	13.0	12.5	0.
2a. PROTOTYPE FRAME: Modelling parameters PROTOTYPE: P2-L2-G1-D1: (L2 = 500 cm; G1 = 2.5 MPa; D1 = 250 mm)						
PARAMETERS OF DECOUPLED AAC INFILL						
K0	DY	FY	DM	FM	DL	FL
kN/mm	mm	kN	mm	kN	mm	kN
10.4	5.0	39.0	10.0	52.0	25.0	0.
2b. PROTOTYPE FRAME: Margins of modelling parameters for practical design PROTOTYPE: P2-L2-G1-D1: (L2 = 500 cm; G1 = 2.5 MPa; D1 = 250 mm)						
1. Effective infill height H_0 = 260 cm = 2600 mm 2. Thickness D1 = 25 cm 3. Contact side area: A_0 = H_0 (cm) *D1(cm) = 260*25 = 6500 cm^2 4. Max side force: N_0 = A_0*G1 = 6500 0.25 = 1625 kN						
Story drift (‰) **(**model-**Dr** / H_0**)**	**1.92**		**3.84**		**9.61**	
H-Force (%) **(**Model-**F** / N_0		**2.40**		**.20**		**0.**

9.3.3 Frame span L2 = 250 cm and infill thickness D2 = 200 mm (Model M2- L2-G1-D2)

Decoupled response of frame and infill: For the selected representative scaled RC frame model (S=1:2) with span L2 = 250 cm, analysed was the effect of considered AAC infill with thickness D2 = 200 mm. Based on the computed nonlinear response of the frame with AAC infill and nonlinear response of non-infilled or only RC frame system, ***the decoupled infill nonlinear response was defined,*** Table 9.3.2**.** In the same table included are the resulting: (1) Modelling parameters of AAC infill for the scaled model, (2a) Modelling parameters of AAC infill for the respective prototype or real-scale system and (2b) Margins of estimated modelling parameters of AAC infill for practical design the real-scale prototype system.

Table 9.3.2. Scaled model M2-L2-G1-D1: Modelling parameters of decoupled AAC infill in frame with span L2 = 250 cm and thickness D2 = 200 mm and results for prototype.

1. SCALED MODEL: Modelling parameters (Micro-Modelling Results) SCALED MODEL: M2-L2-G1-D2: (L2 = 250 cm; G1 = 2.5 MPa; D2 = 200 mm)						
MODEL PARAMETERS OF DECOUPLED AAC INFILL						
K0 = 2.0*FM/DM	DY = 0.5*DM	FY = 0.75*FM	DM	FM	DL = 2.5*DM	FL
kN/mm	mm	kN	mm	kN	mm	kN
7.69	2.6	15.0	5.2	20.0	13.0	0.
2a. PROTOTYPE FRAME: Modelling parameters PROTOTYPE: P2-L2-G1-D2: (L2 = 500 cm; G1 = 2.5 MPa; D2 = 400 mm)						
PARAMETERS OF DECOUPLED AAC INFILL						
K0	DY	FY	DM	FM	DL	FL
kN/mm	mm	kN	mm	kN	mm	kN
15.38	5.2	60.0	10.4	80.0	26.0	0.
2b. PROTOTYPE FRAME: Margins of modelling parameters for practical design PROTOTYPE: P2-L2-G1-D2: (L2 = 500 cm; G1 = 2.5 MPa; D2 = 400 mm)						
1. Effective infill height H_0 = 260 cm = 2600 mm 2. Thickness D2 = 40 cm 3. Contact side area: $A_0 = H_0$ (cm) *D2(cm) = 260*40 = 10400 cm^2 4. Max side force: $N_0 = A_0 * G1 = 10400\ 0.25 = 2600$ kN						
Story drift (‰) (model-**Dr** / H_0**)**	**2.0**		**4.0**		**10.0**	
H-Force (%) (Model-**F** / N_0		**2.31**		**3.02**		**0.**

9.3.4 Frame span L2 = 250 cm and infill thickness D3 = 250 mm (Model M2- L2-G1-D3)

Decoupled response of frame and infill: For the selected representative scaled RC frame model (S=1:2) with span L2 = 250 cm, analysed was the effect of considered AAC infill with thickness D3 = 250 mm. Based on the computed nonlinear response of the frame with AAC infill and nonlinear response of non-infilled or only RC frame system, ***the decoupled infill nonlinear response was defined,*** Table 9.3.3***.*** In the same table included are the resulting: (1) Modelling parameters of AAC infill for the scaled model, (2a) Modelling parameters of AAC infill for the respective prototype or real-scale system and (2b) Margins of estimated modelling parameters of AAC infill for practical design the real-scale prototype system.

Table 9.3.3. Scaled model M2-L2-G1-D3: Modelling parameters of decoupled AAC infill in frame with span L2 = 250 cm and thickness D3 = 250 mm and results for prototype.

1. SCALED MODEL: Modelling parameters (Micro-Modelling Results) SCALED MODEL: M2-L2-G1-D3: (L2 = 250 cm; G1 = 2.5 MPa; D3 = 250 mm)						
MODEL PARAMETERS OF DECOUPLED AAC INFILL						
K0 = 2.0*FM/DM	DY = 0.5*DM	FY = 0.75*FM	DM	FM	DL = 2.5*DM	FL
kN/mm	mm	kN	mm	kN	mm	kN
16.0	3.0	36.0	6.0	48.0	15.0	0.
2a. PROTOTYPE FRAME: Modelling parameters PROTOTYPE: P2-L2-G1-D3: (L2 = 500 cm; G1 = 2.5 MPa; D3 = 500 mm)						
PARAMETERS OF DECOUPLED AAC INFILL						
K0	DY	FY	DM	FM	DL	FL
kN/mm	mm	kN	mm	kN	mm	kN
32.0	6.0	144	12.0	192.0	30.0	0.
2b. PROTOTYPE FRAME: Margins of modelling parameters for practical design PROTOTYPE: P2-L2-G1-D3: (L2 = 500 cm; G1 = 2.5 MPa; D3 = 500 mm)						
1. Effective infill height H_0 = 260 cm = 2600 mm 2. Thickness D3 = 50 cm 3. Contact side area: $A_0 = H_0$ (cm) *D3(cm) = 260*50 = 13000 cm^2 4. Max side force: $N_0 = A_0 * G1 = 13000\ 0.25$ = 3250 kN						
Story drift (‰) (model-**Dr** / H_0)	**2.30**		**4.60**		**11.50**	
H-Force (%) (Model-**F** / N_0		**4.43**		**5.90**		**0.**

9.4 Effect of Infill Thickness on Response of Frame with Span L3 = 300 cm

9.4.1 Parametric Study of Frame with Span L3 = 300 cm and Computed Result

Parametric study of the selected frame with Span L3 = 300 cm was performed based on formulated and implemented three representative nonlinear micro-models considering the identically reinforced RC frames and three different AAC infill thicknesses:

D1 = 125 mm (Model M1-L3-G1-D1);

D2 = 200 mm (Model M1-L3-G1-D2);

D3 = 250 mm (Model M1-L3-G1-D3);

Compressive strength of AAC infill was considered identical G1 = 2.5 MPa. Geometrical characteristics of the analyzed frames and other related conceptual details used as the basis during formulation of related nonlinear micro-model were presented in all necessary details in the previous chapters. Computed results enabling understanding of nonlinear responses are comparatively presented in Fig. 9.4.2.

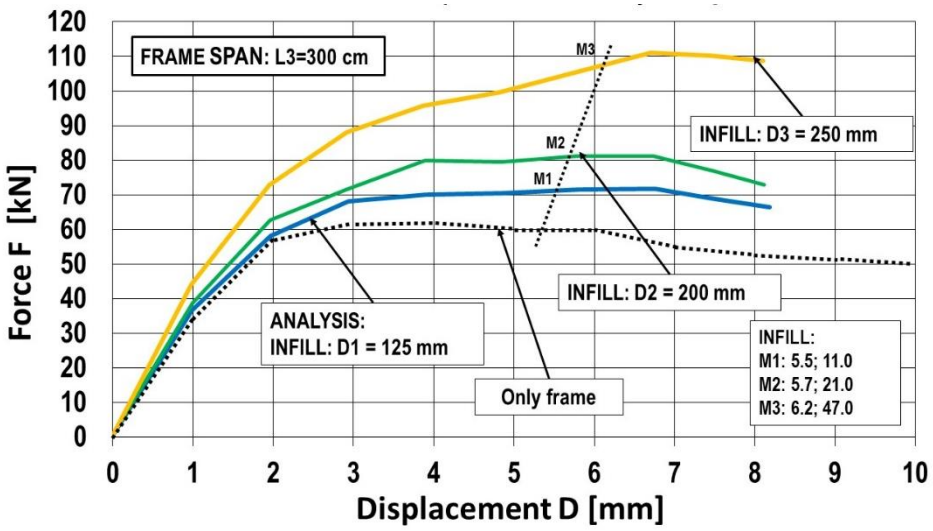

Fig. 9.4.1. Scaled model M3-L3-G1-3D: Computed nonlinear response of AAC infilled frame with span L3 = 300 cm and three infill thicknesses D1, D2 and D3

9.4.2 Frame span L3 = 300 cm and infill thickness D1=125 mm (Model M3-L3-G1-D1)

Decoupled response of frame and infill: For the selected representative scaled RC frame model (S=1:2) with span L3 = 300 cm, analysed was the effect of considered AAC infill with thickness D1 = 125 mm. Based on the computed nonlinear response of the frame with AAC infill and nonlinear response of non-infilled or only RC frame system, ***the decoupled infill nonlinear response was defined,*** Table 9.4.1**.** In the same table included are the resulting: (1) Modelling parameters of AAC infill for the scaled model, (2a) Modelling parameters of AAC infill for the respective prototype or real-scale system and (2b) Margins of estimated modelling parameters of AAC infill for practical design the real-scale prototype system.

Table 9.4.1. Scaled model M3-L3-G1-D1: Modelling parameters of decoupled AAC infill in frame with span L3 = 300 cm and thickness D1 = 125 mm and results for prototype.

1. SCALED MODEL: Modelling parameters (Micro-Modelling Results) SCALED MODEL: M3-L3-G1-D1: (L3 = 300 cm; G1 = 2.5 MPa; D1 = 125 mm)						
MODEL PARAMETERS OF DECOUPLED AAC INFILL						
K0 = 2.0*FM/DM	DY = 0.5*DM	FY = 0.75*FM	DM	FM	DL = 2.5*DM	FL
kN/mm	mm	kN	mm	kN	mm	kN
4.0	2.75	8.25	5.5	11.0	13.75	0.
2a. PROTOTYPE FRAME: Modelling parameters PROTOTYPE: P3-L3-G1-D1: (L3 = 600 cm; G1 = 2.5 MPa; D1 = 250 mm)						
PARAMETERS OF DECOUPLED AAC INFILL						
K0	DY	FY	DM	FM	DL	FL
kN/mm	mm	kN	mm	kN	mm	kN
8.0	5.5	33.0	11.0	44.0	27.5	0.
2b. PROTOTYPE FRAME: Margins of modelling parameters for practical design PROTOTYPE: P3-L3-G1-D1: (L3 = 600 cm; G1 = 2.5 MPa; D1 = 250 mm)						
1. Effective infill height H_0 = 260 cm = 2600 mm 2. Thickness D1 = 25 cm 3. Contact side area: A_0 = H_0 (cm) *D1(cm) = 260*25 = 6500 cm^2 4. Max side force: N_0 = A_0*G1 = 6500 0.25 = 1625 kN						
Story drift (‰) **(**model-**Dr** / H_0**)**	**2.11**		**4.23**		**10.57**	
H-Force (%) **(**Model-**F** / N_0		**2.03**		**2.70**		**0.**

9.4.3 Frame span L3 = 300 cm and infill thickness D2 = 200 mm (Model M3- L3-G1-D2)

Decoupled response of frame and infill: For the selected representative scaled RC frame model (S=1:2) with span L3 = 300 cm, analysed was the effect of considered AAC infill with thickness D2 = 200 mm. Based on the computed nonlinear response of the frame with AAC infill and nonlinear response of non-infilled or only RC frame system, ***the decoupled infill nonlinear response was defined,*** Table 9.4.2**.** In the same table included are the resulting: (1) Modelling parameters of AAC infill for the scaled model, (2a) Modelling parameters of AAC infill for the respective prototype or real-scale system and (2b) Margins of estimated modelling parameters of AAC infill for practical design the real-scale prototype system.

Table 9.4.2. Scaled model M3-L3-G1-D2: Modelling parameters of decoupled AAC infill in frame with span L2 = 300 cm and thickness D2 = 200 mm and results for prototype.

1. SCALED MODEL: Modelling parameters (Micro-Modelling Results) SCALED MODEL: M3-L3-G1-D2: (L3 = 300 cm; G1 = 2.5 MPa; D2 = 200 mm)						
MODEL PARAMETERS OF DECOUPLED AAC INFILL						
K0 = 2.0*FM/DM	DY = 0.5*DM	FY = 0.75*FM	DM	FM	DL = 2.5*DM	FL
kN/mm	mm	kN	mm	kN	mm	kN
7.36	2.85	15.75	5.7	21.0	14.25	0.
2a. PROTOTYPE FRAME: Modelling parameters PROTOTYPE: P3-L3-G1-D2: (L3 = 600 cm; G1 = 2.5 MPa; D2 = 400 mm)						
PARAMETERS OF DECOUPLED AAC INFILL						
K0	DY	FY	DM	FM	DL	FL
kN/mm	mm	kN	mm	kN	mm	kN
14.73	5.7	63.0	11.4	84.0	28.5	0.
2b. PROTOTYPE FRAME: Margins of modelling parameters for practical design PROTOTYPE: P3-L3-G1-D2: (L3 = 600 cm; G1 = 2.5 MPa; D2 = 400 mm)						
1. Effective infill height H_0 = 260 cm = 2600 mm 2. Thickness D2 = 40 cm 3. Contact side area: A_0 = H_0 (cm) *D2(cm) = 260*40 = 10400 cm^2 4. Max side force: N_0 = A_0*G1 = 10400 0.25 = 1625 kN						
Story drift (‰) (model-**Dr** / H_0**)**	**2.19**		**4.38**		**10.96**	
H-Force (%) (Model-**F** / N_0		**2.42**		**3.23**		**0.**

9.4.4 Frame span L3 = 300 cm and infill thickness D3 = 250 mm (Model M3-L3-G1-D3)

Decoupled response of frame and infill: For the selected representative scaled RC frame model (S=1:2) with span L3 = 300 cm, analysed was the effect of considered AAC infill with thickness D3 = 250 mm. Based on the computed nonlinear response of the frame with AAC infill and nonlinear response of non-infilled or only RC frame system, ***the decoupled infill nonlinear response was defined,*** Table 9.4.3***.*** In the same table included are the resulting: (1) Modelling parameters of AAC infill for the scaled model, (2a) Modelling parameters of AAC infill for the respective prototype or real-scale system and (2b) Margins of estimated modelling parameters of AAC infill for practical design the real-scale prototype system.

Table 9.4.3. Scaled model M3-L3-G1-D3: Modelling parameters of decoupled AAC infill in frame with span L3 = 300 cm and thickness D3 = 250 mm and results for prototype.

1. SCALED MODEL: Modelling parameters (Micro-Modelling Results) SCALED MODEL: M3-L3-G1-D3: (L3 = 300 cm; G1 = 2.5 MPa; D3 = 250 mm)						
MODEL PARAMETERS OF DECOUPLED AAC INFILL						
K0 = 2.0*FM/DM	DY = 0.5*DM	FY = 0.75*FM	DM	FM	DL = 2.5*DM	FL
kN/mm	mm	kN	mm	kN	mm	kN
15.16	3.1	35.25	6.2	47.0	15.5	0.
2a. PROTOTYPE FRAME: Modelling parameters PROTOTYPE: P3-L3-G1-D3: (L3 = 600 cm; G1 = 2.5 MPa; D3 = 500 mm)						
PARAMETERS OF DECOUPLED AAC INFILL						
K0	DY	FY	DM	FM	DL	FL
kN/mm	mm	kN	mm	kN	mm	kN
30.32	6.2	141.0	12.4	188.0	31.0	0.
2b. PROTOTYPE FRAME: Margins of modelling parameters for practical design PROTOTYPE: P3-L3-G1-D3: (L3 = 600 cm; G1 = 2.5 MPa; D3 = 500 mm)						
1. Effective infill height H_0 = 260 cm = 2600 mm 2. Thickness D3 = 50 cm 3. Contact side area: A_0 = H_0 (cm) *D1(cm) = 260*50 = 13000 cm^2 4. Max side force: N_0 = A_0*G1 = 13000 0.25 = 3250 kN						
Story drift (‰) (model-**Dr** / H_0)	**2.36**		**4.76**		**11.92**	
H-Force (%) (Model-**F** / N_0		**4.33**		**5.78**		**0.**

9.5 Effect of Frame Span on Infilled Frame Response

9.5.1 Parametric Study of Frame with Three Spans and Computed Results

Parametric study of AAC infilled frames with three spans L1 = 200 cm, L2 = 250 cm and L3 = 300 cm were performed based on formulated and implemented three representative nonlinear micro-models considering the identically reinforced RC frames:

Model M4-L1-G1-D1.

Model M4-L2-G1-D1.

Model M4-L3-G1-D1.

Compressive strength of AAC infill and thickness were considered identical, G1 = 2.5 MPa and D1 = 125 mm. Geometrical characteristics of the analyzed frames and other related conceptual details used as the basis during formulation of related nonlinear micro-models were presented in all necessary details in the previous chapters. The computed results enabling understanding of nonlinear responses are comparatively presented in Fig. 9.5.1.

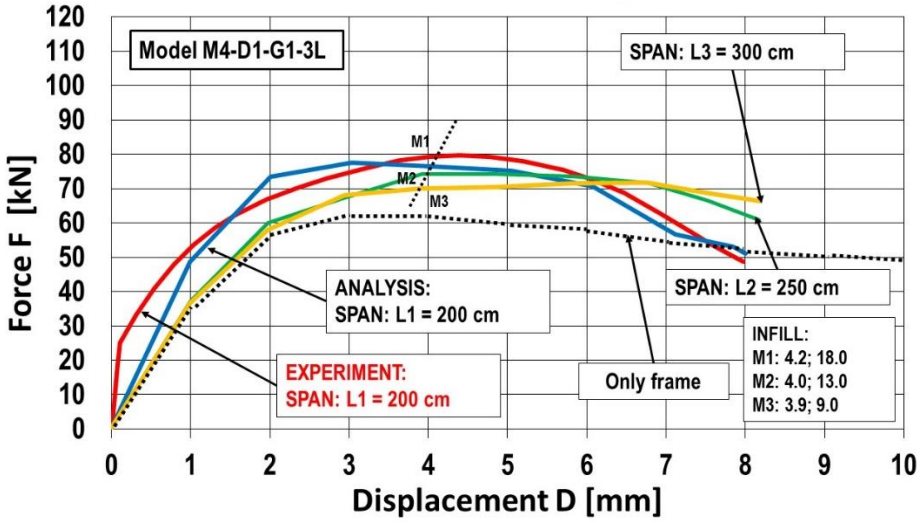

Fig. 9.5.1. Scaled model M4-D1-G1-3L: Computed nonlinear response of AAC infilled frame with infill thickness D1 = 125 mm and three infill spans L1, L2 and L3

9.6 Effect of Frame Span on Non-Infilled Frame Response

9.6.1 Parametric Study of Non-Infilled Frame with Three Spans and Computed Results

Parametric study of non-infilled frames with three spans L1 = 200 cm, L2 = 250 cm and L3 = 300 cm were performed based on formulated and implemented three representative nonlinear micro-models considering the identically reinforced RC frames:

Model M5=M0-L1.

Model M5=M0-L2.

Model M5=M0-L3.

Geometrical characteristics of the analyzed frames and other related conceptual details used as the basis during formulation of related nonlinear micro-models were presented in all necessary details in the previous chapters. The computed results enabling understanding of nonlinear responses are comparatively presented in Fig. 9.6.1.

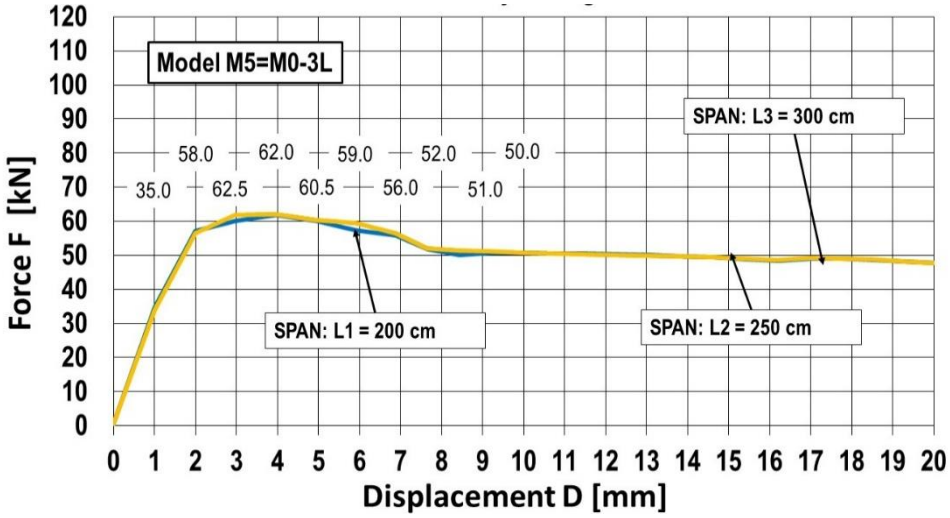

Fig. 9.6.1. Scaled model M5=M0-3L: Computed nonlinear response of non-infilled RC frames with three spans L1, L2 and L3

9.7 Effect of Infill Strength on Response of Frame with Span L1 = 200 cm

9.7.1 Parametric Study of Frame with Span L1 = 200 cm and Computed Results

Parametric study of the selected frame with Span L1 = 200 cm was performed based on formulated and implemented three representative nonlinear micro-models considering the identically reinforced RC frames and three different AAC infill strengths:

G1 = 2.5 MPa (Model M6-L1-D1-G1).

G2 = 3.75 MPa (Model M6-L1-D1-G2).

G3 = 5.0 MPa (Model M6-L1-D1-G3).

Thickness of AAC infill was considered identical D1 = 125 mm. Geometrical characteristics of the analyzed frames and other related conceptual details used as the basis during formulation of related nonlinear micro-model were presented in all necessary details in the previous chapters. The computed results enabling understanding of nonlinear responses are comparatively presented in Fig. 9.7.1.

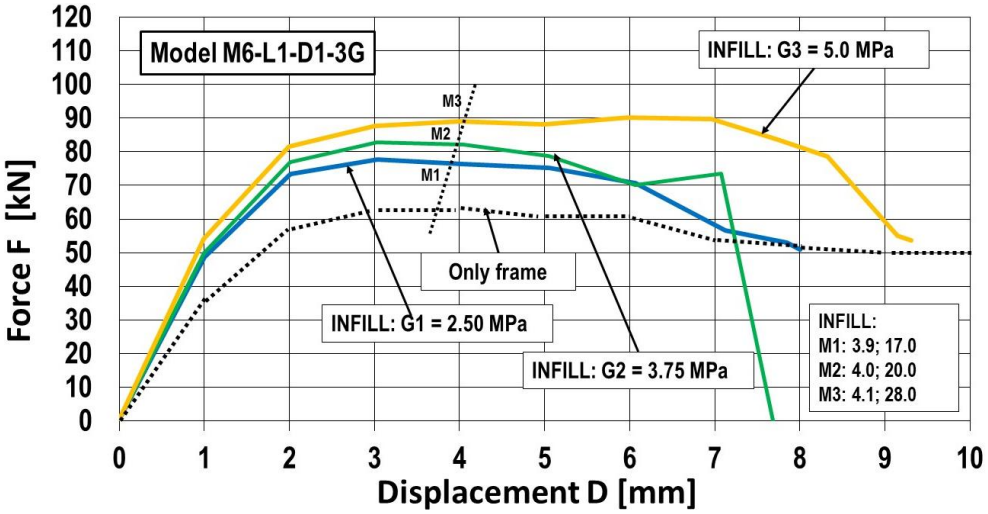

Fig. 9.7.1. Scaled model M6-L1-D1-3G: Computed nonlinear response of AAC infilled frame with span L1 = 200 cm, thickness D1 and three infill strengths G1, G2 and G3

9.7.2 Frame span L1 = 200 cm and infill strength G1 = 2.5 MPa (Model M6-L1-G1-D1)

Decoupled response of frame and infill: For the selected representative scaled RC frame model (S=1:2) with span L1 = 200 cm, analysed was the effect of considered AAC infill with strength G1 = 2.5 MPa. Based on the computed nonlinear response of the frame with AAC infill and nonlinear response of non-infilled or only RC frame system, ***the decoupled infill nonlinear response was defined,*** Table 9.7.1**.** In the same table included are the resulting: (1) Modelling parameters of AAC infill for the scaled model, (2a) Modelling parameters of AAC infill for the respective prototype or real-scale system and (2b) Margins of estimated modelling parameters of AAC infill for practical design the real-scale prototype system.

Table 9.7.1. Scaled model M6-L1-G1-D1: Modelling parameters of decoupled AAC infill in frame with L1 = 200 cm, D1 = 125 mm, compressive strength G1 = 2.5 MPa and results for prototype.

1. SCALED MODEL: Modelling parameters (Micro-Modelling Results) SCALED MODEL: M6-L1-G1-D1: (L1 = 200 cm; D1 = 125 mm; G1 = 2.5 MPa)						
MODEL PARAMETERS OF DECOUPLED AAC INFILL						
K0 = 2.0*FM/DM	DY = 0.5*DM	FY = 0.75*FM	DM	FM	DL = 2.5*DM	FL
kN/mm	mm	kN	mm	kN	mm	kN
8.72	1.95	12.75	3.9	17.0	9.75	0.
2a. PROTOTYPE FRAME: Modelling parameters PROTOTYPE: P6-L1-G1-D1: (L1 = 400 cm; D1 = 250 mm; G1 = 2.5 MPa)						
PARAMETERS OF DECOUPLED AAC INFILL						
K0	DY	FY	DM	FM	DL	FL
kN/mm	mm	kN	mm	kN	mm	kN
17.44	3.9	51.0	7.8	68.0	19.5	0.
2b. PROTOTYPE FRAME: Margins of modelling parameters for practical design PROTOTYPE: P6-L1-G1-D1: (L1 = 400 cm; D1 = 250 mm; G1 = 2.5 MPa)						
1. Effective infill height H_0 = 260 cm = 2600 mm 2. Thickness D1 = 25 cm 3. Contact side area: A_0 = H_0 (cm) *D1(cm) = 260*25 = 6500 cm^2 4. Max side force: N_0 = A_0*G1 = 6500 0.25 = 1625 kN						
Story drift (‰) (model-**Dr** / H_0**)**	**1.50**		**3.00**		**7.50**	
H-Force (%) (Model-**F** / N_0		**3.13**		**4.18**		**0.**

9.7.3 Frame span L1 = 200 cm and infill strength G2 = 3.75 MPa (Model M6-L1-G2-D1)

Decoupled response of frame and infill: For the selected representative scaled RC frame model (S=1:2) with span L1 = 200 cm, analysed was the effect of considered AAC infill with strength G2 = 3.75 MPa. Based on the computed nonlinear response of the frame with AAC infill and nonlinear response of non-infilled or only RC frame system, ***the decoupled infill nonlinear response was defined,*** Table 9.7.2***.*** In the same table included are the resulting: (1) Modelling parameters of AAC infill for the scaled model, (2a) Modelling parameters of AAC infill for the respective prototype or real-scale system and (2b) Margins of estimated modelling parameters of AAC infill for practical design the real-scale prototype system.

Table 9.7.2. Scaled model M6-L1- G2-D1: Modelling parameters of decoupled AAC infill in frame with L1 = 200 cm, D1 = 125 mm, compressive strength G2 = 3.75 MPa and results for prototype.

1. SCALED MODEL: Modelling parameters (Micro-Modelling Results) SCALED MODEL: M6-L1-G2-D1: (L1 = 200 cm; D1 = 125 mm; G2 = 3.75 MPa)						
MODEL PARAMETERS OF DECOUPLED AAC INFILL						
K0 = 2.0*FM/DM	DY = 0.5*DM	FY = 0.75*FM	DM	FM	DL = 2.5*DM	FL
kN/mm	mm	kN	mm	kN	mm	kN
10.0	2.0	15.0	4.0	20.0	10.0	0.
2a. PROTOTYPE FRAME: Modelling parameters PROTOTYPE: P6-L1-G2-D1: (L1 = 400 cm; D1 = 250 mm; G2 = 3.75 MPa)						
PARAMETERS OF DECOUPLED AAC INFILL						
K0	DY	FY	DM	FM	DL	FL
kN/mm	mm	kN	mm	kN	mm	kN
20.0	4.0	60.0	8.0	80.0	20.0	0.
2b. PROTOTYPE FRAME: Margins of modelling parameters for practical design PROTOTYPE: P6-L1-G2-D1: (L1 = 400 cm; D1 = 250 mm; G2 = 3.75 MPa)						
1. Effective infill height H_0 = 260 cm = 2600 mm 2. Thickness D1 = 25 cm 3. Contact side area: $A_0 = H_0$ (cm) *D1(cm) = 260*25 = 6500 cm^2 4. Max side force: $N_0 = A_0 * G2 = 6500\ 0.375 = 2437$ kN						
Story drift (‰) (model-**Dr** / H_0)	**1.53**		**3.07**		**7.69**	
H-Force (%) (Model-**F** / N_0		**2.46**		**3.28**		**0.**

9.7.4 Frame span L1 = 200 cm and infill strength G3 = 5.0 MPa (Model M6-L1-G3-D1)

Decoupled response of frame and infill: For the selected representative scaled RC frame model (S=1:2) with span L1 = 200 cm, analysed was the effect of considered AAC infill with strength G3 = 5.0 MPa. Based on the computed nonlinear response of the frame with AAC infill and nonlinear response of non-infilled or only RC frame system, ***the decoupled infill nonlinear response was defined,*** Table 9.7.3***.*** In the same table included are the resulting: (1) Modelling parameters of AAC infill for the scaled model, (2a) Modelling parameters of AAC infill for the respective prototype or real-scale system and (2b) Margins of estimated modelling parameters of AAC infill for practical design the real-scale prototype system.

Table 9.7.3. Scaled model M6-L1-G3-D1: Modelling parameters of decoupled AAC infill in frame with L1 = 200 cm, D1 = 125 mm, compressive strength G3 = 5.0 MPa and results for prototype.

1. SCALED MODEL: Modelling parameters (Micro-Modelling Results) SCALED MODEL: M6-L1-G3-D1: (L1 = 200 cm; D1 = 125 mm; G3 = 5.0 MPa)						
MODEL PARAMETERS OF DECOUPLED AAC INFILL						
K0 = 2.0*FM/DM	DY = 0.5*DM	FY = 0.75*FM	DM	FM	DL = 2.5*DM	FL
kN/mm	mm	kN	mm	kN	mm	kN
6.82	2.05	21.0	4.1	28.0	10.25	0.
2a. PROTOTYPE FRAME: Modelling parameters PROTOTYPE: P6-L1-G3-D1: (L1 = 400 cm; D1 = 250 mm; G1 = 5.0 MPa)						
PARAMETERS OF DECOUPLED AAC INFILL						
K0	DY	FY	DM	FM	DL	FL
kN/mm	mm	kN	mm	kN	mm	kN
13.65	4.1	84.0	8.2	112.0	20.5	0.
2b. PROTOTYPE FRAME: Margins of modelling parameters for practical design PROTOTYPE: P6-L1-G3-D1: (L1 = 400 cm; D1 = 250 mm; G3 = 5.0 MPa)						
1. Effective infill height H_0 = 260 cm = 2600 mm 2. Thickness D1 = 25 cm 3. Contact side area: A_0 = H_0 (cm) *D1(cm) = 260*25 = 6500 cm^2 4. Max side force: N_0 = A_0*G3 = 6500 0.5 = 3250 kN						
Story drift (‰) (model-**Dr** / H_0)	**1.69**		**3.15**		**7.88**	
H-Force (%) (Model-**F** / N_0		**2.58**		**3.44**		**0.**

9.8 Effect of Infill Strength on Response of Frame with Span L2 = 250 cm

9.8.1 Parametric Study of Frame with Span L2 = 250 cm and Computed Results

Parametric study of the selected frame with Span L2 = 250 cm was performed based on formulated and implemented three representative nonlinear micro-models considering the identically reinforced RC frames and three different AAC infill strengths:

G1 = 2.5 MPa (Model M7-L2-D1-G1);

G2 = 3.75 MPa (Model M7-L2-D1-G2);

G3 = 5.0 MPa (Model M7-L2-D1-G3);

Thickness of AAC infill was considered identical D1 = 125 mm. Geometrical characteristics of the analyzed frames and other related conceptual details used as the basis during formulation of related nonlinear micro-model were presented in all necessary details in the previous chapters. Computed results enabling understanding of nonlinear responses are comparatively presented in Fig. 9.8.1.

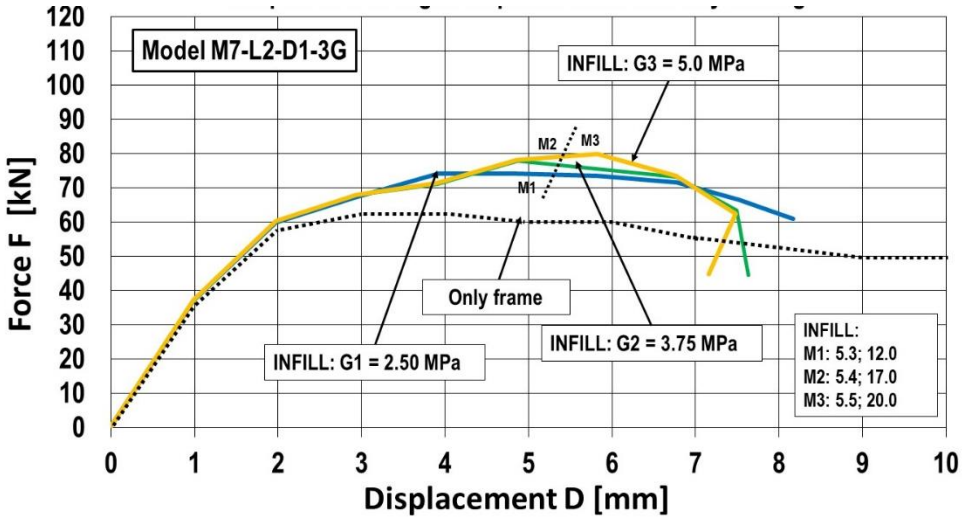

Fig. 9.8.1. Scaled model M7-L2-D1-3G: Computed nonlinear response of AAC infilled frame with span L2 = 250 cm, thickness D1 and three infill strengths G1, G2 and G3

9.8.2 Frame span L2 = 250 cm and infill strength G1 = 2.5 MPa (Model M7-L2-G1-D1)

Decoupled response of frame and infill: For the selected representative scaled RC frame model (S=1:2) with span L2 = 250 cm, analysed was the effect of considered AAC infill with strength G1 = 2.5 MPa. Based on the computed nonlinear response of the frame with AAC infill and nonlinear response of non-infilled or only RC frame system, ***the decoupled infill nonlinear response was defined,*** Table 9.8.1**.** In the same table included are the resulting: (1) Modelling parameters of AAC infill for the scaled model, (2a) Modelling parameters of AAC infill for the respective prototype or real-scale system and (2b) Margins of estimated modelling parameters of AAC infill for practical design the real-scale prototype system.

Table 9.8.1. Scaled model M7-L2-G1-D1: Modelling parameters of decoupled AAC infill in frame with L2 = 250 cm, D1 = 125 mm, compressive strength G1 = 2.5 MPa and results for prototype.

1. SCALED MODEL: Modelling parameters (Micro-Modelling Results) SCALED MODEL: M7-L2-G1-D1: (L2 = 250 cm; D1 = 125 mm; G1 = 2.5 MPa)						
MODEL PARAMETERS OF DECOUPLED AAC INFILL						
K0 = 2.0*FM/DM	DY = 0.5*DM	FY = 0.75*FM	DM	FM	DL = 2.5*DM	FL
kN/mm	mm	kN	mm	kN	mm	kN
2.26	2.65	9.0	5.3	12.0	13.25	0.
2a. PROTOTYPE FRAME: Modelling parameters PROTOTYPE: P7-L2-G1-D1: (L2 = 500 cm; D1 = 250 mm; G1 = 2.5 MPa)						
PARAMETERS OF DECOUPLED AAC INFILL						
K0	DY	FY	DM	FM	DL	FL
kN/mm	mm	kN	mm	kN	mm	kN
4.52	5.3	36.0	10.6	48.0	26.5	0.
2b. PROTOTYPE FRAME: Margins of modelling parameters for practical design PROTOTYPE: P7-L2-G1-D1: (L2 = 500 cm; D1 = 250 mm; G1 = 2.5 MPa)						
1. Effective infill height H_0 = 260 cm = 2600 mm 2. Thickness D1 = 25 cm 3. Contact side area: $A_0 = H_0$ (cm) *D1(cm) = 260*25 = 6500 cm^2 4. Max side force: $N_0 = A_0$*G1 = 6500 0.25 = 1625 kN						
Story drift (‰) (model-**Dr** / H_0**)**	**2.03**		**4.07**		**10.19**	
H-Force (%) (Model-**F** / N_0		**2.21**		**2.95**		**0.**

9.8.3 Frame span L2 = 250 cm and infill strength G2 = 3.75 MPa (Model M7- L2-G2-D1)

Decoupled response of frame and infill: For the selected representative scaled RC frame model (S=1:2) with span L2 = 250 cm, analysed was the effect of considered AAC infill with strength G2 = 3.75 MPa. Based on the computed nonlinear response of the frame with AAC infill and nonlinear response of non-infilled or only RC frame system, ***the decoupled infill nonlinear response was defined,*** Table 9.8.2***.*** In the same table included are the resulting: (1) Modelling parameters of AAC infill for the scaled model, (2a) Modelling parameters of AAC infill for the respective prototype or real-scale system and (2b) Margins of estimated modelling parameters of AAC infill for practical design the real-scale prototype system.

Table 9.8.2. Scaled model M7-L2-G2-D1: Modelling parameters of decoupled AAC infill in frame with L2 = 250 cm, D1 = 125 mm, compressive strength G2 = 3.75 MPa and results for prototype.

1. SCALED MODEL: Modelling parameters (Micro-Modelling Results) SCALED MODEL: M7-L2-G2-D1: (L2 = 250 cm; D1 = 125 mm; G2 = 3.75 MPa)						
MODEL PARAMETERS OF DECOUPLED AAC INFILL						
K0 = 2.0*FM/DM	DY = 0.5*DM	FY = 0.75*FM	DM	FM	DL = 2.5*DM	FL
kN/mm	mm	kN	mm	kN	mm	kN
6.29	2.7	12.75	5.4	17.0	13.5	0.
2a. PROTOTYPE FRAME: Modelling parameters PROTOTYPE: P7-L2-G2-D1: (L2 = 500 cm; D1 = 250 mm; G2 = 3.75 MPa)						
PARAMETERS OF DECOUPLED AAC INFILL						
K0	DY	FY	DM	FM	DL	FL
kN/mm	mm	kN	mm	kN	mm	kN
12.59	5.4	51.0	10.8	68.0	27.0	0.
2b. PROTOTYPE FRAME: Margins of modelling parameters for practical design PROTOTYPE: P7-L2-G2-D1: (L2 = 500 cm; D1 = 250 mm; G2 = 3.75 MPa)						
1. Effective infill height H_0 = 260 cm = 2600 mm 2. Thickness D1 = 25 cm 3. Contact side area: A_0 = H_0 (cm) *D1(cm) = 260*25 = 6500 cm^2 4. Max side force: N_0 = A_0*G2 = 6500 0.375 = 2437 kN						
Story drift (‰) (model-**Dr** / H_0)	**2.07**		**4.15**		**10.38**	
H-Force (%) (Model-**F** / N_0		**2.09**		**2.79**		**0.**

9.8.4 Frame span L2 = 250 cm and infill strength G3 = 5.0 MPa (Model M7- L2-G3-D1)

Decoupled response of frame and infill: For the selected representative scaled RC frame model (S=1:2) with span L2 = 250 cm, analysed was the effect of considered AAC infill with strength G3 = 5.0 MPa. Based on the computed nonlinear response of the frame with AAC infill and nonlinear response of non-infilled or only RC frame system, ***the decoupled infill nonlinear response was defined,*** Table 9.8.3***.*** In the same table included are the resulting: (1) Modelling parameters of AAC infill for the scaled model, (2a) Modelling parameters of AAC infill for the respective prototype or real-scale system and (2b) Margins of estimated.

Table 9.8.3. Scaled model M7-L2- G3-D1: Modelling parameters of decoupled AAC infill in frame with L2 = 250 cm, D1 = 125 mm, compressive strength G3 = 5.0 MPa and results for prototype.

1. SCALED MODEL: Modelling parameters (Micro-Modelling Results) SCALED MODEL: M7-L2-G3-D1: (L2 = 250 cm; D1 = 125 mm; G3 = 5.0 MPa)						
MODEL PARAMETERS OF DECOUPLED AAC INFILL						
K0 = 2.0*FM/DM	DY = 0.5*DM	FY = 0.75*FM	DM	FM	DL = 2.5*DM	FL
kN/mm	mm	kN	mm	kN	mm	kN
7.27	2.75	15.0	5.5	20.0	13.75	0.
2a. PROTOTYPE FRAME: Modelling parameters PROTOTYPE: P7-L2-G3-D1: (L2 = 500 cm; D1 = 250 mm; G3 = 5.0 MPa)						
PARAMETERS OF DECOUPLED AAC INFILL						
K0	DY	FY	DM	FM	DL	FL
kN/mm	mm	kN	mm	kN	mm	kN
14.54	5.5	60.0	11.0	80.0	27.5	0.
2b. PROTOTYPE FRAME: Margins of modelling parameters for practical design PROTOTYPE: P7-L2-G3-D1: (L2 = 500 cm; D1 = 250 mm; G3 = 5.0 MPa)						
1. Effective infill height H_0 = 260 cm = 2600 mm 2. Thickness D1 = 25 cm 3. Contact side area: A_0 = H_0 (cm) *D1(cm) = 260*25 = 6500 cm^2 4. Max side force: N_0 = A_0*G3 = 6500 0.5 = 3,250 kN						
Story drift (‰) (model-**Dr** / H_0)	**2.11**		**4.23**		**10.57**	
H-Force (%) (Model-**F** / N_0		**1.84**		**2.46**		**0.**

9.9 Effect of Infill Strength on Response of Frame with Span L3 = 300 cm

9.9.1 Parametric Study of Frame with Span L3 = 300 cm and Computed Results

Parametric study of the selected frame with Span L3 = 300 cm was performed based on formulated and implemented three representative nonlinear micro-models considering the identically reinforced RC frames and three different AAC infill strengths:

G1 = 2.5 MPa (Model M8-L3-D1-G1);

G2 = 3.75 MPa (Model M8-L3-D1-G2);

G3 = 5.0 MPa (Model M8-L3-D1-G3);

Thickness of AAC infill was considered identical D1 = 125 mm. Geometrical characteristics of the analyzed frames and other related conceptual details used as the basis during formulation of related nonlinear micro-model were presented in all necessary details in the previous chapters. The computed results enabling understanding of nonlinear responses are comparatively presented in Fig. 9.9.1.

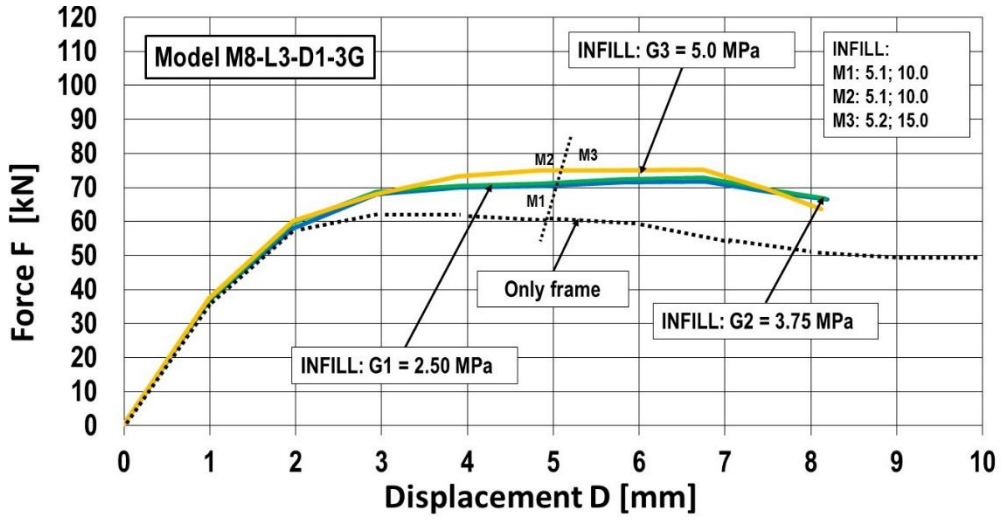

Fig. 9.9.1. Scaled model M8-L3-D1-3G: Computed nonlinear response of AAC infilled frame with span L3 = 300 cm, thickness D1 and three infill strengths G1, G2 and G3

9.9.2 Frame span L3 = 300 cm and infill strength G1 = 2.5 MPa (Model M8-L3-G1-D1)

Decoupled response of frame and infill: For the selected representative scaled RC frame model (S=1:2) with span L3 = 300 cm, analysed was the effect of considered AAC infill with strength G1 = 2.5 MPa. Based on the computed nonlinear response of the frame with AAC infill and nonlinear response of non-infilled or only RC frame system, ***the decoupled infill nonlinear response was defined,*** Table 9.9.1**.** In the same table included are the resulting: (1) Modelling parameters of AAC infill for the scaled model, (2a) Modelling parameters of AAC infill for the respective prototype or real-scale system and (2b) Margins of estimated

Table 9.9.1. Scaled model M8-L3-G1-D1: Modelling parameters of decoupled AAC infill in frame with L3 = 300 cm, D1 = 125 mm, compressive strength G1 = 2.5 MPa and results for prototype.

1. SCALED MODEL: Modelling parameters (Micro-Modelling Results) SCALED MODEL: M8-L3-G1-D1: (L3 = 300 cm; D1 = 125 mm; G1 = 2.5 MPa)						
MODEL PARAMETERS OF DECOUPLED AAC INFILL						
K0 = 2.0*FM/DM	DY = 0.5*DM	FY = 0.75*FM	DM	FM	DL = 2.5*DM	FL
kN/mm	mm	kN	mm	kN	mm	kN
3.92	2.55	7.5	5.1	10.0	12.75	0.
2a. PROTOTYPE FRAME: Modelling parameters PROTOTYPE: P8-L3-G1-D1: (L3 = 600 cm; D1 = 250 mm; G1 = 2.5 MPa)						
PARAMETERS OF DECOUPLED AAC INFILL						
K0	DY	FY	DM	FM	DL	FL
kN/mm	mm	kN	mm	kN	mm	kN
7.84	5.1	30.0	10.2	40.0	25.5	0.
2b. PROTOTYPE FRAME: Margins of modelling parameters for practical design PROTOTYPE: P8-L3-G1-D1: (L3 = 600 cm; D1 = 250 mm; G1 = 2.5 MPa)						
1. Effective infill height H_0 = 260 cm = 2600 mm 2. Thickness D1 = 25 cm 3. Contact side area: A_0 = H_0 (cm) *D1(cm) = 260*25 = 6500 cm^2 4. Max side force: N_0 = A_0*G1 = 6500 0.25 = 1625 kN						
Story drift (‰) (model-**Dr** / H_0)	**1.96**		**3.92**		**9.80**	
H-Force (%) (Model-**F** / N_0		**1.84**		**2.46**		**0.**

9.9.3 Frame span L3 = 300 cm and infill strength G2 = 3.75 MPa (Model M8- L3-G2-D1)

Decoupled response of frame and infill: For the selected representative scaled RC frame model (S=1:2) with span L3 = 300 cm, analysed was the effect of considered AAC infill with strength G2 = 3.75 MPa. Based on the computed nonlinear response of the frame with AAC infill and nonlinear response of non-infilled or only RC frame system, ***the decoupled infill nonlinear response was defined,*** Table 9.9.2***.*** In the same table included are the resulting: (1) Modelling parameters of AAC infill for the scaled model, (2a) Modelling parameters of AAC infill for the respective prototype or real-scale system and (2b) Margins of estimated.

Table 9.9.2. Scaled model M8-L3-G2-D1: Modelling parameters of decoupled AAC infill in frame with L3 = 300 cm, D1 = 125 mm, compressive strength G2 = 3.75 MPa and results for prototype.

1. SCALED MODEL: Modelling parameters (Micro-Modelling Results) SCALED MODEL: M8-L3-G2-D1: (L3 = 300 cm; D1 = 125 mm; G2 = 3.75 MPa)						
MODEL PARAMETERS OF DECOUPLED AAC INFILL						
K0 = 2.0*FM/DM	DY = 0.5*DM	FY = 0.75*FM	DM	FM	DL = 2.5*DM	FL
kN/mm	mm	kN	mm	kN	mm	kN
3.92	2.55	7.5	5.1	10.0	12.75	0.
2a. PROTOTYPE FRAME: Modelling parameters PROTOTYPE: P8-L3-G2-D1: (L3 = 600 cm; D1 = 250 mm; G2 = 3.75 MPa)						
PARAMETERS OF DECOUPLED AAC INFILL						
K0	DY	FY	DM	FM	DL	FL
kN/mm	mm	kN	mm	kN	mm	kN
7.84	5.1	30.0	10.2	40.0	25.5	0.
2b. PROTOTYPE FRAME: Margins of modelling parameters for practical design PROTOTYPE: P8-L3-G2-D1: (L3 = 600 cm; D1 = 250 mm; G2 = 3.75 MPa)						
1. Effective infill height H_0 = 260 cm = 2600 mm 2. Thickness D1 = 25 cm 3. Contact side area: A_0 = H_0 (cm) *D1(cm) = 260*25 = 6500 cm^2 4. Max side force: N_0 = A_0*G2 = 6500 0.375 = 2437 kN						
Story drift (‰) **(**model-**Dr** / H_0**)**	**1.96**		**3.92**		**9.80**	
H-Force (%) **(**Model-**F** / N_0		**1.23**		**1.64**		**0.**

9.9.4 Frame span L3 = 300 cm and infill strength G3 = 5.0 MPa (Model M8-L3-G3-D1)

Decoupled response of frame and infill: For the selected representative scaled RC frame model (S=1:2) with span L3 = 300 cm, analysed was the effect of considered AAC infill with strength G3 = 5.0 MPa. Based on the computed nonlinear response of the frame with AAC infill and nonlinear response of non-infilled or only RC frame system, ***the decoupled infill nonlinear response was defined,*** Table 9.9.3***.*** In the same table included are the resulting: (1) Modelling parameters of AAC infill for the scaled model, (2a) Modelling parameters of AAC infill for the respective prototype or real-scale system and (2b) Margins of estimated.

Table 9.9.3. Scaled model M8-L3-G3-D1: Modelling parameters of decoupled AAC infill in frame with L3 = 300 cm, D1 = 125 mm, compressive strength G3 = 5.0 MPa and results for prototype.

1. SCALED MODEL: Modelling parameters (Micro-Modelling Results) SCALED MODEL: M8-L3-G3-D1: (L3 = 300 cm; D1 = 125 mm; G3 = 5.0 MPa)						
MODEL PARAMETERS OF DECOUPLED AAC INFILL						
K0 = 2.0*FM/DM	DY = 0.5*DM	FY = 0.75*FM	DM	FM	DL = 2.5*DM	FL
kN/mm	mm	kN	mm	kN	mm	kN
5.76	2.6	11.25	5.2	15.0	13.0	0.
2a. PROTOTYPE FRAME: Modelling parameters PROTOTYPE: P8-L3-G3-D1: (L3 = 600 cm; D1 = 250 mm; G3 = 5.0 MPa)						
PARAMETERS OF DECOUPLED AAC INFILL						
K0	DY	FY	DM	FM	DL	FL
kN/mm	mm	kN	mm	kN	mm	kN
11.53	5.2	45.0	10.4	60.0	26.0	0.
2b. PROTOTYPE FRAME: Margins of modelling parameters for practical design PROTOTYPE: P8-L3-G3-D1: (L3 = 600 cm; D1 = 250 mm; G3 = 5.0 MPa)						
1. Effective infill height H_0 = 260 cm = 2600 mm 2. Thickness D1 = 25 cm 3. Contact side area: $A_0 = H_0$ (cm) *D1(cm) = 260*25 = 6500 cm^2 4. Max side force: $N_0 = A_0$*G3 = 6500 0.5 = 3,250 kN						
Story drift (‰) (model-**Dr** / H_0)	**2.0**		**4.0**		**10.0**	
H-Force (%) (Model-**F** / N_0		**1.38**		**1.84**		**0.**

9.10 Uniform Methodology Implemented for Evaluation of Infill Nonlinear Response

Systematic evaluation of decoupled response of AAC infill was performed using the adopted uniform methodology created based on observations from the conducted experimental tests and from the generated new results with the conducted extensive parametric studies. Based on computed nonlinear responses of the frame with AAC infill and nonlinear response of non-infilled or only RC frame systems, decoupling of infill nonlinear response was made possible. The used procedure is shown herein for one typical analysed example: Frame with span L1 = 200 cm, infill thickens D1 = 125 mm and infill strength G1 = 2.5 MPa, Fig. 9.10.1.

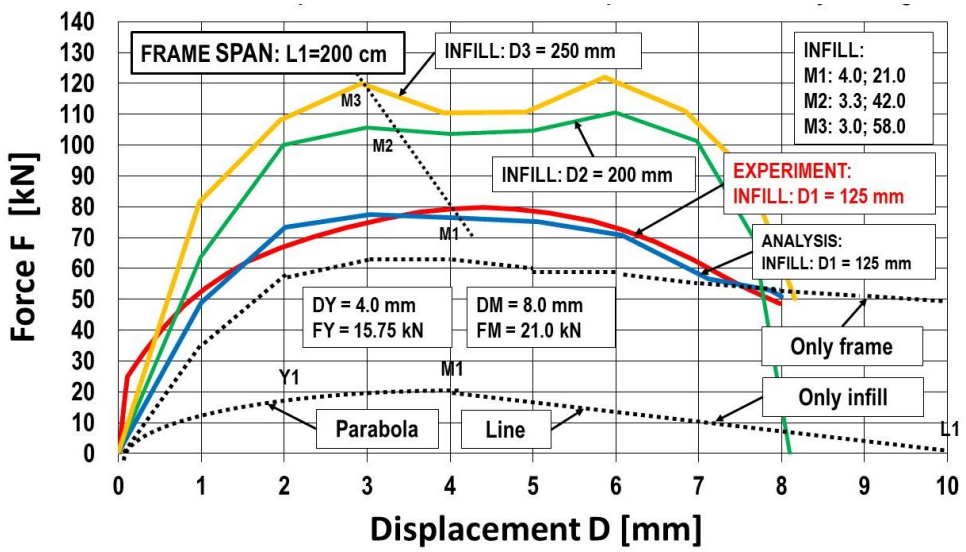

Fig. 9.10.1. Scaled model M1-L1-G1-3D: Computed nonlinear response of AAC infilled frame with span L1 = 200 cm and three infill thicknesses D1, D2 and D3

Firstly, from the computed results, defined is infill M point representing recorded maximum force FM = 21.0 kN and respective relative displacement DM = 4.0 mm. Regarding the observed actual infill responses, in the range of the initial infill relative displacements, smaller than DM, the envelope infill curve was properly represented by second order parabola $y = a\,x^2 + b$, where:

$$a = - FM / DM^2 \quad (1) \quad \text{and} \quad b = 2FM / DM \quad (2)$$

The point Y, representing significant stiffness change was uniformly defined on parabola, considering its representative relative displacement DY = 0.5DM and computed respective force FY = 0.75FM. The initial infill stiffness was represented by parabola tangent slope at zero point, K0 = 2FM / DM. Finally, in the range of relative displacements larger than DM, the infill envelope was uniformly represented by straight line ending at point L with relative displacement DL = 2.5DM and FL = 0.

The required modelling infill parameters for prototypes frames, presented in all related tables, were obtained using similarity low relations for constructed and laboratory tested scaled experimental models. Considering the presented uniform procedure, in respective tables included are the defined resulting data, including: (1) Modelling parameters of AAC infill for the scaled models, (2a) Modelling parameters of AAC infill for the respective prototype or real-scale systems and (2b) Margins of the estimated modelling parameters applicable for the future practical design purposes.

9.11 Discussion of Parametric Results

9.11.1 Influence of Frame Span Length

To evaluate the influence of the frame span length on the global nonlinear behavior of AAC-infilled RC frames, a complete set of models was analyzed across the full parametric matrix. Three span lengths (L = 200, 250, 300 cm) were examined within two primary slices thickness-controlled (fixed G = 2.5 MPa) and strength-controlled (fixed D = 125 mm) as well as a baseline slice including reference infilled and bare frames. All models were subjected to identical boundary conditions, constant vertical load (N = 62.5 kN), and monotonic displacement-controlled lateral loading. This configuration isolates the geometric influence of the span-to-height ratio (L/H) from the effects of infill thickness and material strength. The corresponding force-displacement curves are shown in Figures 9.2.x.

(a) Force-Displacement Response

Increasing the span length reduces initial stiffness and peak strength while increasing ultimate displacement. Short spans (L = 200 cm) are the stiffest and strongest; long spans (L = 300 cm) are more flexible with reduced lateral capacity. This behaviour is consistent for all infill thicknesses and AAC strengths, confirming that L/H is the dominant parameter. Bare frames form the lower-bound envelope, with the advantage of infill diminishing as L increases.

(b) Stiffness

Initial stiffness decreases systematically with increasing span. Thicker and stronger infills increase absolute stiffness but do not change the rate of stiffness reduction with L. Thus, geometry governs stiffness behaviour, while D and G act only as vertical offsets. Earlier stiffness degradation occurs for larger spans, supporting the need for span-dependent stiffness-modification factors.

(c) Strength

Ultimate lateral strength declines as L increases. Short spans mobilize a continuous diagonal strut and achieve higher resistance; longer spans transition to bending-dominated behaviour, reducing infill engagement. Higher infill thickness or strength improves capacity but cannot

compensate for the geometric reduction caused by increasing span. The L/H ratio therefore remains the primary determinant of global capacity.

(d) Ductility

The ductility ratio ($\mu\Delta = Du/Dy$) remains approximately constant across all spans. Longer spans reach larger absolute displacements, but ductility does not increase proportionally. With high-strength infills, post-peak degradation becomes sharper for larger spans. Geometry influences deformation amplitude rather than ductility capacity.

(e) Infill Contribution

Infill participation in resisting lateral load decreases as span increases. At short spans, the infill dominates through diagonal strut action; at intermediate spans, resistance is shared; at long spans, the frame dominates and the infill becomes secondary. Although thicker and stronger infills delay this transition, they cannot prevent it. Infill contribution is therefore strongly geometry-dependent.

(f) Failure Modes

Failure mechanisms follow the geometric progression of L/H.
– Short spans: infill-dominated behavior with diagonal cracking and corner crushing.
–Intermediate spans: mixed infill-frame mechanisms.
– Long spans: frame-dominated response with column flexure, joint rotations, and infill-frame separation.
Higher D and G delay damage but do not alter this transition.

(g) Key Findings

Span length is the most influential geometric parameter, controlling stiffness loss, strength reduction, and the qualitative failure mode. Infill thickness and strength enhance performance but cannot overcome the geometric penalties of large L/H ratios. Ductility remains nearly unaffected by span, while drift demand increases. Infill contribution diminishes with span, and for $L \geq 300$ cm the behavior becomes primarily frame-controlled. Therefore, design enhancements for long spans should focus on the RC frame, while for short-to-medium spans infill strengthening (larger D, higher G) remains effective. Analytical models should incorporate geometry-dependent stiffness and strength modification factors derived from nonlinear simulations.

9.11.2 Influence of AAC Infill Thickness

The influence of AAC infill thickness on the nonlinear behavior of RC frames was examined using analytical models in which all frame properties were kept constant while the infill thickness was varied (D = 125, 200, 250 mm). The AAC strength was fixed at G = 2.5 MPa and the vertical load at N = 62.5 kN. Three spans (L = 200, 250, 300 cm) were analyzed to evaluate the combined effects of thickness and geometry. The results show that increasing wall thickness significantly enhances stiffness and lateral strength for all spans, while ductility remains largely unaffected. Representative force-displacement curves for the 300 cm span are shown in Figure 9.3.1, with similar trends also recorded for the shorter spans.

(a) Force-Displacement Response

Thicker infills generate steeper initial slopes, higher peak forces and delayed stiffness degradation. Thin walls (D = 125 mm) crack earlier and soften faster, whereas 200-250 mm infills maintain their stiffness over a wider displacement range. The thickness-to-span ratio (D/L) governs the effectiveness of the diagonal compression strut; thicker walls improve confinement and load transfer, although the benefit decreases for larger spans due to increased frame flexibility.

(b) Effect on Stiffness

Initial stiffness (K_o) increases with infill thickness across all spans. The effect is strongest for L = 200 cm, noticeable but reduced for L = 250 cm, and becomes limited for L = 300 cm where frame deformations dominate. This shows that the influence of thickness diminishes as span increases, indicating that geometry (L/H) defines the upper limit of stiffness enhancement.

(c) Effect on Strength

Ultimate strength consistently increases with thickness. Short-span frames benefit the most because the diagonal strut is strongly mobilized. For intermediate spans, improvements remain steady but moderate. For long spans, the flexible frame reduces infill engagement, leading to smaller relative strength gains. Thus, the strengthening effect of D is most effective for compact frame geometries.

(d) Effect on Ductility

The ductility ratio ($\mu\Delta$) remains nearly constant for all thicknesses and spans. Although thicker walls improve stiffness and strength, they do not significantly influence the deformation capacity before failure. For D = 250 mm, the post-peak response becomes slightly steeper, indicating mild brittleness, but without major changes in overall ductility.

(e) Enhancement Factors with Thickness

Stiffness and strength increase nonlinearly with thickness. The improvement from D = 125 mm to D = 200 mm is substantial, whereas the gain from D = 200 mm to 250 mm is smaller and begins to approach saturation. Beyond 250 mm, additional thickness provides minimal mechanical benefit while increasing mass, especially in frames with long spans.

(f) Optimal Thickness Range

Considering stiffness, strength, ductility and practical construction limits, the optimal AAC infill thickness lies between 200 mm and 250 mm. Thinner infills (<150 mm) exhibit early cracking and insufficient stiffness, while thicker walls (>250 mm) add weight with little structural benefit. The range D = 200-250 mm therefore represents an efficient compromise for seismic applications.

(g) Key Findings and Design Implications

Infill thickness is a key parameter affecting stiffness and strength, but its influence is geometry-dependent. Increasing D from 125 mm to 250 mm significantly enhances performance, yet the efficiency of this enhancement decreases for long spans where frame flexibility limits the infill contribution. Ductility remains mostly unchanged. For spans up to 250 cm, increasing thickness is effective; for longer spans, attention should shift toward frame detailing rather than further thickening of the infill. These results justify the use of thickness-dependent stiffness and strength modification factors in macro-model calibration.

9.11.3 Influence of AAC Infill Strength

The influence of AAC compressive strength on the nonlinear behavior of RC frames was assessed using analytical models with three strength levels (G = 2.5, 3.75, 5.0 MPa) and three spans (L = 200, 250, 300 cm). All geometric parameters, boundary conditions, and infill thickness (D = 125 mm) were kept constant, while models were analyzed under the same vertical load (N = 62.5 kN) and monotonic lateral displacement. The results show that higher AAC strength increases initial stiffness and peak resistance, while ductility and deformation capacity remain nearly unchanged. Representative force-displacement curves across the three spans confirm that compressive strength influences resistance magnitude but does not modify the overall deformation pattern.

(a) Force-Displacement Response

Increasing AAC strength uniformly shifts the force-displacement curves upward, producing steeper initial slopes, delayed cracking, and higher lateral forces for a given displacement. The deformation shape remains similar, indicating that strength scales capacity rather than altering the global mechanism. The effect is strongest in short spans, moderate in medium spans, and limited in long spans, where frame flexibility restricts infill engagement.

(b) Effect on Stiffness

Initial stiffness (K_o) increases with AAC strength across all spans, with the largest improvement in short frames where confinement is stronger. As span length increases, the stiffness gain diminishes due to frame bending and partial interface separation. This confirms that stiffness enhancement is strength-dependent but controlled primarily by geometry (L/H).

(c) Effect on Peak Load

Peak lateral strength increases consistently with AAC strength. Stronger infills develop more stable diagonal strut action and delayed cracking. The improvement is pronounced for short spans, moderate for medium spans, and small for long spans, where frame flexibility limits the participation of the AAC panel.

(d) Effect on Ductility

The ductility ratio ($\mu\Delta = Du/Dy$) remains nearly constant regardless of AAC strength. While stronger AAC increases load capacity, it does not expand the deformation range before failure. At higher strength levels and longer spans, the post-peak branch becomes slightly steeper, indicating reduced ductility and a more brittle response.

(e) Effect on Energy Dissipation

Energy dissipation increases only modestly with AAC strength. Most of the added energy absorption comes from the elastic phase, while inelastic hysteretic capacity remains limited. For longer spans, the mechanism transitions from infill-driven energy absorption to frame flexure, further reducing the influence of AAC strength on dissipation.

(f) Failure Mode Variations

Failure modes evolve consistently with both span and AAC strength.
– Short spans: diagonal cracking and corner crushing dominate; higher strength intensifies these effects.
– Medium spans: mixed infill and frame damage; stronger AAC delays interface separation.
– Long spans**:** frame-dominated failure, with AAC strength having limited influence.
Thus, AAC strength affects local damage characteristics, while the global mechanism is governed by the L/H ratio.

(g) Key Findings and Design Implications

AAC compressive strength strongly affects stiffness and lateral capacity but has minimal influence on ductility. Its efficiency diminishes with increasing span, as frame flexibility limits infill engagement. Increasing strength beyond 4-5 MPa provides little additional benefit and may promote brittle response, making moderate strength (~3.5 MPa) more appropriate for balanced seismic performance. Recommended design considerations:
- Short spans: high AAC strength (3.5-5.0 MPa) is effective for enhancing resistance.
- Medium spans: moderate strength (~3.5 MPa) provides optimal stiffness-ductility balance.
- Long spans: lower to moderate strength (2.5-3.5 MPa) maintains flexibility and avoids brittle failure.

These findings support the development of strength-dependent stiffness modifiers and reduction factors for macro-model calibration of AAC-infilled RC frame systems.

9.11.4 Comparative analysis and parameter sensitivity

A comparative synthesis of the parametric analyses clearly shows the relative influence of frame span length (L), infill thickness (D), and AAC compressive strength (G) on the nonlinear behavior of RC frames with AAC infills. Among all parameters, the span length (L) governs the response most strongly, since it directly controls frame flexibility, confinement conditions, and the activation of the diagonal strut. Increasing L reduces stiffness and peak strength, while increasing the global deformation capacity. Infill thickness (D) has a substantial positive effect on stiffness and strength, but limited influence on ductility. AAC strength (G) provides moderate improvements to capacity and initial stiffness, with negligible effect on deformation and ductility.

a) Interaction Effects

The efficiency of parameters depends strongly on geometric-material coupling.

– **L-D:** Thicker infills are most effective in short spans; for large L, frame flexibility reduces the benefit of added thickness.

– **L-G:** Higher AAC strength improves capacity only in compact frames; in large spans its influence becomes marginal.

– **D-G:** Combining larger thickness with higher strength increases stiffness but may lead to a slightly more brittle post-peak response.

b) Dominant vs. Secondary Response Quantities

Stiffness (K_0), peak strength (Fm), yield displacement (Dy), ductility ratio ($\mu\Delta$), and ultimate displacement (Du) represent the dominant performance parameters. Secondary indicators—energy dissipation, stiffness degradation rate, post-peak slope and failure patterns—affect qualitative response trends but do not control the primary stiffness-strength relationship.

c) Summary of Parameter Sensitivity

Span length is the primary driver of global behavior, reducing stiffness and strength significantly as L/H increases. Infill thickness improves stiffness and strength effectively up to $D \approx 200\text{-}250$ mm; beyond this range benefits plateau. AAC strength contributes moderately up to $G \approx 3.5\text{-}4.0$ MPa, with limited improvement beyond this level. Overall ductility remains approximately constant across parameter variations, confirming that geometry dominates the deformation capacity while material variations chiefly scale strength and stiffness.

Table 9.11.1 Comparative influence of L, D, and G on the global response of AAC-infilled RC frames

Parameter	Primary Effect on Global Behaviour	Relative Influence	Interaction Sensitivity	Key Design Implications
Frame Span (L)	↑L → large reduction in stiffness and peak load; higher flexibility and drift	**Dominant**	Strong L-D & L-G coupling; geometry controls efficiency of D and G	Control L/H ratio; short spans allow full infill participation
Infill Thickness (D)	↑D → higher stiffness and lateral strength; minimal effect on ductility	**Secondary-Dominant**	Strong dependence on span (L); effect reduces in long spans	Optimal range D = 200-250 mm for stiffness-weight balance
AAC Strength (G)	↑G → moderate increase in capacity and initial stiffness; small ductility changes	**Secondary**	Moderate coupling with L and D; strong effect only in short spans	G ≈ 3.5-4.0 MPa preferred; >4.5 MPa gives diminishing returns
Combined L-D-G Effect	Defines global stiffness-strength envelope and failure mode	—	Highly nonlinear, geometry-controlled	Balanced configuration needed to achieve efficient and ductile seismic response

In Table 9.11.1, the comparative influence of the main parameters frames spans length (L), infill thickness (D), and AAC compressive strength (G) is summarized.

9.12 Practical procedure for defining modelling parameters of decoupled AAC Infill

Presented in the preceding sub-chapters of Chapter 9 is the methodological concept of defining nonlinear macro-modelling parameters, provided that two basic parameters are previously defined: (1) The maximum restoring force FM of the decoupled AAC masonry infill and (2) The relative displacement DM of point M representing the maximum restoring force. The values of these two basic parameters were accurately defined based on the results from the parametric analyses performed by application of the experimentally verified nonlinear micro-models.

Within its frames, sub-chapter 9.10 presents the new direct, consistent and practically applicable procedure for successful definition of a complete set of nonlinear macro-modelling parameters of a decoupled AAC infill for specified different frame span lengths of existing real buildings.

The formulated consistent procedure was formulated based on the results from the performed parametric analyses. The series of parametric analyses were conducted using the experimentally verified nonlinear micro-models. To obtain reliable results for the main parameters for a large number of representative cases of frame structures, the analyses were carried out by varying three representative parameters, namely: (1) Analysis of representative frames with variable spans between the columns; (2) Analysis of representative frames with variable thickness of the AAC infill and (3) Analysis of representative frames with variable compressive strength of the AAC masonry infill. From the conducted study, the two main parameters DM and FM were "accurately" defined for each analyzed model scaled to a large-scale M = 1: 2. Using the adopted parabolic approximation, the location of the characteristic point Y was defined. Consequently, the calculation of the needed three parameters DY, FY and K0 was enabled. The representative point L from the envelope of the decoupled AAC masonry infill was approximated based on the results recorded from the performed experimental tests.

Applying the existing valid criteria of similarity between the models and the prototype frames, in the second phase, all the parameters defined for the analyzed scaled models were directly transferred into corresponding "accurate" parameters for the corresponding prototype frame structures, Table 9.12.1. The table clearly shows that the related study included realized two series of nine analyses (18 in total), considering the identical changes of spans.

In the first series of performed nine analyses with different spans (L1, L2, L3), the representative change of thickness of the AAC infill (D1, D2, D3) was included. However, during all analyses, the infill strength parameter was kept identical (G1) in order to enable a representative set of the main parameters DM and FM for all analyzed spans L1, L2 and L3 of the prototype frame structures, Fig. 9.12.1 and Fig. 9.12.2.

Table 9.12.1. Modelling parameters of decoupled AAC infill defined for analysed prototype frames

No.	Prototype frame	Frame span L(cm)	Infill thickness D (mm)	Infill strength G (MPa)
1	L1-D1-G1	400	250	2.5
2	L1-D2-G1	400	400	2.5
3	L1-D3-G1	400	500	2.5
4	L2-D1-G1	500	250	2.5
5	L2-D2-G1	500	400	2.5
6	L2-D3-G1	500	500	2.5
7	L3-D1-G1	600	250	2.5
8	L3-D2-G1	600	400	2.5
9	L3-D3-G1	600	500	2.5
10	L1-D1-G1	400	250	2.5
11	L1-D1-G2	400	250	3.75
12	L1-D1-G3	400	250	5.0
13	L2-D1-G1	500	250	2.5
14	L2-D1-G2	500	250	3.75
15	L2-D1-G3	500	250	5.0
16	L3-D1-G1	600	250	2.5
17	L3-D1-G2	600	250	3.75
18	L3-D1-G3	600	250	5.0

In the second series of nine analyses with different spans (L1, L2, L3), the representative change of the AAC infill strength (G1, G2, G3) was included. Analogously, during all the analyses, the AAC infill thickness parameter was kept identical (D1) in order to enable the obtaining of a representative set of the main parameters DM and FM for all analyzed spans L1, L2 and L3 of the prototype frame structures, Fig. 9.12.3 and Fig. 9.12.4.

The presented Fig. 9.12.1 shows the computed specific values of the maximum FM of the decoupled AAC infill with different thickness, but with considered specified distinct dimensions of spans L1, L2 and L3.

Analogously, Fig. 9.12.2 shows the computed corresponding values of the relative displacements DM of the decoupled AAC infill with different thickness for the same three distinctly specified values spans L1, L2 and L3.

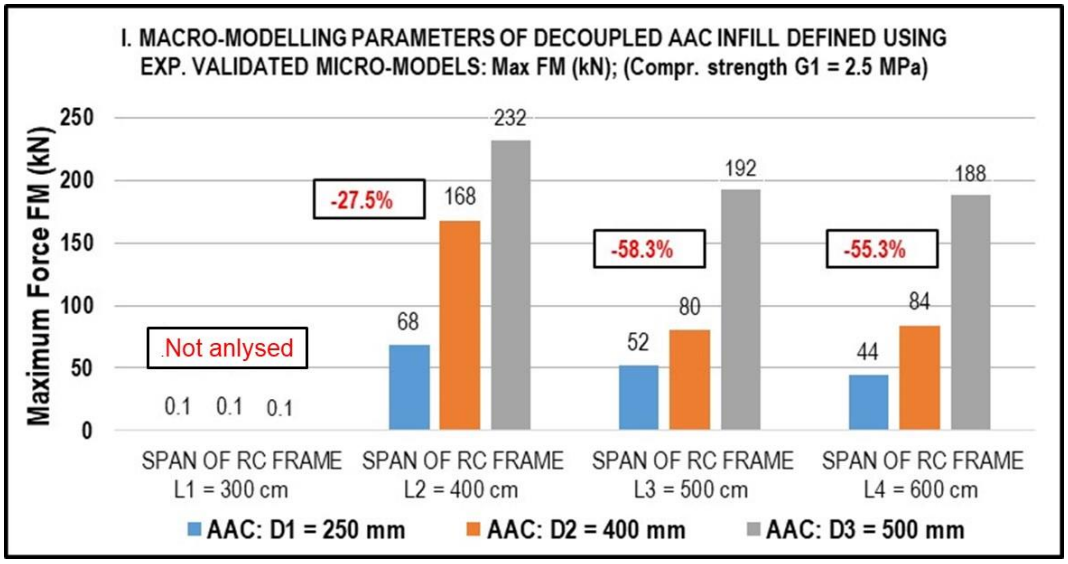

Fig. 9.12.1. Maximum forces FM of decoupled AAC infill with different thickness

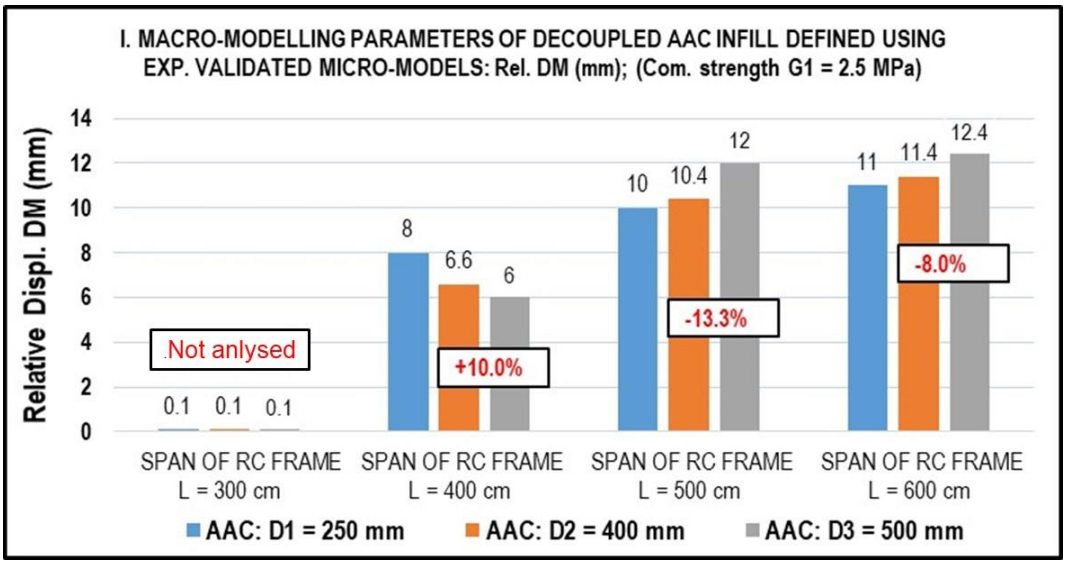

Fig. 9.12.2. Relative displacement DM of decoupled AAC infill with different thickness

Table 9.12.1. Practical procedure and formulas for defining macro-modelling parameters of decoupled AAC infill in RC frames with spans L = 400 - 600 cm (D1 = 250 mm and G1 = 2.5 MPa)

CALCULATION OF NONLINEAR MACRO-MODELLING PARAMETERS OF DECOUPLED AAC INFILL IN RC FRAMES (Infill thickness D1 = 250 mm & Strength G1 = 2.5 MPA)	
Calculation form-1	
Frames with spans L = 400 - 500 cm	**Frames with spans L = 500 - 600 cm**
Point-M:	Point-M:
FM (kN) = - 0.16 L (cm) + 132	FM (kN) = - 0.08 L (cm) + 92
DM (mm) = 0.02 L (cm)	DM (mm) = 0.01 L (cm) + 5
Point-Y: DY = 0.5*DM and FY = 0.75*FM	
Point-L: DL = 2.5*DM and FL = 0.	
Initial stiffness: K0 (kN/mm) = 2.0*FM / DM	

Table 9.12.2. Practical procedure and formulas for defining macro-modelling parameters of decoupled AAC infill in RC frames with spans L = 400 - 600 cm (D2 = 400 mm and G1 = 2.5 MPa)

CALCULATION OF NONLINEAR MACRO-MODELLING PARAMETERS OF DECOUPLED AAC INFILL IN RC FRAMES (Infill thickness D2 = 400 mm & Strength G1 = 2.5 MPA)	
Calculation form-2	
Frames with spans L = 400 - 500 cm	**Frames with spans L = 500 - 600 cm**
Point-M:	Point-M:
FM (kN) = - 0.88 L (cm) + 520	FM (kN) = 0.04 L (cm) + 64
DM (mm) = 0.038 L (cm) – 8.6	DM (mm) = 0.01 L (cm) + 5.4
Point-Y: DY = 0.5*DM and FY = 0.75*FM	
Point-L: DL = 2.5*DM and FL = 0.	
Initial stiffness: K0 (kN/mm) = 2.0*FM / DM	

Table 9.12.3. Practical procedure and formulas for defining macro-modelling parameters of decoupled AAC infill in RC frames with spans L = 400 - 600 cm (D3 = 500 mm and G1 = 2.5 MPa)

CALCULATION OF NONLINEAR MACRO-MODELLING PARAMETERS OF DECOUPLED AAC INFILL IN RC FRAMES (Infill thickness D3 = 500 mm & Strength G1 = 2.5 MPA)	
Calculation form-3	
Frames with spans L = 400 - 500 cm	**Frames with spans L = 500 - 600 cm**
Point-M:	Point-M:
FM (kN) = - 0.4 L (cm) + 392	FM (kN) = - 0.04 L (cm) + 212
DM (mm) = 0.06 L (cm) - 18	DM (mm) = 0.004 L (cm) + 10
Point-Y: DY = 0.5*DM and FY = 0.75*FM	
Point-L: DL = 2.5*DM and FL = 0.	
Initial stiffness: K0 (kN/mm) = 2.0*FM / DM	

Considering the evident need for and importance of extending the practical application of these results that will enable definition of the main modelling parameters FM and DM for spans in the range of L = 400 - 600 cm, corresponding accurate interpolation formulas were defined for all sub-span cases. In this way, successful definition of all necessary macro-modelling parameters was enabled for all spans in the domain as well as for all different thicknesses of the AAC masonry infill. For consistent practical use of the procedure for computation of parameters of the nonlinear macro-models, prepared are three related calculation forms.

Table 9.12.1 shows calculation form - 1 that enables definition of the parameters of the macro-models for all spans and for the specified thickness of the AAC infill of D1 = 250 mm. Analogously, tables 9.12.2 and 9.12.3 show the calculation form - 2 and calculation form - 3 that enable calculation of parameters of macro-models for all spans and for the specified thickness of the AAC infill of D2 = 400 mm and D3 = 500 mm, respectively.

Similarly, the results from the parametric analyses that refer to parameters FM and DM defined for different values of compressive strength of the AAC infill, G1 = 2.5 MPa, G2 = 3.75 MPa and G3 = 5.0 MPa, are shown in Fig. 9.10.3 and Fig. 9.10.4, respectively.

Derived based on used the same interpolation procedure, in Table 9.12.4 presented is calculation form - 4 that enables calculation of all the parameters of the macro-models for all spans and an AAC infill with a compressive strength of G1 = 2.5 MPa. Consequently, in Table 9.12.5 and Table 9.12.6 shown are calculation form - 5 and calculation form - 6, that enable calculation of related parameters of nonlinear macro-models for all spans and for a corresponding value of compressive strength of the AAC infill of G2 = 3.75 MPa and G3 = 5.0 MPa, respectively.

Finally, in the last Table 9.12.7, presented is one typical example of implementation of the procedure for calculation of the macro-modelling parameters of the decoupled AAC infill of an RC frame with a span of L = 550 cm, D1 = 250 mm and G1 = 2.5 MPa. Considering the achieved success in the presented example, the great practical applicability of the developed calculation procedure was clearly demonstrated.

Actually, the presented procedure can be widely applied to calculate full set of necessary parameters of nonlinear macro-models of a decoupled AAC infill including, different RC frame spans, common AAC infill thicknesses and different compressive AAC infill strengths.

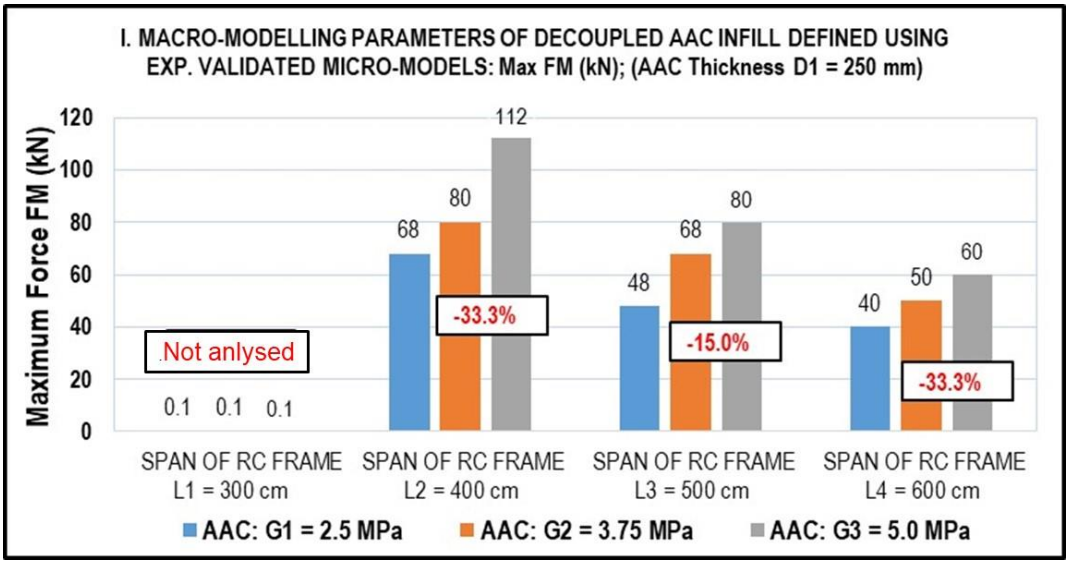

Fig. 9.12.3. Maximum forces FM of decoupled AAC infill with different strength

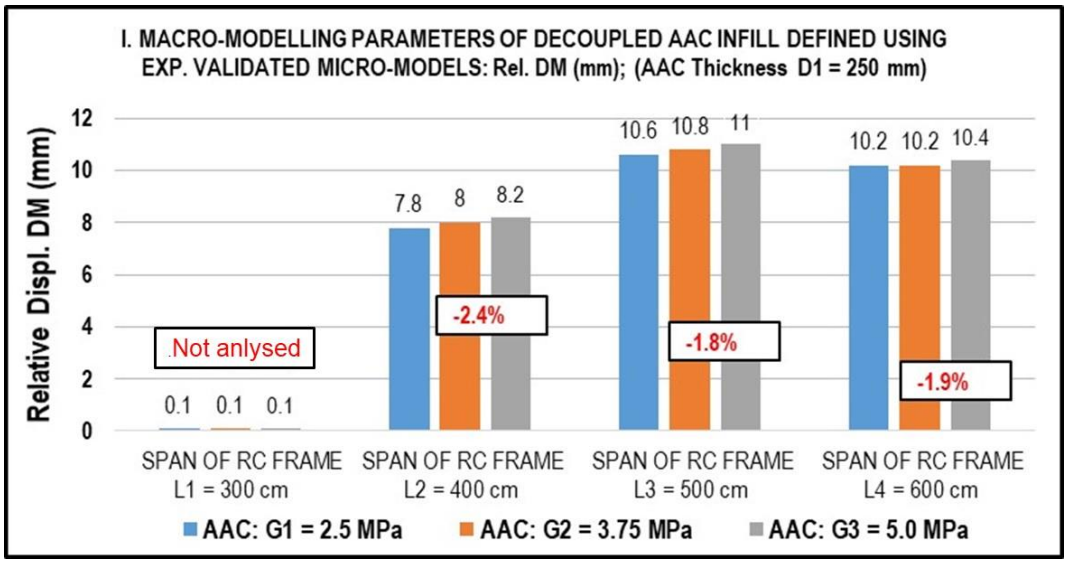

Fig. 9.12.4. Relative displacement DM of decoupled AAC infill with different strength

Table 9.12.4. Practical procedure and formulas for defining macro-modelling parameters of decoupled AAC infill in RC frames with spans L = 400 - 600 cm (D1 = 250 mm and G1 = 2.5 MPa)

CALCULATION OF NONLINEAR MACRO-MODELLING PARAMETERS OF DECOUPLED AAC INFILL IN RC FRAMES (Infill thickness D1 = 250 mm & Strength G1 = 2.5 MPA)	
Calculation form-4	
Frames with spans L = 400 - 500 cm	**Frames with spans L = 500 - 600 cm**
Point-M:	Point-M:
FM (kN) = - 0.2 L (cm) + 148	FM (kN) = - 0.08 L (cm) + 88
DM (mm) = 0.028 L (cm) – 3.4	DM (mm) = - 0.004 L (cm) + 12.6
Point-Y: DY = 0.5*DM and FY = 0.75*FM	
Point-L: DL = 2.5*DM and FL = 0.	
Initial stiffness: K0 (kN/mm) = 2.0*FM / DM	

Table 9.12.5. Practical procedure and formulas for defining macro-modelling parameters of decoupled AAC infill in RC frames with spans L = 400 - 600 cm (D1 = 250 mm and G2 = 3.75 MPa)

CALCULATION OF NONLINEAR MACRO-MODELLING PARAMETERS OF DECOUPLED AAC INFILL IN RC FRAMES (Infill thickness D1 = 250 mm & Strength G2 = 3.75 MPA)	
Calculation form-5	
Frames with spans L = 400 - 500 cm	**Frames with spans L = 500 - 600 cm**
Point-M:	Point-M:
FM (kN) = - 0.12 L (cm) + 128	FM (kN) = - 0.18 L (cm) + 158
DM (mm) = - 0.028 L (cm) – 3.2	DM (mm) = - 0.006 L (cm) + 13.8
Point-Y: DY = 0.5*DM and FY = 0.75*FM	
Point-L: DL = 2.5*DM and FL = 0.	
Initial stiffness: K0 (kN/mm) = 2.0*FM / DM	

Table 9.12.6. Practical procedure and formulas for defining macro-modelling parameters of decoupled AAC infill in RC frames with spans L = 400 - 600 cm (D1 = 250 mm and G3 = 5.0 MPa)

CALCULATION OF NONLINEAR MACRO-MODELLING PARAMETERS OF DECOUPLED AAC INFILL IN RC FRAMES (Infill thickness D1 = 250 mm & Strength G3 = 5.0 MPA)	
Calculation form-6	
Frames with spans L = 400 - 500 cm	**Frames with spans L = 500 - 600 cm**
Point-M:	Point-M:
FM (kN) = - 0.32 L (cm) + 240	FM (kN) = - 0.2 L (cm) + 180
DM (mm) = 0.028 L (cm) - 3	DM (mm) = - 0.006 L (cm) + 14
Point-Y: DY = 0.5*DM and FY = 0.75*FM	
Point-L: DL = 2.5*DM and FL = 0.	
Initial stiffness: K0 (kN/mm) = 2.0*FM / DM	

Table 9.12.7. Example of practical procedure for defining of macro-modelling parameters of decoupled AAC infill of RC frame with spans **L = 550 cm** (D1 = 250 mm and G1 = 2.5 MPa)

Use appropriate calculation form-1 to calculate macro-modelling parameters of decoupled AAC infill of RC frame with L = 550 cm; Infill thickness D1 = 250 mm & Strength G1 = 2.5 MPa	
Calculation form-1: L = 550 cm	
Frames with spans L = 400 - 500 cm	**Frames with spans L = 500 - 600 cm**
Point-M:	**Point-M:**
FM (kN) = - 0.16 L (cm) + 132	FM = - 0.08 x 550 + 92 = 48 kN
DM (mm) = 0.02 L (cm)	DM = 0.01 x 550 + 5 = 10.5 mm
Point-Y: DY = 0.5*DM = 0.5 x 10.5 = 5.25 mm; FY = 0.75*FM =0.75 x 48 = 36 kN	
Point-L: DL = 2.5*DM = 26.25 mm; FL = 0.	
Initial stiffness: K0 (kN/mm) = 2.0*FM / DM = 2 x 48 / 10.5 = 9.143 kN / mm	

9.13 Concluding Remarks

The extensive analytical parametric study conducted within this research can be regarded as highly successful “analytical experiments”, since the adopted analytical micro-models were comprehensively verified through direct comparison with the results obtained from experimental testing. The excellent agreement between analytical predictions and experimental measurements confirms the validity and robustness of the adopted modelling approach.

By following a unified data processing methodology, several key modelling parameters were systematically defined and summarized in dedicated tables, including:
(1) modelling parameters of AAC infill for the scaled laboratory models;
(2a) corresponding parameters for the prototype or real-scale RC frame-infill systems; and
(2b) indicative ranges of the estimated parameters that can be used as reference values for future analytical and design applications.

Based on the results of the verified analytical study, a consistent and practical concept for deriving nonlinear macro-modelling parameters for decoupled AAC infills was successfully established. The developed macro-model formulation enables the reliable representation of the nonlinear force-displacement relationship and stiffness degradation pattern of AAC-infilled RC frames under seismic loading.

The formulated macro-models represent a significant step forward, as they provide a solid analytical basis for simplified yet accurate modelling in engineering practice. They allow broad applicability for seismic assessment and design of RC frames with AAC masonry infill, ensuring that the complex interaction mechanisms captured through micro-modelling can be efficiently transferred into macro-modelling schemes suitable for performance-based seismic design.

Furthermore, the results obtained from this comprehensive research contribute to a deeper understanding of the mechanical behavior, interaction mechanisms, and sensitivity of key parameters governing AAC-infilled RC frames. This knowledge provides valuable guidance for developing design recommendations, calibrating analytical tools, and improving the reliability of seismic performance evaluations of AAC-based structural systems.

10 CHAPTER 10 - DEVELOPMENT OF PRACTICAL FE MODEL FOR STRUCTURAL ANALYSIS OF RC FRAMES WITH AAC INFILL

10.1 Objective of the Seismic Response Study of RC Frame with AAC Infill

Presented and defined in Chapter 9 were the main parameters that enable formulation of individual macro-models for simulation of the nonlinear behavior of both the elements of the RC frame structure and the AAC infill. The main parameters of the macro models were defined based on the performed parametric analyses of the representative frame by application of experimentally verified models. The performed parametric study provided an insight into the high complexity of application of micro-models. From these reasons, the following conclusions are drawn:

(1) The application of micro-models in simulation of the nonlinear behavior of RC frames with AAC infill has a great importance for detailed study of the nonlinear behavior by successful detection of occurrence of nonlinear phenomena at "local" level. However, the application of micro-models for practical design needs is very complex and cannot be recommended for modelling of AAC structures.

(2) To enable analysis of the nonlinear behavior of reinforced concrete frame with AAC infill, it is necessary to formulate corresponding nonlinear "macro-models" that enable simulation of the nonlinear characteristics at the level of a storey of the RC frame.

(3) Due to the need for exploring the characteristics of the nonlinear behavior of the bearing reinforced concrete elements and non-bearing masonry consisting of AAC elements, the need for formulation of individual corresponding macro-models for both components was imposed.

(4) The main objective of the performed study presented in this chapter was to define a practical concept of a new phenomenological nonlinear macro-model that will enable formulation of nonlinear models of buildings that represent systems formed of standard RC frames as structural elements and masonry infill consisting of AAC elements in the form of nonstructural elements.

The practical relevance and capability of the developed concept were demonstrated through a two-phase analysis process. In the first phase, a model was developed and calibrated based on experimental data, with the objective of ensuring a high level of consistency between the theoretical behavior and the experimentally observed response. This model served as the foundation for the formulation and verification of a phenomenological macro-model, capable of realistically but efficiently representing the nonlinear interaction between the reinforced concrete (RC) frame and the AAC infill. In the second phase, the developed macro-model was applied in a case study involving a five-storey RC frame structure with AAC infill, to analyze the seismic response of the building as an integral system. The results obtained confirm that the developed concept has a high potential for practical application, offering a reliable balance

between the necessary engineering detail and the simplicity required for modeling multi-storey structures.

The proposed macro-model is applicable to low and mid-rise reinforced concrete frame structures with nonstructural AAC infill walls, where global inelastic behavior is primarily governed by flexural response of frame members and diagonal compression failure of infill panels. The model is suitable for nonlinear static (pushover) and dynamic analyses, allowing efficient prediction of global capacity, stiffness degradation, and interaction effects between the RC frame and AAC infill. It can be implemented within standard engineering software environments to support both performance-based design and seismic vulnerability assessment of buildings incorporating AAC masonry infills.

10.2 Phenomenological Nonlinear Model M2-A RC Frame with AAC Infill

10.2.1 Concept of Phenomenological Model-M1 of AAC Infilled RC Frame

The analytical nonlinear phenomenological model formulated for the M1 frame with AAC infill, considered in this study as representative, is shown in Fig. 10.2.1. In this conceptual representation, the beams are modeled as rigid elements, while the columns are represented by nonlinear link elements that reproduce their nonlinear behavior. The AAC infill is represented by a central nonlinear link element, which is connected to the surrounding frame through rigid diagonal elements that ensure the transfer of loads to the link without introducing additional deformation. This configuration provides a simplified yet realistic representation of the interaction between the frame and the infill, as well as the global nonlinear behavior of the system. The proposed model was developed and verified in SAP2000 [63], but it can be implemented in any structural analysis software that supports link elements for simulating the nonlinear behavior of materials.

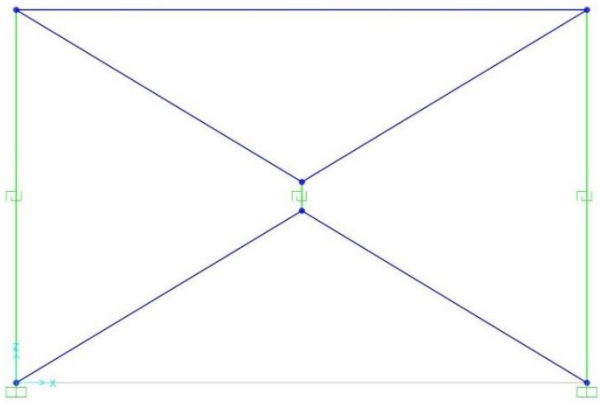

Fig. 10.2.1. Model-M1: Proposed phenomenological nonlinear model of RC frame with AAC infill (AACF-Model)

10.2.2 Modelling of Reinforced Concrete Columns (Model M1)

In the M1 model, the nonlinear behavior of the reinforced concrete columns was represented using nonlinear link elements governed by the Takeda hysteretic model. This model was selected because it can closely reproduce the degradation of stiffness and the pinching effects that typically occur in reinforced concrete members under cyclic seismic loading. It describes the cyclic moment-rotation relationship through an envelope that includes yielding, post-yield stiffness, and reloading branches that degrade progressively with increasing deformation.

The model parameters, such as the yield and ultimate rotations, the initial stiffness, the ratio of post-yield stiffness, and the degradation factor of unloading stiffness, were calibrated based on the experimental results of the tested frame to ensure close agreement between the simulated and measured hysteretic response. The hysteretic rules adopted in this study follow the classical formulation proposed by Takeda, Sozen, and Nielsen (1970) [62], which accurately captures the stiffness degradation, energy dissipation, and strength deterioration observed in reinforced concrete members during cyclic loading. This approach allowed a reliable simulation of the cyclic behavior of the RC columns in the M2A model, maintaining consistency with the experimentally observed nonlinear response.

Tab. 10.2.1. Model parameters of nonlinear links representing RC columns

DY (m)	FY (kN)	DU (m)	FU (kN)	DL (m)	FL (kN)
0.0003	2 × 17.5	0.002	2 × 28	0.004	2 ×30.75

The displacement and force parameters were used to define the corresponding envelope relationship with three characteristic points marked as Y, U, and L. Point Y, defined by DY and FY, represents the yielding point; point U, defined by DU and FU, corresponds to the maximum resisting force; while point L, defined by DL and FL, enables the closely representation of the post-peak branch of the envelope curve.

The representative values of deformations (DY, DU, DL) and the corresponding resistance forces (FY, FU, FL) were determined based on the results of the parametric analyses (Chapter 9) of the representative frame cases previously developed and verified through detailed nonlinear micro-modelling. The numerical values shown in Table 10.2.1 were directly read from the reference case, which provided the calibrated relationship between deformation capacities and resistance forces. In this way, the adopted parameters ensure full consistency between the simplified nonlinear link representation and the experimentally verified response of the RC columns.

10.2.3 Modelling of AAC Infill (Model M2)

The nonlinear behavior of the AAC infill wall was simulated using nonlinear link elements defined based on the experimentally obtained force-displacement relationship. The model reproduces the ascending branch up to the maximum strength point, while the post-peak part of the curve was intentionally excluded to prevent numerical instability during nonlinear analysis. The modelling parameters of the nonlinear links representing the AAC infill are presented in Table 10.2.2. These parameters, defining the characteristic deformation and strength points (DY, FY, DU, FU), were determined according to the formulations and parametric relations developed and verified in Chapter 9. The defined nonlinear response envelope accurately represents the experimental behavior of the AAC infill up to point U, which corresponds to the real maximum restoring force FU and the associated displacement DU. The descending branch of the curve was not implemented in the analytical model because, in the applied software, specific nonlinear link properties for capturing softening behavior are not directly available, and their inclusion could lead to convergence and stability issues. Nevertheless, the adopted definition of the nonlinear envelope ensures full consistency with the experimentally observed behavior within the stable range of response.

Tab. 10.2.2. Model parameters of used nonlinear links representing AAC infill

DY (m)	FY (kN)	DU (m)	FU (kN)	DL (m)	FL (kN)
0.002	15.75	0.004	21	0.01	21

Figure 10.2.2 presents the comparison between the experimental results and the nonlinear macro-model developed for the tested RC frame with AAC infill (Model M2). The macro-model was developed through a pushover analysis, providing a simplified representation of the nonlinear behavior of the frame.

A certain discrepancy is observed in the initial elastic range, where the numerical model exhibits slightly higher stiffness compared to the experimental curve. This difference mainly results from the idealized boundary conditions and material parameters used in the numerical simulation, where perfect contact was assumed between the RC frame and the AAC infill. In the experimental test, the initial stiffness was reduced due to local cracking, micro-defects within the AAC elements, and partial separation between the frame and infill, which are not fully captured in the analytical model. However, this discrepancy affects only the early elastic response and does not influence overall nonlinear behavior.

In the subsequent nonlinear phase, a good correlation is observed between the model and the experiment in terms of ultimate strength and post-peak response, confirming that the proposed macro-model provides a reliable representation of the global behavior of the AAC-infilled system.

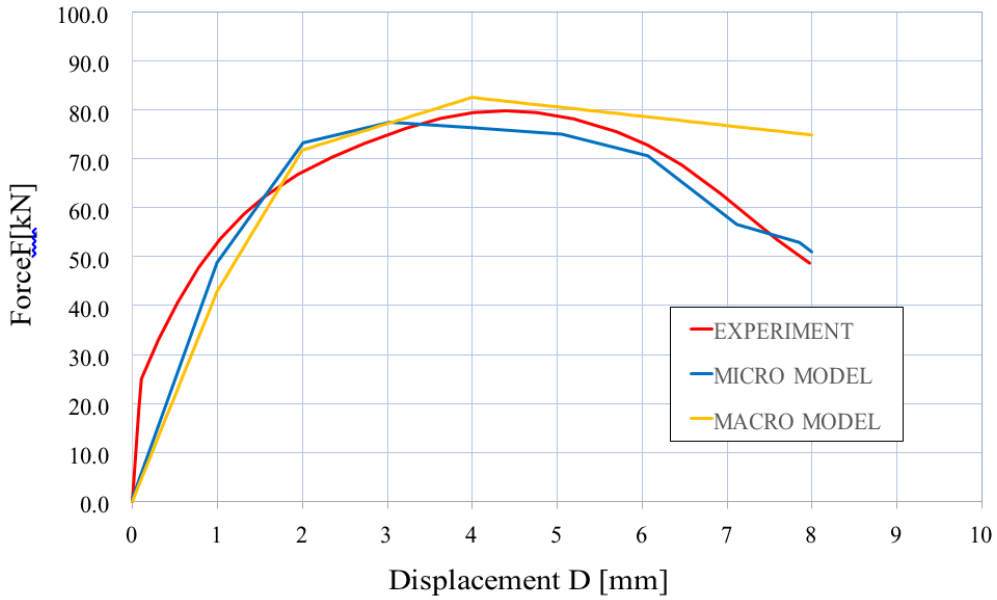

Figure 10.2.2. Experimental verification of the macro-model for the RC frame with AAC infill (Model - M1)

The basic concept of the formulated macro-nonlinear analytical model of an AAC infilled frame (AACF Model) was proposed for practical purposes following the widely applied shear-type multi-frame building modelling concept. The proposed AACF nonlinear macro frame model possesses several advantages as follows:

(1) It enables a closely simulation of the nonlinear behavior of the structural elements of the RC frame as well as the masonry infill in the form of AAC units.
(2) The frame structure can be modelled with different levels of refinement, starting from micro to macro level, which is a great advantage in realization of the numerous necessary nonlinear analyses for practical needs;
(3) The nonlinear behavior of the AAC infill masonry can be very successfully simulated with adequate macro-models with predefined main parameters based on conducted complex experimental tests or parametric analyses realized with experimentally verified nonlinear models;
(4) With the adopted diagonal rigid elements created are two stiff triangular shapes. Since their central points do not touch (remain at small vertical distance), conditions for application of the suitable macro-model for simulation of the nonlinear behavior of the AAC infilled masonry by nonlinear link elements were created;
(5) Great advantages were created with the provided modelling of the AAC masonry infill with link elements. Wide opportunity was created for modelling of the infill with diverse types of analytical models that are the most realistic for the corresponding nonlinear link elements. The parameters of the nonlinear link elements can be successfully defined by experimentally verified nonlinear micro-models, as confirmed with the presently realized extensive parametric studies.
(6) With the application of the created AACF model, the large opportunities for simulation of the nonlinear behavior of the AAC infill of different complexity are provided. A

particularly important advantage is achieved with the created conditions for simulation of the nonlinear behavior of the infill with different topologies of openings for doors and windows, different thickness of the walls, different spans, different strength and deformability of the infill as well as in the case of asymmetry of the hysteretic relationships for cyclic deformations in positive and negative direction.

(7) The proposed AACF nonlinear macro-model enables its practical use for modelling of the nonlinear seismic behavior of building structures that are designed with RC frame structures and with infill composed of complex masonry consisting of AAC elements that are characterized by different geometry, different mechanical characteristics and different topology of openings.

The advantages of the proposed AACF nonlinear macro-model for realization of the specific study of the seismic response of actual structures are presented through the analyzed representative individual RC frame with AAC infill as a part of the real five storey building.

10.3 Phenomenological Nonlinear Model of Five Storey RC Frame with AAC Infill

10.3.1 Concept of Phenomenological Model-M2 of AAC Infilled RC Frame

The formulated analytical nonlinear phenomenological model of the five-storey RC frame with AAC infill considered in this study as representative is shown in Fig. 10.3.1.

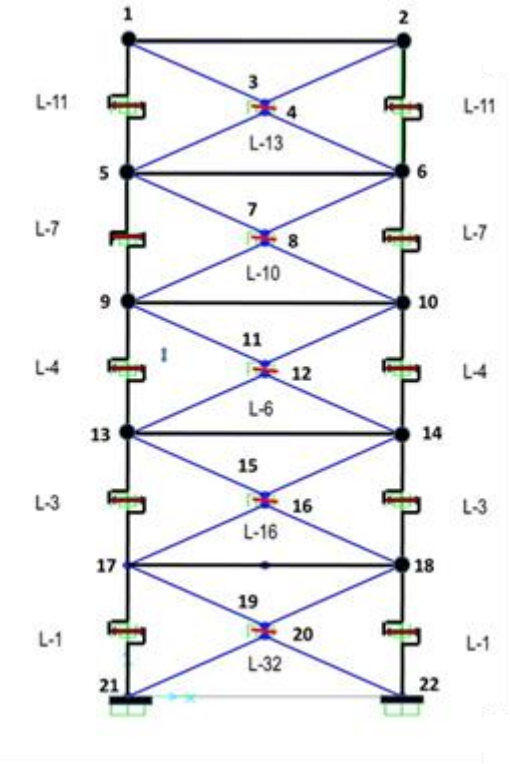

Fig. 10.3.1. Model-M2: Formulated phenomenological nonlinear model of five storey RC frame with AAC infill (AACF-Model)

The considered RC frame represents part of a real building. The reinforced concrete columns are with the same cross-section 50 x 50 cm, whereas, at all storeys, the masonry is constructed of AAC elements with thickness of 250 mm. The reinforced concrete beams are modeled, in this case, as rigid elements, whereas the storey height is adopted identical and amounts to 300 cm. The span between the floor beams, the distance between the columns, is adopted identical in both directions, amounting to 400 cm. The beam was modeled as a rigid element because its effects were already indirectly included in the experimental force-displacement (F-D) results used for model calibration. The corresponding effective masses concentrated at the nodal points were computed based on the actual dimensions of the floor structure.

10.3.2 Representative Discrete Masses

In the formulated nonlinear AACF analytical model presented in Figure 10.2.1, the corresponding storey masses are defined at two discrete nodal points of each storey, representing the left and right column joints. This approach allows the total floor mass to be

distributed symmetrically, ensuring dynamic equivalence with the real structure. The values of the effective masses are presented in Table 10.3.1.

The calculation of these masses was based on the actual geometry and self-weight of the floor structure. For a bay with dimensions of 4.0 × 4.0 m, the self-weight of the slab, the contribution of beams, finishing layers, and the live load were all considered. Based on these components, the total effective load per bay was determined to be approximately 224 kN.

This load represents the total gravity load carried by the two columns at each storey level and is equally distributed to their top joints, resulting in 2 × 112 kN per storey. The corresponding effective masses were derived from these loads and directly implemented in the analytical model to ensure that the dynamic characteristics of the system are consistent with those of the experimental prototype.

Tab. 10.3.1. Considered weights (masses) at storey left and right discrete joints

Storey	Weight (kN)	Mass (t)
1	2 x 112	2 x 11.42
2	2 x 112	2 x 11.42
3	2 x 112	2 x 11.42
4	2 x 112	2 x 11.42
5	2 x 112	2 x 11.42
Total	1120	114.2

10.3.3 Modelling of RC Columns

At each frame storey, the nonlinear behavior of both RC columns was simulated with the corresponding nonlinear link elements. The nonlinear hysteretic relationship of both RC columns was simulated separately with adopted the widely used Takeda model. For each link element, the respective Takeda model was defined using six input parameters, Table 10.3.2.

Tab. 10.3.2. Model parameters of nonlinear links representing RC storey columns

Storey	DY (m)	FY (kN)	DU (m)	FU (kN)	DL (m)	FL (kN)
1	0.0036	2 x 72	0.0202	2 x 110	0.0396	2 x 112
2	0.0036	2 x 72	0.0202	2 x 105	0.0396	2 x 107
3	0.0036	72 x 2	0.0202	2 x 100	0.0396	2 x 102
4	0.0036	2 x 72	0.0202	2 x 95	0.0396	2 x 97
5	0.0036	2 x 72	0.0202	2 x 90	0.0396	2 x 92

The shear force-displacement relationships obtained for each storey, based on the parameters presented in Table 10.3.2, are shown in Figure 10.3.2. The diagram illustrates the nonlinear response of the RC storey columns represented by the calibrated link elements.

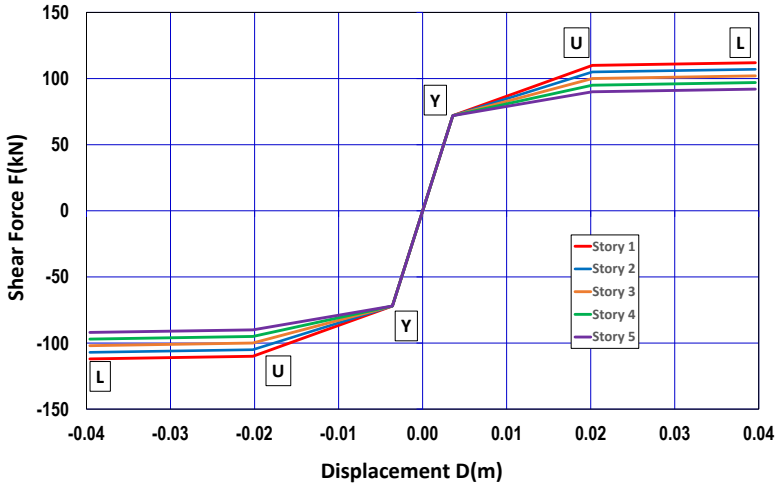

Figure 10.3.2. Force-displacement (F-D) relationship of RC storey columns for the analytical model.

The displacement and force parameters were used to define the corresponding envelope relationship with three characteristic points marked as Y, U and L. Point Y defined by DY and FY refers to the yielding point, point U defined by DU and FU refers to the value of the maximum resisting force, while point L defined by DL and FL enables modelling of the second slope of the envelope line. The representative values of deformations DY, DU and DL and the corresponding resistance forces FY, FU and FL, were defined by means of analyses performed by application of the experimentally verified nonlinear micro-models.

10.3.4 Modelling of AAC Infill

The modelling parameters of the nonlinear links representing an AAC infill are presented in Table 10.3.3. The defined nonlinear response envelope is perfectly represented up to point U representing the real maximum restoring force FU and the corresponding displacement DU. However, in the present case, the descending part of the envelope curve was not included to avoid solution problems. In the software used, specific nonlinear link properties are not presently available.

Tab. 10.3.3. Model parameters of used nonlinear links representing AAC storey infill

Storey	DY (m)	FY (kN)	DU (m)	FU (kN)	DL (m)	FL (kN)
1	0.004	63	0.008	84	0.2	100
2	0.004	63	0.008	84	0.2	100
3	0.004	63	0.008	84	0.2	100
4	0.004	63	0.008	84	0.2	100
5	0.004	63	0.008	84	0.2	100

In the software used, specific nonlinear link properties are not presently available. This inconsistency did not significantly affect the computed results due to the reduced participation of the infill restoring forces. This statement is supported by the close agreement between the computed and experimental force-displacement envelopes, which show nearly identical stiffness, strength, and deformation capacity despite the simplified link definition. The similarity of the global response indicates that the missing software options for defining advanced link hysteresis did not significantly influence the overall accuracy of the results. Nevertheless, software improvement with new modelling options incorporating a dedicated nonlinear AAC macro-model could be an important research direction for future development.

The nonlinear numerical model of the AAC-infilled RC frame was developed in SAP2000 [63], using a simplified macro-modelling approach based on experimentally calibrated link elements. The modelling aimed to reproduce the global nonlinear behavior of the tested prototype frame by representing the essential stiffness, strength, and deformation characteristics obtained from the experimental results.

The model geometry was defined by two vertical RC columns connected by a rigid beam at each storey level to ensure equal horizontal displacements and load transfer between the columns. The columns were divided into segments corresponding to each storey height, and in the middle of each segment, a nonlinear link element was introduced to represent the experimentally obtained force-displacement behavior of the RC columns. These links were defined as multi-linear elastic-plastic with characteristic points (yield, peak, and limit) taken directly from the F-D diagrams presented in Chapter 9.

The AAC infill wall was represented by a single nonlinear link positioned at the mid-plane of the panel. To correctly transfer the in-plane actions of the infill towards this central link, stiff connection strips with very high stiffness were introduced from the corner joints of the frame to the central node of the link. These stiff members do not represent real structural elements but serve to channel the in-plane forces of the wall to the defined nonlinear link. The mechanical properties of the infill link were determined directly from the experimental force-displacement curve of the AAC panel, described in Chapter 9, including the characteristic points corresponding to the yielding, peak, and limit states. The nonlinear envelope of the link was defined according to these values, and the descending branch was not included to avoid convergence issues, while maintaining a capped plateau until the limit value, as indicated in Table 10.3.3. The behavior of the link was calibrated to reproduce the nonlinear deformation, compressive response, and progressive stiffness degradation of the AAC infill observed during experimental testing.

At the base level, the supports of both columns were fully fixed, while a constant vertical load of N_1 = 62.5 kN was applied to each column. The lateral loading was simulated through a displacement-controlled pushover analysis applied at the top node of the rigid beam. The obtained numerical results showed a satisfactory agreement with the experimental global force-displacement curve in terms of initial stiffness, peak strength, and overall deformation capacity.

In the analysis process, the beam at each storey was considered rigid to ensure uniform displacement distribution. The nonlinear behavior of both columns and infill was governed by the link elements calibrated from experimental data. The AAC infill was assumed to act in compression within the nonlinear range and to gradually lose stiffness with increasing deformation, in accordance with the experimentally observed cracking and detachment from the RC frame. The interaction between the frame and the infill was simulated through the central link and stiff connection strips, which ensured load transfer without introducing artificial tensile resistance. Geometric nonlinearity (P-Δ effects) was included to capture second-order deformations. The link parameters for each storey were adopted according to the values listed in Table 10.3.3.

A nonlinear static pushover analysis was conducted with displacement control applied at the top of the frame. The global nonlinear behavior of the system was fully governed by the defined link elements, while convergence was verified for all loading steps. The primary output of the analysis consisted of the global force-displacement relationship and the activation history of the nonlinear links, which were used for comparison with the experimental findings presented in Chapter 9.

The shear force-displacement (F-D) relationship of the nonlinear link representing the AAC infill, defined according to the parameters presented in Table 10.3.3, is shown in Figure 10.3.3. The diagram illustrates the nonlinear compressive response of the AAC infill link.

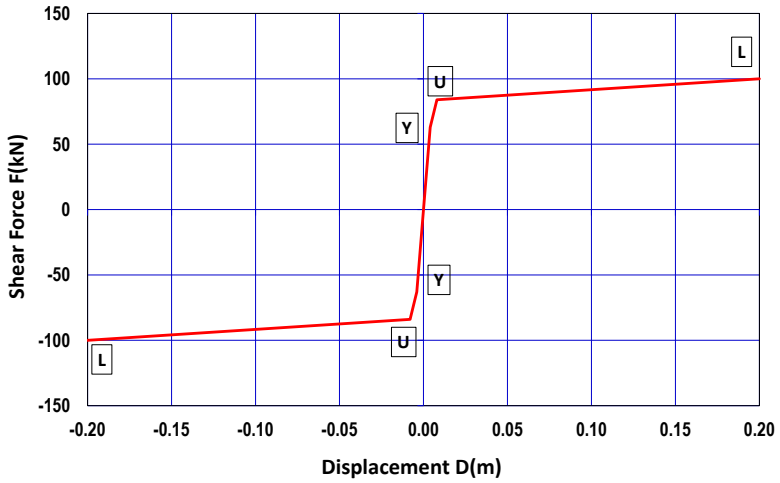

Figure 10.3.3. Force-displacement (F-D) relationship of the nonlinear link representing the AAC infill.

10.3.5 Selected Earthquake Ground Motions

To demonstrate the practical applicability of the proposed AACF model in nonlinear seismic response analysis of buildings, the present case study involving nonlinear seismic response analysis of the selected representative AAC infilled RC frame was conducted.

In the present seismic response analysis, seismic response analyses under selected two intensity levels of the widely used Ulcinj-Albatros earthquake record were conducted, including:

(1) Seismic response analysis considering PGA = 0.22g, Figure 10.3.4,

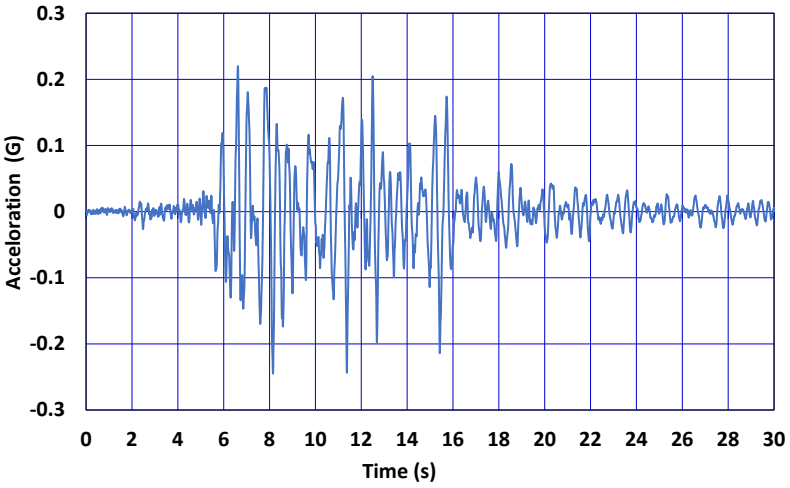

Figure 10.3.4. Acceleration time-history of the Ulcinj-Albatros earthquake (PGA = 0.22 g)

(2) Seismic response analysis considering PGA = 0.30 g, Figure 10.3.5

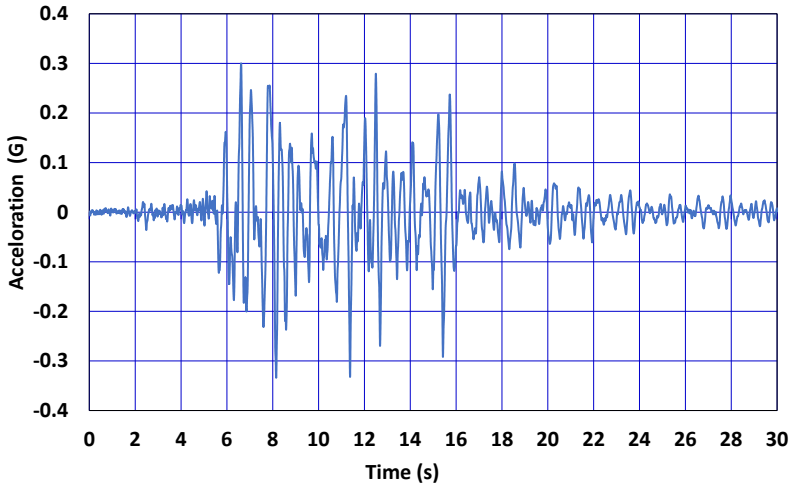

Figure 10.3.5. Acceleration time-history of the Ulcinj-Albatros earthquake (PGA = 0.3g)

The studies enabled a detailed insight into the changes of the characteristics of the structural seismic response under simulated two earthquake intensities.

10.4 Dynamic Characteristics of Five Storey RC Frame with AAC Infill

Prior to realization of the nonlinear seismic response analysis of the five-storey reinforced concrete frame with masonry infill consisting of AAC elements, calculations of the main dynamic characteristics of the system were performed using the developed macro AACF model shown in Fig. 10.4.1. The obtained periods and the corresponding frequencies for the first five modes of vibration are shown in Table 10.4.1.

Tab. 10.4.1. Periods and frequencies of five storey RC frame with AAC infill

Mode	Period T (s)	Frequency f (cyc/s)	Participation factor Γx = UX (kN·m)	Modal mass ratio UX (-)
1	0.334	2.997	-10.022	0.87953
2	0.114	8.749	-3.155	0.08718
3	0.073	13.791	1.663	0.02422
4	0.056	17.717	-0.926	0.00751
5	0.049	20.207	-0.423	0.00157

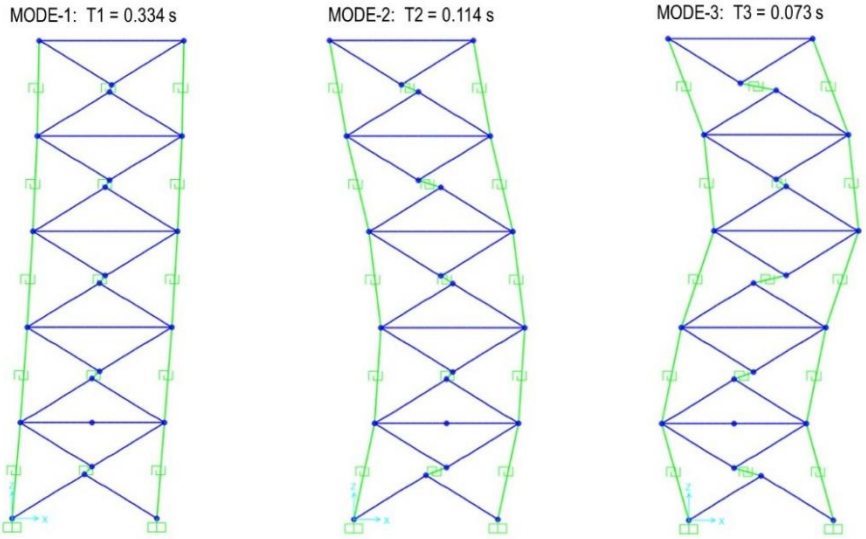

Fig. 10.4.1. Model-M2: Computed mode shapes and periods of modelled five storey RC frame with AAC infill (AACF-Model)

The obtained specific mode shapes of the first three modes are clearly shown in Figure 10.4.1. The first mode, with a period of T1 = 0.334 s, represents a global lateral sway of the entire height of the structure, where all storeys drift in the same direction with an almost uniform deformation pattern. Such a short period, compared to bare frames, confirms the increased initial stiffness provided by the AAC masonry infill. The second mode (T2 = 0.114 s) exhibits a higher-order bending deformation with a distinct point of inflection near mid-height, indicating that the upper and lower parts of the structure deform with different curvature. The third mode (T3 = 0.073 s) shows a combined torsional lateral deformation in which the storeys rotate slightly around the vertical axis while also displacing laterally, a behavior associated with small stiffness irregularities introduced by the infill configuration. Although the presence of masonry significantly increases the initial stiffness, higher seismic intensities lead to

cracking and degradation of the infill at certain storeys, which consequently reduces the stiffness and results in an increase of the effective vibration periods as damage progresses, even though the RC frame itself maintains satisfactory stability.

10.5 Seismic Response Under Earthquake Intensity EQI=1

The obtained characteristics of the nonlinear seismic response of the analyzed representative RC frame with AAC masonry infill are presented in a graphic form. To obtain detailed insight into the computed results, characteristic time histories of displacements, time histories of velocity, time histories of acceleration, hysteretic responses of the reinforced concrete columns per storeys as well as hysteretic responses of the AAC infill per storeys are presented in corresponding figures.

10.5.1 EQI=0.22g: Displacements of AAC Infilled RC Frame

Fig. 10.5.1 shows the time history response of displacement of storey 1 of the AAC infilled RC frame under the simulated Ulcinj-Albatros earthquake scaled to peak ground acceleration PGA = 0.22 g. The computed maximum displacement amounts to maxD = 1.98 cm. Similarly, Fig. 10.5.2 shows the time history response of floor 5. The maximum displacement of storey 5 amounts to maxD = 3.7 cm.

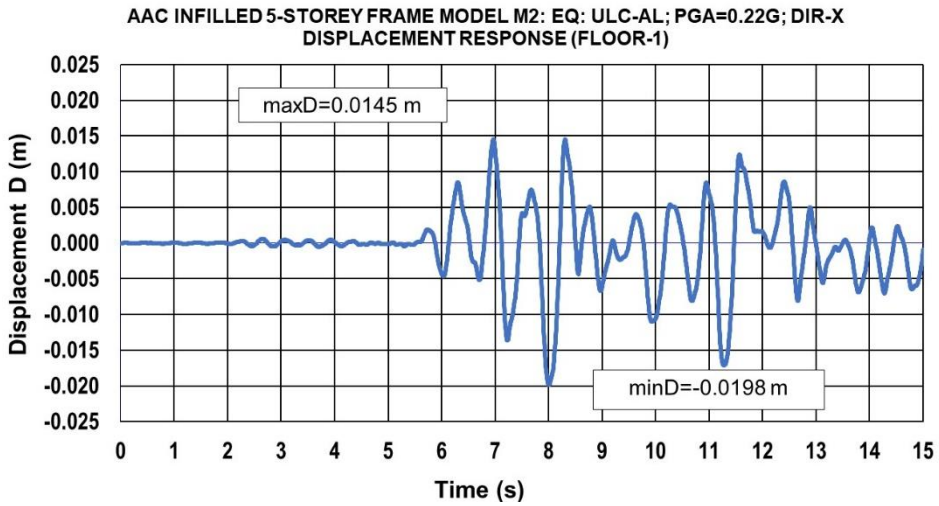

Fig. 10.5.1. Model-M2 under earthquake intensity EQI1=0.22g: Displacements time history response of storey-1

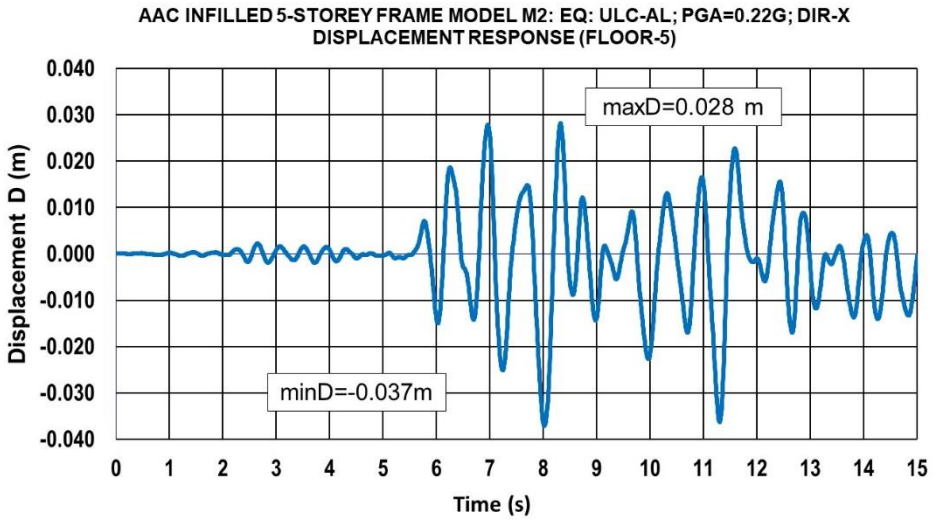

Fig. 10.5.2. Model-M2 under earthquake intensity EQI1=0.22g: Displacements time history response of storey-5

10.5.2 EQI=0.22g: Velocities of AAC Infilled RC Frame

The velocity time history response of storey 1 is presented in Fig. 10.5.3. The computed maximum value of velocity amounts to maxV = 2.15 m/s. Analogously, Fig. 10.5.4 shows the time history of velocity for storey 5. The maximum value of velocity is greater and amounts to maxV = 3.77 m/s.

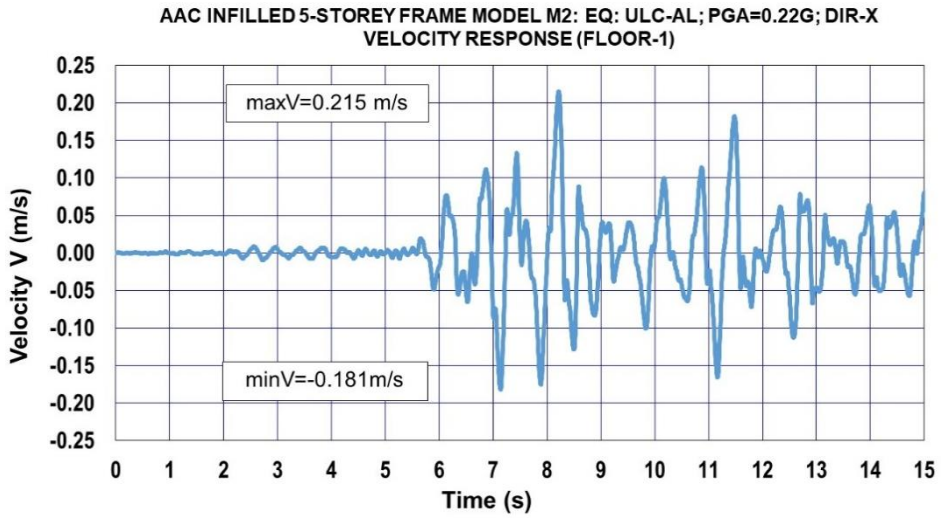

Fig. 10.5.3. Model-M2 under earthquake intensity EQI1=0.22g: Velocity time history response of storey-1

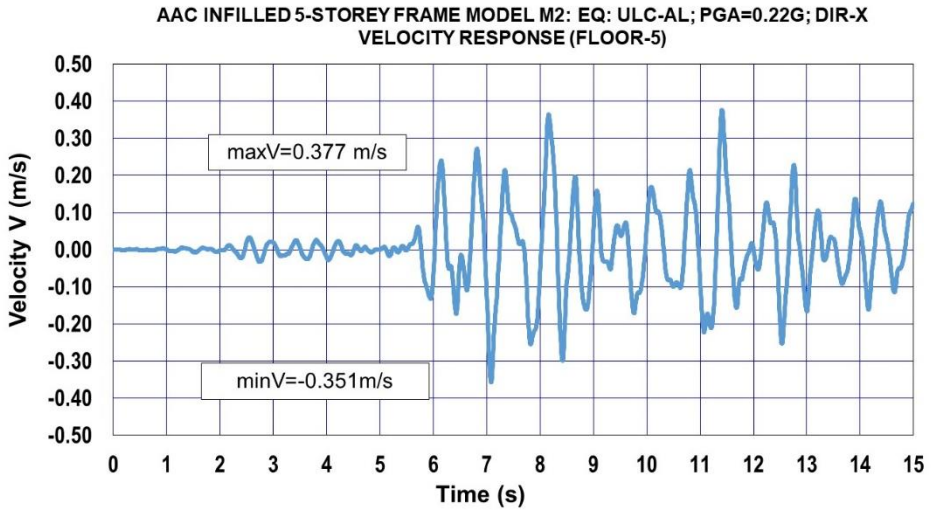

Fig. 10.5.4. Model-M2 under earthquake intensity EQI1=0.22g: Velocity time history response of storey-5

10.5.3 EQI=0.22g: Accelerations of AAC Infilled RC Frame

The acceleration time history response of storey 1 is presented in Fig. 10.5.5. The maximum value of the acceleration amounts to maxA = 4.36 m/s^2. Analogously, for storey 5, the time history response is presented in Fig. 10.5.6. At storey 5, the computed maximum value of acceleration amounts to maxA = 4.491 m/s^2. If the maximum response value is compared with the input peak acceleration amounting to PGA = 0.22 g = 2.158 m/s^2, the significant dynamic amplification factor, DAF = 4.491/2.158 = 2.08, was obtained.

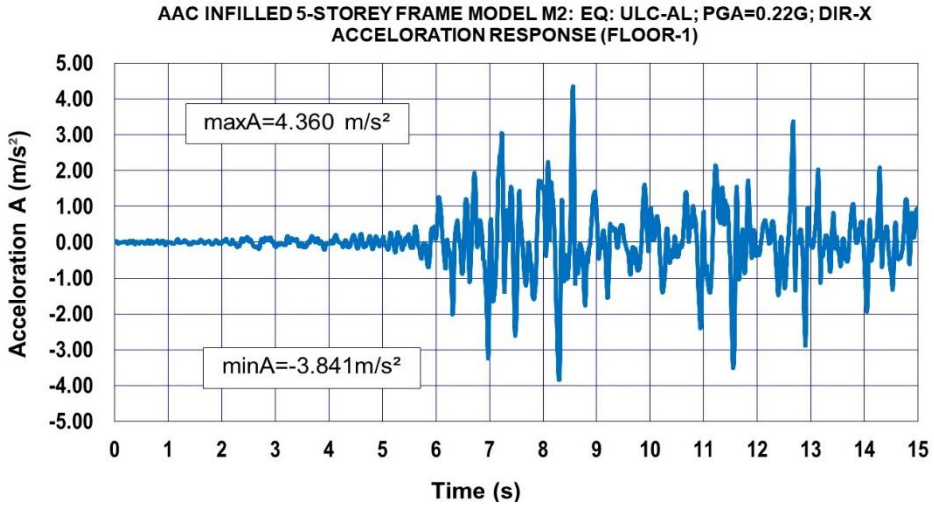

Fig. 10.5.5. Model-M2 under earthquake intensity EQI1=0.22g: Acceleration time history response of storey-1

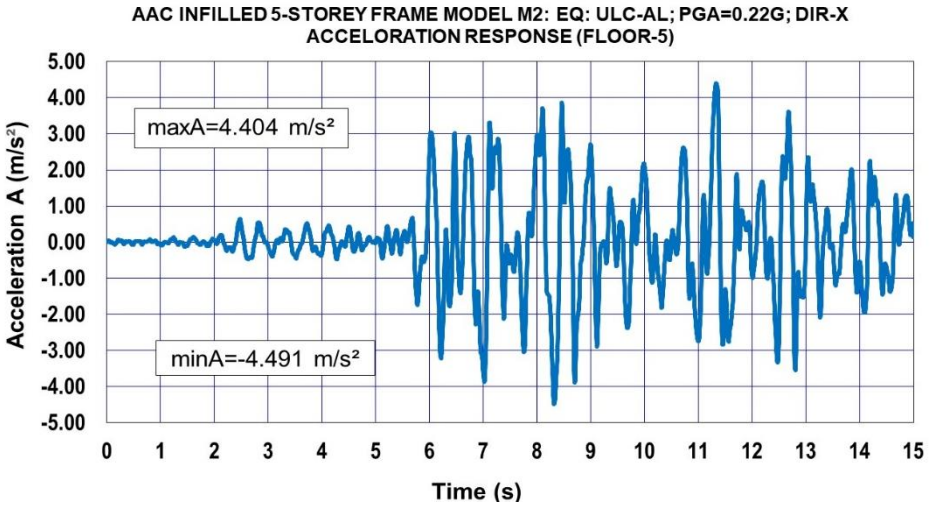

Fig. 10.5.6. Model-M2 under earthquake intensity EQI1=0.22g: Acceleration time history response of storey-5

10.5.4 EQI=0.22g: Hysteretic Response of RC Columns

To enable complete monitoring of the development of the hysteretic response of the RC columns along the height, the hysteretic responses of the left modelled columns at all storeys (marked by nonlinear link elements L1, L3, L4, L7 and L11) are presented in Figures 10.5.7 through 10.5.11.

In Figure 10.5.7, the hysteretic response of the RC column located on the first storey (LINK-L1) of Model M2 is presented for the earthquake intensity level EQI = 0.22 g. The blue lines represent the complete cyclic hysteretic loops of the column during loading and unloading, while the red line indicates the model envelope curve that connects the maximum shear force and corresponding displacement in both positive and negative loading directions.

The differences between the blue and red curves arise from the cyclic nonlinear behavior of the column element. The blue response curve illustrates the actual force-displacement history during cyclic loading, where stiffness and strength gradually degrade due to cracking, yielding of reinforcement, and energy dissipation through hysteretic damping. The envelope curve, on the other hand, represents the idealized maximum response envelope that bounds all cycles and is used to define the ultimate capacity. Therefore, the two curves differ because the envelope shows only the outermost limits, whereas the hysteretic loops record the real cyclic degradation within those limits.

The asymmetry between the positive and negative branches is caused by the residual deformation and partial loss of stiffness that develops after the first major yielding in one direction. Once cracks and local yielding occur, the column does not return to its original configuration upon unloading. This results in a shifted origin (residual displacement) and a difference between the positive and negative envelope branches. Furthermore, the interaction between the RC frame and the AAC infill produces additional eccentric effects and unequal

stiffness in tension and compression zones, which further increase the asymmetry of the hysteretic loops [64], [65].

Although the columns in the lower storeys, such as LINK-L1, exhibit more pronounced hysteretic deformations, all recorded displacements remain below the failure limit of Df = 3.0 cm. This value, determined from the parametric analyses presented in Chapter 9, is consistent with the deformation limits for RC columns defined in Eurocode 8 and FEMA 356, confirming that the nonlinear behavior remains controlled and within the expected range. The same approach was used for analyzing the responses of other storey-level link elements shown in the subsequent figures.

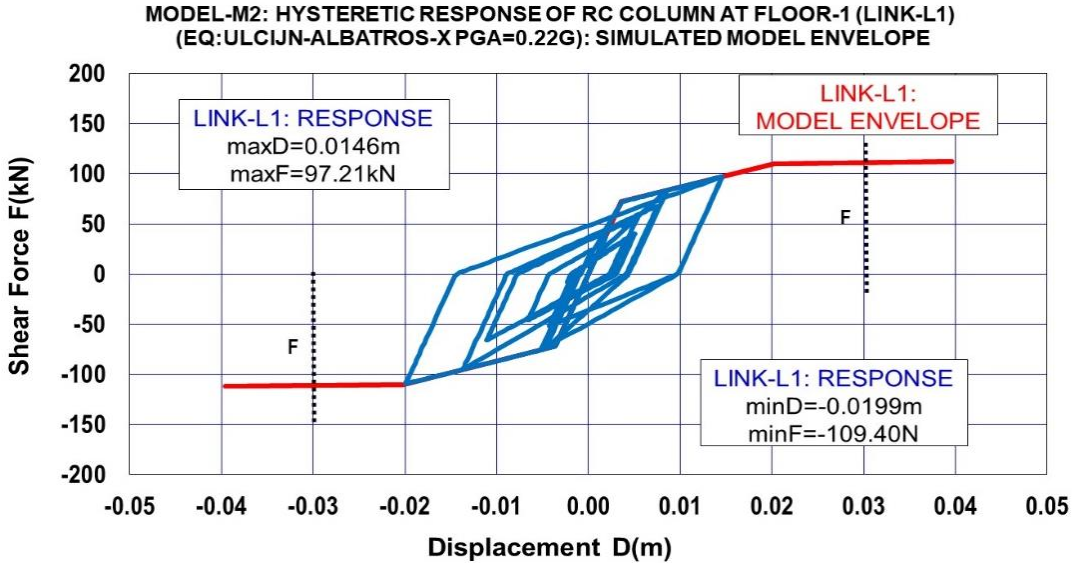

Fig. 10.5.7. Model-M2 under earthquake intensity EQI1=0.22g: Hysteretic response of RC column at storey-1

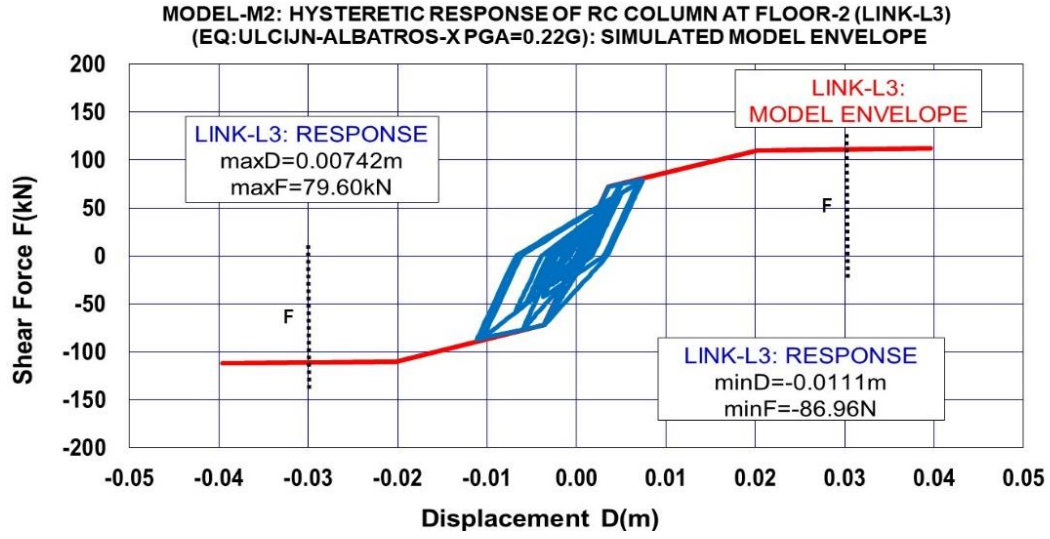

Fig. 10.5.8. Model-M2 under earthquake intensity EQI1=0.22g: Hysteretic response of RC column at storey-2

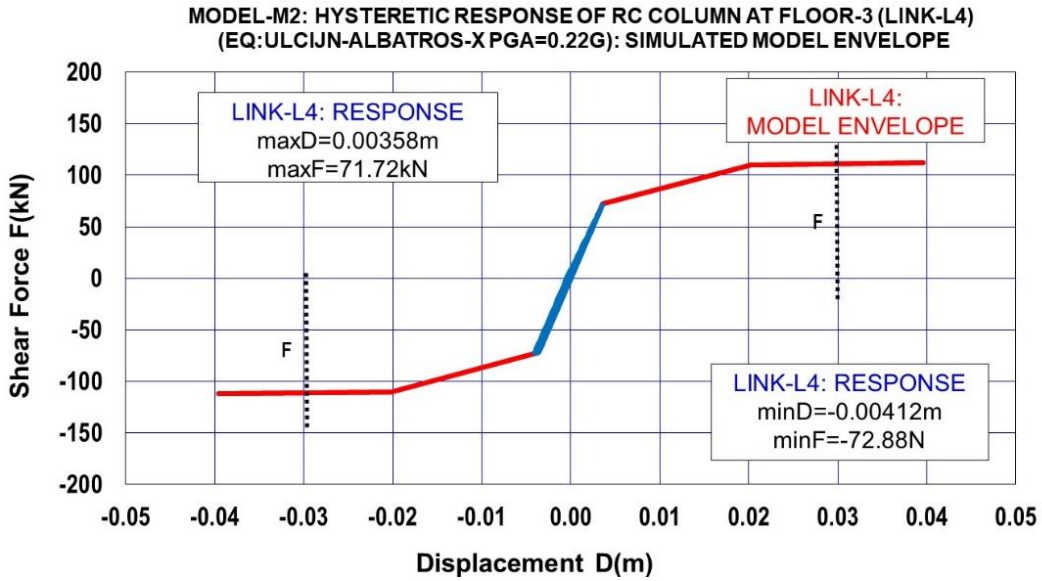

Fig. 10.5.9. Model-M2 under earthquake intensity EQI1=0.22g: Hysteretic response of RC column at storey-3

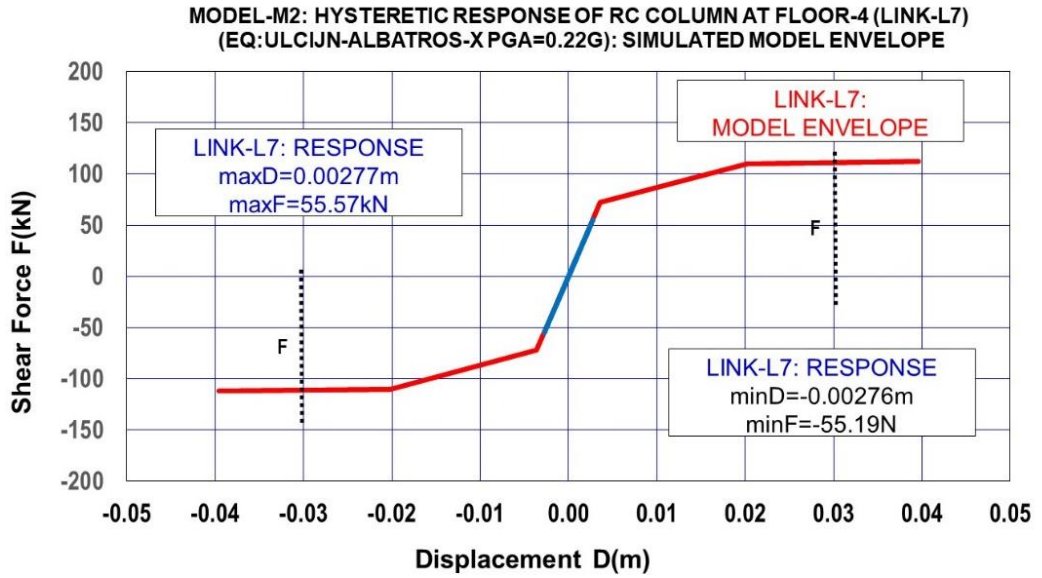

Fig. 10.5.10. Model-M2 under earthquake intensity EQI1=0.22g: Hysteretic response of RC column at storey-4

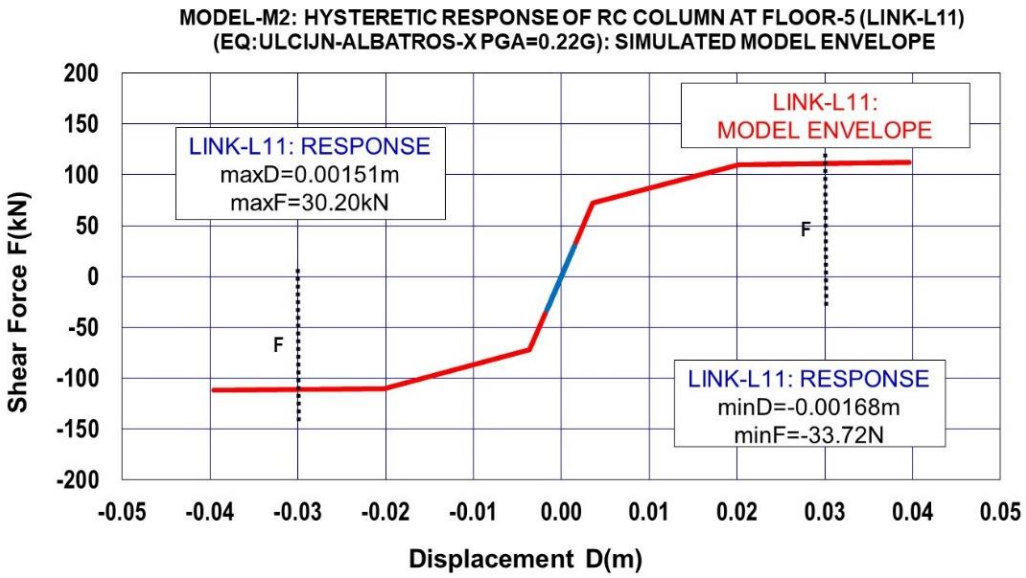

Fig. 10.5.11. Model-M2 under earthquake intensity EQI1=0.22g: Hysteretic response of RC column at storey-5

10.5.5 EQI=0.22g: Hysteretic Response of AAC Infill

The hysteretic response of the AAC infill along storeys (1 to 5) was simulated by the nonlinear link elements L32, L16, L6, L10 and L13. The obtained hysteretic responses are analogously presented in five figures, from Fig. 10.5.12 to Fig. 10.5.16. Since, for the AAC infill, the failure deformation amounts to Df = 1.5 cm, infill failure is present only at storey 1. Although the AAC infill wall in the lower storeys exhibits more pronounced hysteretic deformations, all recorded displacements remain below the failure limit adopted for AAC masonry, Df = 1.5 cm. This value, determined from the parametric analyses presented in Chapter 9, is consistent with deformation limits reported in experimental studies and international guidelines for stiff masonry infill panels. This indicates that the nonlinear behavior of the infill remains controlled and within the expected range. The same criterion was applied when evaluating the responses of the other masonry infill panels presented in the subsequent figures. For the modelled storeys 3, 4 and 5, the response of the AAC infill is almost linear. However, at storey 2, there is a nonlinear response characterized by distributed fine cracks.

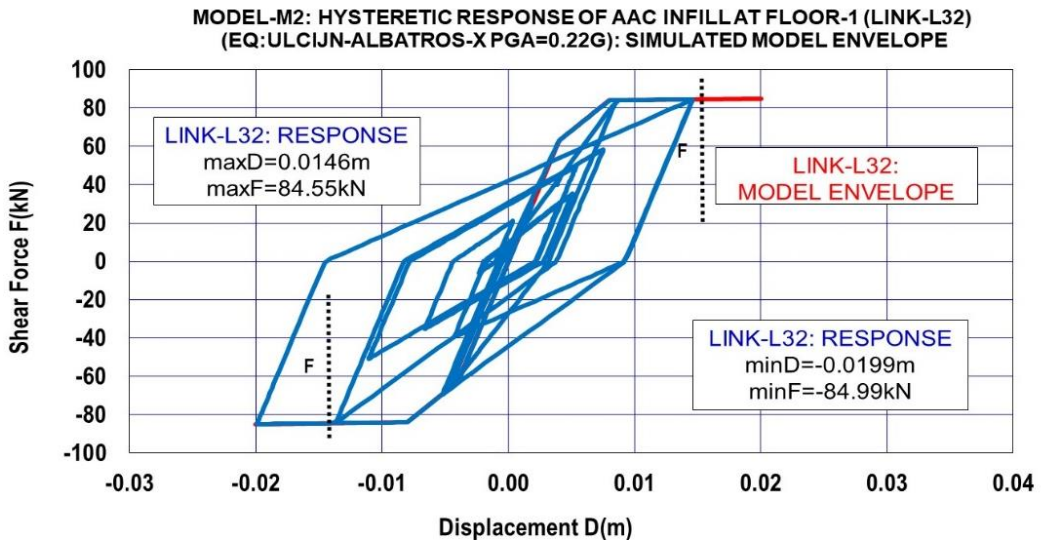

Fig. 10.5.12. Model-M2 under earthquake intensity EQI1=0.22g: Hysteretic response of AAC infill at storey-1

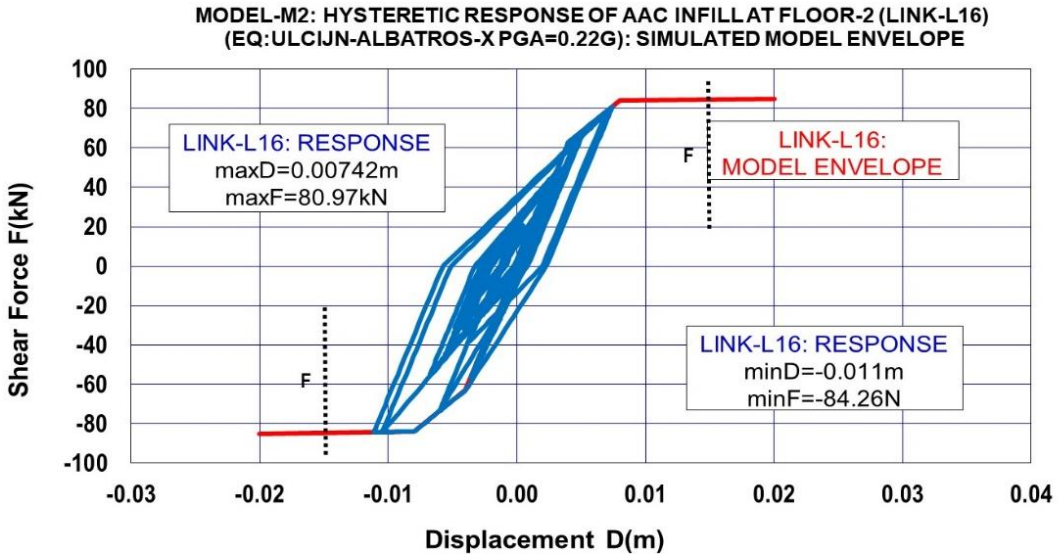

Fig. 10.5.13. Model-M2 under earthquake intensity EQI1=0.22g: Hysteretic response of AAC infill at storey-2

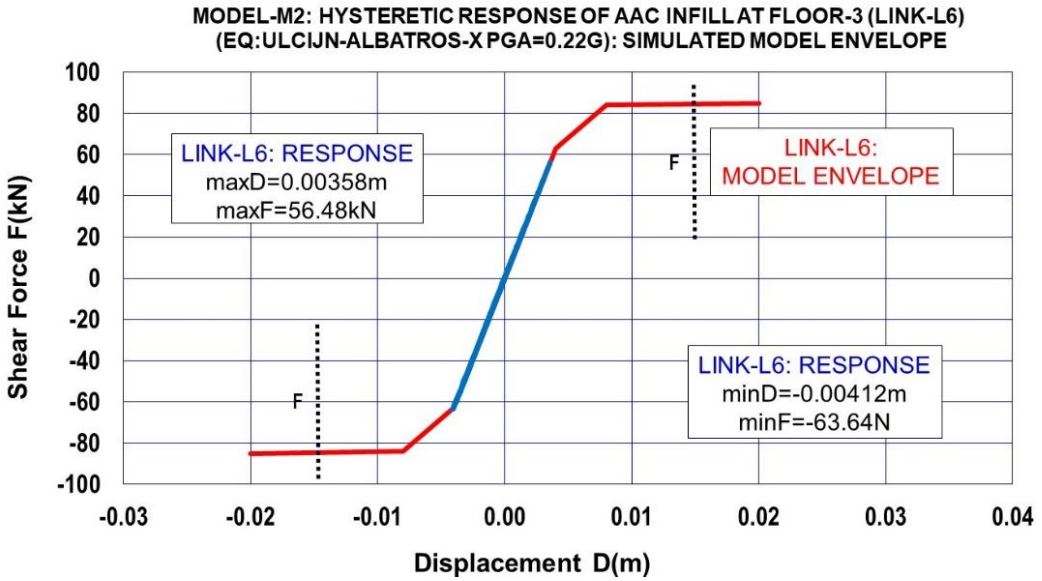

Fig. 10.5.14. Model-M2 under earthquake intensity EQI1=0.22g: Hysteretic response of AAC infill at storey-3

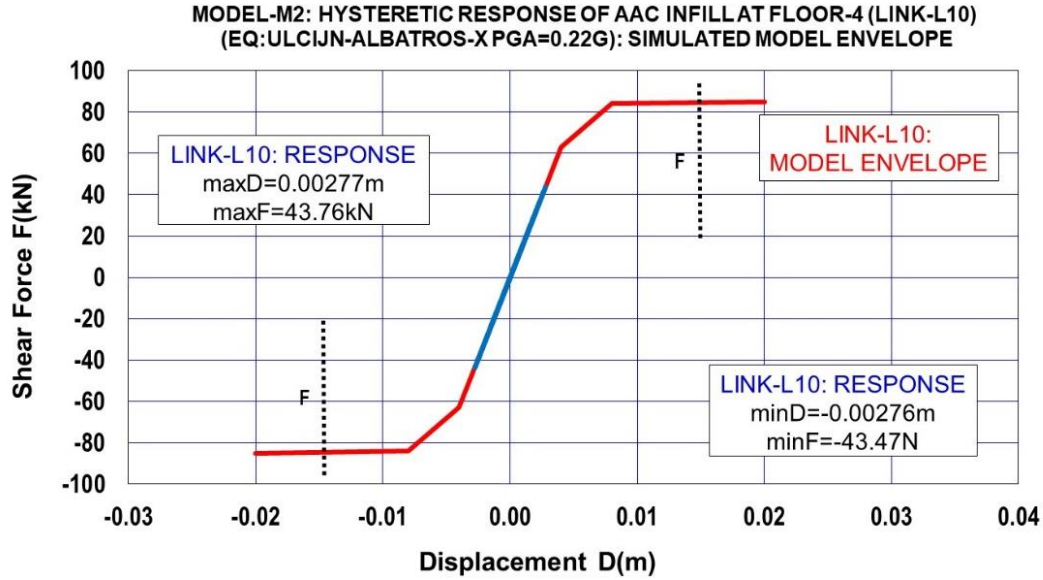

Fig. 10.5.15. Model-M2 under earthquake intensity EQI1=0.22g: Hysteretic response of AAC infill at storey-4

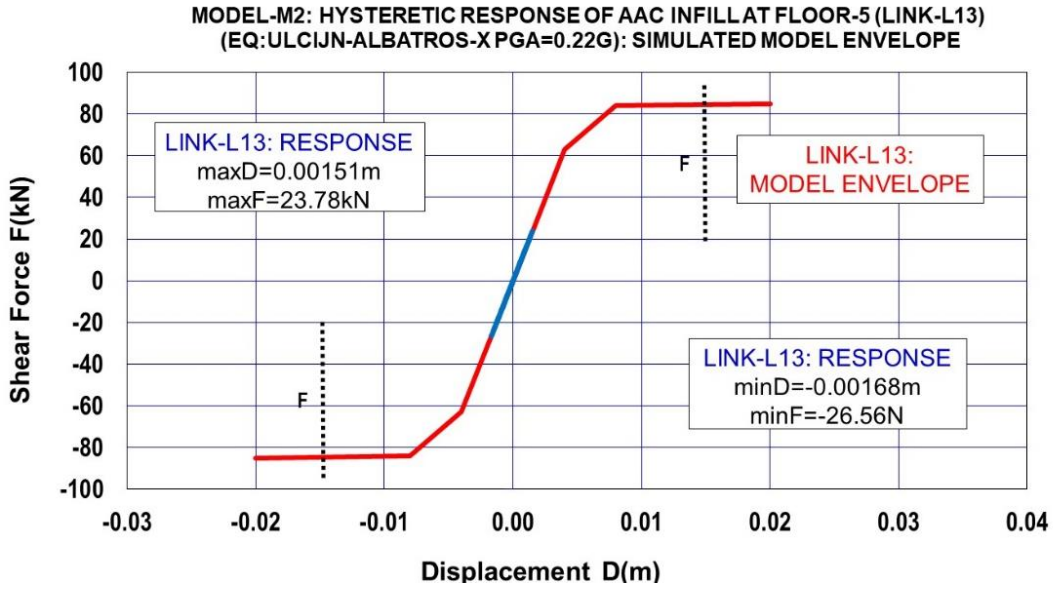

Fig. 10.5.16. Model-M2 under earthquake intensity EQI1=0.22g: Hysteretic response of AAC infill at storey-5

The main objective of this section is to verify the reliability of the proposed nonlinear macro-model in reproducing the overall hysteretic behavior of the RC frame with AAC infill, rather than to provide a detailed analysis of local damage mechanisms. The hysteretic diagrams represent the complete cyclic response of the system, including stiffness degradation, strength reduction, and residual deformations, which are clear indicators of damage progression. Therefore, the presented results adequately capture both the global and local nonlinear behavior of the structure, consistent with the purpose of this study. In Figure 10.5.11, the hysteretic response of the AAC infill link located at the top storey (LINK-L13) of Model M2 is presented for the earthquake excitation level EQI = 0.22 g. The blue curve represents the simulated cyclic response of the link, while the red curve denotes the model envelope connecting the maximum shear forces and corresponding displacements.

The almost linear shape of the response loop indicates that the AAC infill at this level remained within the elastic or quasi-elastic range during the applied excitation. This behavior is expected, since the upper storeys experience smaller inter-storey drifts and lower shear demands compared with the lower levels of the frame. As a result, the deformation of the infill is limited, and no significant cracking or nonlinearity develops within the AAC panel. Consequently, the link element behaves linearly up to the attained displacement amplitude.

10.6 Seismic Response Under Simulated Earthquake Intensity EQI=2

To provide comparative insight into the change of the nonlinear behavior of the modelled AAC infilled RC frame, presented are analogous results from the performed nonlinear seismic analysis with increased earthquake intensity characterized by PGA = 0.30 g.

10.6.1 EQI=0.30g: Displacements of AAC Infilled RC Frame

The displacement time histories of storey 1 and storey 5 are presented in Fig. 10.6.1 and Fig. 10.6.2, respectively. For the first floor, the computed maximum displacement amounts to maxD = 3.72 cm. Since the failure relative displacement of the modelled RC columns amounts to Df = 3.0 cm, this means that the global stability of storey 1 is endangered.

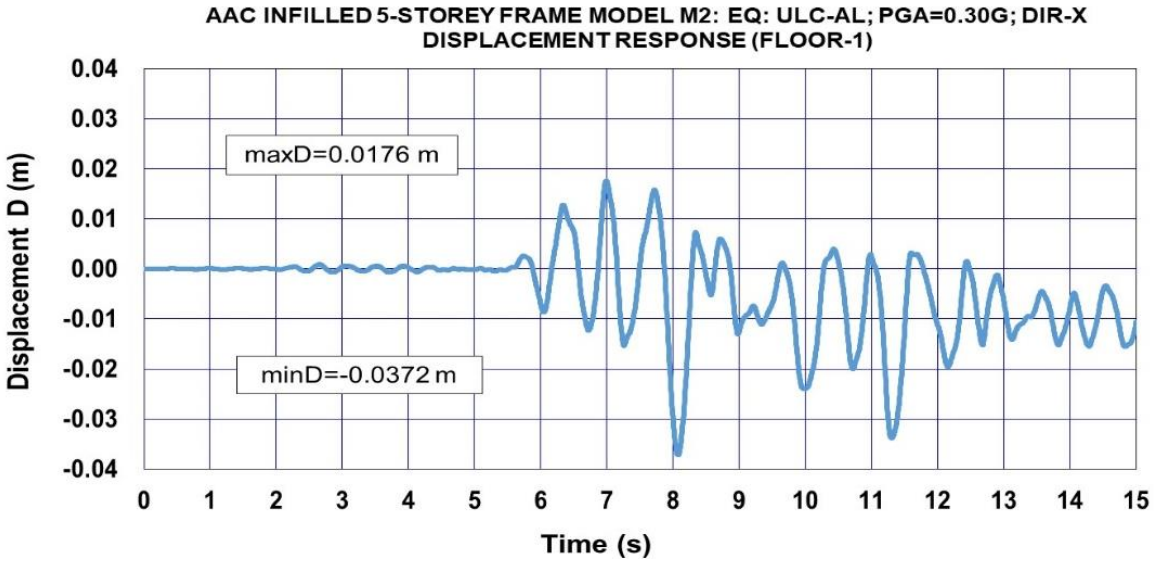

Fig. 10.6.1. Model-M2 under earthquake intensity EQI2=0.30g: Displacements time history response of storey-1

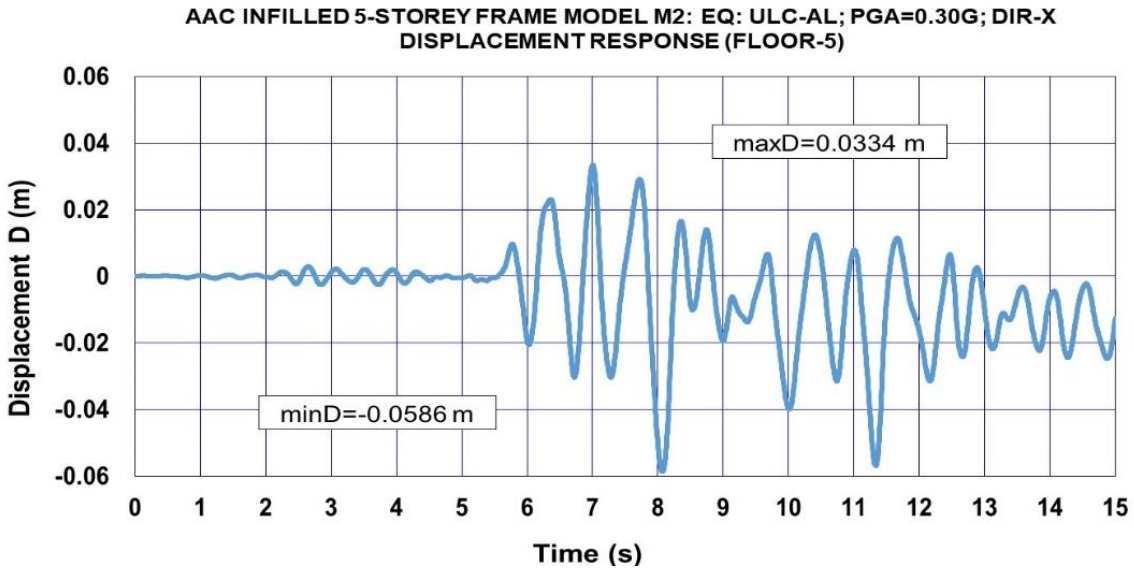

Fig. 10.6.2. Model-M2 under earthquake intensity EQI2=0.30g: Displacements time history response of storey-5

10.6.2 EQI=0.30g: Velocities of AAC Infilled RC Frame

The velocity time histories of storey 1 and storey 5 are presented in Fig. 10.6.3 and Fig. 10.6.4, respectively. The maximum computed value of velocity is maxV = 0.496 m/s.

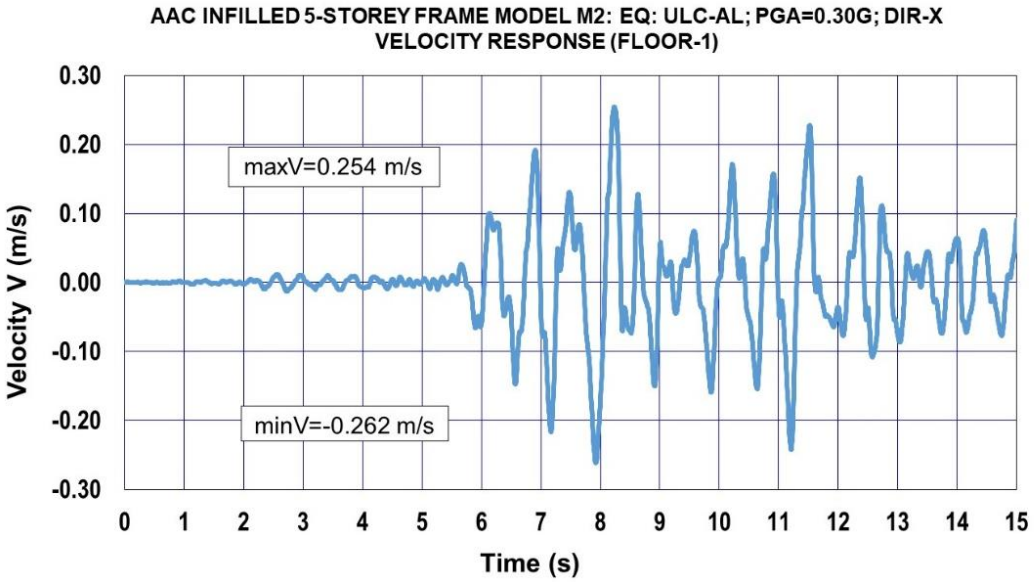

Fig. 10.6.3. Model-M2 under earthquake intensity EQI2=0.30g: Velocity time history response of storey-1

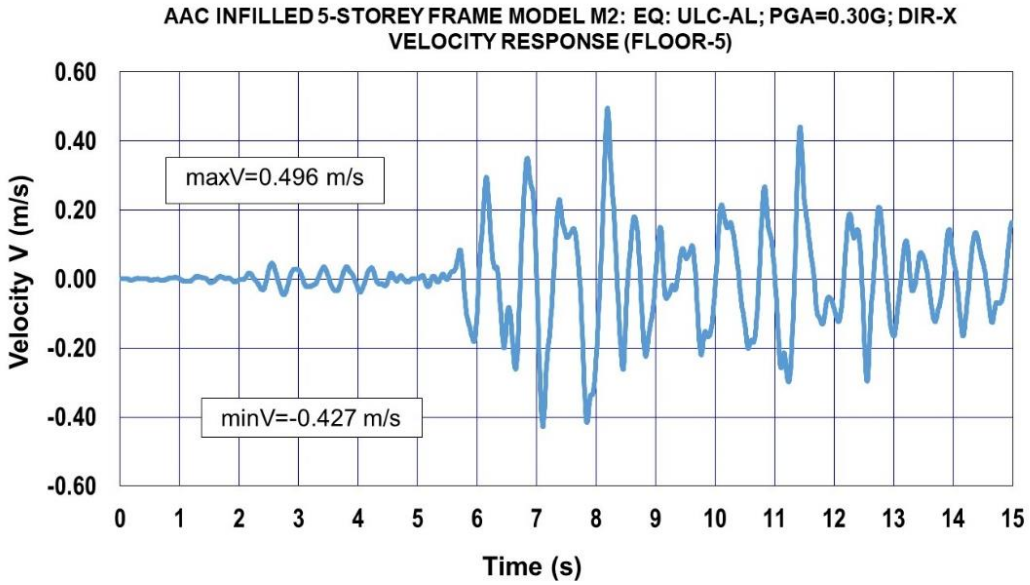

Fig. 10.6.4. Model-M2 under earthquake intensity EQI2=0.30g: Velocity time history response of storey-5

10.6.3 EQI=30g: Accelerations of AAC Infilled RC Frame

The acceleration time history responses of storey 1 and storey 5 are presented in Fig. 10.6.5 and Fig. 10.6.6, respectively. Also, in this case, the maximum values are within the expected range. For example, the maximum acceleration at storey 5 amounts to maxA = 5.538 m/s^2. Consequently, in this case, the dynamic amplification factor amounts to DAF = 5.538/2.943 = 1.88. The value of DAF in this case is smaller since an increased degree of nonlinear behavior of the columns was induced.

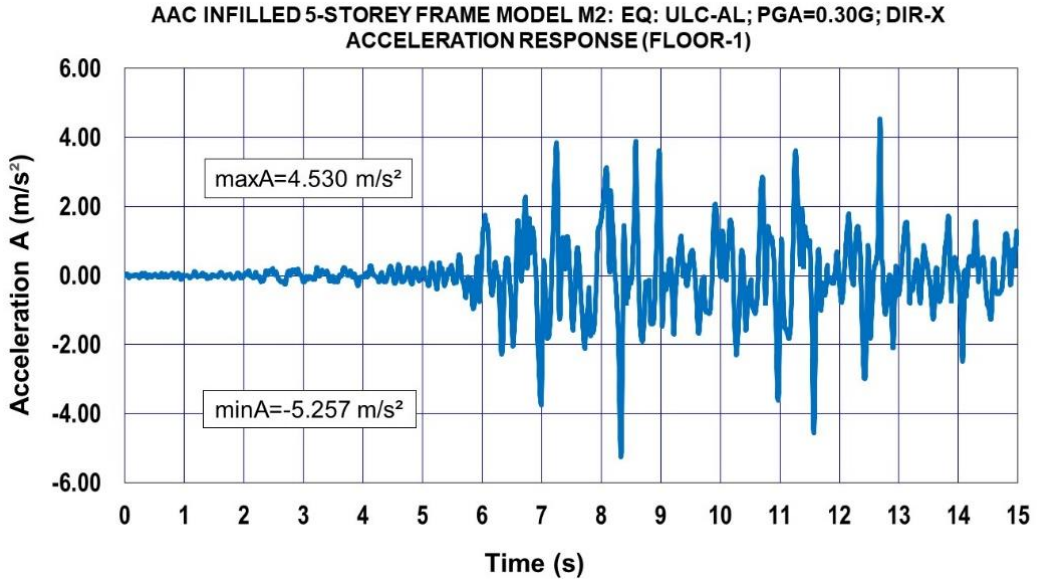

Fig. 10.6.5. Model-M2 under earthquake intensity EQI2=0.30g: Acceleration time history response of storey-1

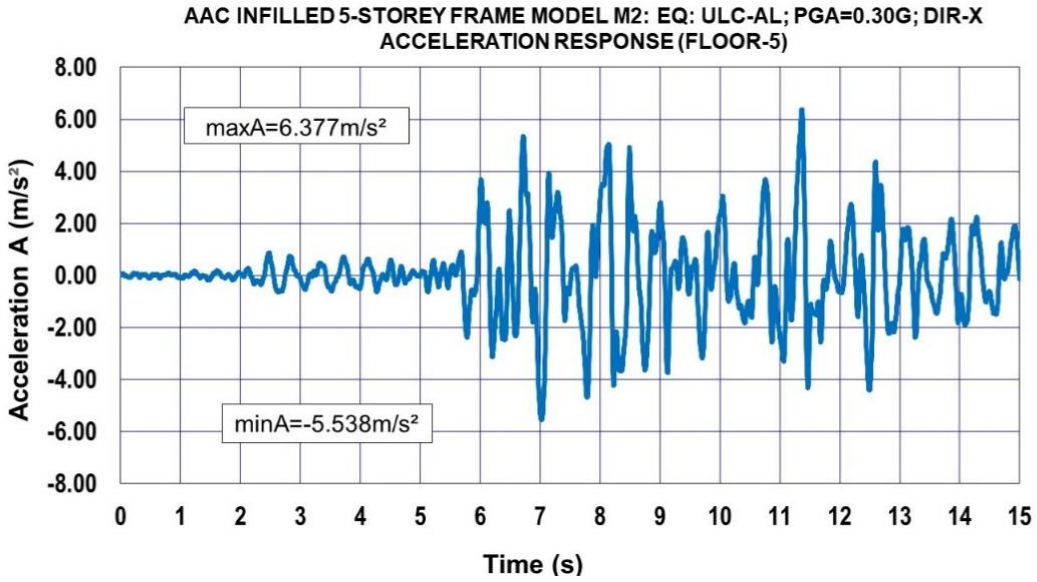

Fig. 10.6.6. Model-M2 under earthquake intensity EQI2=0.30g: Acceleration time history response of storey-5

10.6.4 EQI=30g: Hysteretic Response of RC Columns

The hysteretic response of the RC columns for all five storeys is presented in Fig. 10.6.7, Fig. 10.6.8, Fig. 10.6.9, Fig. 10.6.10 and Fig. 10.6.11.

It is characteristic that deformation is larger than the deformation capacity of the column amounting to 3.0 cm takes place only at the first storey.

Since all the remaining columns of storey 2, storey 3, storey 4 and storey 5 do not exhibit much expressed nonlinear response and remain stable, it turns out that failure of the structure is conditioned by local effects. Such critical local instabilities can be very avoided by carrying out additional advanced nonlinear expert analyses developed for specific design goals. The formulated AACF nonlinear macro model gives the opportunity for identification of possible critical segments and advancement of the seismic safety of the structural systems in the final phase of design of structures exposed to potential strong earthquake effects.

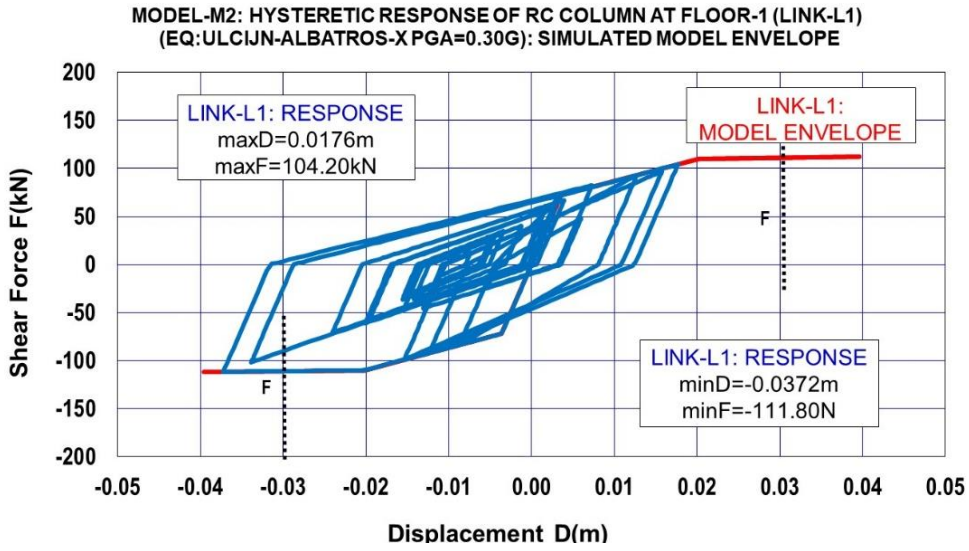

Fig. 10.6.7. Model-M2 under earthquake intensity EQI2=0.30g: Hysteretic response of RC column at storey-1

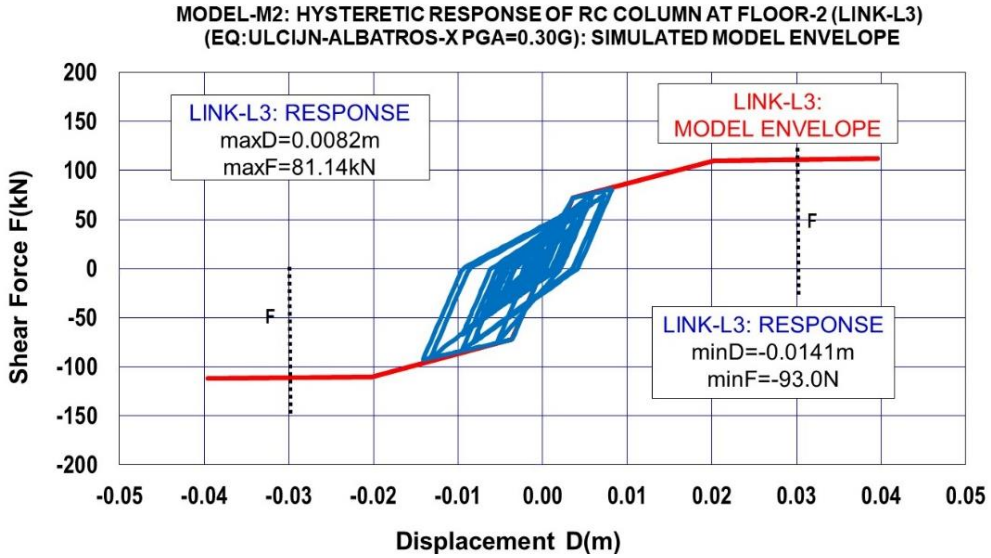

Fig. 10.6.8. Model-M2 under earthquake intensity EQI2=0.30g: Hysteretic response of RC column at storey-2

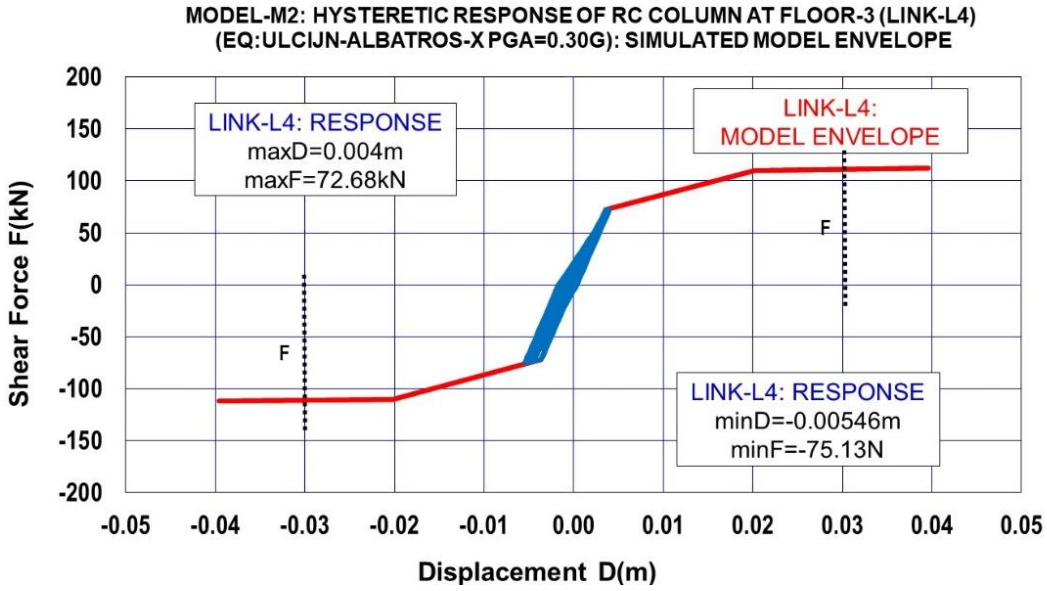

Fig. 10.6.9. Model-M2 under earthquake intensity EQI2=0.30g: Hysteretic response of RC column at storey-3

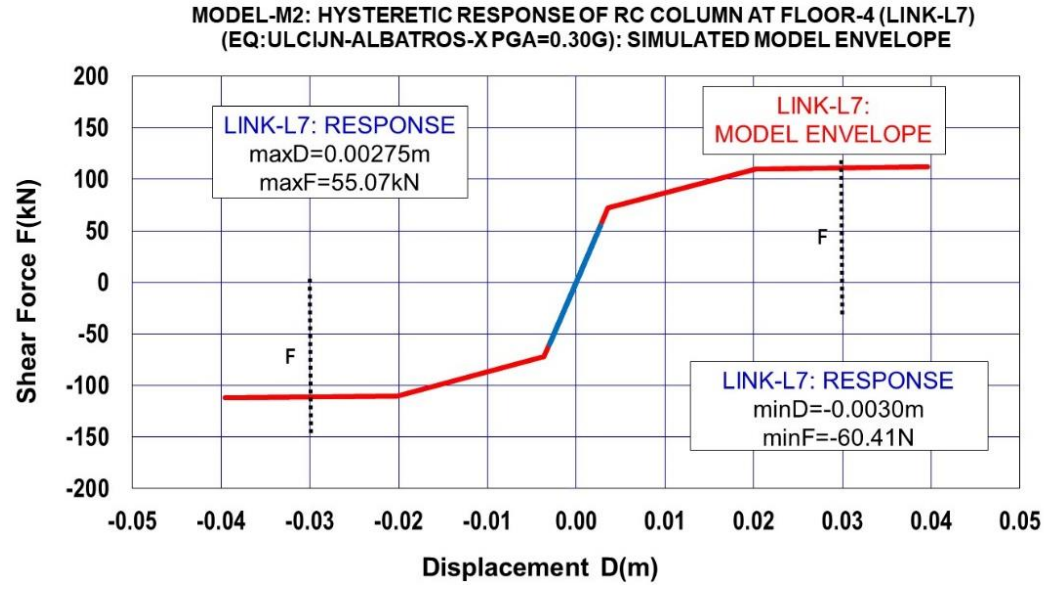

Fig. 10.6.10. Model-M2 under earthquake intensity EQI2=0.30g: Hysteretic response of RC column at storey-4

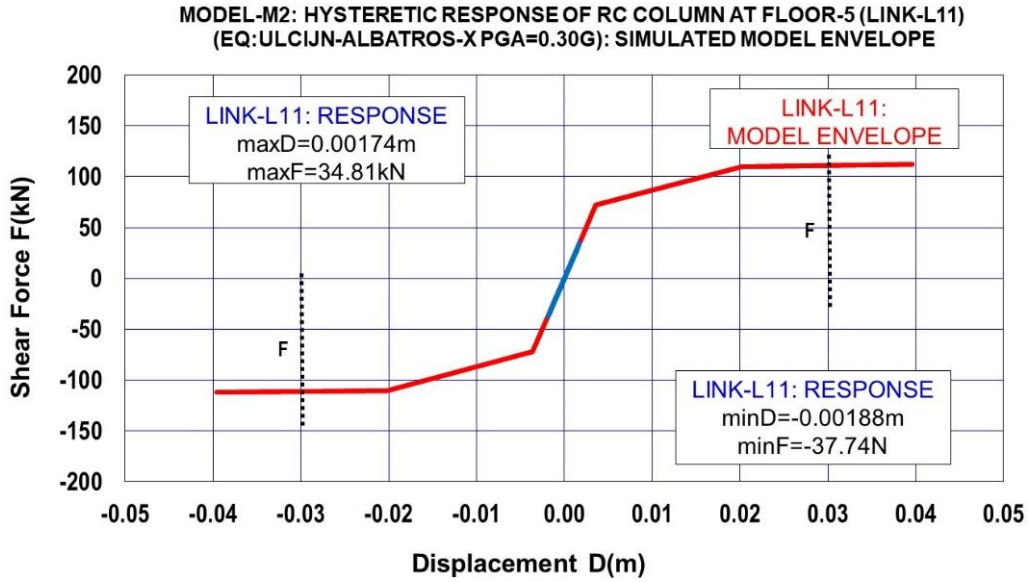

Fig. 10.6.11. Model-M2 under earthquake intensity EQI2=0.30g: Hysteretic response of RC column at storey-5

10.6.5 EQI=30g: Hysteretic Response of AAC Infill

The hysteretic response of the AAC infill per storeys is shown analogously in Fig. 10.6.12 through Fig. 10.6.16. The stated results show that the infill at the first storey that is modeled by the nonlinear link element L32 experiences total failure, Fig. 10.6.12. At the next storey 2, the AAC infill experiences intensive cracks, but not failure, Fig. 10.6.13, showing nonlinear response of link element L16.

The AAC infill at storey 3, storey 4 and storey 5 does not experience any damage since its behavior generally remains in the linear domain, Fig. 10.6.14, Fig. 10.6.15 and Fig. 10.6.16.

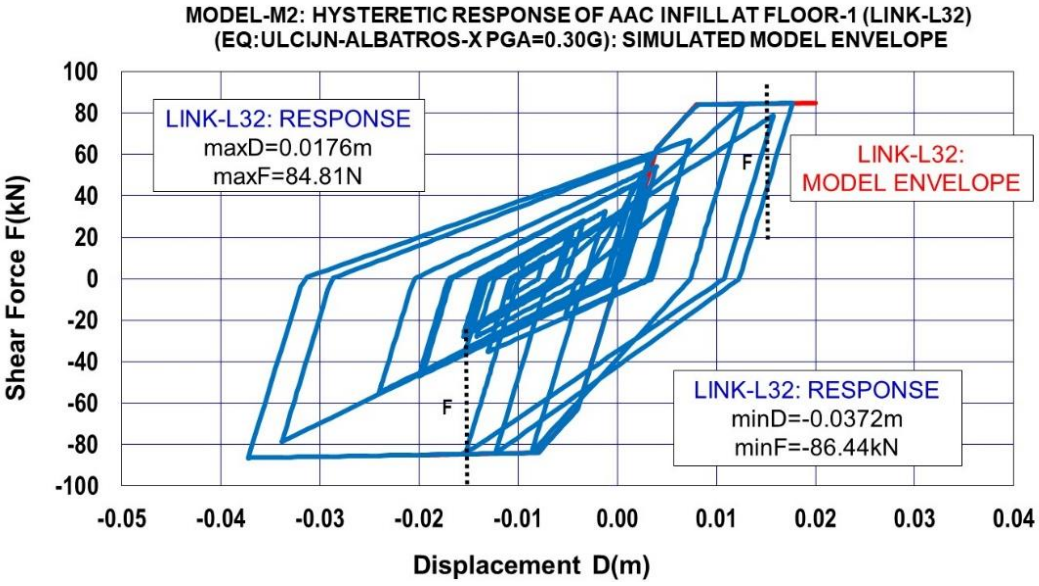

Fig. 10.6.12. Model-M2 under earthquake intensity EQI2=0.30g: Hysteretic response of AAC infill at storey-1

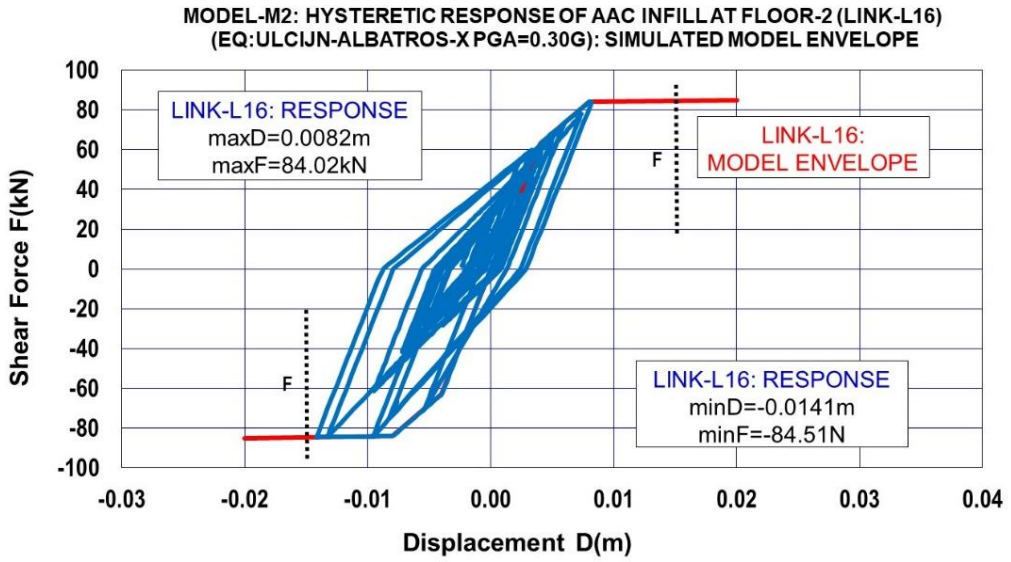

Fig. 10.6.13. Model-M2 under earthquake intensity EQI2=0.30g: Hysteretic response of AAC infill at storey-2

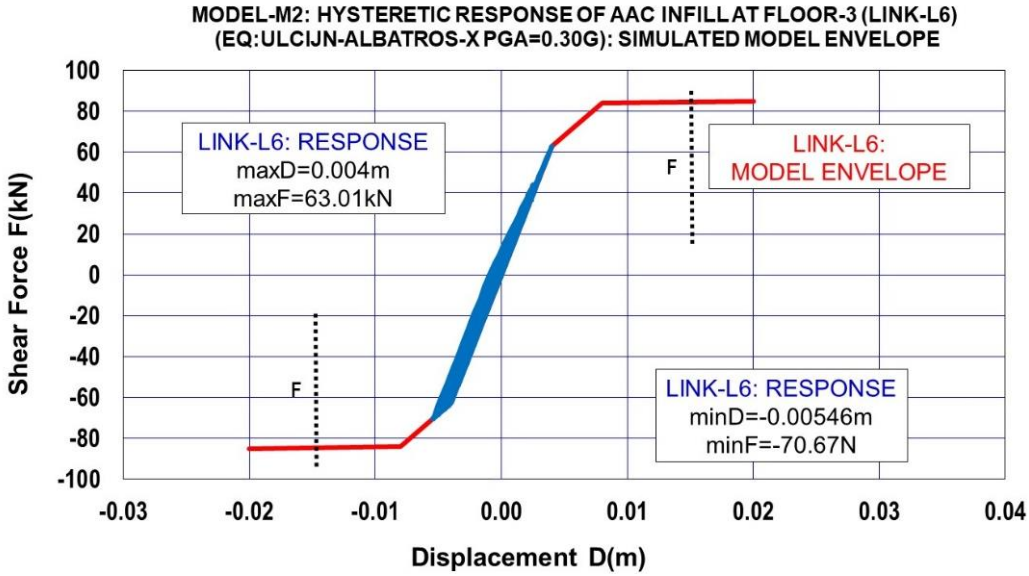

Fig. 10.6.14. Model-M2 under earthquake intensity EQI2=0.30g: Hysteretic response of AAC infill at storey-3

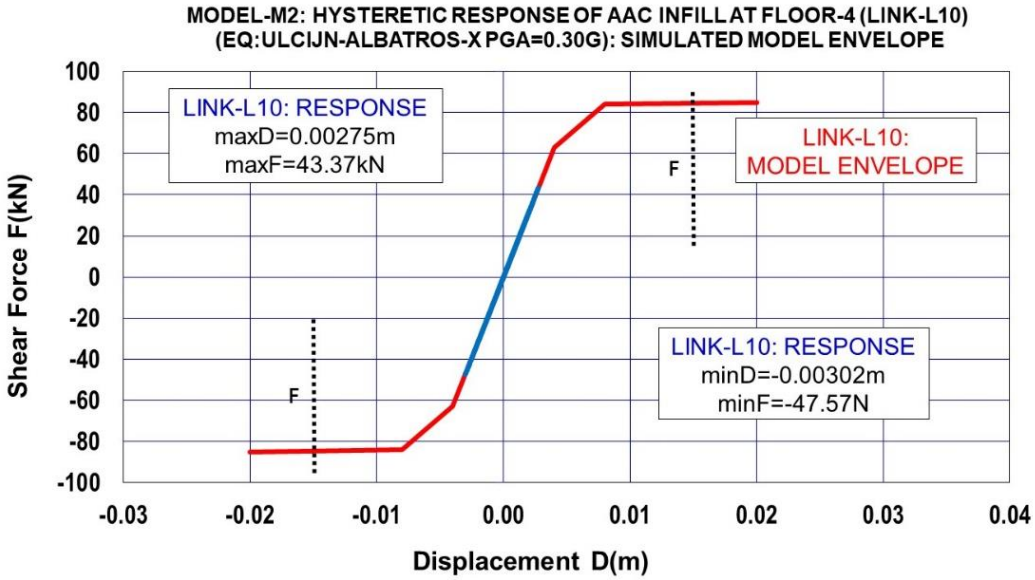

Fig. 10.6.15. Model-M2 under earthquake intensity EQI2=0.30g: Hysteretic response of AAC infill at storey-4

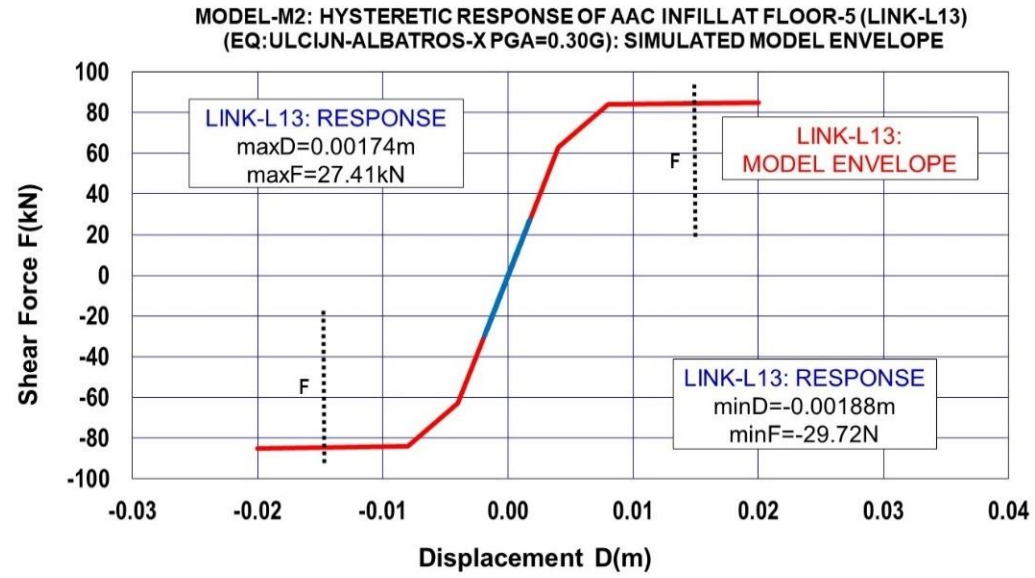

Fig. 10.6.16. Model-M2 under earthquake intensity EQI2=0.30g: Hysteretic response of AAC infill at storey-5

10.7 Concluding Remarks

The nonlinear macro-model of the AAC infill demonstrated a consistent ability to reproduce the cumulative storey envelope, as illustrated in Fig. 10.7.1. For this purpose, two pushover analyses were performed in SAP2000, one in the positive and one in the negative loading direction, [63]. The pushover analysis was carried out by gradually increasing the horizontal force at the control node of the first storey until the model reached its nonlinear capacity, generating the characteristic force-displacement curve for each direction. The results of these monotonic analyses were then combined to obtain the cumulative model pushover envelope, shown in the figure with red lines. This envelope is directly compared with the hysteretic storey response obtained from cyclic loading, represented by the blue curves.

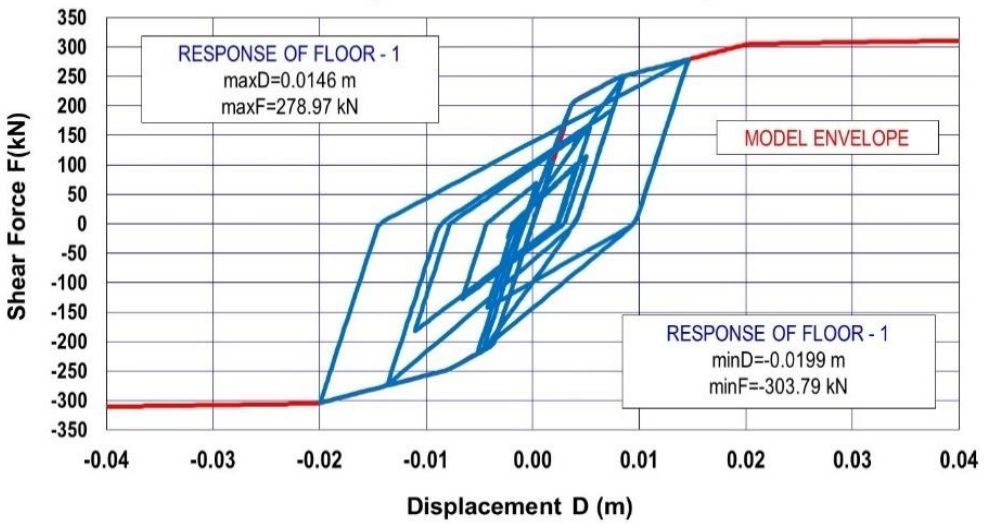

Fig. 10.7.1. Confirmed capability of AACF nonlinear macro-model for simulation of cumulative storey envelope computed with positive and negative push-over analysis and with earthquake response analysis including two RC columns and AAC infill at storey-1

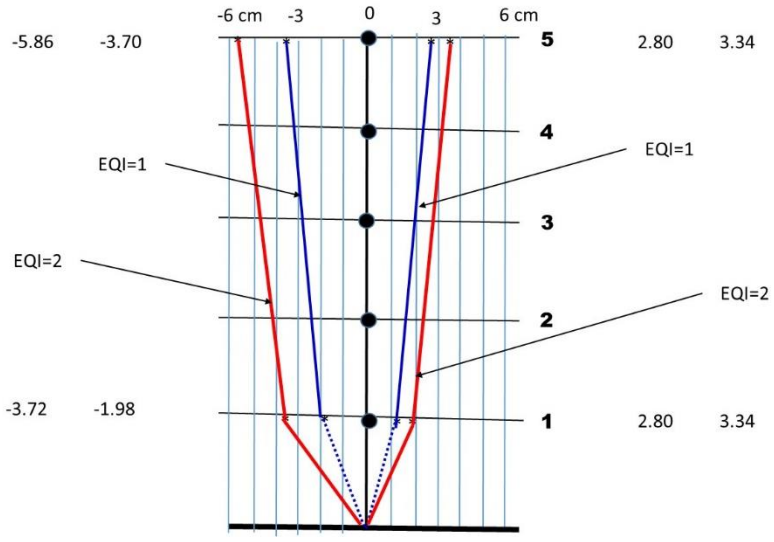

Fig. 10.7.2. Model-M2 under earthquake intensity EQI1=0.22g and EQI2=0.30g: Computed maximum positive and negative storey displacements of the analysed AAC infilled frame

Using results from the performed earthquake response analysis, including two RC columns and AAC infill at storey-1, obtained was cumulative storey hysteretic response by summation of computed restoring forces of left column, right column and existing infill segment of storey-1 Figure 10.7.1. Comparing the two cases, the obtained perfect agreement is evidenced (subchapter 10.3.3).

Fig. 10.7.2 shows the computed maximum positive and negative storey displacements of the analyzed AAC infilled frame. The presented deformation profiles computed for earthquake intensity EQI1 = 0.22 g and EQI2 = 0.30 g, provide an insight into the critical storey deformations which are, in this case, concentrated at the first storey.

Considering the presented results from the performed analyses for two selected earthquake intensities, the following conclusions are summarized:

(1) The proposed nonlinear AACF macro model possesses a pronounced ability to simulate the characteristics of the frame structures of buildings with AAC infill.
(2) The structural elements of the RC frame structures can be successfully modelled with different levels of refinement, depending on the objective of the analysis. In this research, two levels of modelling refinement were applied: a simplified macro-model using nonlinear link elements calibrated from the experimental results, and a more refined micro-model developed in DIANA FEA for local stress and cracking analysis.
    The comparison between these modelling levels confirmed that both approaches provided consistent global responses, while the refined model offered additional insight into local damage mechanisms. The AAC infill can be effectively modelled by using nonlinear link elements. Within this study, the nonlinear behavior of the AAC infill was successfully simulated and verified through analytical calibration against experimental results.
(3) The AAC infill can be modelled by the application of nonlinear link elements calibrated from experimental results. In this research, a single level of modelling accuracy was applied, corresponding to the macro-modelling approach, which reproduces the overall nonlinear behavior of the infill in terms of stiffness, strength, and degradation. The reference to different degrees of accuracy relates to the general modelling concept, where the nonlinear response of AAC infills can be simulated at different refinement levels from simplified single-link representations to detailed micro-modelling of cracking and crushing mechanisms. In the present study, the simplified macro-model was adopted, which is sufficiently accurate for reproducing the global behavior observed experimentally. The asymmetric response of the infilled frame was not separately modelled but was captured inherently through the nonlinear hysteretic properties of the link elements calibrated from the experimental force-displacement

curves, which already contained the asymmetry induced by cracking and partial separation between the frame and the infill.

(4) The proposed AACF nonlinear model provides the possibility for the formulation of complete macro-nonlinear models of multi-storey RC frame structures with AAC infill in panels without openings. Although the current study focuses on infill walls without openings, the developed modelling concept can be further extended in future research to simulate the nonlinear behavior of infilled frames with openings or with complex wall topologies. This would require additional calibration of the link parameters to account for the local stress concentrations and reduced stiffness introduced by the openings.

11 CHAPTER 11 - CONCLUSIONS AND REOMENDATIONS

11.1 Conclusions

Based on the results obtained from the experimental testing of the constructed large-scale reinforced concrete (RC) bare frame models and RC frame models with autoclaved aerated concrete (AAC) infill, as well as the findings derived from the complementary parametric analytical study, the following detailed conclusions are presented:

1) The experimental tests performed on the large-scale prototype models of RC bare frames, which included one model subjected to the combined action of vertical and cyclic horizontal loading (M1-A) and another model subjected to vertical loading followed by monotonic horizontal loading (M1-B), confirmed that the type of loading pattern applied in the tests did not significantly affect the global structural response. This was clearly demonstrated by the fact that the nonlinear envelope curves generated in both cases were almost identical in shape, resistance, and deformation characteristics. The similarity of these curves verifies that for this particular frame configuration, the distinction between cyclic and monotonic horizontal loading does not play an essential role in modifying the overall nonlinear behavior.
2) A similar conclusion was reached for the RC frame models with AAC infill. These models were also tested under two types of loading conditions that simulated real structural demands, including the interactive combination of vertical and cyclic horizontal loading (M2-A) and the identical vertical loading followed by monotonic horizontal loading (M2-B). The comparison of the resulting nonlinear envelope curves revealed very small differences between the two loading procedures. This indicates that the AAC infilled RC frame system exhibits a comparable global response regardless of whether cyclic or monotonic horizontal loading is applied under the same vertical load.
3) The results of the conducted tests demonstrated that the RC frames were designed with sufficient ductility. At higher relative deformation levels, the frames exhibited nonlinear behavior accompanied by crack formation at critical regions. Despite this, the frames retained their overall stability throughout the loading process. In contrast, the AAC infill experienced substantial and irreparable damage under larger relative displacements. Although the RC frame itself did not fail and its structural integrity remained intact, the extent of damage suffered by the AAC infill became very severe and economically unjustifiable, indicating that the infill is considerably more vulnerable than the surrounding RC frame elements.
4) The advanced nonlinear micro-model developed for the tested RC bare frame successfully reproduced the experimentally observed response. The model demonstrated strong capability in capturing essential nonlinear characteristics of the frame system and is therefore suitable for conducting further investigations, including simulations of RC frame behavior under combined vertical and horizontal loading effects. Its validity is supported by the high level of agreement between the numerical and experimental results.

5) The analytical micro-modelling study confirmed that variations in the axial load level have a major influence on the nonlinear response of RC frames. Changes in axial forces significantly affect the stiffness, strength, and deformation capacity of the structural system. This observation highlights that the effect of varying axial loads cannot be ignored during the seismic design of RC frame structures located in earthquake-prone regions.
6) The analyses performed using the refined nonlinear micro-model further demonstrated that RC frames subjected to significantly increased axial load levels exhibit a notable reduction in ductility. When axial loads rise to higher values, the frame becomes more vulnerable and is more likely to experience critical damage or complete structural failure. This finding emphasizes the importance of correctly assessing axial load variations during design and evaluation processes.
7) The predicted nonlinear force deformation relationship produced by the refined nonlinear micro-model showed very strong agreement with the experimentally obtained nonlinear envelope curve. The maximum resisting force from the experimental test was 80.0 kN, while the analytically predicted maximum resisting force was 82.0 kN. The difference between these values was only 2.5 percent, which confirms the high accuracy of the developed model. This close correlation represents a significant achievement, indicating that the refined model can be reliably used for extended research, including detailed parametric studies and other specialized analytical investigations.
8) The analytical simulation study of RC frames with AAC infill, which considered three different axial load levels, confirmed that increasing axial loads in the columns results in a significant reduction in their ductility. This reduction introduces a critical structural condition, especially during strong seismic events, where changes in axial force levels are unavoidable. The cracks observed in the RC columns were generally localized and appeared in the critical regions near the column bases where stress concentrations were the highest.
9) The cracks that developed in the AAC infill were typically widespread throughout the panel. Larger cracks formed along extended diagonally oriented paths, while concentrated and more severe damage occurred at the corners of the infill panel. An important observation is that the nonlinear behavior of AAC infill is highly complex. At the initial loading stages, the infill contributes positively by increasing the global stiffness and the resisting force of the structural system. However, both initial and extended cracking appear very early at relatively small deformation levels. More extensive failure of the AAC infill also occurs at relatively small displacements. After this significant deterioration, the stability of the entire system depends on the capacity of the RC columns to provide adequate ductility.
10) In the extended analytical simulation considering the asymmetric placement of the AAC infill, where the infill was located only in the left half-span of the RC frame, unexpected but important results were obtained. Despite the asymmetric configuration, the structural response displayed symmetry. The maximum resisting forces obtained for positive and negative deformations were very close in magnitude, with values of 72.5 kN and 73.5 kN. The small difference of only 1.4 percent indicates that the nonlinear response of the system remained nearly symmetrical.

11) The reason for the symmetrical response lies in the geometric transformation that occurred during deformation. Both positive and negative deformations altered the initial rectangular shape of the infill panel and forced it into an oblique rectangular configuration. Since the geometric transformation for the positive and negative deformation directions was nearly identical, the resulting resisting forces were also symmetrical.
12) Using the experimentally verified micro-models, extensive analytical parametric studies were performed. These studies functioned as successful analytical experiments and provided valuable insights into the behavior of AAC infill under different configurations. Based on the results of these detailed analytical investigations, a new practically applicable procedure was formulated. This procedure offers an advanced capability for defining the complete set of required nonlinear macro-modelling parameters for uncoupled AAC infill panels used in RC frames with different spans, optional thicknesses, and variable compressive strengths.
13) The proposed AACF nonlinear macro-model can be applied successfully for the modelling of multi-storey RC frame buildings with AAC infill. It has demonstrated strong capability and reliability in representing the behavior of AAC infill panels without openings, making it suitable for modeling a wide range of RC frame structures that incorporate such infill walls.
14) The research results indicated that AAC infill is highly susceptible to extensive damage or failure in certain critical regions of the panels. To prevent or reduce potential damage, it is necessary to develop and implement new protective measures for the infill. Future research should focus on creating innovative technical solutions aimed at reducing the vulnerability of AAC masonry elements, which possess diverse geometric configurations and distinct nonlinear mechanical characteristics.

11.2 Recommendations for Future Research

The findings of this study highlight the important role and the inherent vulnerability of AAC infills under seismic actions. Although meaningful progress has been made in understanding their nonlinear behavior, several aspects require further development. In line with the reviewer's comments, the following recommendations summarize the necessary extensions, research gaps, advanced studies, and practical implications arising from the present work.

11.2.1 Extensions of the Current Work

Future investigations should broaden the scope of the current study by including parameters and configurations that were not examined here. These extensions should cover:

- additional geometric and material variables that influence the frame-infill interaction;
- a wider range of axial load levels and boundary conditions;

- different infill configurations, particularly partial infills, mixed layouts, or infills with openings.

Such extensions would allow a more comprehensive understanding of the sensitivity of AAC-infilled frames to multiple structural and loading parameters.

11.2.2 Identified Research Gaps

Several limitations of the present study should be addressed in future work:

- The current analyses were focused on a limited set of parameters; broader parametric combinations remain unexplored.
- Certain questions arising from the observed behavior, such as local damage mechanisms, interface degradation, and post-cracking stiffness evolution require deeper investigation.
- Scenarios related to long-term behavior (aging, moisture, or degradation of AAC) were not considered but may affect the overall performance of infilled frames.

Addressing these gaps would significantly refine the understanding of AAC performance under seismic loading.

11.2.3 Advanced Studies

To further improve the reliability and applicability of AAC-infilled frame models, the following advanced studies are recommended:

- investigation of complex structural conditions such as 3D effects, torsional responses, vertical irregularities, and soft-storey mechanisms;
- analyses that consider long-term effects, such as durability, environmental exposure, or time-dependent degradation of AAC units;
- exploration of alternative materials or hybrid construction techniques that could improve the ductility and seismic resilience of AAC infills.

These advanced studies would contribute to a more realistic representation of AAC-infilled buildings under real earthquake scenarios.

11.2.4 Recommendations for Engineering Practice-Design Guidelines

The results of this research emphasize that the influence of AAC infills should not be neglected in seismic design. Practitioners should:

- account for the stiffness and strength modification induced by AAC infills;

- apply the findings of this study when determining effective stiffness and capacity parameters for analysis;
- consider appropriate safety factors or design margins when infill properties or construction quality are uncertain.

11.2.5 Practical Implementation

For engineering applications, the simplified macro-modeling approach developed in this study can be used in practice, provided that:

- the model is calibrated within the appropriate parameter ranges;
- implementation in design software follows the same modelling principles demonstrated in this research;
- adequate quality control is ensured during construction, especially regarding joint quality, alignment, and material consistency.

11.2.6 Recommendations for Experimental Work

Future experimental studies are necessary to strengthen the validation of analytical findings. These should include:

- Full scale or large-scale cyclic tests of AAC-infilled RC frames;
- alternative loading protocols to simulate different earthquake scenarios;
- improved instrumentation using advanced measurement systems for crack monitoring, deformation tracking, and interface behavior observation.

These efforts would provide high-quality data needed to refine analytical and numerical models.

11.2.7 Recommendations for Numerical Modeling

To further advance the modeling accuracy of AAC infills:

- more sophisticated constitutive relationships should be developed, including micro-modelling of AAC units and mortar joints when needed;
- models should be enhanced to capture localized cracking, interface slip, degradation, and post-peak softening behavior;
- computational efficiency should be improved to enable large-scale parametric studies.

11.2.8 Validation Requirements

Additional validation against different structural configurations, loading regimes, and boundary conditions is essential to ensure broad applicability of the proposed modeling approach.

11.2.9 Final Summary

The overall results demonstrate that AAC infills remain vulnerable under strong earthquakes and require careful analytical treatment. Progressing from the current study toward more comprehensive parametric, experimental, and numerical investigations will be essential for developing improved design strategies and safer engineering applications. The recommendations above provide a structured roadmap for future research and practical implementation aligned with the reviewer’s expectations.

12 REFERENCES

[1] Willem van Boggelen (2014) History of Autoclaved Aerated Concrete: The short story of a long-lasting building material. Publishing Date: April 2014.

[2] Basavachetana Gudugurmath, Prajwala, Divya L, Hemantha R, Kavya B (2023) Autoclaved Aerated Blocks. International Journal of Engineering Research & Technology (IJERT), Volume 11, Issue 05, ICEI – 2023.

[3] Ytong Modular Building System: Ultrafast and energy-efficient housing construction. XEL50225/A Silka, Ytong and Xella are registered trademarks of the Xella Group dmix/1215/1.000. www.xella.co.uk

[4] Savetnik o YTONG Materijalu i Sistemu Gradnje. www.xella.co.yu. ytong-serbia@xella.com. Januar 2006.

[5] Furkan Gökmen (2017) Seismic Behavior of Autoclaved Aerated Concrete Reinforced Vertical Panel Buildings. MSc Thesis, Middle East Technical University, Turkey, 2017.

[6] Matthew John Brightman (2000) AAC Shear Wall Specimens: Development of Test Setup and Preliminary Results. MSc Thesis, Faculty of the Graduate School, University of Texas at Austin, 2000.

[7] Nina Löfman and Victor Molander (2024) Investigation of Reinforced Autoclaved Aerated Concrete Structures. MSc Thesis, Royal Institute of Technology, KTH, Department of Civil and Architectural Engineering, Division of Concrete Structures, Stockholm, Sweden, 2024.

[8] Vassilios Soulis (2020) The Seismic Behavior of Single- and Three-Story Masonry Infilled R/C Frames Utilizing Non-linear Numerical Models. International Journal of Science and Engineering Investigations vol. 9, issue 99, 2020.

[9] Jun Yu; Yi-Ping Gan; Jun Liu (2020) Numerical study of dynamic responses of RC infilled frames subjected to progressive collapse. Advances in Structural Engineering, November 2020: DOI: 10.1177/1369433220965273

[10] Carlo Del Gaudio, Maria Teresa De Risi & Gerardo Mario Verderame (2021): Seismic Loss Prediction for Infilled RC Buildings via Simplified Analytical Method, Journal of Earthquake Engineering, DOI: 10.1080/13632469.2021.1875940

[11] Hashemi, M. Javad; Tsang, Hing-Ho; Al-Ogaidi, Yassamin; Wilson, John L.; Al-Mahaidi, Riadh (2017) Collapse assessment of reinforced concrete building columns

through multi-axis hybrid simulation. Year: 2017, ACI Structural Journal, Volume: 114, Issue: 2, Pages: 437-449, URL: https://hdl.handle.net/1959.3/434767

[12] Moment Resisting Frames with Infill Panels, C7, (2017) Ministry of Business, Innovation and Employment, the Earthquake Commission, the New Zealand Society for Earthquake Engineering, the Structural Engineering Society and the New Zealand Geotechnical Society.

[13] Avadhoot Bhosale; Nikhil P. Zade; Robin Davis; and Pradip Sarkar (2019) Experimental Investigation of Autoclaved Aerated Concrete Masonry. J. Mater. Civ. Eng., 2019, 31(7): 04019109. https://doi.org/10.1061/(ASCE)MT.1943-5533.0002762

[14] Miha Tomaževič; Matija Gams (2019) Shaking table study and modelling of seismic behaviour of confined AAC masonry buildings. Bull Earthquake Eng (2012) 10:863–893. DOI 10.1007/s10518-011-9331-x

[15] Lourenço, P. B. (1996). Computational strategies for masonry structures. Ph.D. Thesis, Delft University of Technology, The Netherlands.

[16] Christiana A. Filippou; Nicholas C. Kyriakides; Christis Z. Chrysostomou; Elpida S. Georgiou (2018) Finite element model of masonry-infilled RC frame. 16th Conference in Earthquake Engineering. Thessaloniki, Greece.

[17] Kewei Ding; Chikun Zhang; Shulin He; and Yunlin Liu (2022) Hysteresis Behavior and Design of the New Autoclaved Lightweight Concrete (ALC) External Panel Connector with the Steel Frame. Advances in Materials Science and Engineering. Volume 2022, Article ID 8319044, 18 pages. https://doi.org/10.1155/2022/8319044

[18] Damir Markulak; Ivan Radić; Vladimir Sigmund (2013) Cyclic testing of single bay steel frames with various types of masonry infill. Engineering Structures, 10.1016/j.engstruct.2013.01.026.

[19] Mostafa Ali Taha Ali Okasha; Mohamed Abdel Razek and Hassan El-Esnawi (2020) Strengthening of existing RC buildings by using autoclaved aerated concrete infill wall. HBRC Journal 2020, VOL. 16, NO. 1, 143–155; https://doi.org/10.1080/16874048.2020.1789392

[20] Mollaei, S.; Babaei Ghazijahani, R.; Noroozinejad Farsangi, E.; Jahani, D. (2022) Investigation of Behavior of Masonry Walls Constructed with Autoclaved Aerated

Concrete Blocks under Blast Loading. Appl. Sci. 2022, 12, 8725. DOI: 10.3390/app12178725.

[21] Tiziana Cardinale; Corradino Sposato; Maria Bruna Alba; Andrea Feo1, Giorgio Leter; Piero De Fazio1 (2020) The Bio-aerated Autoclaved Concrete: A New Solution for a Sustainable Product in the Building Sector. TECNICA ITALIANA-Italian Journal of Engineering Science, Vol. 64, No. 2-4, June, 2020, pp. 341-346, DOI: 10.18280/ti-ijes.642-432.

[22] Xiaogang Huang; Zhen Zhou; Yuhang Wang (2021) Investigation of the seismic behaviour of masonry infilled self-centring beam moment frames using a new infill material model. Bulletin of Earthquake Engineering (2021) 19:4887–4910. https://doi.org/10.1007/s10518-021-01150-9

[232] Wang, X.; Xiong, L.; Wang, Z. (2024) Simplified Model Study of Autoclaved Aerated Concrete Masonry Flexible Connection Infilled Frames with Basalt Fiber Grating Strips. Buildings 2024, 14, 1033. https://doi.org/10.3390/buildings14041033

[24] A. A. Costa; A. Penna; G. Magenes; and A. Galasco (2008) Seismic performance assessment of autoclaved aerated concrete (AAC) masonry buildings. The 14th World Conference on Earthquake Engineering, October 12-17, 2008, Beijing, China.

[25] Li, X.; Ma, D.; Zhang, Q.; Zhang, Z.; Bao, H.; Yao, Y. Seismic (2024) Performance of Full-Scale Autoclaved Aerated Concrete Panel-Assembled Walls: Experimental Study and Numerical Modeling. Buildings 2024, 14, 1333. https://doi.org/10.3390/buildings14051333

[26] Yun Liu; Gonglian Chen; ZhipengWang; Zhen Chen; Yujia Gao; and Fenglan Li (2020) On the Seismic Performance of Autoclaved Aerated Concrete Self-Insulation Block Walls. Materials 2020, 13, 2942, https://doi.org/10.3390/ma13132942

[27] ASTM E519-81 Standard Test Method for Diagonal Tension (Shear) of Masonry Assemblages.

[28] CUR (1994). Masonry Structures: Materials, Design and Construction Recommendations. CUR Report 171, Centre for Civil Engineering Research and Codes (CUR), Gouda, The Netherlands.

[29] D'Altri AM et al. (2019): Modeling Strategies for the Computational Analysis of Unreinforced Masonry Structures: Review and Classification. Archives of Computational Methods in Engineering, vol. 27, pp. 1153-1185, https://doi.org/10.1007/s11831-019-09377-x

[30] Castellazzi, G., Ciancio, D., Ubertini, F. A (2015): Simplified Micro-Modeling Approach for Historical Stone Masonry Walls. Key Eng. Mater, vol. 624, pp. 74-79. DOI: 10.4028/www.scientific.net/KEM.624.74

[31] Baraldi, D., Cecchi, A (2016): Three-dimensional Nonlinear Behaviour of Masonry Walls Modeled with Discrete Elements. ECCOMAS Congr. Proc. 7th Eur. Congr. Comput. Methods Appl. Sci. Eng, vol.3, pp. 5248-5261. DOI: 10.7712/100016.2177.10185.

[32] Baloevic. G., Radnic, J., Matesan, D., Grgic, N., Banovic, I (2016): Comparison of Developed Numerical Macro and Micro Masonry Models for Static and Dynamic Analysis of Masonry-infilled Steel Frames. Lat. Am. J. Solids Struct, vol. 13 (12), pp.2251-2265. DOI: 10.1590/1679-78252520

[33] Furtado, A., Rodrigues, H., Arede, A., Varum, H (2016): Simplified Macro-Model for Infill Masonry Walls Considering the Out-of-Plane Behaviour. Earthq. Eng. Struct. Dyn, vol. 45, pp. 507-524. DOI: 10.1002/eqe.2663.

[34] Mohammad, A. K (2020): Analysis of Autoclaved Aerated Concrete (AAC) Blocks with Reference to its Potential and Sustainability. Journal of Building Materials and Structures. 7, 76-86, DOI: 10.5281/zenodo.3950489.

[35] Kalpana, M., Mohith, S (2020): Study on Autoclaved Aerated Concrete: Review. Materials Today. Proceedings, Volume 22, Part 3, Pages 894-896. https://doi.org/10.1016/j.matpr.2019.11.099.

[36] Saranya, G., Gunasekaran, M., Elamaran, L., Sakthivel, P (2016): Development of Light Weight Concrete by Using Autoclaved Aerated Concrete. International Journal for Innovative Research in Science & Technology, Volume 2, Issue 11, ISSN (online): 2349-6010, April 2016.

[37] Nitin, K., Prakash, N. O (2017): Application of AAC Blocks in Residential Buildings. International Journal of Engineering Sciences & Research, ISSN: 2277-9655, March, 2017.

[38] American Concrete Institute. (2009) Guide for Design and Construction with Autoclaved Aerated Concrete Panels. Reported by ACI Committee 523

[39] Shendkar M., Kontoni N., Isik E (2022) Influence of Masonry Infill on Seismic Design Factors of Reinforced-Concrete Buildings. Hindawi, Shock and Vibration, Volume 2022, Article ID 5521162, 15 pages, https://doi.org/10.1155/2022/5521162

[40] Khaliq, A., Verma, A (2022) Strength Analysis of Concrete by Using Aerated Concrete Material, International Journal of Scientific Research & Engineering Trends, Volume 8, Issue 1, Jan-Feb-2022, ISSN (Online): 2395-566X

[41] DIANA FEA (2014). DIANA -User´s Manual. Delft, The Netherlands

[42] Ristic, D. “Nonlinear behavior and stress-strain based modelling of reinforced concrete structures under earthquake induced bending and varying axial loads.” Doctoral Dissertation, School of Civil Engineering, Kyoto University, Japan, 1988.

[43] Seismosoft. SeismoStruct – A computer program for static and dynamic nonlinear analysis of framed structures Seismosoft, Pavia, Italy. 2021. http://www.seismosoft.com/en/SeismoStruct.aspx

[44] Misini, Labeat, Jelena Ristic, Viktor Hristovski, and Danilo Ristic. “Performance testing of roof beam–column connections for precast N-system.” Magazine of Concrete Research 2024, Published Online: January 05, 2024. doi:10.1680/jmacr.23.00037.

[45] Churilov, S. (2012). Experimental and analytical research of strengthening techniques for masonry. PhD thesis, University "Ss. Cyril and Methodius", Faculty of Civil Engineering- Skopje. (http://ktk.gf.ukim.edu.mk)

[46] EN 12602:2008. Prefabricated reinforced components of autoclaved aerated concrete. European Committee for Standardization (CEN), Brussels.

[47] Drysdale, R. G., Hamid, A. A., & Baker, L. R. (1999). Masonry structures: Behavior and design. The Masonry Society, Boulder, CO, USA.

[48] Müller, H. S., Haist, M., & Vogel, M. (2017). Tensile strength and fracture energy of autoclaved aerated concrete (AAC). Materials and Structures, 50(1), 1–12. Springer.

[49] Wittmann, F. H. (2002). Crack formation and fracture energy of normal and high strength concrete. Sadhana – Academy Proceedings in Engineering Sciences, 27(4), 413–423. Springer.

[50] Atkinson, B. K., Meredith, P. G., & Meredith, P. G. (1989). Fracture of brittle rock and concrete materials. In: B. K. Atkinson (Ed.), Fracture Mechanics of Rock (pp. 111–166). Academic Press, London.

[51] Nakamura, H., & Higai, T. (2001). Compressive fracture energy and fracture zone length of concrete. In: Fracture Mechanics of Concrete Structures (FRAMCOS-4), ed. by V. C. Li, K. Y. Leung, K. J. Willam, & S. L. Billington, Aedificatio Publishers, Freiburg, Germany, pp. 259–268.

[52] Fardis, M. N. (2009). Seismic design, assessment and retrofitting of concrete buildings: based on EN-Eurocode 8. Springer, Dordrecht.

[53] Dolšek, M., & Fajfar, P. (2002). Mathematical modelling of an infilled reinforced concrete frame structure based on the results of pseudo-dynamic tests. Earthquake Engineering & Structural Dynamics, DOI: 10.1002/eqe.147

[54] Stavridis, A., & Shing, P. B. (2010). Finite-element modeling of nonlinear behavior of masonry-infilled RC frames. Journal of Structural Engineering, ASCE, 136(3), DOI: 10.1061/(ASCE)ST.1943-541X.0000123

[55] EN 772-1:2011+A1:2015. Methods of test for masonry units – Part 1: Determination of compressive strength of masonry units.

[56] EN 1015-11:2019. Methods of test for mortar for masonry – Part 11: Determination of flexural and compressive strength of hardened mortar.

[57] EN 12390-3:2019. Testing hardened concrete – Part 3: Compressive strength of test specimens.

[58] EN ISO 6892-1:2019. Metallic materials — Tensile testing — Part 1: Method of test at room temperature.

[59] CEN (2005). EN 1998-3: Eurocode 8 – Design of Structures for Earthquake Resistance – Part 3: Assessment and Retrofitting of Buildings. Brussels: European Committee for Standardization.

[60] Priestley, M. J. N., Calvi, G. M., & Kowalsky, M. J. (2007). Displacement-Based Seismic Design of Structures. Pavia, Italy: IUSS Press.

[61] Brzev, S. (2012). Earthquake-Resistant Design of Masonry and Reinforced Concrete Buildings. Earthquake Engineering Research Institute (EERI), Oakland, CA, USA. ISBN 978-1-932884-46-3.

[62] Takeda, T., Sozen, M. A., & Nielsen, N. N. (1970). Reinforced concrete response to simulated earthquakes. Journal of the Structural Division, ASCE, 96(12), 2557–2573.

[63] Computers and Structures, Inc. (CSI). SAP2000 Integrated Software for Structural Analysis and Design – Analysis Reference Manual. Version 23. Berkeley, California, USA: Computers and Structures, Inc., 2021.

[64] Omar A. H. et al. (2025) – Investigation of Hysteresis Behavior for Frames with and Without Infill Masonry Concrete Block Wall in Various Aspect Ratios, Journal of Civil Engineering & Construction, https://doi.org/10.32732/jcec.2025.14.3.136

[65] Pedone L. et al. (2023) – Displacement incompatibility shape functions between infill and frame interaction, Bulletin of Earthquake Engineering, https://doi.org/10.1007/s10518-023-01634-w

[66] Nakamura, H., et al. (2016). "Observed damage of RC buildings during the 2016 Kumamoto Earthquake." Journal of Advanced Concrete Technology, Vol. 14 (11), pp. 620–635. (ResearchGate), DOI**:** https://doi.org/10.3151/jact.14.620

[67] Dogan, S., Korkmaz, K., & Yildiz, S. (2024). "Investigation of RC structure damages after the February 6, 2023 Kahramanmaraş earthquake in the Hatay region." Bulletin of Earthquake Engineering (Springer), DOI: 10.1007/s10518-024-01965-2

[68] Ferretti, D.; Michelini, E.; Pongiluppi, N.; Cerioni, R. (2020) Damage assessment of autoclaved aerated concrete buildings: some Italian case studies. Applied Sciences, Vol. 10 (3), Article 338308014.

[69] Adnan, S. M. N.; Matsukawa, K.; Haga, Y.; Islam, M. M. (2022) A nonlinear macro-model for simulating the in-plane behavior of unreinforced masonry (URM) infilled frames. Bulletin of Earthquake Engineering, Vol. 20 (2), pp. 657–678.

[70] Oyguc, R.; Oyguc, E. (2017) The 2011 Van Earthquakes: Lessons from Damaged Masonry Structures. Journal of Performance of Constructed Facilities, Vol. 31 (5)